THE UNIVERSITY OF
SYDNEY

Functional and Structural Characterisation of Mutant Tropoelastin Constructs

Giselle Chua Yeo

A thesis submitted in fulfilment of the requirements
for the degree of Doctor of Philosophy

School of Molecular Bioscience
University of Sydney
June 2013

Declaration

I declare that the work described in this thesis is entirely my own except where specifically stated in the text. This work has not been previously submitted for any degree at any institution.

_____

Giselle Chua Yeo

Acknowledgements

I am foremost indebted to my supervisors, Prof Anthony Weiss and Dr Suzanne Mithieux, for their continued guidance, insightful advice, kind encouragement and optimism throughout my PhD candidature. Their extensive knowledge and unbridled enthusiasm have been a source of inspiration. I could not have asked for better mentors.

I am especially grateful for the technical assistance and scientific expertise offered by many people during the course of this work. In particular, I thank Dr Clair Baldock at the University of Manchester for her invaluable assistance with the SAXS data acquisition and analyses of tropoelastin constructs; Dr Manfred Roessle and Dr Anne Tuukkanen at DESY Hamburg for their help with the SAXS data processing; Dr Renee Whan, Mrs Ellie Kable, Mr Dennis Dwarte and Dr Patrick Trimby at the Australian Centre for Microscopy and Microanalysis for technical instructions on confocal, SEM and micro-CT imaging; Dr Steven Wise for running mass spectrometry of the tropoelastin constructs; Dr Daniel Bax for his expert knowledge on cell-based assays; and Dr Suzanne Mithieux for helpful advice on elastic fibre assembly assays.

To all past and current members of the Weiss Lab – especially Sue, Steve, Dan, Yannie, Jess, Jelena, Anna, Kevin, Lisa, Matti, Pearl, Alan, Ed and Behnaz – thank you for the witty repartees, the animated discussions, the constant encouragement, and most especially, for the warm friendship that has made my stay in the lab so enjoyable.

Finally, I am eternally grateful for the unwavering love and support of friends and family. I thank Papa, Aku Juan, Amah, Clarence and Anthony for steadfastly believing in me and supporting me every step of the way. Above all, I dedicate this work to Mom, memories of whom continue to inspire and drive me to reach for goals that were as much hers as they are mine.

Summary

Elastic fibres provide structural integrity and elasticity to tissues such as skin, lungs and blood vessels. The major component of elastic fibres is elastin, which is formed from its soluble precursor, tropoelastin. The tropoelastin nanostructure, which has only recently been described, is characterised by an elastic N-terminal coil region, a flexible hinge region, an exposed bridge region, and a cell-interactive C-terminal foot region. The process of assembling tropoelastin into elastic fibres, known as elastogenesis, consists of distinct stages of tropoelastin synthesis, coacervation, microfibrillar deposition, and cross-linking into mature, insoluble fibres. However, the contributions of specific structural regions in tropoelastin to elastic fibre assembly are insufficiently understood.

This thesis explores the functional significance of specific residues and regions in human tropoelastin. Mutant tropoelastin constructs were designed in which the R515 residue in the bridge region, the E345/E414 residues near the hinge region, or the D72 residue in the N-terminal region have been inactivated by alanine substitution. Another mutant construct that contains domain 22 (EX22), which is typically spliced out in the hinge region of native human tropoelastin, was also produced.

As functional impairment of the R515A isoform has previously been reported in assays modelling individual stages of assembly, a system was optimised to define the elastogenic potential of R515A tropoelastin in a cellular environment. When added exogenously to human dermal fibroblasts and human retinal pigmented epithelium cells, R515A tropoelastin assembled less efficiently into elastic fibres possessing atypical morphology. This may be partially attributed to a significantly altered structure around the bridge and C-terminal regions.

The E345A, E414A, E345A+E414A, D72A and EX22 constructs were extensively characterised *de novo*, via their ability to coacervate, to cross-link into hydrogels with

standard compositional and swelling properties, to interact with cells, and to form elastic fibres in elastogenic environments. All mutant constructs displayed varying degrees of impaired self-assembly. The solution shapes of the mutant species were further analysed to correlate their observed functional attributes to structural effects of the mutation/s. All mutant constructs possessed conformational changes consistent with their biochemical properties and the expected location of the mutation site.

The results described in this work identify for the first time the role of several residues, or the advantage of specific domain exclusion, in maintaining the wild-type structure of human tropoelastin, and the importance of this native structure to normal tropoelastin assembly and function.

Publications arising from this work

Publications:

Wise, S. G., Yeo, G. C., Hiob, M. A., Rnjak-Kovacina, J., Kaplan, D. L., Ng, M. K. & Weiss, A. S. Tropoelastin – a versatile assembly module for bioactive and elastic applications. *Acta Biomaterialia*, submitted June 2013.

Yeo, G. C., Baldock, C., Tarakanova, A., Wise, S. G., Buehler, M. J. & Weiss, A. S. (2013) Biological and structural properties of human tropoelastin with a revived "fossil" domain. *Proceedings of the National Academy of Sciences of the United States of America*, submitted March 2013.

Yeo, G. C., Baldock, C., Tuukkanen, A., Roessle, M., Dyksterhuis, L. B., Wise, S. G., Matthews, J., Mithieux, S. M. & Weiss, A. S. (2012) Tropoelastin bridge region positions the cell-interactive C terminus and contributes to elastic fiber assembly. *Proceedings of the National Academy of Sciences of the United States of America* 109:2878-2883.

Yeo G. C., Keeley F. W., & Weiss A. S. (2011) Coacervation of tropoelastin. *Advances in Colloid and Interface Science* 167:94-103.

Conference Proceedings:

Yeo, G. C., Baldock, C., Tuukkanen, A., Roessle, M. Dyksterhuis, L. B., Wise, S. G., Matthews, J., Mithieux, S. M. & Weiss, A. S. (2012) Tropoelastin bridge region positions the cell-interactive C-terminus and contributes to elastic fibre assembly. Oral presentation. Bosch Institute Young Investigators Symposium, NSW, Australia.

Yeo, G. C., Baldock, C., Tuukkanen, A., Roessle, M. Dyksterhuis, L. B., Wise, S. G., Matthews, J., Mithieux, S. M. & Weiss, A. S. (2012) Role of the tropoelastin bridge region in elastic fibre assembly. Oral presentation. Sydney University Tissue Engineering Network (SuTEN) Tissue Engineering Symposium, NSW, Australia.

Yeo, G. C., Baldock, C., Tuukkanen, A., Roessle, M. Dyksterhuis, L. B., Wise, S. G., Matthews, J., Mithieux, S. M. & Weiss, A. S. (2012) The tropoelastin bridge region in elastic fibre assembly. Poster presentation. Strategies in Tissue Engineering, Würzburg, Germany.

Yeo, G. C., Dyksterhuis, L. B., Mithieux, S. M. & Weiss, A. S. (2010) The tropoelastin bridge region in elastin assembly and cell interactions. Poster presentation. AINSE/ANBUG Neutron Scattering Symposium, NSW, Australia.

Yeo, G. C., Dyksterhuis, L. B., Mithieux, S. M. & Weiss, A. S. (2010) The tropoelastin bridge region in elastin assembly and cell interactions. Poster presentation. OzBio: The Molecules of Life, Melbourne, Australia.

Abbreviations

A	Alanine
ABTS	2,2’-azino-bis(3-ethylbenzothiazoline-6-sulfonic acid)diammonium salt
ADCL	Autosomal dominant cutis laxa
ANOVA	Analysis of variance
ARCL	Autosomal recessive cutis laxa
ARPE-19	Human retinal pigmented epithelial cells
BS3	Bis-sulfosuccinimidyl suberate
BSA	Bovine serum albumin
CAI	Codon adaptation index
CD	Circular dichroism
CRALBP	Cellular retinaldehyde-binding protein
D	Aspartic acid/aspartate
DAPI	4',6-diamidino-2-phenylindole
DEPC	diethylpyrocarbonate
DMEM	Dulbecco’s modified eagle medium
DMSO	Dimethyl sulfoxide
E	Glutamic acid/glutamate
E345A	Synthetic human tropoelastin with the glutamate 345 residue mutated to an alanine
E414A	Synthetic human tropoelastin with the glutamate 414 residue mutated to an alanine
E345A+E414A	Synthetic human tropoelastin with the glutamate 345 and glutamate 414 residues mutated to alanines

EBP	Elastin binding protein
EDTA	Ethylenediaminetetraacetic acid
ELISA	Enzyme-linked immunosorbent assay
EX22	Synthetic human tropoelastin with domain 22
FBS	Foetal bovine serum
FITC	Fluorescein isothiocyanate
FLIM	Fluorescence lifetime imaging microscopy
GAG	Glycosaminoglycan
GM3348	Human dermal fibroblast cell line
HDF	Human dermal fibroblast
IPTG	Isopropyl β-D-1-thiogalactopyranoside
kDa	Kilo-dalton
LB	Luria-Bertani
LOX	Lysyl oxidase
LOXL1	Lysyl oxidase-like 1
MES	2-(N-morpholino)ethanesulfonic acid
Micro-CT	Micro-computed tomography
MMP	Matrix metalloproteinase
MQW	Milli-Q water
NHF8909	Neonatal human fibroblasts
PB	Phosphate buffer
PBS	Phosphate buffered saline
PCR	Polymerase chain reaction
PMSF	Phenylmethylsulphonyl fluoride
PPII	Polyproline II

R	Arginine
R515A	Synthetic human tropoelastin with the arginine 515 residue mutated to an alanine
RPE65	Retinal pigmented epithelium-specific 65 kDa protein
rpm	Revolutions per minute
RT-PCR	Reverse transcriptase polymerase chain reaction
SAXS	Small angle x-ray scattering
SDS	Sodium dodecyl sulfate
SDS-PAGE	Sodium dodecyl sulfate polyacrylamide gel electrophoresis
SEM	Scanning electron microscopy
SNP	Single nucleotide polymorphism
SVAS	Supravalvular aortic stenosis
TBE	Tris/borate/EDTA
Tris	tris(hydroxymethyl)aminomethane
TRITC	Tetramethyl rhodamine isothiocyanate
WT	Synthetic human wild-type tropoelastin without domains 22 and 26A

Table of Contents

1. General Introduction

1.1 Elastic fibres

Elastic fibres are a component of the extracellular matrix of vertebrate tissues such as blood vessels, lungs, skin, and elastic ligaments [1]. Elastic fibres have distinct tissue-specific architectures, forming thin concentric lamellar sheets in vascular walls [2], large three-dimensional honeycomb structures in elastic cartilage, and highly-branched networks in lungs and skin [3, 4]. Apart from maintaining the structural integrity of elastic tissues [5, 6], they also confer the elastic and recoil properties required for repetitive and reversible stretching during normal function [1, 2, 7].

Elastic fibres have been shown to consist of peripheral microfibrils and a core material identified as elastin [8-10]. Microfibrils are beaded structures 8-16 nm in diameter [6], and are composed of proteins such as fibrillins, matrix-associated glycoproteins, and fibulins [4]. Interspersed with the unbranched microfibrils is the elastin core, which comprises more than 90% of the elastic fibre [4, 11]. Initially, elastin was thought to be amorphous [12], but has since been described as hydrated, laterally-packed 5 nm-wide filaments [8, 13] with a twisted structure [14].

Elastin imparts the elastic properties of elastic fibres, as evidenced by the loss of tissue resilience in diseases arising from elastin mutations [15]. In addition, elastin also regulates various cellular processes. Its biological activity is supported by elastin knockout studies where phenotypic abnormalities cannot be attributed to loss of tissue elasticity alone [16]. Through interactions with cell receptors, elastin can promote the formation of actin fibres [2], inhibit smooth muscle cell proliferation [17], regulate cell migration [18], and facilitate arterial morphogenesis, vasodilation, and chemotaxis of monocytes [1, 19].

1.2 Tropoelastin

1.2.1 The *ELN* gene

The elastin polymer is assembled from a soluble precursor known as tropoelastin [1, 20]. Tropoelastin is coded by a single vertebrate-specific gene (*ELN*) [7, 21], believed to have coincided evolutionarily with the development of a closed, high pressure circulatory system [22]. The human *ELN* was mapped by *in situ* hybridisation to the q11.2 locus of chromosome 7 [23]. It has been sequenced [24] and its regulatory elements are well-characterised [21, 25]. The tropoelastin gene sequence is highly repetitive [26] and contains numerous Alu repeats, which may contribute to the occurrence of disease due to frequent recombination events [4].

The human *ELN* spans 45 kb of genomic DNA [21]. Interspersed between large introns are 34 exons [4, 7], each coding for a hydropathically distinct domain [21]. Intron-exon splice junctions are well-conserved and functionally equivalent [7, 21, 27, 28]. This allows extensive alternative splicing of almost 30% of exons [8], particularly exons 22, 23, 24, 26A, 32, and 33 [29, 30]. For instance, exon 22 appears to be constitutively spliced out in tropoelastin transcripts of humans but not in other mammals [31-35]. Exon 26A is unique to the human *ELN*, but is commonly excluded [29, 31, 36] except in aged [4] or disease states [37]. The alternate usage of exons conceptually allows the production of functionally diverse tropoelastin isoforms from a single gene sequence [30], which is supported by the tight regulation of the splicing process [38]. To date, at least 13 human tropoelastin isoforms have been documented, which appear to be age-related [4] rather than tissue-specific [39, 40].

1.2.2 Sequence features of tropoelastin

Tropoelastin has alternating hydrophilic and hydrophobic domains [4]. This unique arrangement of domains has evolved convergently in elastomeric proteins, and if altered can significantly affect protein assembly and function [41, 42]. Hydrophilic regions are shorter [43] and possess lysines separated by proline or poly-alanine residues [27, 44], which give rise to the cationic nature of these domains [45, 46]. While hydrophilic regions are relatively conserved among species [27, 47], hydrophobic sequences are more variable. They commonly contain three- to nine-peptide repeats of glycine, valine, alanine, and proline in varying arrangements, which comprise up to 75% of the tropoelastin sequence [4, 28]. The hydrophobic peptides, when liberated from tropoelastin by protease digestion, are bioactive [36] and can stimulate the expression of matrix proteins including tropoelastin itself [48].

Another distinct feature of tropoelastin is the C-terminal domain 36. Over 70% of its sequence is highly conserved among different species, particularly the terminal RKRK residues [24, 49]. The C-terminus contains both hydrophobic and highly basic residues, as well as the only two cysteines in the protein which are stabilised by a disulfide bond to create a positively-charged pocket [27, 50, 51]. The domain structure of human tropoelastin is illustrated in Figure 1.1.

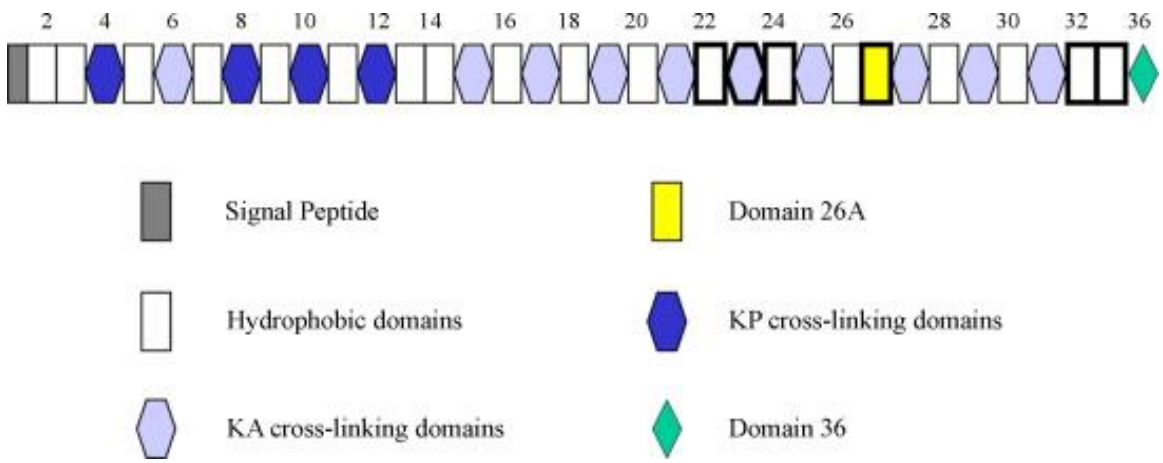

Figure 1.1. Schematic representation of the domain structure of human tropoelastin obtained from [7]. Domains are traditionally numbered to maintain consistency between homologous domains in the bovine tropoelastin. Domains outlined in bold are subject to alternative splicing.

1.2.3 Structure of tropoelastin

The earliest structural insights into elastin originated from infrared absorption and circular dichroism (CD) studies on α-elastin, a product derived from acid hydrolysis of elastin [52]. These reports indicated that solubilised elastin has a predominantly disordered structure. Nuclear magnetic resonance studies revealed that the majority of backbone carbonyl carbon atoms in the polypeptides are highly mobile [53]. Sequence-based structure prediction algorithms likewise estimated approximately 75% disorder in the structure of the tropoelastin monomer [54]. Subsequent CD and Raman spectroscopy studies on recombinant tropoelastin and elastin-like peptides also confirmed a large proportion of highly disordered regions, which were attributed to hydrophobic domains [54, 55].

The abundance of disordered structures in tropoelastin, defined as a preferential adoption of transient local structural motifs over stably-bonded secondary structures, is manifested in the flexibility of the molecule [56]. Elastin-based polypeptides oscillate between different conformations in equilibrium, giving rise to a conformational ensemble

that includes β-turns, β-strands and polyproline II (PPII) structures [57-60]. PPII structures are defined by an absence of intramolecular and intermolecular hydrogen bonds, and can therefore interconvert into other conformations [58]. In a hydrated environment, tropoelastin presents a highly flexible form [54]. The structural dynamics of the elastin backbone is mainly achieved by the proportion of rigid proline and flexible glycine residues [61]. The steric constraints imposed by proline and the entropic disadvantage of glycine confinement determine the possible backbone conformations [56, 62]. The placement of recurring proline and glycine residues promotes the formation of labile β-turns, which contribute significantly to flexibility within the protein [63]. Accordingly, skewing the ratio of proline to glycine in elastic-like polypeptides has been shown to promote the formation of β-structure-rich amyloid-like fibrils, which show a greater degree of conformational restriction than the native elastin structure [62].

In addition to PPII and other labile structures, the hydrophobic repeat units in tropoelastin also form more compact motifs such as short β-sheets or β-turns [27, 55, 64, 65]. In contrast, the hydrophilic domains are associated with a small percentage of α-helices [27, 66-68]. The presence of independent clusters of structure in tropoelastin is consistent with the gradual unfolding transition observed upon urea treatment [54].

Obtaining the tertiary structure of tropoelastin has been hindered by its inability to form resolvable crystals. In addition, the insoluble nature of polymerised elastin precludes the use of classical spectroscopic techniques [69]. Nevertheless, the binding of hydrophobic probes to tropoelastin and the ability of hydrophobic sequences to be cleaved in protease mapping experiments indicate the presence of solvent-exposed hydrophobic regions, which suggests that tropoelastin hydrophobic domains are not restricted to the core unlike classical globular proteins that have buried hydrophobic residues and solvent-contacting polar

residues [54, 70]. Furthermore, a large percentage of the monomer, including hydrophobic regions, remain partially accessible in the cross-linked elastin structure [71].

Small angle X-ray and neutron scattering analyses of recombinant human tropoelastin in solution revealed an extended asymmetrical shape with a long narrow rod from one terminus that branches into a larger region at the other terminus [72] (Figure 1.2). By comparing the solution structures of full-length tropoelastin and mutant isoforms truncated at various lengths from the N-terminus, specific domains were assigned to distinct spatial locations within the model. An elongated coil region encompasses the N-terminus to domain 18, and leads downstream to a spur containing domains 20-24 that corresponds to a predicted hinge region [73, 74]. The model shows a protrusion around domains 25-26 that was assigned as a bridge region, which connects to an open foot region at the C-terminus.

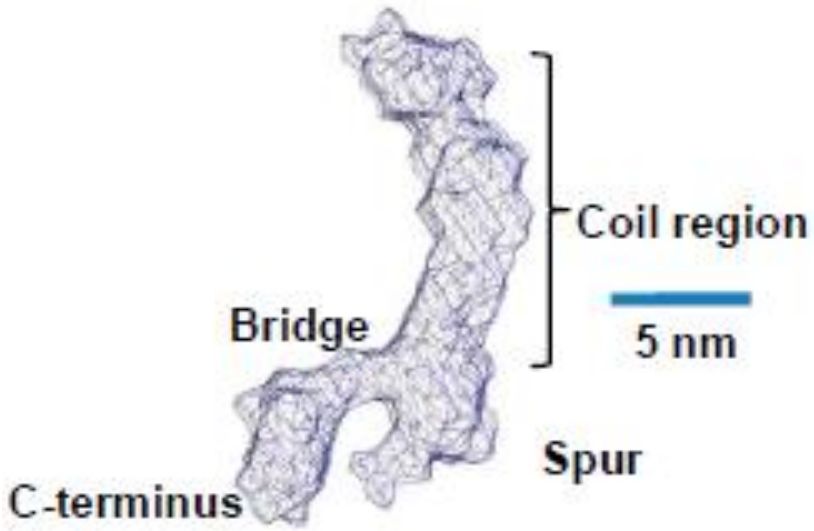

Figure 1.2. Model of full-length tropoelastin with the proposed locations of the N-terminal coil, spur and bridge regions, and the C-terminus. Obtained from [72].

The tropoelastin structure provides an indication of how the elastomeric properties of the protein are conferred [47, 69, 75]. The flexibility of the polypeptide chains contributes to the high entropy of the relaxed state. When elastin is stretched in an aqueous environment,

the hydrophobic sequences, most likely those in the coil region [72], become more exposed to the solvent and constrain the local order of water molecules [55]. This decrease in entropy acts as a driving force for spontaneous elastic recoil back to the native disordered state [76-78].

1.3 Elastogenesis

Elastogenesis refers to the assembly of tropoelastin monomers into elastic fibres. In the classical model, this process is marked by distinct stages of tropoelastin synthesis, coacervation, microfibrillar deposition, and cross-linking to form mature elastic fibres. A summary of the steps is illustrated in Figure 1.3.

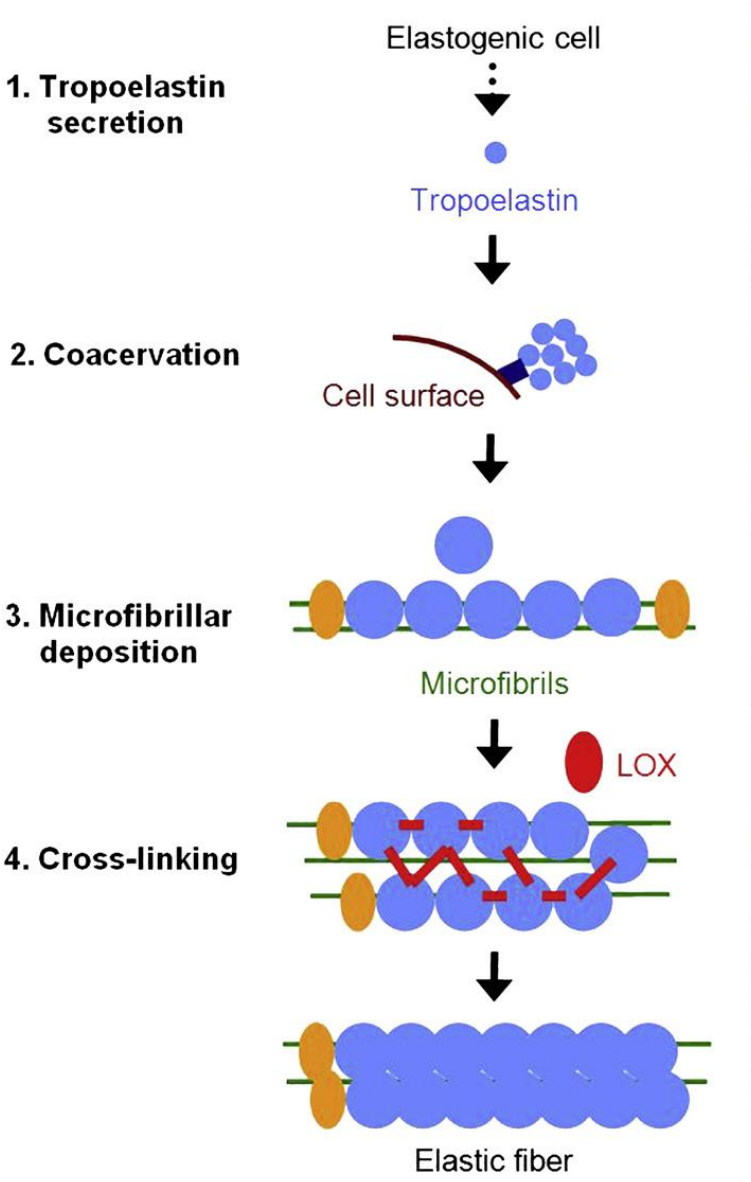

Figure 1.3. The classical model of elastic fibre assembly. Tropoelastin is secreted by elastogenic cells and coacervate into assemblies that remain attached to the cell-surface until deposition onto microfibrils. Microfibrillar proteins recruit lysyl oxidase (LOX), which cross-links tropoelastin at specific lysine residues for the formation of stable and insoluble elastic fibres. Adapted from [7].

1.3.1 Tropoelastin synthesis

Tropoelastin is produced by elastogenic cells such as smooth muscle cells, endothelial cells and fibroblasts [1, 8] in response to stimuli, including mechanical stress [8], glucocorticoids, cytokines such as tumour necrosis factor-α and interleukin-1β [79]. The rate of tropoelastin synthesis is age-dependent and maximal during perinatal development [80, 81]. While elastin synthesis in adults is minimal, it may be reactivated to repair damaged or degraded elastic fibres in aging and pathological conditions such as atherosclerosis and chronic obstructive pulmonary disease [82, 83].

Human tropoelastin is initially translated as a 724-residue polypeptide, but the 26-amino acid signal sequence is cleaved in the endoplasmic reticulum to yield the mature ~60 kDa form [7]. Tropoelastin is not glycosylated and undergoes little, if any, post-translational modification [84, 85]. Hydroxylation of some proline residues has been reported [10], although this does not appear to be functionally important for elastogenesis and if in excess, even appears to be detrimental for fibre maturation [80].

Intracellular tropoelastin may be bound by the elastin binding protein (EBP) via hydrophobic residues located in the central domains, predominantly in domain 24 [45]. This is thought to prevent premature intracellular aggregation and direct tropoelastin secretion to specific elastin assembly sites on the cell surface [3, 80, 86, 87]. Tropoelastin is secreted from elastogenic cells as nanoparticles consistent with the size of tropoelastin-enriched secretory vesicles [88, 89]. Once the protein complexes are localised to the extracellular space, the EBP chaperone protein is thought to interact with cell-surface galactosides, which leads to the release of tropoelastin [80, 90].

1.3.2 Coacervation

In the extracellular space, tropoelastin self-aggregates in a process known as coacervation. The soluble 15 nm monomers assemble outward to form progressively larger spherical globules of 2-6 μm [3, 11, 91], which appear unfused under light microscopy [11]. This process may be facilitated by glycosaminoglycans (GAGs) abundant on the surface of elastogenic cells [92], particularly at low tropoelastin concentrations [91]. Tropoelastin-GAG interactions neutralise positive charges on the tropoelastin chain that may contribute to intermolecular repulsion [93, 94], which results in molecular conformational transitions that trigger self-aggregation into the droplets observed on the cell surface [3].

Coacervation is a thermodynamically favourable process, which occurs due to the energy-driven disruption of hydrogen bonds in clathrate water around surface hydrophobic domains at physiological temperature [95]. This exposes the hydrophobic segments, which spontaneously interact and result in protein aggregation [4, 96]. The collapse of tropoelastin chains into a more ordered, assembled state decreases the entropy of the protein. This, however, is overcompensated by the increase in solvent entropy associated with the conversion of clathrate water into bulk water [97]. While water molecules can be present between associating tropoelastin filaments [98], they are fewer in number and less structured than the clathrate water surrounding hydrophobic regions of tropoelastin monomers [99]. The tropoelastin backbone also remains disordered even after coacervation due to limited self-interactions, and this contributes favourably to the entropy increase driving the coacervation process [56].

The requirement for hydrophobic domains in coacervation is supported by studies demonstrating the aggregation of elastin-like peptides containing hydrophobic motifs [47], and the abolishment of this ability in peptides with only hydrophilic sequences [100]. Furthermore, *in vitro* models have demonstrated that coacervation follows a rapid inverse

temperature transition, which is classically indicative of hydrophobic interactions [11, 101]. Specifically, the hydrophobic domains 16, 18, 20, 24, 26 and 30 are proposed to be important for self-assembly [70, 102, 103], because of their ability as isolated domains to exhibit reversible phase separation similar to the full-length tropoelastin *in vitro* [58]. Domain 20 may be a major contributor to coacervation, since it uniquely displays supramolecular fibril-like features similar to full-length tropoelastin [64]. Domain 26 is also thought to play a central role in coacervation, as its deletion or disruption abolishes the self-association ability of tropoelastin [70]. Furthermore, it represents the longest hydrophobic unit repeat in tropoelastin [26], and is well-conserved [104] and surface exposed for optimal intermolecular contacts [70]. Its proximity to the anti-parallel domain 25-domain 19 cross-link [105] places it in a position to interact with domain 18. This arrangement also implies hydrophobic contacts between domains 20 and 24 [70]. There is also evidence that domains 16-17 are involved in coacervation, as tropoelastin constructs without these domains gave rise to atypically small aggregates with a reduced propensity to form mature elastin [103].

While coacervation has classically been defined as an intrinsic property of hydrophobic sequences, the process may also be regulated by additional electrostatic contacts between charged residues [11], as suggested by pH dependence of the assembly process [106]. However, these interactions are believed to be insignificant during critical assembly conditions where hydrophobic forces play the dominant role [107].

Nevertheless, coacervation does not seem to be governed by overall hydrophobicity alone. Amino acid sequence is crucial, as evidenced by deficient or abnormal aggregation of peptides with scrambled hydrophobic residues [64, 70]. Furthermore, contextual position of the hydrophobic domains appears significant, as indicated by the decreased coacervation of a construct in which domain 26 was translocated to the C-terminus [108]. These findings suggest that self-assembly of tropoelastin is intrinsically dictated by protein sequence, and is

further supported by the propensity of isolated domains to form different structures during *in vitro* coacervation [64].

The specific requirements for coacervation suggest that the process does not result in a simple aggregated protein mass. Numerous studies have shown that tropoelastin is more ordered in the coacervate state than as monomers in solution [54, 62, 98, 101, 109-114], although it is unclear whether these structural changes precede or follow the changes in hydration state [115]. It is believed that coacervation induces the formation of regularly-spaced β-turns in hydrophobic domains which promote monomer-monomer interactions [60, 116]. The increasingly hydrophobic environment, as evidenced by enhanced surface binding of hydrophobic probes [54], also leads to a structural transformation of KA-rich domains from nascent helices into α-helices [117]. These changes limit the accessible protein conformations and stabilise the coacervate [67]. An important consequence of this process is the concentration and alignment of tropoelastin monomers essential for downstream events [44, 60, 67, 100, 101, 118-120]. The crucial role of coacervation in elastogenesis is supported by cellular studies in which incubation of smooth muscle cells below the coacervation temperature of tropoelastin led to decreased elastic fibre formation [119].

1.3.3 Microfibrillar deposition

Coacervated tropoelastin remains attached via the C-terminus to cell-surface integrins and glycosaminoglycans [3, 45] until deposition on microfibrillar bundles [121] as observed via time-lapse microscopy [3] and electron microscope immunohistochemistry [5]. Microfibrillar association is most likely dominated by domain 36, as suggested by deletion [102] and targeted antibody [45] studies. The disulfide-bonded cysteine residues in domain 36 are proposed to form a hairpin loop, creating a positively-charged pocket which contacts acidic glycoproteins in microfibrils [50]. In support of this model, disruption of the disulfide

bond and oxidation of the C-terminal tetrabasic residues decreased the integration of tropoelastin into elastic fibres [83]. However, tropoelastin constructs lacking domain 36 still bound microfibrils to some degree, suggesting the involvement of other regions in the molecule [122]. Possible candidates include domains 16, 17 and 30, as deletion constructs also exhibited reduced microfibrillar deposition [103].

The microfibrillar proteins known to interact with tropoelastin to aid extracellular deposition include matrix-associated glycoproteins, fibrillins, and fibulins [123-126]. MAGP-1 is thought to bind tropoelastin in the presence of Ca^{2+} at multiple sites spanning the entire molecule, including the domain 25-26 junction [124, 127]. Fibrillins, the major component of microfibrils [128], are thought to contact tropoelastin lysine residues [129] via glycine- and cysteine-rich domains [130] and EGF-like motifs [128]. Fibrillin-1 has been shown to regulate the expansion of tropoelastin coacervates and facilitate deposition onto microfibrils [131]. The same role is shared by fibulins such as fibulin-2, fibulin-4 and fibulin-5 [83]. As evidence, fibulin-4 and fibulin-5 deficiencies in humans are associated with abnormally large tropoelastin globules that are not optimal for incorporation into microfibrils [132, 133]. The role of fibulins in tropoelastin deposition is further supported by a lack of elastin assembly in fibulin-free fibroblast cultures [12], and the disorganised and fragmentated elastic fibres in fibulin-knockout mice [125, 126].

Microfibrillar deposition of tropoelastin is essential in elastogenesis, since microfibrils act as scaffolds which direct elastic fibre shape and orientation [3, 64, 80]. This is consistent with reports that microfibrils are the first ultrastructural indication of elastic fibres and precede the appearance of elastin [9, 134]. Binding of tropoelastin with microfibrillar proteins may also promote further self-assembly [12, 125, 126, 135] and alignment of intermolecular cross-linking domains required for elastin maturation [121, 128].

1.3.4 Cross-linking

Tropoelastin cross-linking is mediated by at least two copper-dependent lysyl oxidases, LOXL1 and LOX [123, 136, 137]. LOXL1 has been found to localise specifically to elastogenic sites [138], while LOX is widely-distributed and may cross-link both elastin and collagen [136, 137]. Lysyl oxidase function has been demonstrated *in vitro* after incubation with tropoelastin led to the disappearance of the monomer and concurrent appearance of insoluble, high molecular weight particulates [139]. *In vivo*, LOX gene inactivation [138] and LOX inhibition by either BAPN [5, 140] or copper deprivation [137] independently resulted in decreased elastin cross-linking and an impaired ability of tropoelastin aggregates to form mature fibres. The resultant elastic fibres also possessed a disorganised structure [141]. In the same manner, knockout mice lacking LOXL1 lack normal elastic fibres concomitant with extracellular tropoelastin accumulation [136].

Lysyl oxidase is thought to be recruited and activated by microfibrillar proteins such as fibulin-5 [12, 136, 142], where it recognises specific lysine residues on deposited tropoelastin. Due to variability in the sequences flanking these residues [137], substrate recognition by lysyl oxidase is believed to be at least partly dependent on local conformation [143]. This is consistent with the need for prior alignment of tropoelastin monomers during coacervation, wherein cross-linking regions are surface-exposed and α-helical [100, 117, 144], with lysines oriented on one side of the helix to allow the spontaneous condensation of cross-link intermediates [30, 128, 145-147].

Lysyl oxidase oxidatively deaminates the ε-amino group of lysine side chains to form allysines [30]. These may react either with other allysines via aldol condensation, or with unoxidised lysines via Schiff base reactions, to form bifunctional allysine aldol and dehydrolysinonorleucine cross-links, respectively [45, 140]. As elastin fibres mature, some of these covalent intra- and inter-molecular linkages [137] may further condense to form

tetrafunctional desmosine and isodesmosine cross-links [28, 140]. These allow elastin fibres to extend into the three-dimensional networks observed in extracellular matrices of elastic tissues [80].

Approximately 88% of all tropoelastin lysine residues, spanning 16 domains, are involved in cross-link formation [3, 36, 148]. The region spanning domains 19 to 25 has been reported to contain a particularly high number of cross-links [1, 143]. The initial point of contact is purported to involve the K353 residue of domain 19, since it participates in cross-links at the lowest cross-linker concentrations [44]. A well-characterised cross-link involves domains 19 and 25 of two anti-parallel elastin chains linked by desmosines, which are bridged by lysinonorleucine links with domain 10 from a third chain [105]. In addition, there may be intramolecular cross-links at the N-terminal domains 12 to 14 [1, 143].

While cross-linking imposes structural restrictions on elastin, the cross-linked material still retains hydration and flexibility due to the highly disordered backbone of the tropoelastin monomer [58]. The presence of covalent linkages render elastic fibres insoluble and stable under mechanical stretching [80, 139]. It has been reported that an increased number of cross-links improves the mechanical stability of elastin, including a higher stress and strain at break [41]. Evolutionarily, this may account for the domain expansion of elastomeric proteins such as tropoelastin and spider silk [41]. The elastic fibres also become more resistant to proteolysis, due to the inaccessibility of cleavage sites in the cross-linked structure [36]. Conversely, the inhibition of cross-linking has been correlated to increased elastin fragmentation [149]. Due to the stability of elastic fibres conferred by the cross-linking process, elastin turnover is very low in healthy tissues [4, 7, 80].

1.4 Elastin mutations and disease

Polymorphisms in the tropoelastin sequence can significantly impact upon the self-assembly of the monomer, as well as the properties of the cross-linked elastin polymer [150]. This is clearly demonstrated in pathological conditions associated with tropoelastin mutations.

Supravalvular aortic stenosis (SVAS), which may be inherited as an isolated trait or as part of Williams-Beuren syndrome [151], is characterized by aortic narrowing caused by the thickening of the media or intima layers of the arterial wall [152]. If left untreated, it can lead to complications such as increased blood pressure, myocardial hypertrophy and heart failure [153]. SVAS is associated with a number of point or translocation mutations in exons 8, 16, 18, 20, 21, 25, 26 of the elastin gene [15, 151, 153-157]. These mutations often prematurely truncate the reading frame and lead to nonsense-mediated decay of the mutant transcript [152, 158]. Accordingly, a decreased level of tropoelastin expression has been reported in skin fibroblasts and smooth muscle cells of SVAS patients [159]. This supports elastin haploinsufficiency as the underlying pathomechanism of the disease [152, 158, 160, 161].

In some cases of SVAS where the mutated tropoelastin is secreted at normal levels, the monomer assembles poorly into elastic fibres despite the ability to interact with microfibrillar components [103]. The mutant isoform, which lacks domains 16-17, displays impaired coacervation and forms atypical fibrils upon aggregation. Similarly, two other truncated tropoelastin mutants associated with SVAS do not coacervate at physiological temperatures, which precludes their participation in fibre assembly and mimics a hemizygous disorder where only products from one allele are functional [153].

Cutis laxa is another elastin-linked disease which comprises a heterogeneous spectrum of acquired and inherited conditions characterised by loose, sagging skin and a

wide range of clinical symptoms [162]. Autosomal dominant cutis laxa (ADCL) presents with redundant skin folds resulting in a prematurely aged appearance, typically with no severe effects on internal organs and neurodevelopment [163, 164]. Unlike SVAS mutations which usually occur in the 5′ and central regions of the elastin gene, ADCL arises from missense or frameshift mutations in the 3′ end, specifically in exons 25, 30, 32 and 33 [15, 43, 162, 165]. These changes are predicted to enable protein translation to proceed into the 3′ untranslated region, resulting in an extended C-terminal missense sequence [166-170]. ADCL-associated tropoelastin has a higher propensity for aggregation, leading to enhanced globule formation in the extracellular space [162]. Consistent with the role of the C-terminus in microfibrillar protein binding, it is poorly deposited onto microfibrils and forms fewer, fragmented and disorganised elastic fibres [159, 162]. The abnormal packing of fibres is also proposed to affect cross-link formation [168], which may deleteriously affect the strength and elasticity of connective tissues [167].

Autosomal recessive cutis laxa (ARCL) is often more severe, and is characterised by vascular abnormalities, pulmonary emphysema, developmental delay, or skeletal defects [35, 132]. Although ARCL commonly arises from mutations in elastogenic proteins other than tropoelastin, such as fibulin-4 and fibulin-5 [132, 171], it has recently also been attributed to a non-conservative substitution in tropoelastin domain 12 [35]. On the other hand, acquired cutis laxa has been linked to missense mutations in exon 4 and 36 [172]. The C-terminal mutation, in particular, introduces additional proteolytic cleavage sites in tropoelastin that renders the protein more susceptible to degradation [166].

However, not all mutations in the elastin gene are associated with diseases. Such sequence variations are typically single nucleotide polymorphisms (SNPs), in contrast to the broader truncation or frameshift mutations previously described. Currently, 110 SNPs have been identified in the human *ELN*, the majority of which are located in introns [55]. Out of

24 exonic mutations, 17 result in non-synonymous substitutions in the amino acid sequence, of which 13 are non-conservative and occur throughout the molecule. Examples include the introduction of a proline in the tropoelastin signal peptide hypothesised to affect protein secretion; the addition of charged residues in conserved hydrophobic domains; the replacement of a cross-linking lysine with an arginine; and the placement of a charged residue in the C-terminus [55]. While these sequence polymorphisms are not currently linked to disease states, their introduction in elastin-like polypeptides and full-length tropoelastin affected the self-assembly and structural integrity of the constructs [55]. These findings confirm a tight correlation between sequence and function in tropoelastin, wherein even single tropoelastin mutations can impact the assembly and mechanical properties of the elastic matrix.

1.5 Project aims

This project identifies previously uncharacterised sites within tropoelastin, which are unique in their conservation among mammalian tropoelastin variants, or conversely, in their rare occurrence within the human tropoelastin sequence. The regions of interest include the highly-conserved, protease-susceptible R515 in domain 26; the only three negatively-charged tropoelastin residues, E345 in domain 19, E414 in domain 21, and D72 in domain 6; and the constitutively spliced domain 22. This study employs targeted mutagenesis of tropoelastin at these sites, and characterises the assembly and structural properties of the resulting mutant isoforms. These findings identify functionally important residues or regions within the tropoelastin molecule, and help improve current understanding of the sequence-structure-function relationship in tropoelastin.

The specific aims of the work described in this thesis are:

1) To express and purify tropoelastin constructs mutated at the site/s of interest
2) To explore the elastogenic potential of the constructs via independent assays that simulate *in vivo* tropoelastin self-assembly and cell interactions
3) To determine the ability of the constructs to form elastic fibres in a cellular environment
4) To characterise the structural features of the constructs
5) To clarify the potential roles of the identified sites in tropoelastin structure and function

2. General materials and methods

2.1 Materials

2.1.1 Reagents

The reagents and suppliers used in this work are listed in Table 2.1.

Table 2.1. List of reagents and suppliers.

Reagents	Supplier
Agar	Difco Laboratories, USA
Ammonium acetate (CH_3COONH_4)	Ajax Finechem Pty Ltd, Australia
Ampicillin	Sigma-Aldrich, USA
Anti-C-terminal peptide rabbit antibody	Biomatik, USA
Anti-elastin antibody (BA4)	Sigma-Aldrich, USA
Anti-mouse IgG conjugated with horseradish peroxidase	Sigma-Aldrich, USA
Anti-mouse IgG conjugated with FITC	Sigma-Aldrich, USA
Anti-rabbit IgG conjugated with horseradish peroxidase	Sigma-Aldrich, USA
Boric acid	ICN Biomedicals Inc., USA
Bovine serum albumin	Sigma-Aldrich, USA
Bromophenol blue	International Biotechnologies Inc., USA
Bis-(sulfosuccinimidyl)-suberate (BS3)	School of Chemistry, University of Sydney
Coomassie Blue G	Sigma-Aldrich, USA
Crystal violet	Sigma-Aldrich, USA
Deoxyribonuclease I	Sigma-Aldrich, USA
Disodium hydrogen phosphate (Na_2HPO_4)	Ajax Finechem Pty Ltd, Australia

Dulbecco's modified eagle medium	Sigma Aldrich, USA
Ethylenediaminetetraacetic acid	Sigma-Aldrich, USA
Ethidium bromide	International Biotechnologies Inc., USA
Foetal bovine serum	Life Technologies, USA
Glucose	Ajax Finechem Pty Ltd, Australia
Glycerol	ICN Biochemicals Inc., USA
Glycine	Ajax Finechem Pty Ltd, Australia
Isopropyl β-D-1-thiogalactopyranoside	Sigma-Aldrich, USA
L-glutamine	Sigma-Aldrich, USA
Lysozyme	Sigma-Aldrich, USA
Lys-C	Calbiochem, USA
Magnesium chloride ($MgCl_2$)	Ajax Finechem Pty Ltd, Australia
Magnesium sulfate ($MgSO_4$)	Ajax Finechem Pty Ltd, Australia
Mark12™ Unstained Standard	Life Technologies, USA
Mercaptoethanol	Sigma-Aldrich, USA
2-(N-morpholino)ethanesulfonic acid	Sigma-Aldrich, USA
Paraformaldehyde	Sigma-Aldrich, USA
Penicillin/streptomycin	Sigma-Aldrich, USA
Phenylmethylsulphonyl fluoride	Sigma-Aldrich, USA
Potassium chloride (KCl)	Ajax Finechem Pty Ltd., Australia
ProLong Gold anti-fade reagent with DAPI	Life Technologies, USA
SDS-PAGE gel, pre-cast	Life Technologies, USA
SDS-PAGE loading dye	Life Technologies, USA
SDS-PAGE running buffer	Life Technologies, USA

Sodium acetate (CH_3COONa)	Ajax Finechem Pty Ltd, Australia
Sodium chloride (NaCl)	Ajax Finechem Pty Ltd, Australia
Sodium dihydrogen phosphate 2-water ($NaH_2PO_4 \cdot 2H_2O$)	Ajax Finechem Pty Ltd, Australia
Sodium fluoride (NaF)	Ajax Finechem Pty Ltd, Australia
Sucrose	Ajax Finechem Pty Ltd, Australia
Tris(hydroxymethyl)aminomethane	Sigma-Aldrich, USA
Triton X-100	Sigma-Aldrich, USA
Trypsin-EDTA	Sigma-Aldrich, USA
Tryptone	Becton-Dickinson, USA
Yeast extract	Becton-Dickinson, USA

2.1.2 Solutions

The solutions used in this study are listed in Table 2.2.

Table 2.2. List of solutions and solution components.

Solution	Components
2TY-ampicillin	1.6% (w/v) tryptone, 1% (w/v) yeast extract, 0.5% (w/v) NaCl, 50 μg/mL ampicillin
ABTS solution	1.04 mg/mL ABTS, 0.05% (v/v) H_2O_2, 10 mM CH_3COONa, 5 mM Na_2HPO_4
Coomassie stain	0.125% (w/v) Coomassie Blue G, 45% (v/v) methanol, 10% (v/v) acetic acid
LB broth	1% (w/v) tryptone, 0.5% (w/v) yeast extract, 1% (w/v) NaCl, 2% (w/v) glucose
LB-ampicillin agar	1% (w/v) tryptone, 0.5% (w/v) yeast extract, 1% (w/v) NaCl, 1.5% (w/v) agar, 100 μg/mL ampicillin
Lysis buffer	50 mM Tris, 1 mM EDTA, 100 mM NaCl
PB	7.76 mM Na_2HPO_4, 2.24 mM $NaH_2PO_4 \cdot 2H_2O$
PBS	7.76 mM Na_2HPO_4, 2.24 mM $NaH_2PO_4 \cdot 2H_2O$, 150 mM NaCl, pH 7.4
SOC	2% (w/v) tryptone, 0.5% (w/v) yeast extract, 10 mM NaCl, 2.5 mM KCl, 10 mM $MgCl_2$, 10 mM $MgSO_4$, 20 mM glucose

2.2 Methods

2.2.1 Bioinformatics analysis of tropoelastin sequences

Mammalian tropoelastin sequences were aligned with the ClustalW 2.0 online program (http://www.ebi.ac.uk/Tools/msa/clustalw2/) using default parameters.

2.2.2 Production of tropoelastin constructs

Recombinant wild-type human tropoelastin (WT) corresponding to amino acid residues 27–724 of GenBank entry AAC98394 was produced in-lab via a large-scale high cell density fermentation process and purified as previously described [26, 153]. Mutant tropoelastin constructs were produced using a small-scale expression system described below.

2.2.2.1 Mutagenesis of tropoelastin sequence

Purified pET-3d plasmid containing the WT tropoelastin sequence was sent to Genscript, USA for site-directed mutagenesis.

2.2.2.2 Bacterial transformation

The pET-3d plasmid construct containing the mutant tropoelastin sequence was added to electrocompetent *E. coli* BL21 cells (2.5 ng DNA/μL cells). Electroporation was performed on a Micropulser™ Electroporation Apparatus according to the protocol supplied by Bio-Rad. Electroporated cells were recovered in SOC medium and incubated at 37˚C for 1 hr with agitation. Cultures were plated on LB-ampicillin agar and incubated at 37˚C overnight. Transformed colonies were identified by growth on the selective medium.

2.2.2.3 Extraction of plasmid DNA

Transformed colonies were used to inoculate LB broth containing 100 μg/mL ampicillin and cultured overnight at 37˚C. Plasmid DNA was extracted using the QIAGEN® QIAprep Spin Miniprep Kit. DNA yield and purity were estimated using a NanoDrop™ spectrophotometer.

2.2.2.4 Sequencing of plasmid DNA

The extracted plasmid DNA was sequenced to confirm that the insert carried the correct mutation/s at the nucleotide level. Plasmid DNA (100 ng/μL) was mixed with 0.8 pmol/μL sequencing primer (Table 2.3). Sequencing was carried out by the Australian Genome Research Facility.

Table 2.3. List of sequencing primers used in this study. The sequence, length and melting temperature of each primer are indicated.

Primer	Sequence (5'-3')	Length (bases)	Tm (°C)
pNeoSeqFor	AAGGCTAGAGTACTTAATACGA	22	65.7
pNeoSeqRev	CTCATCAATGTATCTTATCATG	22	63.9
pNeoSeqMid	AAGGCAGCAGCAAAATTCGG	20	68.3
pNeoSeqMid2	CGGGTGCAGGTGTAAAACC	19	59.5
pNeoSeqMid3	TACCCAGGCGCGGGTCTGGGT	21	77.3
pNeoSeqMid4	GTTTCGGCGTTGGTGTTGGTGG	22	65.8

2.2.2.5 Glycerol storage of transformants

An overnight culture of transformed *E. coli* was mixed with 15% (v/v) sterile glycerol, frozen rapidly in liquid nitrogen, and stored at –80˚C.

2.2.2.6 Tropoelastin expression

Transformants from glycerol stocks were streaked on LB-ampicillin agar plates and incubated overnight at 37˚C. To prepare starter cultures, a single colony from each plate was grown overnight at 37˚C in LB broth containing 50 μg/mL ampicillin. Starter culture (5% (v/v)) was added to 2TY-ampicillin medium and incubated at 37˚C and 260 rpm for ~1.5 hrs until the absorbance at 600 nm reached 0.8. Protein expression was then induced with 1 mM IPTG for 2 hrs.

2.2.2.7 Tropoelastin purification

Bacterial culture was pelleted at 10,000 rpm for 10 min at 4˚C and lysed in 10 volumes of chilled lysis buffer containing 0.1% (w/v) lysozyme and 1 mM PMSF in isopropanol. The cell suspension was divided into ~5 mL aliquots and freeze-thawed five times until highly viscous. Aliquots were pooled and mixed with 10 mM $MgCl_2$, 10 mg/mL deoxyribonuclease and 1 mM PMSF at 4˚C for 45 min until viscosity was reduced. This allowed degradation of DNA while inhibiting proteolysis of the tropoelastin species. To remove cell debris, the cell suspension was centrifuged at 15,000 rpm for 20 min at 4˚C. The supernatant was progressively mixed with 1.5 volumes of n-propanol and 2.5 volumes of n-butanol over a 5-hr period for the selective solubilisation of tropoelastin overnight at 4˚C. The mixture was centrifuged at 12,000 rpm for 10 min at 4˚C, and the solubilised tropoelastin was recovered via rotary evaporation at 60˚C and 25 mbar. The residue was washed overnight with chloroform, air-dried and dissolved in 50 mM ammonium acetate, pH 5.0. The tropoelastin solution was dialysed with SnakeSkin® 10 kDa-cutoff pleated dialysis tubing against 50 mM ammonium acetate at 4˚C for 2 days, then further purified via centrifugation at 5,000 rpm for 5 min. Finally, the supernatant was lyophilised to obtain dry, purified tropoelastin.

2.2.3 Confirmation of purified tropoelastin

2.2.3.1 Sodium dodecyl sulfate polyacrylamide gel electrophoresis (SDS-PAGE)

Purified tropoelastin was analysed via SDS-PAGE to estimate the molecular weight and extent of degradation. Samples were mixed with 1x SDS-PAGE loading dye and denatured at 70 ˚C for 10 min, then loaded into a NuPAGE® 4-12% Bis-Tris gel with Mark12™ Unstained Standards. Electrophoresis was performed in SDS-PAGE running buffer at 200 V until the marker dye was ~1 cm from the base of the gel. The gel was fixed in 50% (v/v) methanol for 1 hr, stained with Coomassie stain solution overnight, and destained with 25% (v/v) methanol and 10% (v/v) acetic acid for 5 hrs.

2.2.3.2 Mass spectrometry

WT and mutant tropoelastin constructs were dissolved to 5 mg/mL in water and digested with 0.05 mg/mL excision grade Lys-C at 25˚C overnight. The samples were then subjected to comparative matrix-assisted laser desorption ionization time-of-flight (MALDI-TOF) mass spectrometry using a QSTAR XL mass spectrometer with the assistance of Dr. Steven Wise (Weiss Lab, School of Molecular Bioscience). A mass/charge window of 800-5000 was applied and the resulting peaks were assigned by comparison with expected monoisotopic peptide masses from a theoretical Lys-C digest. These theoretical mass values, obtained using PeptideMass (http://au.expasy.org/tools/peptide-mass.html), were of singly-charged peptides ($[M+H]^+$) containing up to one missed cleavage. The mass peaks from the WT and mutant tropoelastin samples were then overlaid and peptide mass shifts corresponding to the mutation were identified.

2.2.4 Coacervation

2.2.4.1 Light spectrophotometry

Tropoelastin constructs dissolved in PBS to 10 mg/mL were placed in quartz cuvettes and monitored in a Shimadzu UV-1601 spectrophotometer heated to a set temperature by a Julabo F4 recirculation waterbath. Light scattering was examined by measuring the absorbance at 300 nm over 600 s at temperatures from 20 to 60˚C. Between each temperature shift, the sample was cooled at 4˚C until turbidity was visibly reduced. The tropoelastin species were assessed according to the time taken to reach maximum turbidity at each temperature, as well as the temperature at which maximum sample turbidity was attained.

2.2.4.2 Particle size analysis

The particle sizes of tropoelastin solutions over a temperature range of 20 to 60˚C were determined via dynamic light scattering using a Malvern Zetasizer Nano (Malvern Instruments, UK). Solutions of 10 mg/mL tropoelastin were equilibrated for 5 min at the set temperature. Three runs of measurements, each with at least 12 data acquisitions, were taken and averaged to obtain the relative percentages of particle sizes present in each tropoelastin solution.

2.2.5 Cross-linking

2.2.5.1 Construction of hydrogels

Tropoelastin constructs were dissolved in PBS to 100 mg/mL at 4 ˚C overnight. The solutions were mixed with BS3 at 4˚C to a final concentration of 10 mM, and 200 μL aliquots were transferred to LabTek® Chamber Slides™. The tropoelastin solutions were cross-linked at 37˚C for 16 hrs, then washed in PB and lyophilised. The extent of tropoelastin cross-linking was estimated by SDS-PAGE analysis of the aqueous solutions left after hydrogel formation.

2.2.5.2 Swelling of hydrogels

Triplicate freeze-dried and pre-weighed hydrogels were swelled in MQW for 24 hrs at 37˚C, 25˚C and 4˚C. Between each temperature shift, excess water was removed and the hydrogels were weighed. At each temperature, the amount of liquid absorbed per gram of hydrogel was recorded.

2.2.5.3 Micro-computed tomography (Micro-CT)

The three-dimensional x-ray structures of freeze-dried hydrogels were determined with a SkyScan 1072 micro-computed tomography system at the Australian Centre for Microscopy and Microanalysis. Each hydrogel was scanned with a 60 kV x-ray beam at a resolution of 3.23 μm. The resulting x-ray projection images were converted into a stack of cross-sections with the cone-beam reconstruction program NRecon 1.4.4. (SkyScan, Belgium) and rendered into a three-dimensional structure with VGStudio Max 1.2.1 (Volume Graphics GmbH, Germany). Images of the 3D structures, as well as horizontal and vertical sections, were taken with the same software. Hydrogel porosity was estimated from the cross-section images using the CTan program (SkyScan, Belgium).

2.2.5.4 Scanning electron microscopy (SEM)

Water-swollen hydrogels were lyophilised, mounted using carbon tape and conductive Silver DAG, and coated with ~20 nm gold. Sample imaging was performed at different magnifications using the Zeiss EVO / Qemscan electron microscope at the Australian Centre for Microscopy and Microanalysis.

2.2.6 Cell attachment assay

Triplicate cell culture wells were coated with 1.25, 2.5, 5, 10, 20 or 30 μg/mL of each tropoelastin construct at 4˚C overnight. After incubation, wells were washed three times with PBS to remove unbound tropoelastin. BSA (10 mg/mL in PBS) was denatured at 80˚C for 10 min then cooled on ice to prevent renaturation. Non-specific binding to wells was blocked with the denatured BSA for 1 hr at room temperature.

GM3348 fibroblast cells grown in DMEM with 10% (v/v) foetal bovine serum were trypsinised with trypsin-EDTA at 37˚C for 2 min. The cells were centrifuged at 800 g for 4 min and resuspended in serum-free DMEM. The blocked wells were washed three times in PBS and seeded with 1.56 x 10^5 cells/cm^2 well surface. To estimate the percentage of cell attachment, cells were diluted in DMEM to 10%, 20%, 50%, 80% and 100% of the cell density used for the experimental wells and added to uncoated and unblocked wells. Cells were allowed to attach at 37˚C in 5% CO_2 for 1.5 hrs. After incubation, non-adherent cells in the experimental wells were removed with two PBS washes. Adherent cells and cells in the standard wells were fixed with 3% (w/v) formaldehyde in PBS for 20 min. All wells were washed three times with PBS and the fixed cells were stained with 0.1% (w/v) crystal violet in 0.2 M MES, pH 5.0 at room temperature for 1 hr. Excess stain was removed with four washes of reverse osmosis water, and the crystal violet was solubilised with 10% (w/v) acetic acid. Absorbance was measured at 570 nm using a plate reader. Absorbance readings from the standard wells were fitted to a linear regression, which was used to convert experimental absorbances into percentage of cell attachment.

2.2.7 Enzyme-linked immunosorbent assay (ELISA)

2.2.7.1 With BA4 anti-elastin antibody

The amount of tropoelastin bound to cell culture wells after overnight coating was determined. Triplicate wells were coated with 1.25, 2.5, 5, 10, 20 or 30 μg/mL of tropoelastin at 4˚C overnight. Unbound tropoelastin was removed with three PBS washes and non-specific antibody binding was blocked with 3% (w/v) BSA for 1 hr at room temperature. Excess BSA was washed off with PBS and the bound tropoelastin was detected with 1:2000 dilution of mouse anti-elastin BA4 antibody for 1 hr at room temperature. Wells were washed thrice with PBS and incubated with 1:5000 dilution of goat anti-mouse IgG conjugated with horseradish peroxidase. Unbound secondary antibody was removed with three PBS washes while the bound species was visualised by incubation with ABTS solution at 37˚C for 1 hr. Sample absorbances at 405 nm were read with a plate reader, and subtracted by the absorbance of BSA-blocked wells without tropoelastin.

2.2.7.2 With anti-domain 6 antibody

To determine the accessibility of the N-terminal domain 6 on surface-coated tropoelastin species, an ELISA was performed following the protocol previously described. A 1:5000 dilution of mouse anti-domain 6 antibody and a 1:5000 dilution of goat anti-mouse horseradish peroxidase-conjugated IgG were used as the primary and secondary antibody, respectively.

2.2.7.3 With anti-C-terminus antibody

To compare the exposure of the C-terminus on surface-coated tropoelastin constructs, another ELISA was performed as described. A 1:5000 dilution of rabbit anti-C-terminal

peptide antibody and a 1:5000 dilution of goat anti-rabbit horseradish peroxidase-conjugated IgG were used as the primary and secondary antibody, respectively.

2.2.8 Immunofluorescent staining of elastin fibers

2.2.8.1 Cell culture

Human dermal fibroblasts (GM3348; obtained from the Coriell Research Institute, Camden, NJ) were cultured in DMEM supplemented with 10% (v/v) fetal bovine serum and 1% (v/v) penicillin/streptomycin. Human retinal pigmented epithelium cells (ARPE-19; obtained from Dr. M. Madigan, Save Sight Institute, NSW, Australia) were cultured in DMEM:Nutrient mixture F12 supplemented with 10% (v/v) fetal bovine serum, 2 mM L-glutamine and 1% (v/v) penicillin/streptomycin.

2.2.8.2 Sample preparation

GM3348 and ARPE-19 cells were seeded on glass coverslips at a density of 18,400 cells/cm^2. At 10 and 14 days post-seeding, respectively, 20 or 200 μg/mL tropoelastin was added to culture medium. At 1, 4, 7 and 10 days after tropoelastin addition, cells were fixed with 4% (w/v) paraformaldehyde for 20 min and quenched with 0.2 M glycine. The cells were incubated with 0.2% (v/v) Triton X-100 for 6 min, blocked with 5% bovine serum albumin at 4 °C overnight, and stained with 1:500 mouse anti-elastin BA4 antibody for 1.5 hr and 1:100 FITC-conjugated anti-mouse IgG antibody for 1 hr. The coverslips were then mounted onto glass slides with ProLong Gold anti-fade reagent with DAPI.

2.2.8.3 Confocal microscopy

Slides from each elastogenic time point were visualized with an Olympus FluoView FV1000 confocal microscope under identical laser settings. Z-stacks were taken from areas distributed across each sample and converted to maximum projection images.

2.2.8.4 Analysis of elastic fibres

Confocal images of elastic fibres were analyzed using ImageJ (http://rsbweb.nih.gov/ij/). To compare fibre fluorescence, a threshold was set to exclude background and saturated pixel intensities. The average intensity of pixels within this threshold was measured for each projection image and averaged for each sample. To compare fibre number, two perpendicular reference lines were drawn in each projection image. The number of fibers intersecting either reference line was counted and averaged for each sample. Fibre width was measured and averaged from a total of ~150 randomly selected sections of elastic fibres. Fibre area was measured by the percentage of fluorescent pixels over the total number pixels per image, then averaged for each sample. The area occupied by cell nuclei was used as a control indicative of cell number and viability in all samples.

2.2.9 Far-UV circular dichroism (CD)

Tropoelastin constructs were dissolved to 0.15 mg/mL in 10 mM phosphate and 150 mM NaF. CD spectra were recorded on a Jasco J-815 spectrometer equipped with a Peltier-controlled sample chamber. Samples were scanned with a band width of 1.0 nm at 20 nm/min. Each spectrum was averaged from five scans, buffer-corrected, and smoothed using 3 point adjacent averaging. Secondary structure composition was estimated from the CD spectrum using the CONTINLL and CDSSTR methods [173] with a reference set of 37 soluble proteins.

2.2.10 Small angle x-ray scattering (SAXS)

Tropoelastin constructs dissolved in PBS were mixed with 2 mM dithiothreitol. SAXS data were collected on the European Molecular Biology Laboratory beamline X33 at the DORISIII light source facilities at Hamburger Synchrotronstrahlungslabor/Deutsches Elektronen-Synchrotron (HASYLAB/DESY). Data were acquired using 4 x 30 sec exposures and a 2.4 meter sample-to-detector distance to cover a momentum transfer interval $0.008 < q < 0.54$ Å $^{-1}$. The modulus of the momentum transfer is defined as $q = 4\pi\sin\theta/\lambda$, where 2θ is the scattering angle, and λ is the wavelength. The q range was calibrated using silver behenate powder based on diffraction spacings of 58.38Å. The scattering images obtained were spherically averaged using in-house software and buffer scattering intensities subtracted using PRIMUS [174]. Particle shapes were generated *ab initio* using GASBOR [175]. Multiple GASBOR runs were performed to generate 10 similar shapes that were combined and filtered to produce an averaged model using the DAMAVER software package [176].

2.2.11 Statistical analyses

All data were reported as mean ± standard error. One- or two-way analysis of variance and Bonferroni post-test were performed using GraphPad Prism version 5.5 for Windows (GraphPad Software, CA). Statistical significance was set at $p<0.05$ or higher, and indicated in the figures as * ($p<0.05$), ** ($p<0.01$) or *** ($p<0.001$).

3. *In vitro* elastic fibre assembly of WT and R515A tropoelastin

3.1 Introduction

3.1.1 The tropoelastin bridge region

Comparative analyses of the nanostructures of tropoelastin species truncated at different lengths from the N-terminus have enabled the mapping of functional regions of tropoelastin to spatial locations within the molecule [72]. Most of the elasticity of the molecule has been proposed to be conferred by the coiled region [177] that extends from the N-terminus to domain 18. A protrusion from the coil region formed by domains 20-24 corresponds to a predicted hinge region [73, 178]. The hinge region then leads to a bridge region that most likely encompasses domains 25-26. The tropoelastin molecule terminates in a foot-like region containing the cell-interactive C-terminus [179].

Unlike the N-terminal elastic spiral and C-terminal cell-interactive foot regions of tropoelastin, little has been described about the functional role of the bridge region. One model proposes that the bridge region may be involved in elastic fibre assembly, as it includes domain 26 which is essential for coacervation, and lies near other large central hydrophobic domains implicated in the process [70, 108]. The bridge region also either partially encompasses or resides proximally to domains 19-25 which dominate inter-molecular cross-linking to form elastin [44, 105, 143]. Structurally, the bridge region directly leads from a region of high flexibility [178] and may therefore contribute to the extensive conformational changes associated with monomer alignment and organisation during elastin assembly [67].

3.1.2 The arginine 515 site

The tropoelastin bridge region contains an arginine 515 (R515) residue at the junction of domains 25 and 26 [70], which is highly conserved within various mammalian tropoelastin sequences (Table 3.1). Interestingly, the R515 site is solvent-exposed, and susceptible to cleavage by a number of serine proteases including kallikrein, thrombin and plasmin [70].

The evolutionary preservation of such a hypersensitive proteolytic cleavage site in tropoelastin implies a significant role in protein function. It has been proposed that specific cleavage of tropoelastin may occur during tissue injury or inflammation to induce cell migratory and chemotactic responses for wound repair [120, 149, 180]. Cleaved tropoelastin peptides may also be a means of regulating tropoelastin expression and synthesis [181, 182]. The significance of the R515 residue may also be unrelated to its protease susceptibility. R515 may modulate important functions associated with the tropoelastin bridge region during elastin assembly, which may account for the selective retention of this potentially disadvantageous proteolytic cleavage site within tropoelastin.

Table 3.1. Alignment of domains 25-26 of various mammalian tropoelastin sequences, partially adapted from Piontkivska et al. (2004) [183]. The human, cow, mouse and rat sequences were obtained from GenBank, while the cat, dog, baboon and chimpanzee sequences were predicted from genomic sequences based on homology with the human sequence. The corresponding arginine 515 site in all sequences are indicated in bold type.

Mouse	GAGSPAAAKSAAKAAAKAQY**R**AAAGLGAGVPGFGAGAGVPGFGAGAGVPGFGAGAGVPGFGAGAGVPGFGAGA
Rat	GAGTPAAAKSAAKAAAKAQY**R**AAAGLGAGVPGLGVGAGVPGFGAGAG----GFGAGAGVPGFGAGA----------
Cat	RVGTPAAAKAAAKAAAKAQY**R**AAAGLPAGVPGFGVGAGVPGFGVGAGVPGFGAGVGVPGFGAGA----------
Dog	GVGTPAAAKAAAKAAAKAQY**R**AAAGLPAGVPGFGVGAGVPGFGVGAGIPGFGVGAGVPGFGAGA----------
Cow	GAGVPAAAKSAAKAAAKAQF**R**AAAGLPAGVPGLGVGVGVPGLGVGVGVPGLGVGAGVPGLGA----------
Baboon	GVGAPEAAKSAAKAAAKAQL**R**AAAGLGA--VPGLGVGA--VPGLGVGVGVPGLGVGAGVPGFGAGA----------
Chimpanzee	----------AAAKSAAKVAAKAQL**R**AAAGLGAGIPGLGVGVGVPGLGVGAGVPGLGVGAGVPGFGA----------
Human	----------AAAKSAAKVAAKAQL**R**AAAGLGAGIPGLGVGVGVPGLGVGAGVPGLGVGAGVPGFGA----------

3.1.3 Consequences of an R515A mutation in tropoelastin

Previous work has characterised a protease-resistant tropoelastin construct in which the bridge region was disrupted by substituting the R515 residue with an alanine (R515A) (Figure 3.1). When compared to mature, full-length human tropoelastin (WT), the R515A mutant displayed impaired or atypical behaviour at each stage of elastogenesis [184].

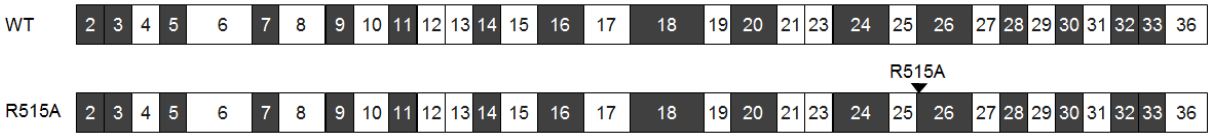

Figure 3.1. Domain structures of WT and R515A tropoelastin constructs. Hydrophobic domains are represented by black boxes, while hydrophilic domains are shown as white boxes. At the 515 site, WT has an arginine residue while R515A has an alanine.

3.1.3.1 Impaired coacervation

R515A tropoelastin possessed greater thermal and temporal requirements for coacervation [184]. Maximum coacervation was achieved at a higher temperature of 40 °C and after a ~30% longer time course compared to WT.

Classically, the number of hydrophobic domains determines the critical temperature [185] and rate [70] of coacervation, but this model does not explain the difference between WT and R515A. The unexpected increase in R515A coacervation temperature conceptually reflects a higher energy requirement for the disruption of bound water and therefore indicates an increase in protein hydration [185, 186] most likely due to a structural deviation from wild-type tropoelastin. The increase in R515A coacervation time also supports a model of a conformational change that affects its ability to associate through either steric hindrance and/or altered relative positions of associating hydrophobic domains.

As coacervation represents the crucial first step that determines the subsequent incorporation of tropoelastin monomers into the elastic fibre [187], the decreased propensity of R515A for self-association may affect its potential for elastogenesis.

3.1.3.2 Abnormal hydrogel formation

Chemical cross-linking of R515A with the amine-reactive bis-sulfosuccinimidyl suberate (BS3), which approximates *in vivo* lysyl oxidase-mediated crosslinking [143], produced hydrogels with obvious morphological differences to the WT constructs [184]. The WT hydrogel consisted of overlapping fibres interspersed with large channels, consistent with the filamentous nature of natural elastin [8, 13]. In contrast, the R515A hydrogels were less porous and composed wholly of compact spherules similar in size to partially cross-linked nascent elastin [11, 94].

The low porosity of R515A hydrogels was coupled with a significantly reduced water uptake compared to the WT constructs. Since the extent of solvent influx in hydrogels is defined by the junctions of the polymer network [188, 189], the decreased swelling of R515A hydrogels suggests atypical cross-linking [190, 191].

The cross-linking of tropoelastin strongly corresponds to its ability to assemble into stable, insoluble elastic fibres [102]. The inability of R515A to form mature cross-linked structures may likewise impact upon its elastogenic capacity.

3.1.3.3 Decreased fibroblast attachment

R515A tropoelastin supported significantly reduced adhesion to human dermal fibroblasts [184], consistent with the decreased exposure of its C-terminal cell-binding motif [179]. In an elastogenic context, tropoelastin-cell interactions are important. During the *in*

vivo coacervation process, weak cell adhesion may lead to the detachment of tropoelastin monomers from the cell surface and therefore preclude incorporation into elastic fibres [18]. Signalling between cells and tropoelastin molecules has also been proposed to be crucial for cell anchorage of the elastic network [179], maintenance of the elastic fibre architecture [3, 6, 94, 172], and regulation of cellular activity [45]. The decreased cell binding ability of R515A may therefore affect its propensity for elastic fibre formation as well as the organisation and stability of the formed fibres.

3.1.3.4 Structural distortion in the bridge and C-terminal regions

The solution structure of R515A, solved by SAXS, revealed greater conformational variability around the bridge and C-terminal regions compared to WT [184]. The structural flexibility adopted by the R515A bridge and C-terminal regions resulted in an averaged shape that exhibited substantial dislocation of the C-terminal foot towards the central axis of the molecule (Figure 3.2). This altered structure may lead to the masking of functionally important domains and contribute to steric hindrances during elastin assembly, which are likely to influence the elastogenic capability of R515A.

SAXS has a resolution limit of ~1.5 nm. In this and subsequent chapters, slight shape changes between the WT models can be attributed to the resolution limit of the technique.

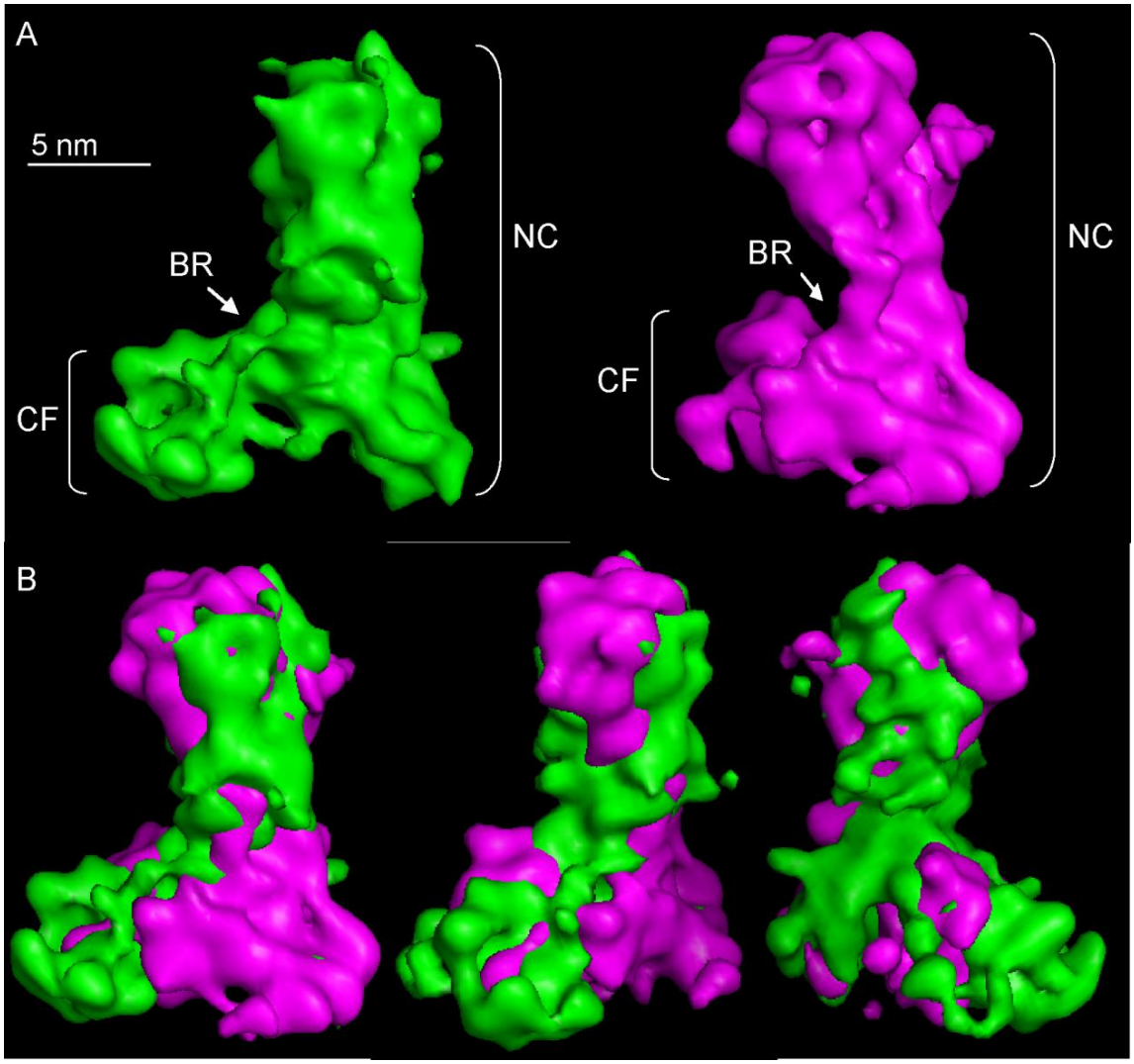

Figure 3.2. (A) Solution structures of WT (green) and R515A (purple) tropoelastin from SAXS [184]. The elastic N-terminal coil region (NC), bridge region (BR) and cell-interactive C-terminal foot region (CF) are indicated. (B) Superimposition of the WT and R515A models illustrates a conformational difference in the R515A bridge and C-terminal regions.

3.1.4 Models of elastic fibre assembly

Early studies modelling elastic fibre assembly utilised the intrinsic ability of elastogenic cells such as aortic smooth muscle cells [192], vascular endothelial cells [193], dermal fibroblasts [194] and auricular chondroblasts [195, 196] to synthesise and assemble elastin *in vitro*. However, the unstable elastogenic phenotype of these cultured cells proved unconducive for longer term studies, as levels of tropoelastin expression decreased with serial passaging [197].

More recently, pigmented epithelial cells obtained from the ciliary body or retina of the eye have been selected as a model system for elastic fibre assembly. The ciliary body pigmented epithelium directly contacts the microfibril-rich connective tissue matrix of the ciliary body [198]. It is continuous with the retinal pigmented epithelium, which likewise rests against a basement membrane that contains matrix proteins including elastic fibre components [199, 200]. Accordingly, pigmented epithelial cells have been shown to produce major elastogenic components including microfibrillar proteins and lysyl oxidase, but not tropoelastin [140, 201]. They therefore represent an ideal model system for assaying the elastogenic capability of tropoelastin species.

Constitutive tropoelastin expression can be initiated in pigmented epithelial cells via stable transfection of the tropoelastin cDNA into the genome. Immortalised ciliary body pigmented epithelial cells transfected with bovine tropoelastin cDNA have been shown to assemble the secreted tropoelastin into elastic fibres [201]. While variations in transfection efficiency may affect tropoelastin expression levels and therefore limit the quantification of assembled fibres [140], this approach still serves as a powerful means of simulating the *in vivo* elastogenic process of WT and mutant tropoelastin constructs.

Another method for studying elastic fibre assembly relies on the direct addition of purified tropoelastin to the culture medium. Previous studies have demonstrated successful

incorporation of exogenous tropoelastin into an elastic fibre network by non-elastogenic cells [202, 203]. Similarly, recombinant human and bovine tropoelastin added to the extracellular environment of retinal pigmented epithelial cells were shown to be assembled into elastic fibres [140]. This model represents a convenient method to study the elastic fibre formation of wild-type or modified tropoelastin molecules.

3.1.5 Aims

This chapter aims to establish a cellular system for assessing the elastogenic potential of WT and R515A tropoelastin constructs. Comparative analysis of WT and R515A elastic fibres will determine if the observed structural deviation and functional impairment of R515A in independent assays modelling various stages of assembly impacts upon its ability to form normal elastic fibres in a cellular environment. These results will improve our understanding of the role of the tropoelastin bridge region in elastic fibre assembly.

3.2 Materials and Methods

3.2.1 Materials

Chemical reagents are listed in Table 3.2. Solutions and solution components are outlined in Table 3.3 General reagents and solutions not specific to this set of work are described in Section 2.1.

Table 3.2. Reagents and suppliers of reagents used in this study.

Reagent	Supplier
1 kb DNA ladder	New England Biolabs, USA
100 bp DNA ladder	New England Biolabs, USA
Ab21610 rabbit anti-elastin antibody	Abcam, USA
BA4 mouse anti-elastin antibody	Sigma Aldrich, USA
BamHI	New England Biolabs, USA
BSA	Sigma Aldrich, USA
DEPC	Sigma Aldrich, USA
DMEM	Sigma Aldrich, USA
DMEM/F12	Sigma Aldrich, USA
DMSO	Sigma Aldrich, USA
DNA polymerase I Klenow fragment	New England Biolabs, USA
*Eco*RI	New England Biolabs, USA
FITC-conjugated anti-mouse antibody	Sigma Aldrich, USA
Foetal bovine serum	Life Technologies, USA
GlutaMAX™	Life Technologies, USA
Lipofectamine® LTX	Life Technologies, USA
MAB1919 mouse anti-fibrillin antibody	Millipore, USA

*Nco*I	New England Biolabs, USA
*Not*I	New England Biolabs, USA
Paraformaldehyde	Sigma Aldrich, USA
pCI-neo mammalian expression vector	Promega Corporation, USA
PLUS™ reagent	Life Technologies, USA
ProLong® Gold anti-fade reagent with DAPI	Life Technologies, USA
Rhodamine phalloidin	Life Technologies, USA
*Sma*I	New England Biolabs, USA
SYBR Green	Applied Biosystems, USA
T4 DNA ligase	New England Biolabs, USA
TRITC-conjugated anti-rabbit	Sigma Aldrich, USA
TRIzol®	Life Technologies, USA
*Xba*I	New England Biolabs, USA

Table 3.3. Solutions and solution components used in this study.

Solution	Components
Annealing buffer	10 mM Tris, 50 mM NaCl, 1 mM EDTA
DEPC-MQW	0.1% (v/v) DEPC in Milli-Q water
DNA loading dye	40% (w/v) sucrose, 0.25% (w/v) bromophenol blue
LB broth	1% (w/v) tryptone, 0.5% (w/v) yeast extract, 1% (w/v) NaCl
LB-ampicillin agar	1% (w/v) tryptone, 0.5% (w/v) yeast extract, 1% (w/v) NaCl, 1.5% (w/v) agar, 100 μg/mL ampicillin
LB-ampicillin broth	1% (w/v) tryptone, 0.5% (w/v) yeast extract, 1% (w/v) NaCl, 2% (w/v) glucose, 100 μg/mL ampicillin
PBS	10 mM phosphate, 150 mM NaCl
SOC	2% (w/v) tryptone, 0.5% (w/v) yeast extract, 10 mM NaCl, 2.5 mM KCl, 10 mM $MgCl_2$, 10 mM $MgSO_4$, 20 mM glucose
TBE	1.08% (w/v) Tris, 0.55% (w/v) boric acid, 2 mM EDTA

3.2.2 Methods

3.2.2.1 Bioinformatics analysis of WT/R515A expression in a human cell system

The likelihood that synthetic WT and R515A tropoelastin sequences could be expressed in human cells was determined using the online Rare Codon Analysis Tool (*www.genscript.com/cgi-bin/tools/rare_codon_analysis*). Specifically, the codon adaptation index, GC content adjustment, and codon frequency distribution of the tropoelastin constructs in a human expression host were assessed.

3.2.2.2 Extraction of the pET-3d-tropoelastin plasmid

Glycerol stocks of *Escherichia coli* BL21 transformed with pET-3d-WT or pET-3d-R515A were streak plated on Luria-Bertani (LB)-ampicillin agar and incubated at 37 °C overnight. LB broth was inoculated with a single colony from either plate and incubated in a shaking water bath at 37 °C overnight. Plasmid DNA was extracted from the bacterial cultures using the QIAGEN® QIAprep Spin Miniprep Kit. DNA yield and purity were estimated using a NanoDrop™ spectrophotometer.

3.2.2.3 Polymerase chain reaction (PCR) amplification of the tropoelastin insert

3.2.2.3.1 Design of PCR primers

Primers for polymerase chain reaction amplification of the tropoelastin sequence were designed to incorporate an *Eco*RI restriction site at the 5′ end and an *Xba*I restriction site at the 3′ end. Primers were checked for similar melting temperatures, potential dimerization and secondary structure formation using Oligonucleotide Primer Check (*http://depts.washington.edu/bakerpg/primertemp/primermelttemp.html*) and NetPrimer (*www.premierbiosoft.com/netprimer/index.html)*. The primers used are outlined in Table 3.4.

Table 3.4. Primers for polymerase chain reaction amplification of tropoelastin. The engineered restriction sites are underlined.

Primer	Sequence (5′ to 3′)	Tm (°C)
p*Eco*RIFor	GGAATTCATGGGTGGCGTTCCGGGT	58
p*Xba*IRev	GCTCTAGACTATCATTATTTACGTTTACGG	58

3.2.2.3.2 Polymerase chain reaction

Plasmid DNA (~200 ng) extracted from WT and R515A bacterial transformants was mixed with 1x AccuTaq buffer, 0.5 μL AccuTaq polymerase, 0.5 mM dATP, 0.5 mM dCTP, 0.5 mM dGTP, 0.5 mM dTTP, 0.4 nmol/mL p*Eco*RIFor, 0.4 nmol/mL p*Xba*IRev, and 2% (v/v) DMSO. A no-template control was included. PCR was performed using a GeneAmp PCR System 2400 following the protocol listed in Table 3.5.

Table 3.5. Running time and temperature of the PCR cycles.

Step	No. of cycles	Time (s)	Temperature (°C)
Initial denaturation	1	30	94
Denaturation	35	10	94
Annealing		30	55/60
Extension		180	68
Final extension	1	600	68

3.2.2.3.3 Gel electrophoresis of PCR products

PCR products were mixed with 10% (v/v) DNA loading dye and loaded onto a 1% (w/v) agarose gel together with a 1 kb DNA ladder. Electrophoresis was performed at 100 V for 1 hr in Tris/borate/EDTA (TBE) buffer. The gel was stained with 1 μg/mL ethidium

bromide for 25 min, destained with reverse osmosis water for 5 min, and viewed under UV transilluminescence.

3.2.2.3.4 Gel extraction of PCR-amplified tropoelastin sequences

Bands on the agarose gel corresponding to the expected size of the WT and R515A tropoelastin inserts were excised and processed according to the QIAGEN® QIAquick Gel Extraction Kit. The yield and purity of extracted DNA were confirmed with a NanoDrop™ Spectrophotometer.

3.2.2.4 Restriction digests of pCI-neo and tropoelastin sequences

3.2.2.4.1 With EcoRI and XbaI

The pCI-neo mammalian expression vector (60 ng/μL) and gel-extracted WT and R515A tropoelastin inserts (30 ng/μL) were digested with *Eco*RI (0.7 U/μL) and *Xba*I (0.7 U/μL) in 1x NEB Buffer 4 and 1x BSA for 1 hr at 37 °C. The restriction enzymes were heat inactivated at 65 °C for 20 min.

3.2.2.4.2 With SmaI

The pCI-neo expression vector was digested with *Sma*I (1 U/μL) in 10% (v/v) Roche Buffer A at 25 °C for 1 hr. To prevent spontaneous re-ligation, alkaline phosphatase (5% v/v) and alkaline phosphatase buffer (10% v/v) were added to the digest and incubated at 37 °C for 1 hr. The reaction was stopped at 65 °C for 20 min.

3.2.2.5 Gel extraction of digested pCI-neo and tropoelastin sequences

The digested pCI-neo and tropoelastin insert sequences were visualised via agarose gel electrophoresis and excised using a QIAGEN® QIAquick Gel Extraction Kit. DNA yield and purity were measured with a NanoDrop™ spectrophotometer.

3.2.2.6 Ligation of pCI-neo and tropoelastin sequences

3.2.2.6.1 Sticky-end ligation

Purified *Eco*RI- and *Xba*I-digested pCI-neo vector and tropoelastin sequences were mixed at a vector:insert ratio of 1:3, 1:5 or 1:10 and ligated with 40 U/μL T4 DNA ligase in 1x T4 buffer at 16 °C overnight. The ligase reaction was inactivated at 70 °C for 10 min.

3.2.2.6.2 Direct ligation

Purified *Sma*I-digested vector DNA was mixed with PCR-amplified WT or R515A sequence from Section 3.2.2.3.4 at a 1:5 molar ratio and ligated with 40 U/μL T4 DNA ligase in T4 buffer at 16 °C overnight. The ligase reaction was inactivated at 70 °C for 10 min.

3.2.2.6.3 Blunt-end ligation

WT and R515A insert sequences were obtained by digesting pET-3d-tropoelastin plasmid constructs from Section 3.2.2.2 with *Nco*I (1 U/μL) and *Bam*HI (1 U/μL) at 37 °C for 2 hrs. The digests were visualised by agarose gel electrophoresis and extracted similarly as described in Section 3.2.2.3.4. The insert sequences were end-filled by incubating with 33 μM each of dATP, dGTP, dCTP, dTTP, 6.8 U/μL DNA polymerase I Klenow fragment, and 10% (v/v) NEB Buffer 4 at 25 °C for 15 min. The reaction was stopped by adding 10 mM EDTA and heating to 75 °C for 20 min. The product was purified by ethanol precipitation.

Purified *Sma*I-digested vector DNA was mixed with the end-filled tropoelastin insert sequence at a 1:5 molar ratio and ligated with 40 U/μL T4 DNA ligase in T4 buffer at 16 °C overnight. The ligase reaction was inactivated at 70 °C for 10 min.

3.2.2.7 Linker cloning of tropoelastin insert sequences into pCI-neo

3.2.2.7.1 Linker construction

Custom-made single-stranded oligonucleotides described in Table 3.6 were dissolved in annealing buffer to equimolar concentrations. Equal volumes of the forward and reverse strands of each linker were mixed, incubated at 95 °C for 2 min, then allowed to cool to room temperature over 1 hr to form the double-stranded *Eco*RI-*Nco*I and *Bam*HI-*Xba*I linker constructs.

Table 3.6. Sequences of single-stranded oligonucleotides used in linker construction.

Linker	Strand	Sequence (5′-3′)
*Eco*RI-*Nco*I	Forward	AATTCCGGCGTCGACGTCCATGC
	Reverse	CATGGCATGGACGTCGACGCCGG
*Bam*HI-*Xba*I	Forward	GATCCCGAACTGCAGAACCGCT
	Reverse	CTAGAGCGGTTCTGCAGTTCGG

3.2.2.7.2 Ligation of pCI-neo, linker constructs and tropoelastin insert sequences

The *Eco*RI- and *Xba*I-digested pCI-neo expression vector (from Section 3.2.2.4.1) was mixed with the *Eco*RI-*Nco*I linker, the *Nco*I- and *Bam*HI-digested tropoelastin insert, and the *Bam*HI-*Xba*I linker in a 1:1:1:1 and 1:3:3:3 molar ratio. A four-way ligation was done with 40 U/μL T4 DNA ligase in T4 buffer at 16 °C overnight and terminated at 70 °C for 10 min.

3.2.2.8 Preparation of electrocompetent E. coli

A volume of LB broth was inoculated with a single colony of *E. coli* DH5α and incubated at 37 °C overnight. The overnight culture was used to inoculate 100 volumes of

LB broth and incubated at 37 °C until its absorbance at 600 nm reached 0.6. The culture was placed on ice for 20 min and centrifuged at 4000 g for 15 min at 4 °C. The supernatant was discarded and the pellet was resuspended in 25 volumes of cold 10% (v/v) glycerol. The mixture was centrifuged again at 4000 g for 15 min at 4 °C. The supernatant was discarded and the pellet was resuspended in 2 volumes of cold 10% (v/v) glycerol. The mixture was spun again at 4000 g for 15 min at 4 °C. The supernatant was discarded and the pellet was resuspended in 1/5 volume of cold 10% (v/v) glycerol. Aliquots (40 μL) of the electrocompetent bacteria were stored at -80 °C.

3.2.2.9 Transformation of E. coli

Competent *E. coli* cells were gently mixed with ligated pCI-neo-tropoelastin (2.5 ng DNA/μL cells) from Section 3.2.2.6 or 3.2.2.7 and incubated on ice for 1 min. Control samples were mixed with non-ligated vector and insert. Electroporation was performed using a Micropulser™ Electrporation Apparatus according to the protocol supplied. Electroporated cells were recovered in SOC medium and incubated at 37 °C for 1 hr. Cultures were plated on LB-ampicillin agar and incubated at 37 °C overnight. Transformed colonies were identified by growth on the selective medium.

3.2.2.10 Confirmation of transformed colonies

3.2.2.10.1 Extraction of the pCI-neo-tropoelastin expression vector

Plasmid DNA was extracted from randomly selected transformed colonies in Section 3.2.2.9 using the QIAGEN® QIAprep Spin Miniprep Kit. DNA yield and purity were estimated using a NanoDrop™ spectrophotometer.

3.2.2.10.2 Restriction analysis of the pCI-neo-tropoelastin expression vector

Extracted plasmid DNA was digested with either *Not*I (2 U/μL) or *Eco*RI (2 U/μL) and *Xba*I (2 U/μL) in 1x NEB Buffer 4 and 1x BSA for 1 hr at 37 °C. The digests were terminated by incubation at 65 °C for 20 min, then analysed via agarose gel electrophoresis following the same protocol described in Section 3.2.2.3.3.

3.2.2.10.3 Design of sequencing primers

Sequencing primers were designed to confirm the tropoelastin insert within the pCI-neo expression vector (Table 3.7). The pNeoSeqFor and pNeoSeqRev primers flank the *Eco*RI and *Xba*I cloning sites of the pCI-neo expression vector, while pNeoSeqMid anneals to a region within the insert.

Table 3.7. Primers used to sequence the insert between the *Eco*RI and *Xba*I cloning sites of the pCI-neo vector. The primer sequence, length and melting temperature are shown.

Primer	Sequence (5'-3')	Length (bases)	Tm (°C)
pNeoSeqFor	AAGGCTAGAGTACTTAATACGA	22	65.7
pNeoSeqRev	CTCATCAATGTATCTTATCATG	22	63.9
pNeoSeqMid	CGGGTGCAGGTGTAAAACC	19	59.5

3.2.2.10.4 Sequencing of the pCI-neo-tropoelastin expression vector

The vector construct extracted from transformants (100 ng//μL) was separately mixed with 0.8 pmol/μL sequencing primer and sent to the Australian Genome Research Facility for sequencing.

3.2.2.11 Cell culture

3.2.2.11.1 Human retinal pigmented epithelial cells (ARPE-19)

ARPE-19 cells (American Type Culture Collections) were obtained from Dr M. Madigan (Sydney Eye Hospital, NSW, Australia). The cells were cultured in DMEM/F12 nutrient medium supplemented with 10% (v/v) foetal bovine serum, 1% (v/v) GlutaMAX and 1% (v/v) penicillin/streptomycin.

3.2.2.11.2 Human dermal fibroblasts (GM3348)

GM3348 cells (Coriell Cell Repositories) were cultured in DMEM supplemented with 10% foetal bovine serum and 1% (v/v) penicillin/streptomycin.

3.2.2.11.3 Neonatal human fibroblasts (NHF8909)

NHF8909 cells were obtained from Dr X. Q. Wang (University of Queensland, QLD, Australia). The cells were cultured in DMEM supplemented with 10% foetal bovine serum and 1% (v/v) penicillin/streptomycin.

3.2.2.12 Testing for mycoplasma contamination in ARPE-19

Conditioned media from ARPE-19 cells was used to test for mycoplasma contamination using LookOut® Mycoplasma PCR Detection Kit (Sigma Aldrich).

3.2.2.13 Production of frozen cell stocks

Cells cultured until ~90% confluency were washed with PBS, trypsinised at 37 °C for 3 min, and dislodged by light tapping. The trypsin was then neutralised with 2.5 volumes of serum-containing culture media. Cells were pelleted at 800 g for 10 min and resuspended in fresh culture media. Approximately 10^6 cells were placed in each cryogenic vial and mixed with 10% (v/v) DMSO. The vials were placed in a rack submerged in isopropanol, incubated overnight at -80 °C, then stored in liquid nitrogen.

3.2.2.14 Transfection

3.2.2.14.1 Optimisation of the transfection protocol

The pCI-neo-WT vector was diluted in serum-free DMEM/F12 (10 μg/mL), mixed well with 1% (v/v) PLUS™ Reagent, and incubated at room temperature for 10 min. Lipofectamine® LTX Reagent was serially diluted in serum-free DMEM/F12 to a concentration range of 1 to 6% (v/v). An equal volume of the pCI-neo-WT:PLUS™ Reagent solution was then added and incubated at room temperature for 30 min to form stock transfection complexes with increasing ratios of vector DNA to lipid. Different volumes of each stock transfection complex were slowly added to wells containing ~70% confluent ARPE-19 cells to test the transfection efficacy of various amounts of vector DNA. The cells were cultured for another 24 hrs and assayed for WT tropoelastin expression.

3.2.2.14.2 Stable transfection

ARPE-19 cells were seeded onto cell culture wells at a density of 15,000 cells/cm^2. After 24 hrs, cells were confirmed to be between 50-80% confluent. Solutions of pCI-neo-WT, pCI-neo-R515A and the empty pCI-neo vector in serum-free DMEM/F12 (390 ng/cm^2 well surface) were mixed 1:1 with the PLUS Reagent and incubated at room temperature for 5 min. The vector DNA solutions were added 1:4 to Lipofectamine® LTX in serum-free DMEM/F12 and incubated at room temperature for 30 min. The ARPE-19 cells were then washed with PBS and provided with fresh medium. The DNA-Lipofectamine® complex was added drop-wise to each well and mixed by gentle rocking.

After 24 hrs, cells were passaged 1:3 into fresh medium. After 48 hrs, 0.6 mg/mL Geneticin® (G418) was added to the culture media. This selective media was changed daily until all cells transfected with the empty vector had died, after which the antibiotic concentration was lowered to 0.3 mg/mL.

3.2.2.14.3 Transient transfection

Cells were transfected as described in Section 3.2.2.14.2 and assayed after 24 hrs. No selective agents were added to the culture media.

3.2.2.15 Assaying for gene expression by real-time reverse transcriptase polymerase chain reaction (RT-PCR)

3.2.2.15.1 RNA extraction

Cells were washed twice with PBS made up in DEPC-MQW and lysed with TRIzol® (0.05 mL/cm^2 well surface). Cell lysates were homogenised through a 21G needle five times and mixed thoroughly with chloroform (300 μL/mL TRIzol) by vortexing for 15 s. The solution was incubated at room temperature for 5 min and centrifuged at 12000 g for 15 min. The aqueous phase was collected in an RNase-free tube and mixed by inversion with an equal volume of 70% (v/v) ethanol in DEPC-MQW. Total RNA was extracted from the mixture using the QIAGEN® RNeasy Mini Kit. RNA yield and purity were analysed with a NanoDrop™ spectrophotometer.

3.2.2.15.2 cDNA synthesis

Reverse transcription of the extracted RNA was undertaken using the SuperScript® VILO™ cDNA Synthesis Kit (Life Technologies).

3.2.2.15.3 Design of real-time RT-PCR primers

For each gene to be assayed, forward and reverse primers were designed using the Primer3 program (http://frodo.wi.mit.edu/). Amplicons were optimised to be between 80-150 base pairs. The primer sequences are listed in

Table 3.8.

Table 3.8. Real-time RT-PCR primers.

Target	Primer	Sequence (5'-3')
18S	18S_For	CCTGCGGCTTAATTTGACTC
	18S_For	AACTAAGAACGGCCATGCAC
WT/R515A	SHEL_For	GCGTAGGTGGTGCTGGCGTT
	SHEL_Rev	AGCTGCCGCTTCCGGGGATA
Endogenous human tropoelastin	HTE_For	AGGGGTTGTGTCACCAGAAG
	HTE_Rev	CAGCTCCAACCCCGTAAGTA
Cellular retinaldehyde-binding protein (CRALBP)	CRALBP_For	ACAAGTATGGCCGAGTGGTC
	CRALBP_Rev	CATTCTCCAGCAGCTTCTCC
Retinal pigmented epithelium-specific 65 kDa protein (RPE65)	RPE65_For	AGGCTGACACAGGCAAGAAT
	RPE65_Rev	TCAGGCTCCAGCCAGATAGT
Fibrillin-1 [140]	Fib1_For	CACCCTATGCCAAGTTGATC
	Fib1_Rev	TGACACTTAAAGCTGCCAATG
Fibulin-4	Fib4_For	CGTCATCAACGACCTACACG
	Fib4_Rev	CACACAGCTGTCCTGATCGT
Fibulin-5	Fib5_For	GCCTGCCGAGGAGACATGAT
	Fib5_Rev	TGCACACTCGTCCACATCCA
Lysyl oxidase	LOX_For	GATATTCCTGGGAATGGGCAC
	LOX_Rev	GCCAGGACTCAATCCCTGTG
Lysyl oxidase-like 1	LOXL1_For	GTCGCTACGTTTCTGCAACA
	LOXL1_Rev	GCTTTGGAAGGGGAGAGATT
Lysyl oxidase-like 2	LOXL2_For	GAGTTGCCTGCTCAGAAACC
	LOXL2_Rev	GTTGTGGATCTGGGAGGAGA

3.2.2.15.4 Real-time RT-PCR

Replicate cDNA samples (1.25-10 ng/μL) were mixed with 50% (v/v) SYBR Green, 0.375 μM forward primer and 0.375 μM reverse primer. No-template controls containing only the RT-PCR reagents were included. All samples were incubated on ice for 10 min. RT-PCR was performed on an Applied Biosystems StepOnePlus Real-time PCR System.

3.2.2.16 Immunohistochemistry analysis of the extracellular matrix

3.2.2.16.1 Preparation of stable transfectants

Transfected ARPE-19 cells that have been cultured in selective media were seeded on sterile glass coverslips at a density of 25,000 cells/cm^2. Cells were fixed and stained 1 and 5 days post-seeding.

3.2.2.16.2 Preparation of transient transfectants

ARPE-19, GM3348 and NHF8909 cells were seeded on glass coverslips at a density of 25,000 cells/cm^2. ARPE-19 cells were transfected 14 days post-seeding, while GM3348 and NHF8909 fibroblasts were transfected 10 days post-seeding. Samples were fixed and stained 1, 4, 7 and 10 days after transfection.

3.2.2.16.3 Exogenous addition of tropoelastin

ARPE-19, GM3348 and NHF8909 cells were seeded on glass coverslips at a density of 18400 cells/cm^2. Cells were stained for fibrillin at various time points to determine the extent of microfibril formation.

When a microfibrillar network has been established (10 and 14 days post-seeding for fibroblasts and ARPE-19 cells, respectively), 20 μg/mL of purified WT or R515A in PBS was added to triplicate wells of each cell type. The culture media was changed every 2 days. Samples were fixed and stained 1, 4, 7 and 10 days after tropoelastin addition.

This experiment was also undertaken with WT or R515A being supplemented during each media change. Samples were fixed and stained 1, 4, 7 and 10 days after the initial tropoelastin addition.

3.2.2.16.4 Fixing and immunostaining

Cells were washed twice in PBS and fixed with 4% (w/v) paraformaldehyde for 20 min. Excess paraformaldehyde was washed off three times with PBS and quenched with 0.2M glycine for 20 min. The cells were rinsed three times in PBS, incubated in 0.2% (v/v) Triton-100 for 6 min, washed again with PBS three times, and coated with 5% (w/v) BSA at 4 °C overnight. Excess BSA was removed with three PBS washes. The cells were then incubated with a primary antibody for 1.5 hrs, washed three times with PBS, and incubated with a fluorophore-conjugated secondary antibody for 1 hr. The sets of antibodies used are listed in Table 3.9. Unstained, no-primary-antibody, and isotype controls with non-specific mouse or rabbit IgG were also prepared. Actin fibres were visualised with 1:1000 rhodamine phalloidin. The cells were washed three times in PBS and mounted on glass microscope slides with ProLong® Gold anti-fade reagent with DAPI.

Table 3.9. Primary and secondary antibodies used to detect extracellular matrix components.

Target	Primary Antibody	Dilution	Secondary Antibody	Dilution
Elastin	Mouse anti-elastin (BA4)	1:500	FITC-conjugated anti-mouse	1:100
Elastin	Rabbit anti-elastin (ab21610)	1:250	TRITC-conjugated anti-rabbit	1:100
Fibrillin	Mouse anti-fibrillin (MAB1919)	1:500	FITC-conjugated anti-mouse	1:100

3.2.2.16.5 Confocal microscopy

Samples were imaged with an Olympus FluoView FV1000 confocal microscope under the 60x oil immersion objective. DAPI, FITC and TRITC fluorescence were detected using the 405, 488 and 559 nm lasers, respectively. Z-stacks were taken from at least 3 areas distributed across each sample and converted to maximum projection images.

3.2.2.16.6 Analyses of elastic fibres

Fibre analyses were performed on maximum projection images from WT and R515A samples. To compare elastic fibre fluorescence, a threshold was set to exclude background and saturated pixel intensities in the FITC or TRITC channel. The average intensity of pixels within the threshold was measured and averaged for each sample. To compare fibre density, two perpendicular reference lines were drawn in each projection image. The number of fibres intersecting either reference line was counted and averaged for each sample. The area occupied by cell nuclei, measured by the number of DAPI-fluorescent pixels above background intensity, was used as a control of cell number and viability in all samples.

3.2.2.17 Fluorescence lifetime imaging (FLIM)

The presence of elastic fibres in ARPE-19 cells transiently transfected with pCI-neo-WT or pCI-neo-R515A was determined by FLIM. Cells were fixed and stained after 1 and 4 days as described in Section 3.2.2.16.4. Time-correlated single-photon-counting fluorescence lifetime imaging was performed using a Leica SP5 II multi-photon microscope. The excitation wavelength was set at 800 nm, and the emission spectrum from 510-560 nm was collected over 200 s. A decay matrix was calculated and used to obtain the fluorescence lifetimes of specific components within each sample.

3.3 Results

3.3.1 Bioinformatics analysis of WT/R515A expression in human cells

The potential for synthetic WT and R515A tropoelastin cDNA to be expressed in a human host system was assessed by analysing the compatibility of the sequences with human-specific codon usage bias. The likely success of heterologous gene expression is directly related to the codon adaptation index (CAI). The CAI of endogenous human tropoelastin was 0.68, while both WT and R515A sequences were calculated to have a slightly lower CAI of 0.55, which was predictive of moderate expression levels in human cells (Figure 3.3).

The majority of codons in the WT and R515A sequences were used at moderate to high frequencies in a human expression system (Figure 3.4). While 12% of the WT and R515A codons were categorised to have low usage frequencies (codon values <30), in contrast with 1% of the native human tropoelastin sequence, they still represented codons that appear naturally in human genes (codon values >20).

The average GC content of endogenous human tropoelastin (64.3%) was similar to that of the WT and R515A sequences (65.7%) (Figure 3.5). Both values fell within the ideal GC content range of 30-70% observed in human sequences, indicating likely heterologous expression of WT and R515A in human cells.

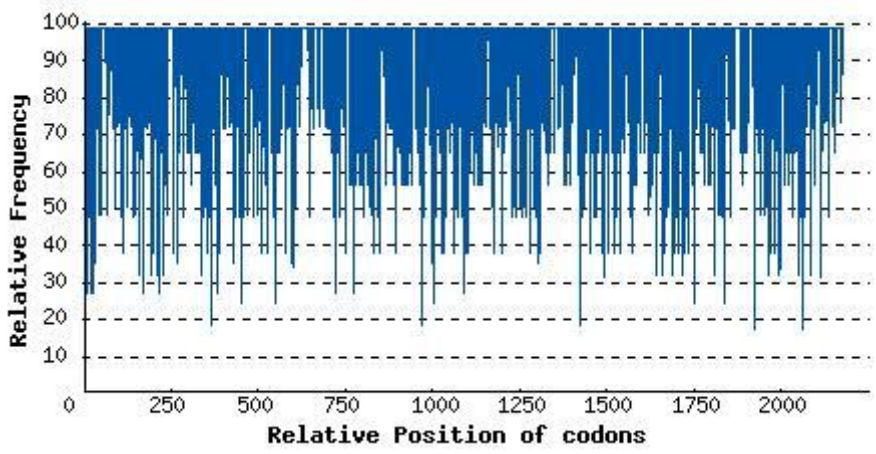

A

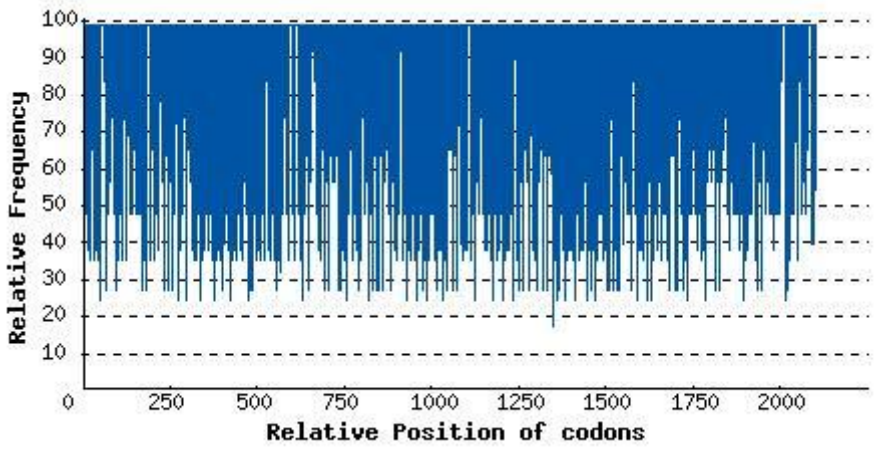

B

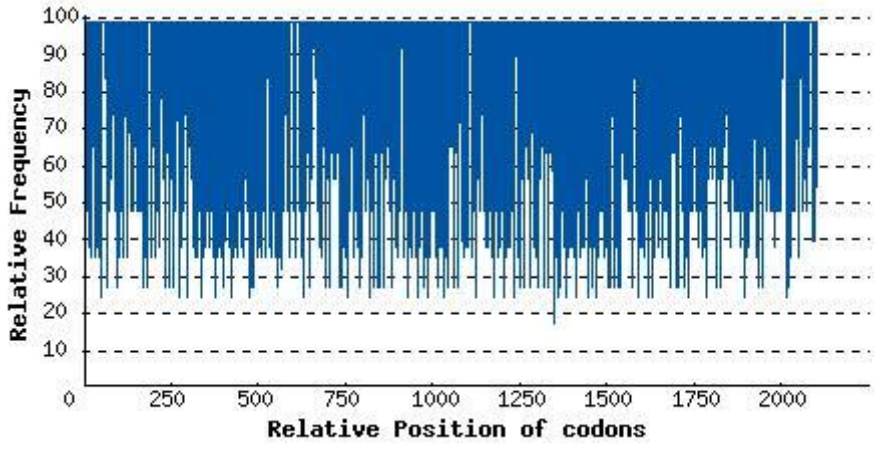

C

Figure 3.3. Codon adaptation index of (A) endogenous human tropoelastin, (B) WT and (C) R515A DNA sequences. The distribution of codon usage frequency along the length of the 2100 bp sequence in a human expression system is shown. The likelihood of protein expression is directly correlated to the relative frequency of codon usage in the specified host.

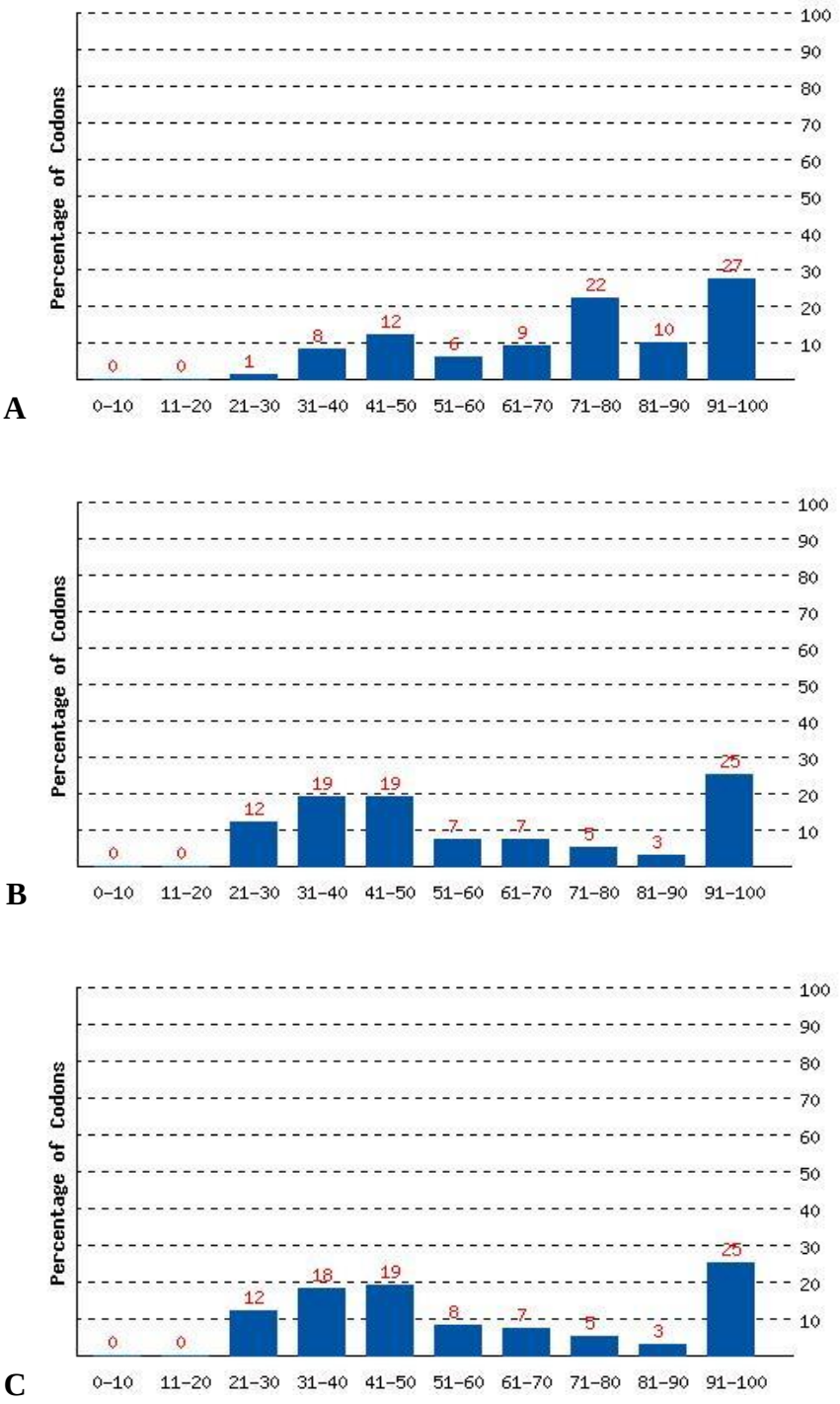

Figure 3.4. Codon frequency distribution of (A) endogenous human tropoelastin, (B) WT and (C) R515A DNA sequences. The percentage distribution of codons in computed 'codon quality' groups are shown. A value of 100 is set for the codon with the highest usage frequency for a given amino acid in the human expression system. Codons with values lower than 30 may decrease expression efficiency.

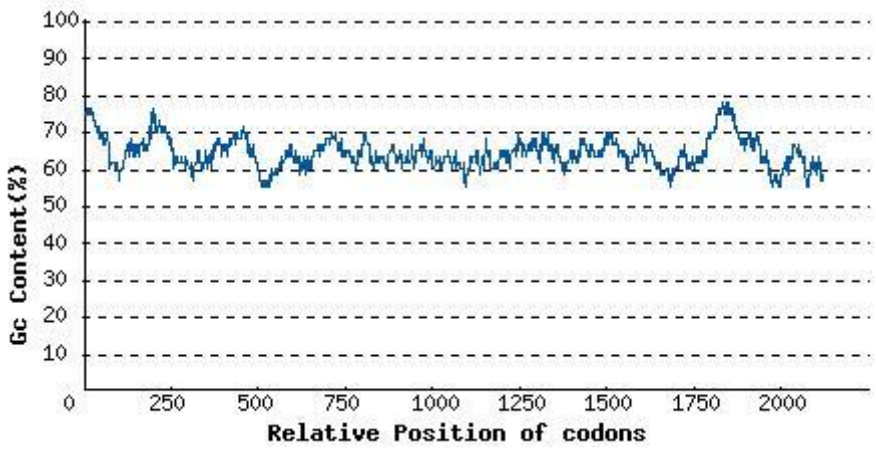

A

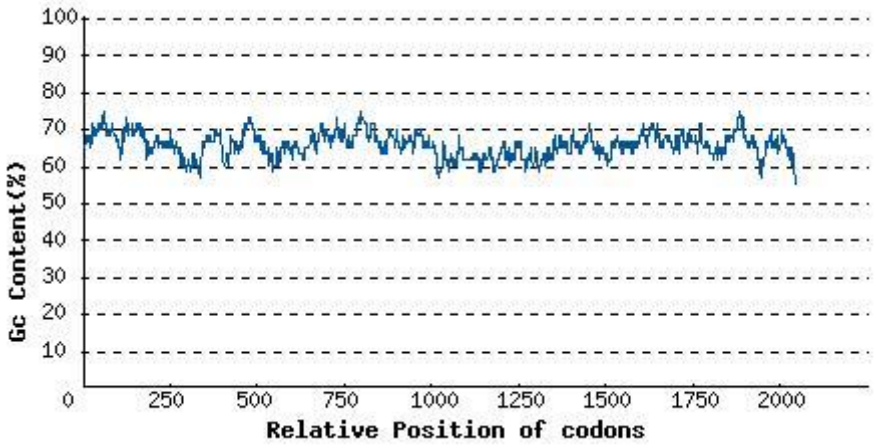

B

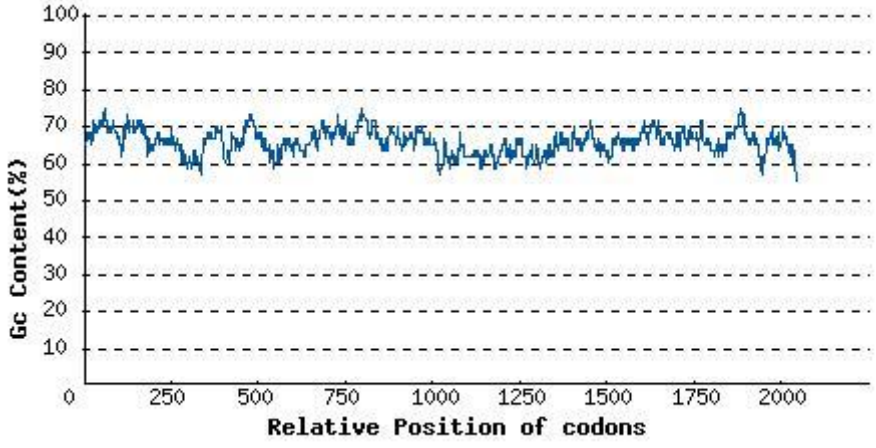

C

Figure 3.5. GC content of (A) endogenous human tropoelastin, (B) WT and (C) R515A DNA sequences.

3.3.2 Construction of the pCI-neo-WT and pCI-neo-R515A expression vectors

To construct the pCI-neo-WT and pCI-neo-R515A mammalian expression vectors, the tropoelastin insert flanked by *Nco*I and *Bam*HI restriction sites within a bacterial pET-3d plasmid had to be cloned into a pCI-neo vector that did not contain *Nco*I and *Bam*HI sites. This was achieved after attempts with several cloning strategies.

3.3.2.1 Cohesive-end cloning

The pET-3d plasmid containing either WT or R515A cDNA (Figure 3.6) was extracted from stock *E. coli* transformants at high purity (A260:A280 ~ 1.8).

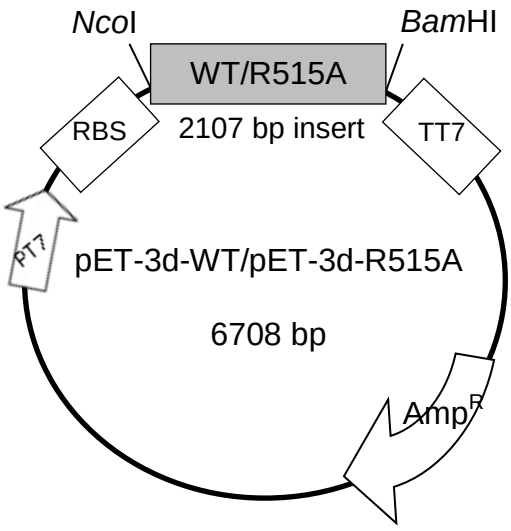

Figure 3.6. Schematic representation of the pET-3d plasmid with the 2107 bp WT or R515A insert. Features of the plasmid construct including the T7 promoter (PT7), ribosome binding site (RBS), T7 terminator (TT7) and ampicillin resistance gene (Amp^R) are indicated.

PCR primers that annealed to flanking regions of the tropoelastin insert were engineered to introduce an *Eco*RI restriction site at the 5′ end and an *Xba*I restriction site at the 3′ end of the insert sequence. PCR amplification of pET-3d-WT and pET-3d-R515A with these primers produced a dominant ~2.1 kb species corresponding to the expected size of the tropoelastin sequences (Figure 3.7). No amplification products were observed for the no template control. The WT and R515A PCR products were gel-extracted and confirmed to be of high purity.

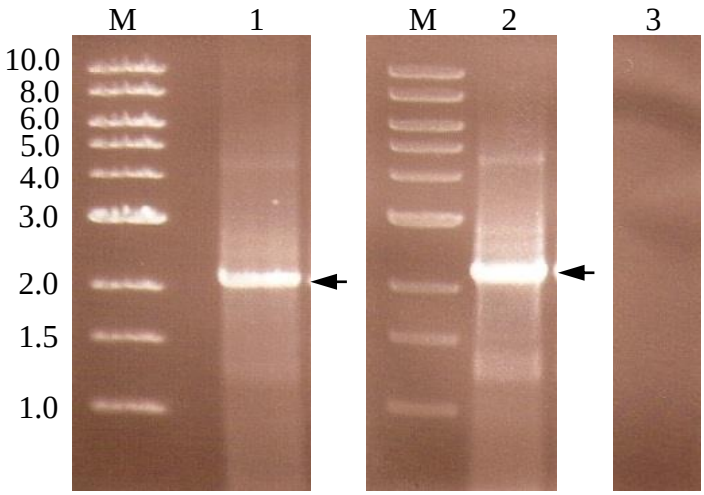

Figure 3.7. Polymerase chain reaction amplification of the WT or R515A tropoelastin insert sequence in pET-3d plasmids extracted from transformed *E. coli* colonies. The ~2.1 kb bands corresponding to the expected size of the tropoelastin sequences are indicated by arrowheads. Lanes: M – DNA ladder (kb); 1 – pET-3d-WT PCR products; 2 – pet-3d-R515A PCR products; 3 – no template control.

The WT/R515A insert sequences and pCI-neo vector sequence (Figure 3.8) were double digested with *Eco*RI and *Xba*I to produce cohesive ends for subsequent directional ligation. DNA gel electrophoresis of the vector digests revealed a ~5.5 kb band corresponding to the pCI-neo sequence, while the insert digests showed a ~2.1 kb band

consistent with the WT/R515A sequence (Figure 3.9). The revelant bands were purified from the agarose gel at high purity.

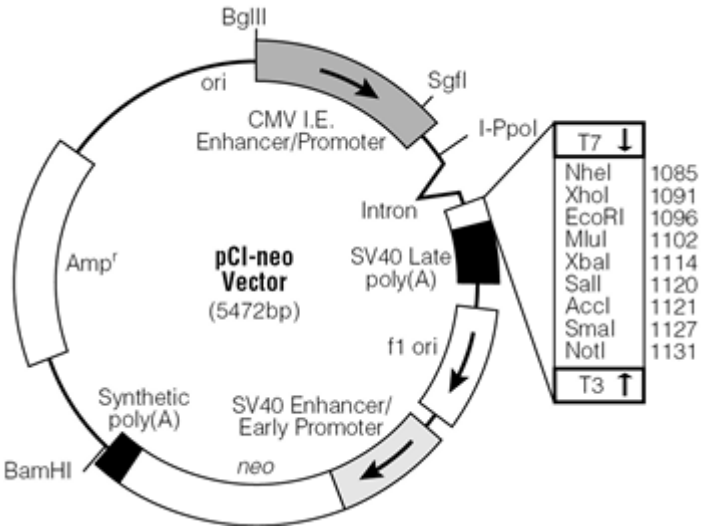

Figure 3.8. Diagram of the ~5.5 kb pCI-neo mammalian expression vector obtained from the manufacturer (Promega).

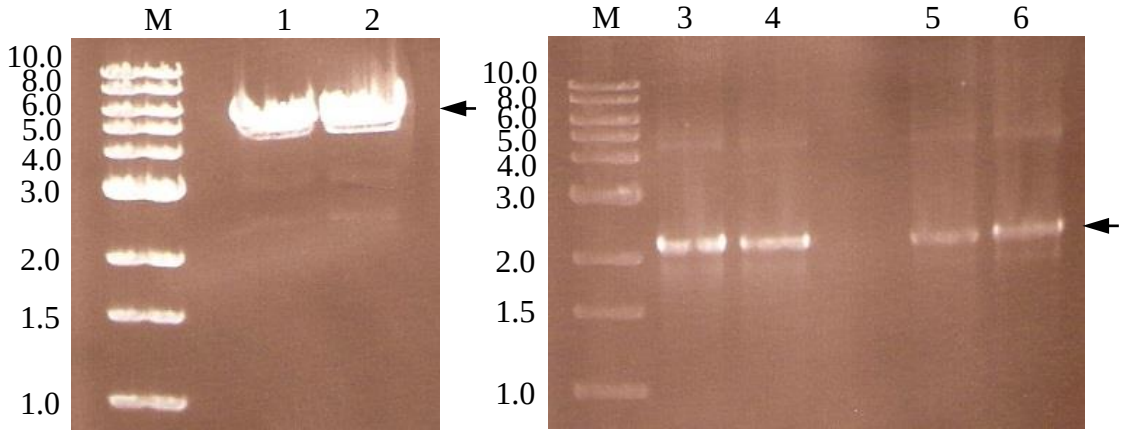

Figure 3.9. Agarose gel showing gel-purified *Eco*RI + *Xba*I digested pCI-neo vector and WT/R515A tropoelastin insert sequences. The main ~5.5 kb vector and ~2.1 kb insert digest products are indicated. Lanes: M – DNA ladder (kb); 1, 2 – pCI-neo vector digests; 3, 4 – WT insert digests; 5, 6 – R515A insert digests.

The digested pCI-neo and WT/R515A sequences were ligated at various vector:insert ratios and used to transform competent *E. coli* cells via electroporation. Colony growth was observed on selective medium, which indicated successful uptake of the ampicillin resistance-conferring pCI-neo. Plasmid DNA was extracted from randomly selected colonies at high yield and purity and screened for the tropoelastin sequence. Restriction analysis with *Eco*RI and *Xba*I showed only a ~5.5 kb band corresponding to the empty vector (Figure 3.10A). Similar results were observed for putative clones analysed with *Not*I (Figure 3.10B). It appeared that the tropoelastin inserts were not incorporated into pCI-neo, and the bacterial cells were subsequently transformed with re-ligated vector DNA.

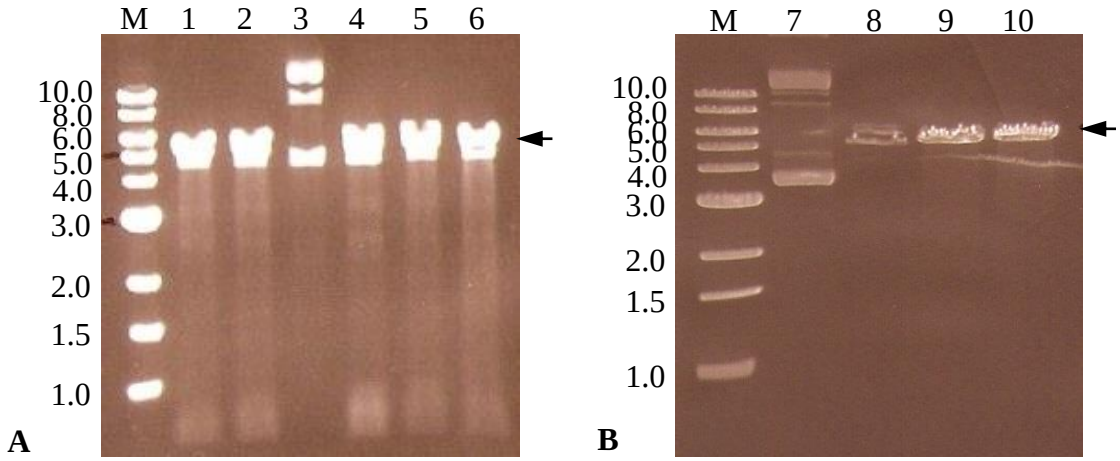

Figure 3.10. Restriction analysis of pCI-neo vector DNA extracted from transformed colonies with (A) *Eco*RI + *Xba*I or (B) *Not*I. Only ~5.5 kb bands corresponding to the empty vector were seen for all samples. Lanes: M – DNA ladder (kb); 1, 2 – *Eco*RI + *Xba*I digest of putative pCI-neo-WT; 3 – undigested pCI-neo; 4, 5, 6 – *Eco*RI + *Xba*I digest of putative pCI-neo-R515A; 7 – undigested pCI-neo; 8 - *Not*I digest of putative pCI-neo-WT; 9, 10 - *Not*I digest of putative pCI-neo-R515A.

3.3.2.2 Direct cloning

A more direct cloning approach was adopted to minimise handling steps that may induce damage to the DNA sequences. The pCI-neo vector was digested with *Sma*I to produce a linearised sequence with blunt ends. DNA gel electrophoresis of the vector digest together with PCR-amplified WT and R515A insert sequences enabled purification of the relevant products (Figure 3.11).

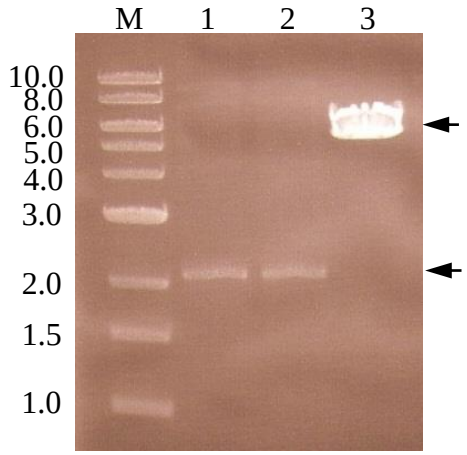

Figure 3.11. Agarose gel showing gel-purified PCR-amplified tropoelastin insert sequences and *Sma*I digested pCI-neo. Lanes: M – DNA ladder (kb); 1 – WT PCR product; 2 – R515A PCR product; 3 – *Sma*I digest of pCI-neo.

PCR-amplified WT/R515A directly ligated with the linearised pCI-neo vector was used to transform competent *E. coli*. These cells did not grow on selective plates, while those transformed with pCI-neo alone exhibited colony formation, suggesting incomplete ligation of the vector and insert sequences.

3.3.2.3 Blunt-end cloning

An alternative cloning method was used to eliminate the need for restriction sites at the ends of the tropoelastin insert that would be compatible with available cloning sites in pCI-neo. The pET-3d-WT and pET-3d-R515A plasmid DNA extracted from transformed *E. coli* stocks were treated with *Nco*I and *Bam*HI to release the WT and R515A cDNA sequences. Gel electrophoresis of the digests enabled purification of the ~2.1 kb tropoelastin insert from the larger ~4.6 kb plasmid fragment (Figure 3.12).

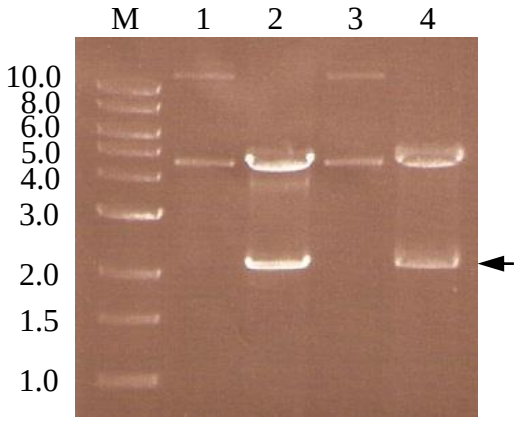

Figure 3.12. *Nco*I and *Bam*HI double digest of pET-3d plasmid containing the WT or R515A insert sequence. The ~2.1 kb bands corresponding to the tropoelastin inserts are indicated. Lanes: M – DNA ladder (kb); 1 – undigested pET-3d-WT; 2 – *Nco*I + *Bam*HI digest of pET-3d-WT; 3 – undigested pET-3d-R515A; 4 - *Nco*I + *Bam*HI digest of pET-3d-R515A.

The WT and R515A sequences were filled at the overhanging 5′ *Nco*I and 3′ *Bam*HI sites to produce blunt-ended constructs, and ligated with *Sma*I-digested pCI-neo. Only 2-3 transformed colonies were observed on selective plates. Screening of the clones via *Not*I restriction analysis of extracted plasmid DNA showed only a ~5.5 kb band consistent with

the empty pCI-neo vector (Figure 3.13), indicating unsuccessful incorporation of the tropoelastin insert into the vector sequence.

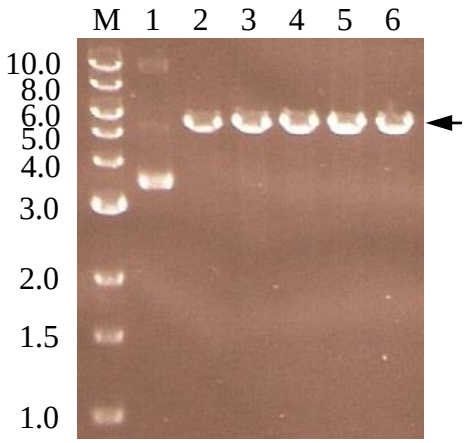

Figure 3.13. Screening for possible pCI-neo-WT and pCI-neo-R515A clones by *Not*I restriction analysis of plasmid DNA extracted from transformed *E. coli*. Only ~5.5 kb bands corresponding to the size of the empty vector were observed. Lanes: M – DNA ladder (kb); 1 – undigested pCI-neo; 2, 3, 4 – *Not*I digests of putative pCI-neo-WT clones; 5, 6 - *Not*I digests of putative pCI-neo-R515A clones.

3.3.2.4 Linker-mediated cloning

A different cloning approach was attempted using linker sequences to attach vector-compatible restriction sites at the ends of the tropoelastin insert. Two linker sequences were constructed (Figure 3.14): an *Eco*RI-*Nco*I linker to adjoin the upstream *Eco*RI site in pCI-neo with the 5′ *Nco*I site in WT/R515A; and a *Bam*HI-*Xba*I linker to connect the 3′ *Bam*HI site in WT/R515A with the downstream *Xba*I site in pCI-neo.

Simultaneous ligation of the *Eco*RI+*Xba*I-digested pCI-neo, *Eco*RI-*Nco*I linker, *Nco*I+*Bam*HI-digested WT/R515A and *Bam*HI-*Xba*I linker was performed. Transformed *E. coli* colonies were screened by *Not*I restriction analysis of extracted plasmid samples. *Not*I will cut pCI-neo-WT or pCI-neo-R515A within the insert and vector sequences to produce

~1.3 kb and ~6.3 kb fragments. This characteristic digest profile was seen in 10 putative WT and 8 putative R515A clones sampled (Figure 3.15).

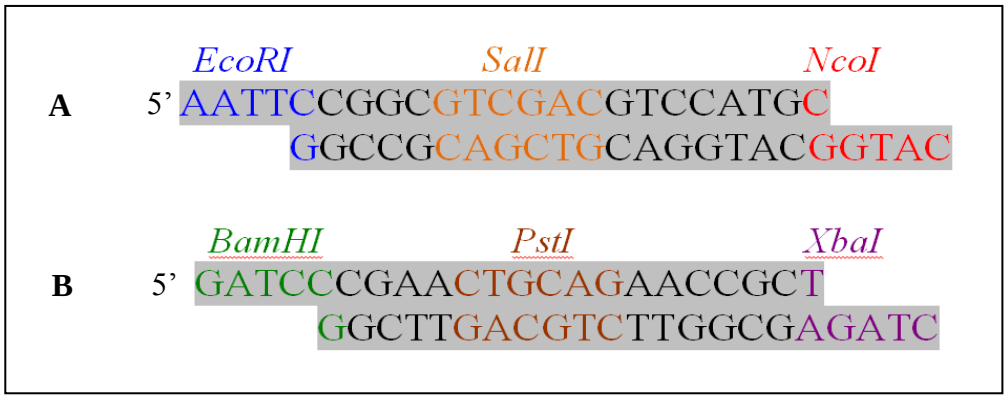

Figure 3.14. Schematic representation of the (A) *Eco*RI-*Nco*I and (B) *Bam*HI-*Xba*I linkers. Restriction enzyme recognition sites are labelled in coloured font.

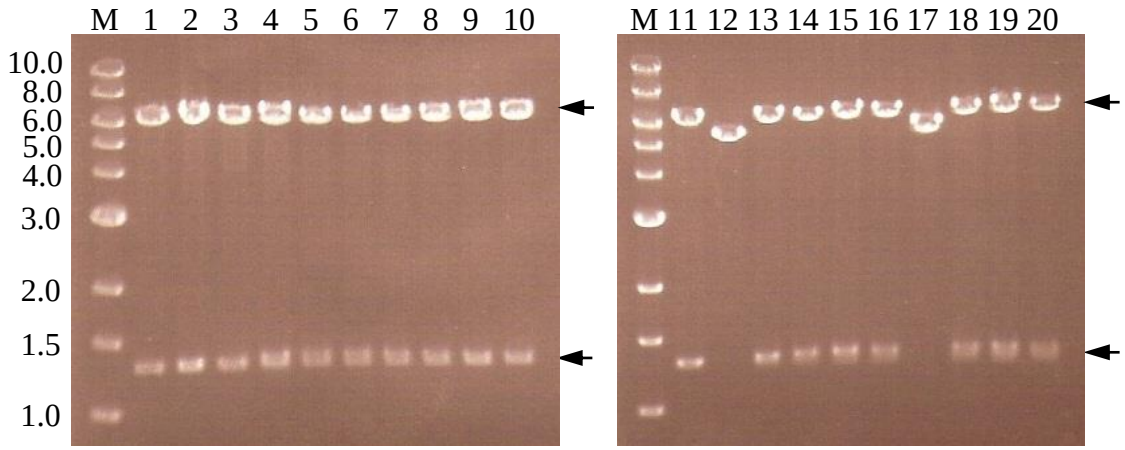

Figure 3.15. *Not*I restriction analysis of putative pCI-neo-WT and pCI-neo-R515A clones extracted from transformed *E. coli*. A ~6.3 kb band and a ~1.3 kb band were seen in all WT and most R515A colonies, indicating the presence of the tropoelastin insert within the vector. Lanes: M – DNA ladder (kb); 1-10 – *Not*I digests of pCI-neo-WT; 11-20 - *Not*I digests of pCI-neo-R515A.

3.3.2.5 Sequence confirmation

Sequencing of plasmid DNA extracted from presumptive WT and R515A transformants confirmed successful cloning of the WT or R515A sequence into the pCI-neo expression vector (Appendix 8.1).

3.3.3 Stable transfection

3.3.3.1 Validation of the ARPE-19 cell line

The ARPE-19 cells were found to be free of mycoplasma contamination (Figure 3.16). Mycoplasma markers were not detected by PCR analysis of the incubation media from different cell passages.

The cultured ARPE-19 cells displayed characteristic retinal pigmented epithelial cell features, including defined cell borders and a general cobblestone appearance. The transcript levels of two retinal pigmented epithelium-specific markers, the cellular retinaldehyde-binding protein (CRALBP) and the retinal pigmented epithelium-specific 65 kDa protein (RPE65), were also detectable (Figure 3.17). Expression levels increased with longer periods in culture and were significantly higher than the background levels in human dermal fibroblasts cultured for the same duration.

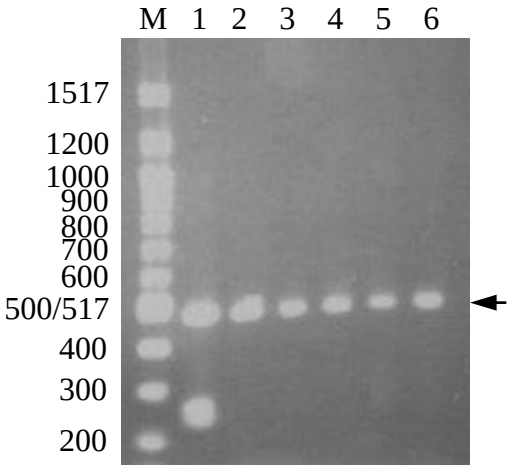

Figure 3.16. PCR detection of mycoplasma markers in the culture media of ARPE-19 cells. Lanes: M – DNA ladder (bp); 1 – positive control; 2 – negative control; 3-6 – culture media from different passages of ARPE-19. All test samples showed the ~489 bp internal control band but not the ~259 bp mycoplasma-specific band.

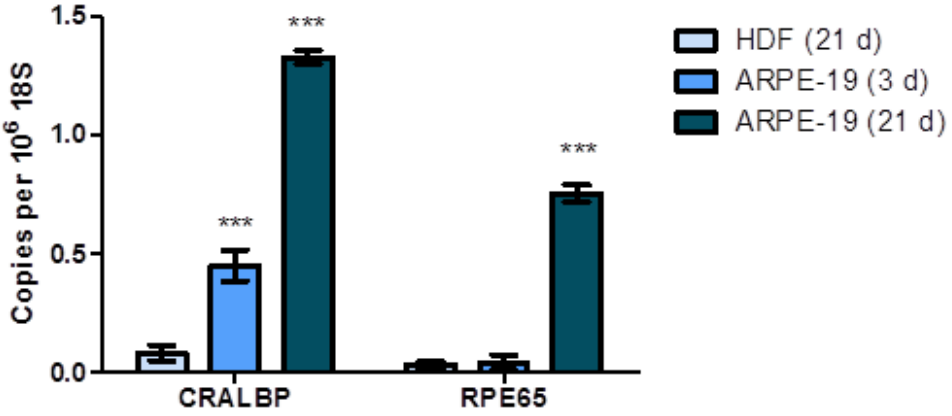

Figure 3.17. Transcript levels of ARPE-19 specific markers after 3 and 21 days in culture. Human dermal fibroblasts (HDF) cultured for 21 days were used as a negative control for gene expression.

3.3.3.2 ARPE-19 RNA expression of elastogenic components

The ARPE-19 cells were shown to express several extracellular matrix proteins involved in elastogenesis, including crucial components such as the major microfibrillar protein fibrillin-1, and the cross-linking enzyme lysyl oxidase (Figure 3.18). ARPE-19 cells displayed variable expression of these genes compared to human dermal fibroblasts (HDF) which have an established elastogenic phenotype. Both fibrilin-1 and fibulin 5 transcript levels were lower in ARPE-19 than HDF, while lysyl oxidase expression was similar in both cell types. In contrast to HDF, however, ARPE-19 did not produce detectable levels of endogenous tropoelastin mRNA.

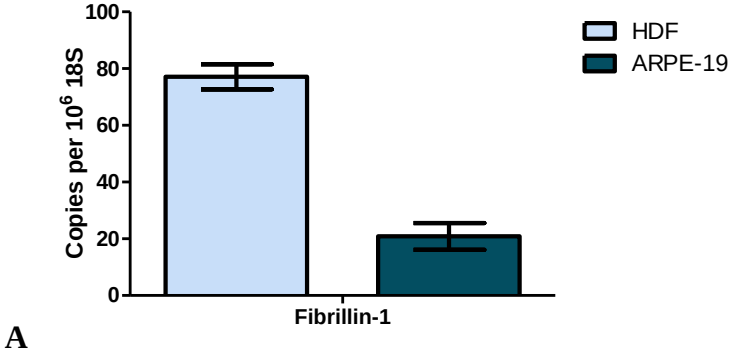

A

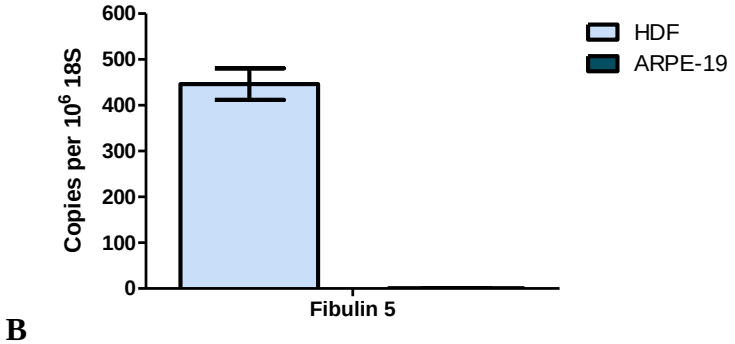

B

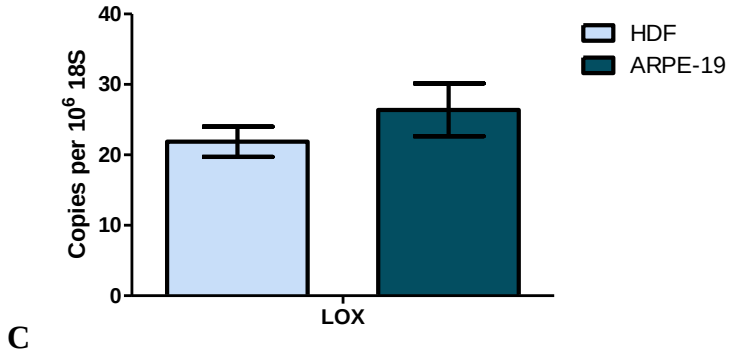

C

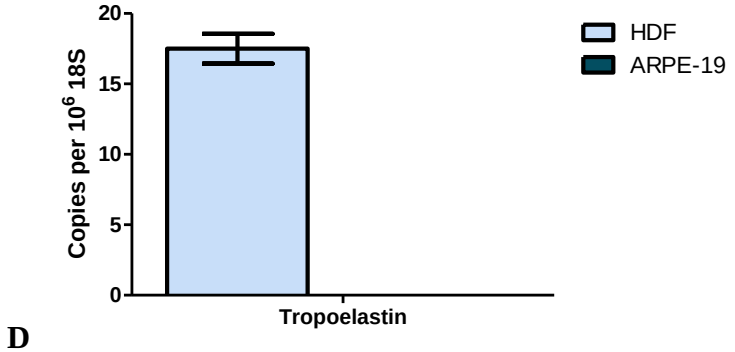

D

Figure 3.18. Comparative expression levels of (A) fibrillin-1, (B) fibulin 5, (C) lysyl oxidase, (D) tropoelastin by ARPE-19 and human dermal fibroblasts.

3.3.3.3 Optimisation of the transfection protocol

ARPE-19 cells were transfected with varying amounts of pCI-neo-WT vector DNA at increasing ratios of the lipid transfection agent to determine optimum transfection parameters (Figure 3.19). Optimal transfection efficiency was found to occur with the following conditions: 750 ng DNA per 2 cm^2 well surface at 4-fold excess of Lipofectamine. Twenty-four hours after transfection, cells exhibited a 4.5 million fold increase in tropoelastin expression compared to untransfected cells.

Introduction of the WT tropoelastin gene into ARPE-19 and the consequent induction of WT tropoelastin mRNA expression did not affect endogenous levels of other elastogenic components. Transfected ARPE-19 displayed similar transcript levels of fibrillin-1, fibulin 5 and lysyl oxidase to untransfected cells (Figure 3.20).

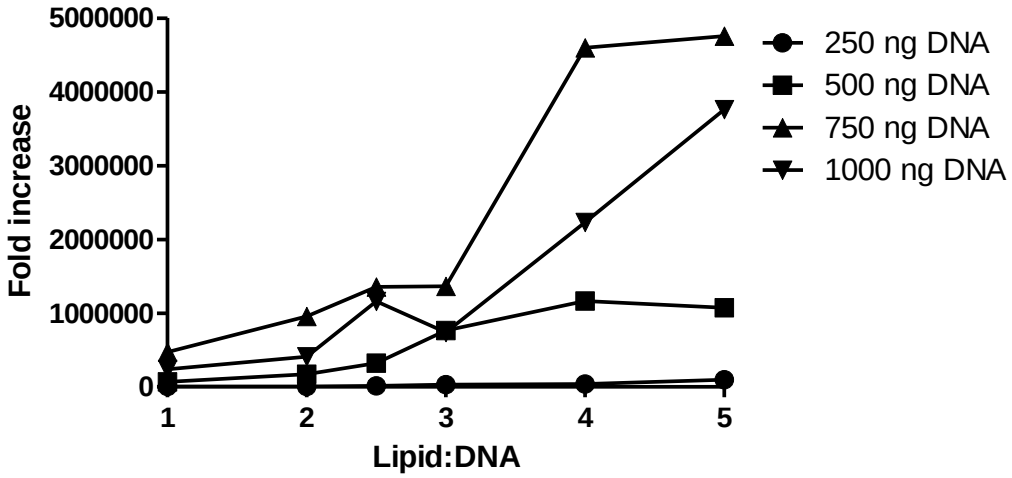

Figure 3.19. WT expression levels of ARPE-19 cells transfected with increasing amounts of pCI-neo-WT and at different ratios of Lipofectamine:DNA. WT tropoelastin transcript levels of transfected cells were assayed 24 hrs after transfection and denoted by the fold increase over expression levels of untransfected cells.

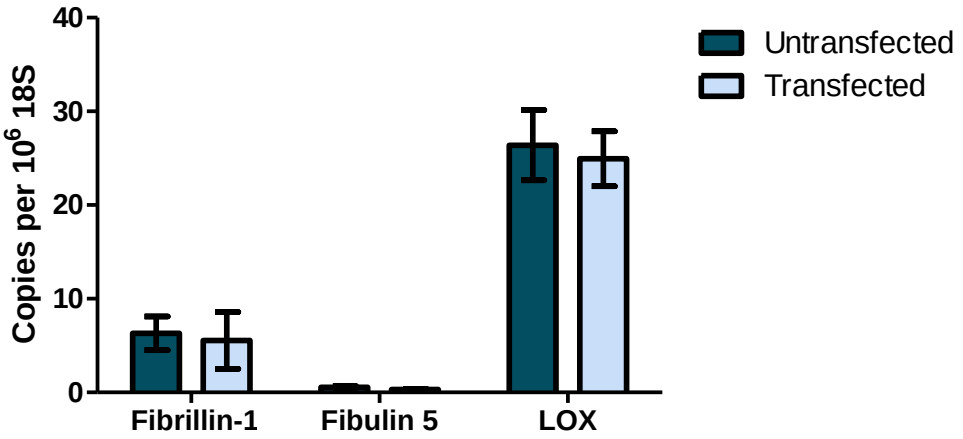

Figure 3.20. Expression of elastogenic components in transfected and untransfected ARPE-19 cells.

3.3.3.4 Propagation of stable transfectants

ARPE-19 transfected with pCI-neo-WT, pCI-neo-R515A or the empty pCI-neo vector were cultured in G418-supplemented nutrient media to select for cells with the neomycin resistance-conferring pCI-neo constructs. Untransfected ARPE-19 cells were cultured under the same conditions to monitor the progress of the antibiotic selection.

Over two weeks after the initial addition of G418 to the culture media, untransfected cells steadily diminished in number with only a few cells visible per field of view on the 16th day (Figure 3.21). In contrast, cells transfected with the empty pCI-neo vector survived and proliferated into dense clusters. Likewise, cells transfected with pCI-neo-WT and pCI-neo-R515A persisted with increasing cell numbers after 16 days in selective media. However, there were visibly more WT than R515A transfectants, suggesting variable transfection rates between samples.

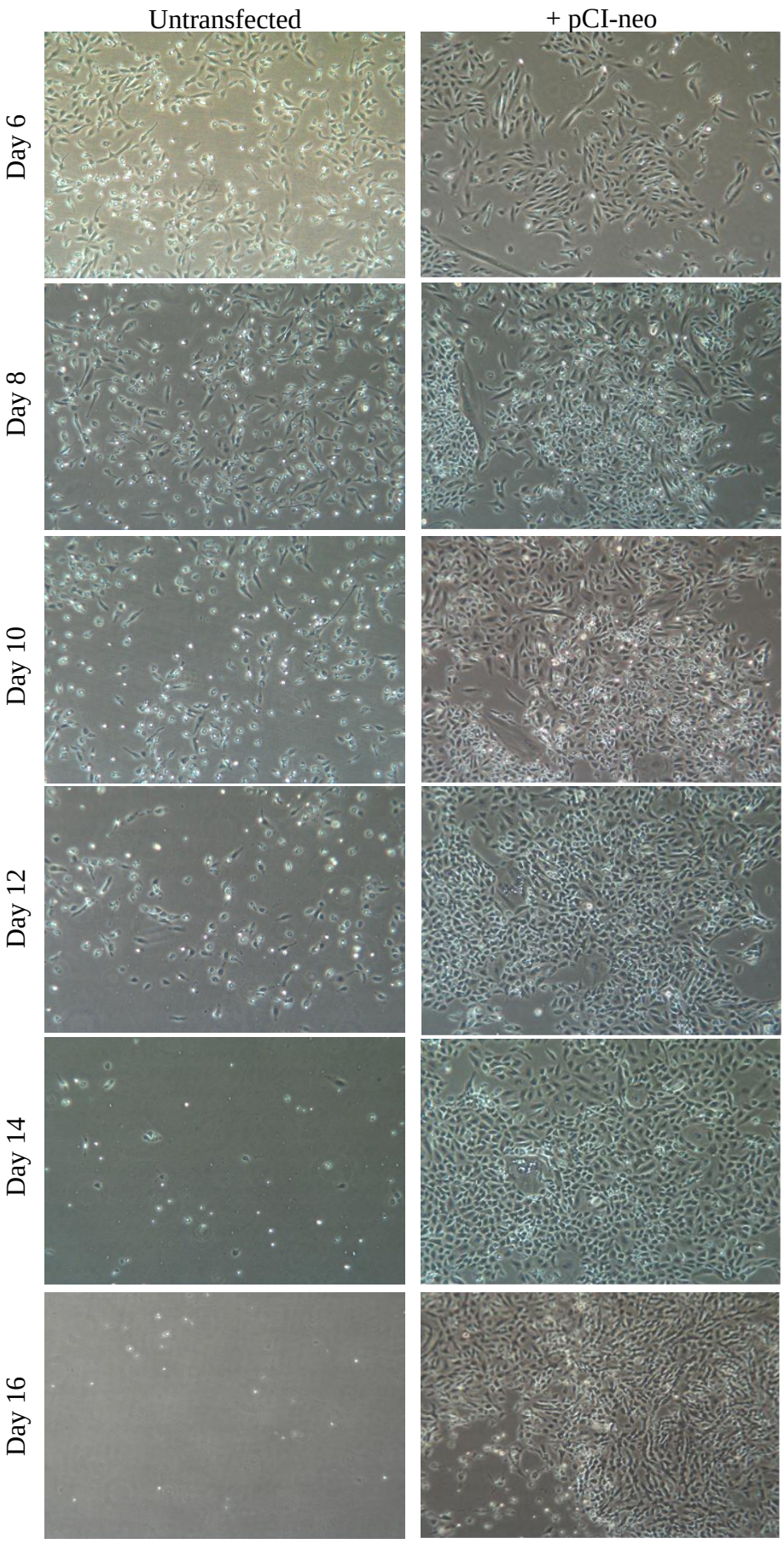
Untransfected
+ pCI-neo
Day 6
Day 8
Day 10
Day 12
Day 14
Day 16

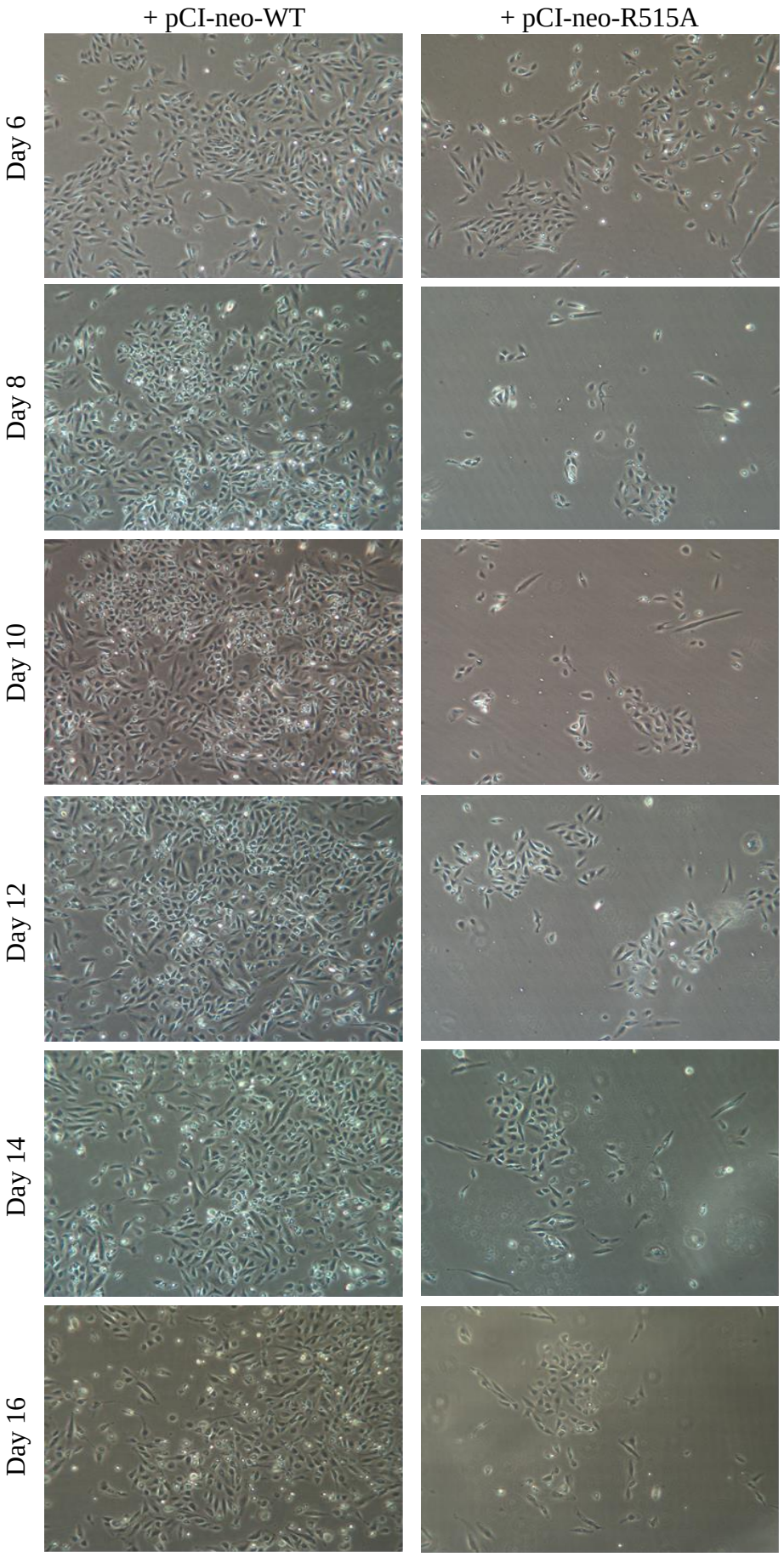
+ pCI-neo-WT
+ pCI-neo-R515A
Day 6
Day 8
Day 10
Day 12
Day 14
Day 16

Figure 3.21. Light microscope images of untransfected, pCI-neo transfected, pCI-neo-WT transfected, and pCI-neo-R515A transfected ARPE-19 at various time points after initial addition of G418 into the culture medium.

3.3.3.5 Probing for elastic fibre formation by transfected ARPE-19

ARPE-19 cells transfected with WT, R515A or the vector alone were propagated for 90 days to achieve sufficient cell numbers for study. Confocal microscopy of the cells stained for fibrillin-1 and elastin showed no definitive elastic fibre network (Figure 3.22). Punctate species and thin microfibres corresponding to fibrillin-1 staining were observed in the extracellular matrix of the cells, suggesting formation of nascent microfibrils. However, there was no discernible elastin production in all samples.

Analysis of WT and R515A transcript levels in the transfectants confirmed a dramatic loss of WT tropoelastin expression that occurred over the course of propagating the transfected cultures (Figure 3.23). This represents a ~300,000-fold decrease in expression levels over three months.

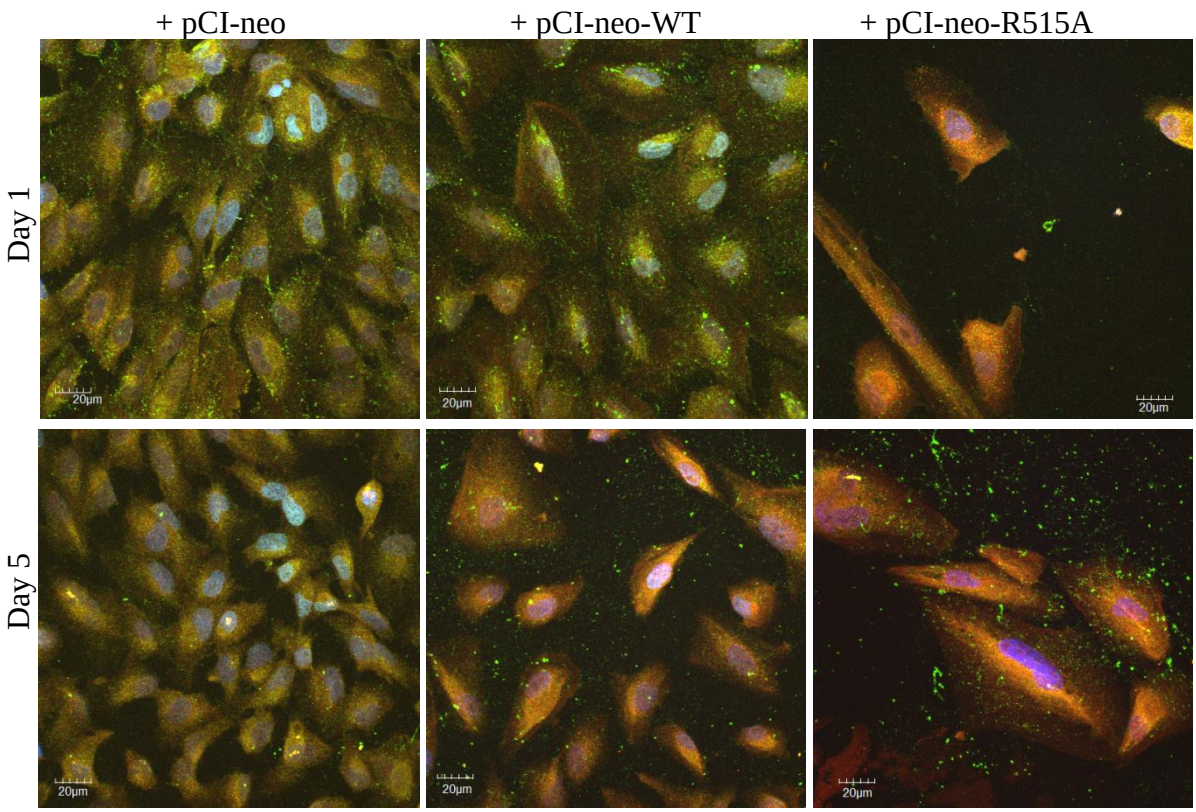

Figure 3.22. Confocal microscopy of transfected ARPE-19 cells stained for cell nuclei (blue), fibrillin-1 (green), and elastin (red). Cells were fixed and stained 1 and 5 days post-seeding.

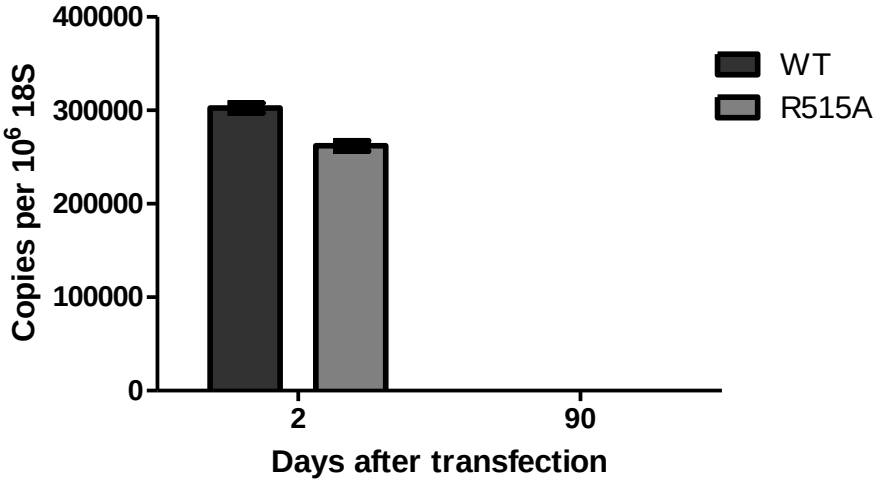

Figure 3.23. Expression levels of WT and R515A tropoelastin in transfected ARPE-19 cells after 90 days in culture.

3.3.4 Transient transfection

3.3.4.1 RNA expression of elastogenic components

ARPE-19 cells and GM3348/NHF8909 fibroblasts were shown to express a number of extracellular matrix proteins involved in elastogenesis, including microfibrillar proteins fibrillin-1, fibulin 4 and fibulin 5, as well as several lysyl oxidase family proteins (Figure 3.24). As previously described, no endogenous tropoelastin transcripts were detected in ARPE-19 cells. However, GM3348 and NHF8909 fibroblasts expressed low levels of tropoelastin consistent with their elastogenic phenotype.

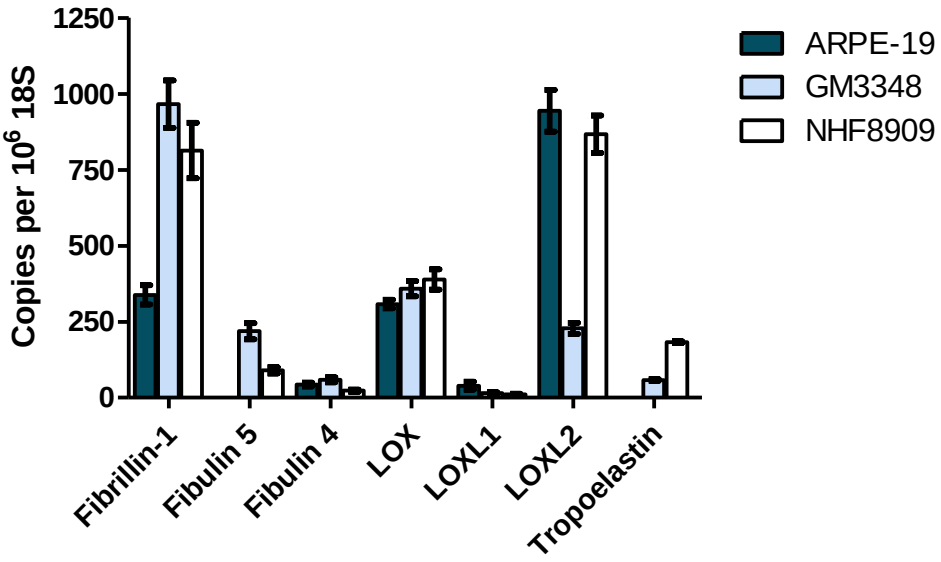

Figure 3.24. Expression of elastogenic components by ARPE-19, GM3348 and NHF8909 cells.

3.3.4.2 Tropoelastin expression in transiently transfected cells

Analysis of WT/R515A transcript levels in transiently transfected cells suggested a steep decline in tropoelastin expression within a few days after transfection (Figure 3.25). Transfection of ARPE-19 cells induced a 150,000-fold increase in tropoelastin expression, which rapidly decreased after 24 hrs. In contrast, tropoelastin expression persisted slightly longer in GM3348 and NHF8909 fibroblasts until 4 days after transfection, but had similarly returned to near-baseline levels by 10 days.

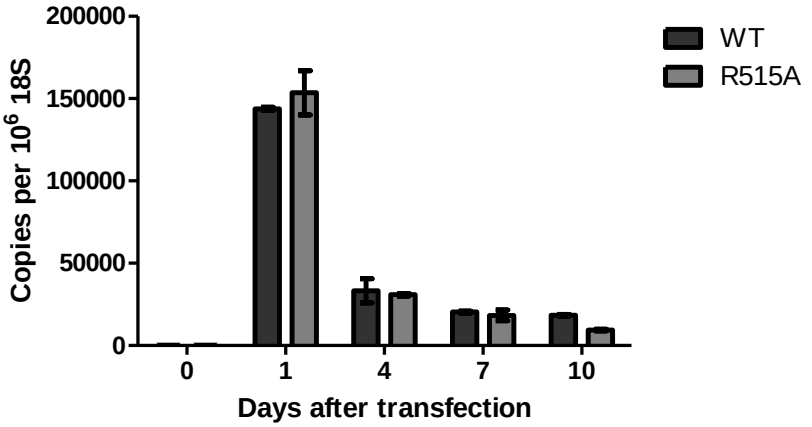

A

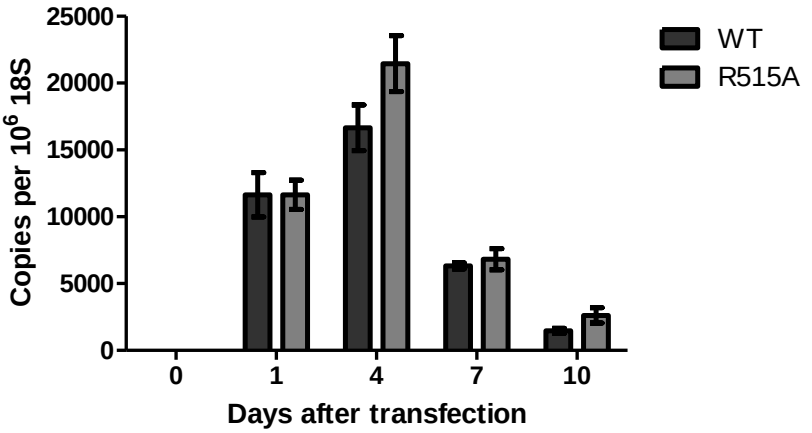

B

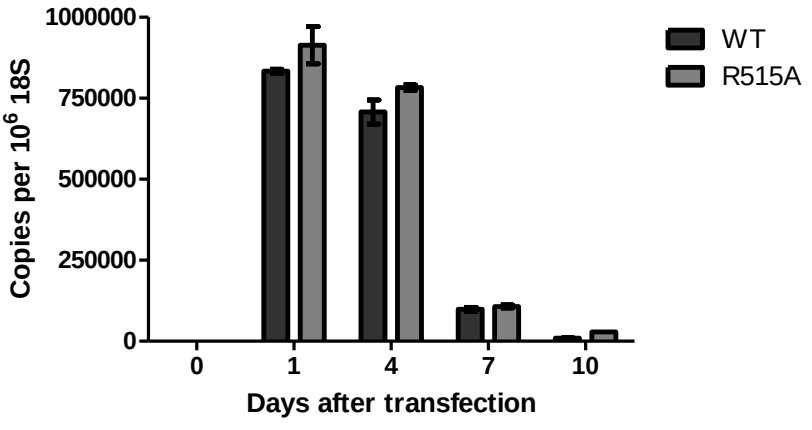

C

Figure 3.25. Transcript expression levels of WT and R515A tropoelastin in transiently transfected (A) ARPE-19, (B) GM3348 and (C) NHF8909 cells. Samples at day 0 represent untransfected cells.

3.3.4.3 Establishment of the microfibrillar network

The temporal progression of microfibrillar development in ARPE-19 cells and human dermal fibroblasts was determined so that ARPE-19 cells could be transfected and tropoelastin expression induced only after a defined network of microfibrils had been established (Figure 3.26). Six days after seeding, ARPE-19 and GM3348 cells stained for fibrillin-1, the dominant component of microfibrils, did not show any visible fibre formation. Ten days after seeding, short fibrillin fibres were observed in ARPE-19 cells, while an extensive fibrillar network was already present in GM3348 fibroblasts. By day 14 post-seeding, microfibrillar development was comparable in both cell types. The staining controls showed no detection of fibrillin species.

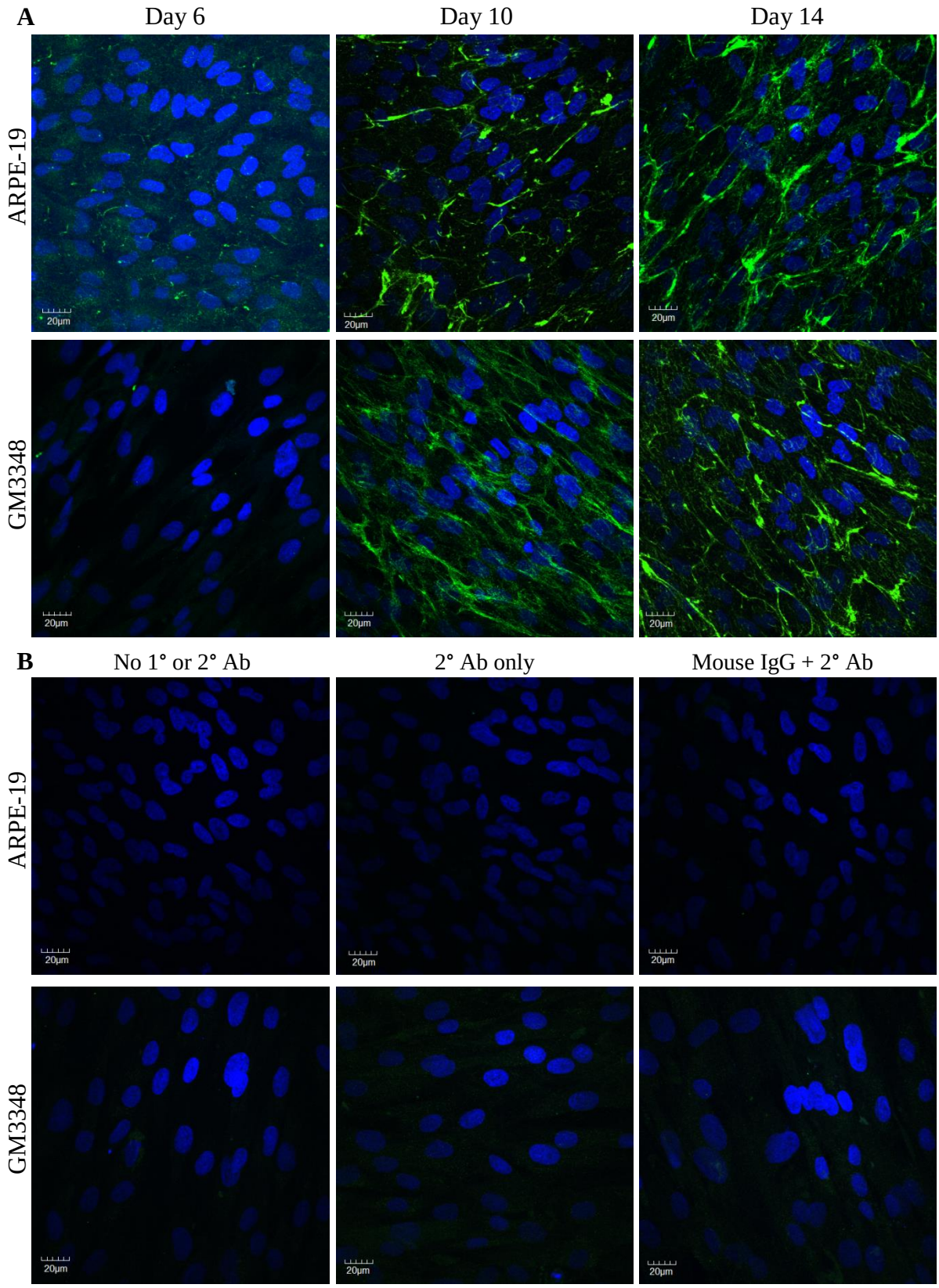

Figure 3.26. Development of a microfibril network in ARPE-19 and GM3348 cells. (A) Fibrillin-1 immunostaining in ARPE-19 and GM3348 cells at 6, 10 and 14 days post-

seeding. (B) Staining controls confirm antibody specificity. Cell nuclei in all samples are indicated by DAPI fluorescence.

3.3.4.4 Elastic fibre assembly by transiently transfected cells

The presence of elastic fibres was probed in ARPE-19 cells and dermal fibroblasts that were transfected with pCI-neo-WT or pCI-R515A after the cultures had established a microfibrillar network, i.e. on days 14 and 10 of culture, respectively. Confocal images were taken in the 500-550 nm range, which captured elastin-specific staining, and in the 600-650 nm range, which reflected sample autofluorescence.

At 1, 4, 7 and 10 days after transfection, ARPE-19 cells transfected with pCI-neo containing either the WT or R515A sequence exhibited no visible elastic fibre formation (Figure 3.27). All sample images showed a diffused background fluorescence without any defined structure similar to those of control cells transfected with the empty pCI-neo.

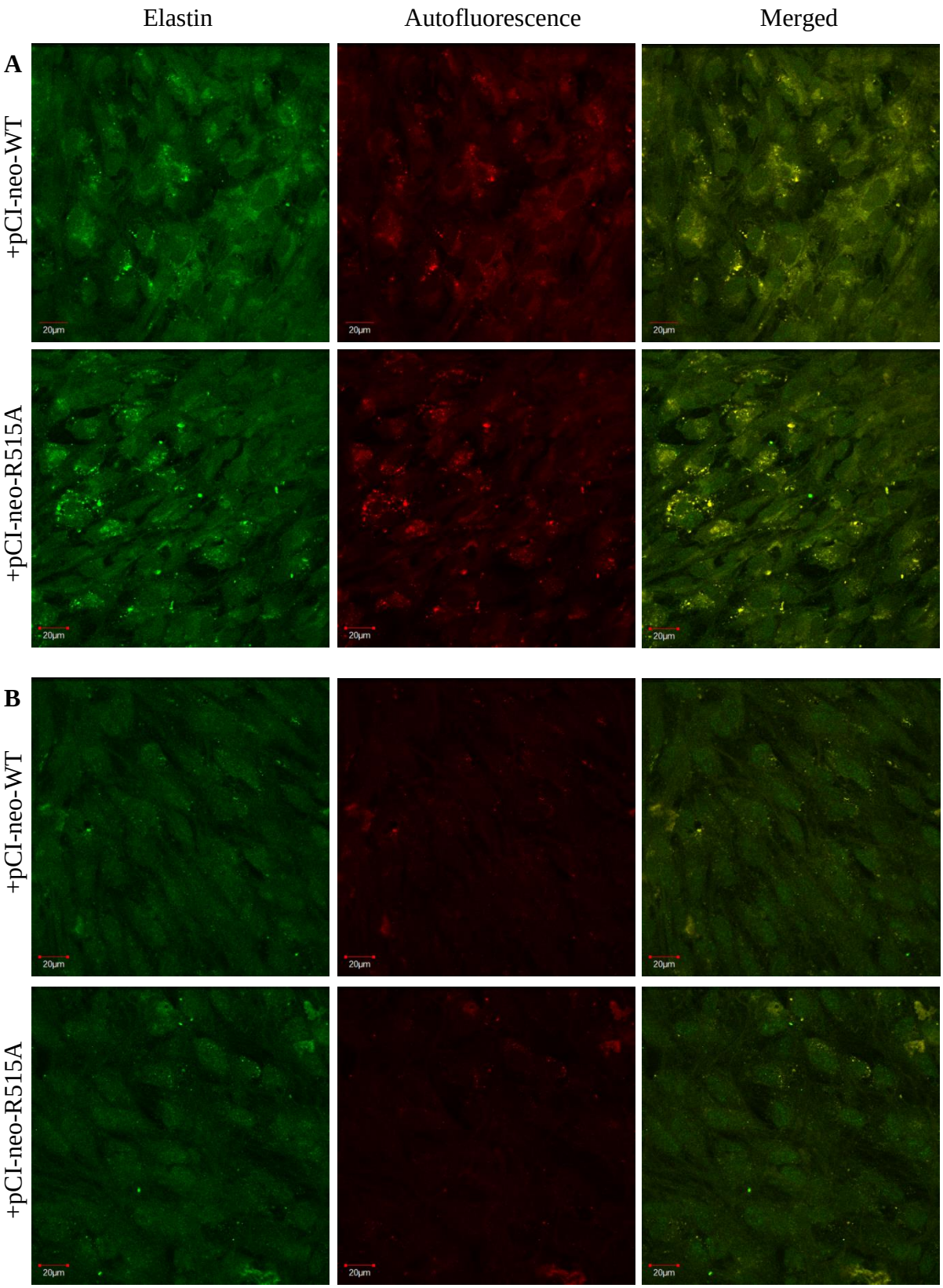
Elastin
Autofluorescence
Merged
A
+pCI-neo-WT
+pCI-neo-R515A
B
+pCI-neo-WT
+pCI-neo-R515A
20µm

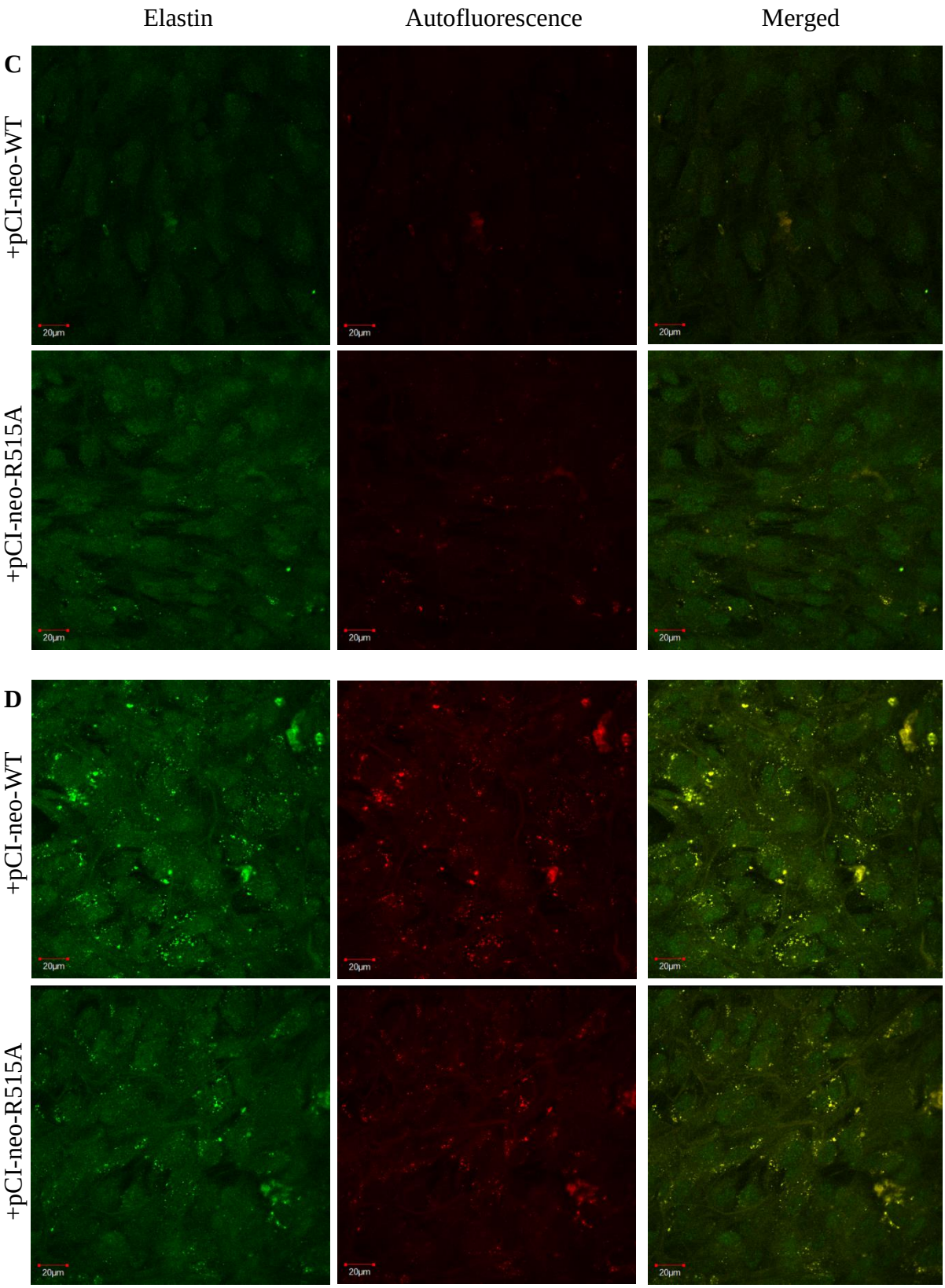
Elastin
Autofluorescence
Merged
C
+pCI-neo-WT
+pCI-neo-R515A
D
+pCI-neo-WT
+pCI-neo-R515A
20µm

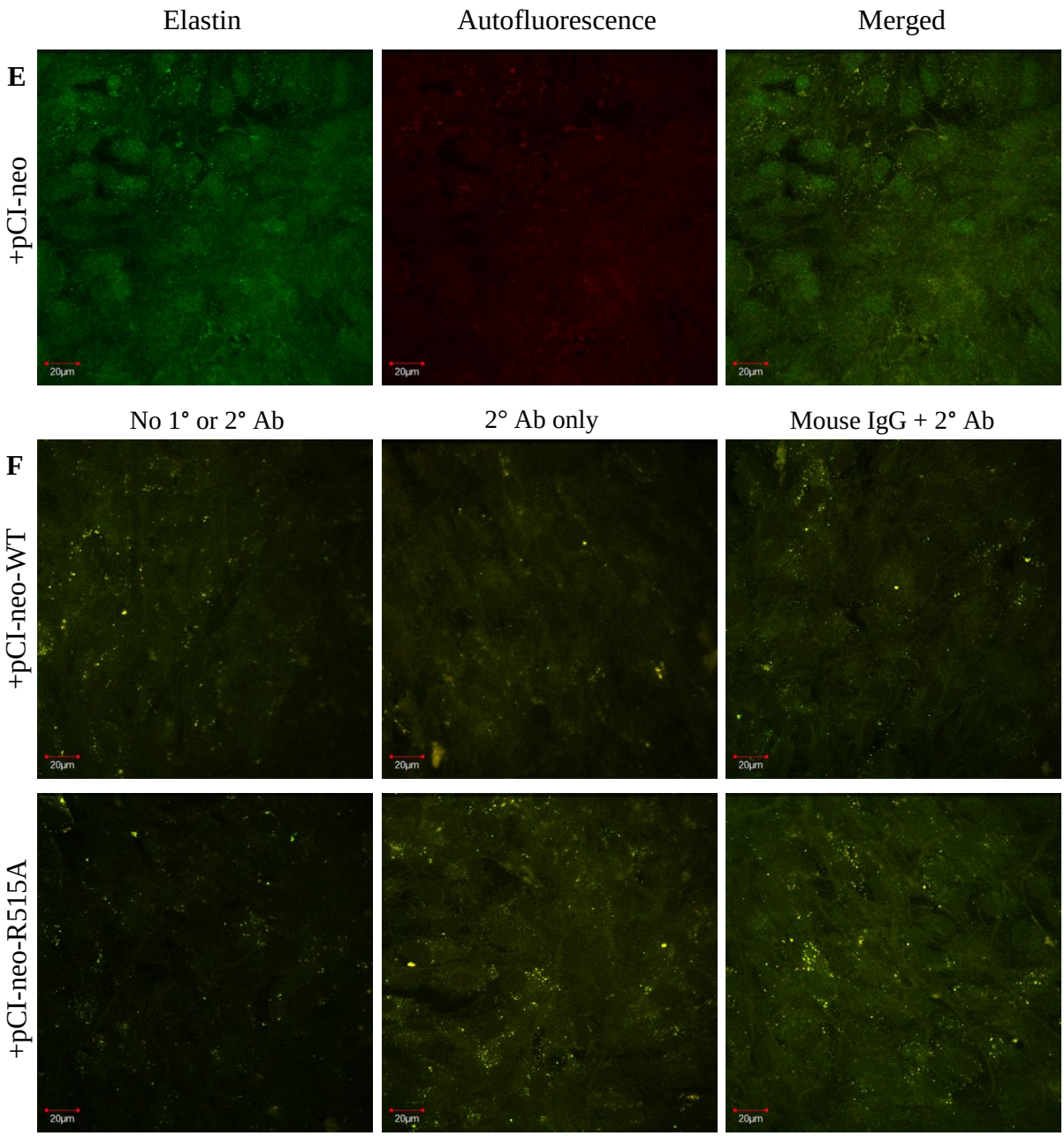

Figure 3.27. Confocal images of WT and R515A transfected ARPE-19 cells stained for elastin with the mouse BA4 and FITC-conjugated anti-mouse antibodies. Images show FITC fluorescence, autofluorescence, and merged channels (A) 1, (B) 4, (C) 7 and (D) 10 days after transfection. (E) Cells 10 days after transfection with the empty pCI-neo vector. (F) Staining controls: no primary or secondary antibody; FITC-conjugated secondary antibody only; non-specific mouse IgG and FITC-conjugated secondary antibody. Controls show images from merged FITC and autofluorescence channels.

In contrast, transiently transfected GM3348 dermal fibroblasts produced fine fibres that were detected by elastin immunostaining (Figure 3.28). However, the faint fibres necessitated visualisation under a high laser power, which also intensified background fluorescence. To isolate these fibres, structures that emitted visibly higher elastin-specific fluorescence than autofluorescence, and hence appeared green rather than yellow/orange on the merged images, were identified.

Fine fibre structures with similar abundance and morphology were seen in both WT and R515A transfected cells at 1, 4 and 7 days after transfection. No such fibres were observed in the samples 10 days after transfection. These structures were also absent in cells transfected with the empty pCI-neo vector and in the staining controls.

Similar results were demonstrated in transiently transfected NHF8909 neonatal human fibroblasts (Figure 3.29). Fibrous assemblies that exhibit elastin-specific staining were present in transfected cells within 7 days after transfection. The fibres were indistinguishable between WT and R515A samples, and were not seen in vector-transfected cells and unstained controls.

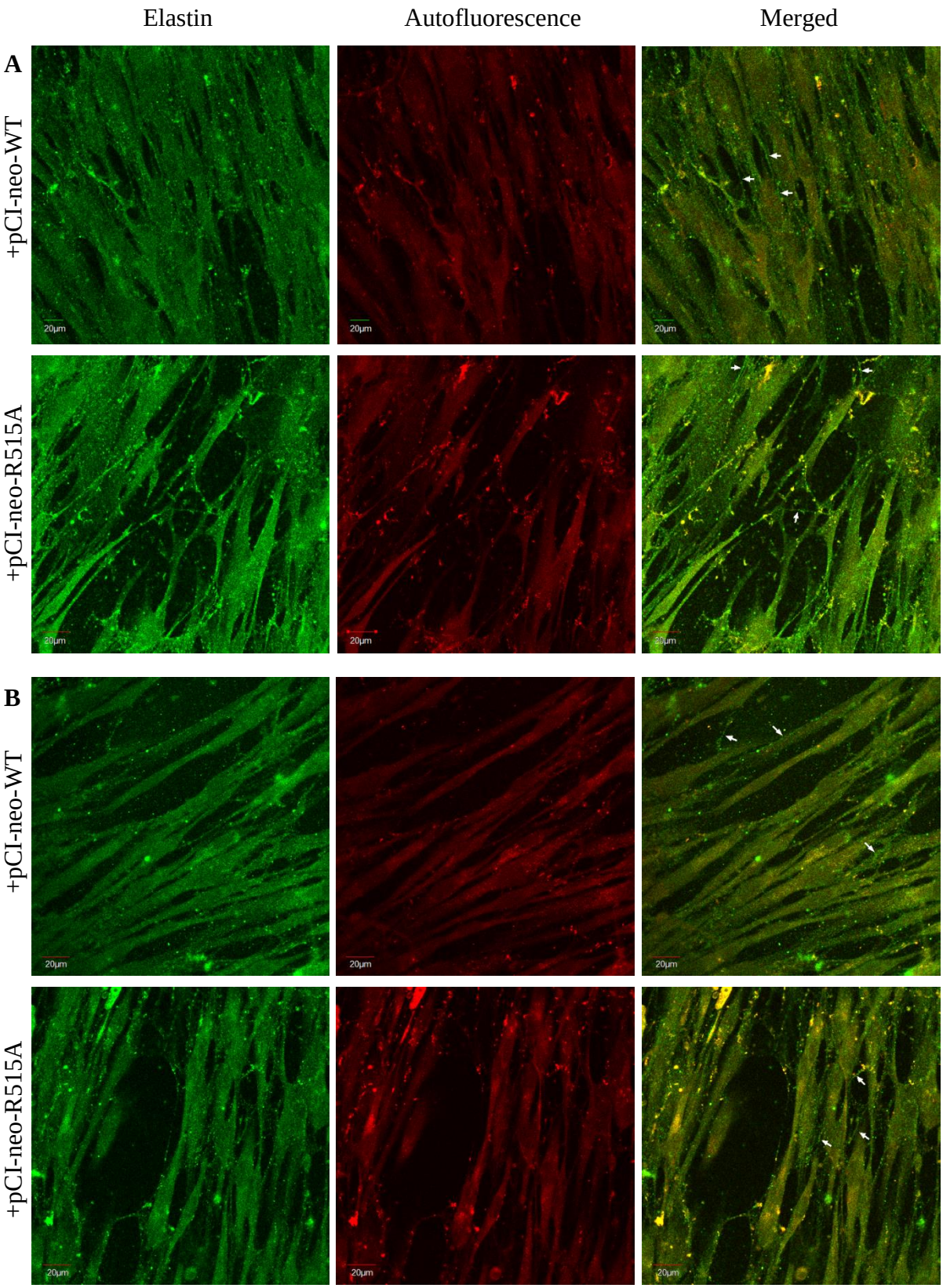
Elastin
Autofluorescence
Merged
A
+pCI-neo-WT
+pCI-neo-R515A
B
+pCI-neo-WT
+pCI-neo-R515A
20µm

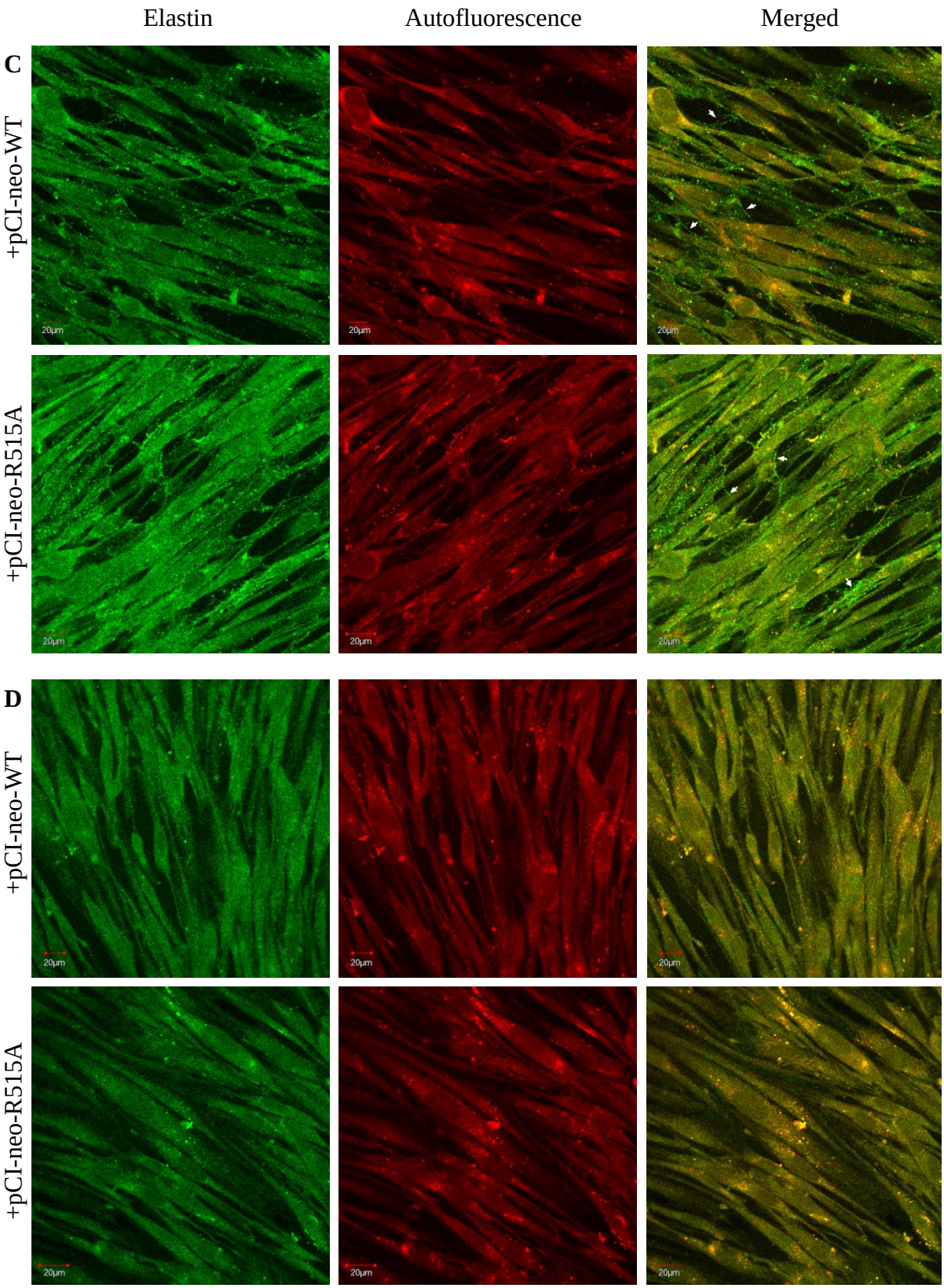
Elastin
Autofluorescence
Merged
C
+pCI-neo-WT
+pCI-neo-R515A
D
+pCI-neo-WT
+pCI-neo-R515A
20µm

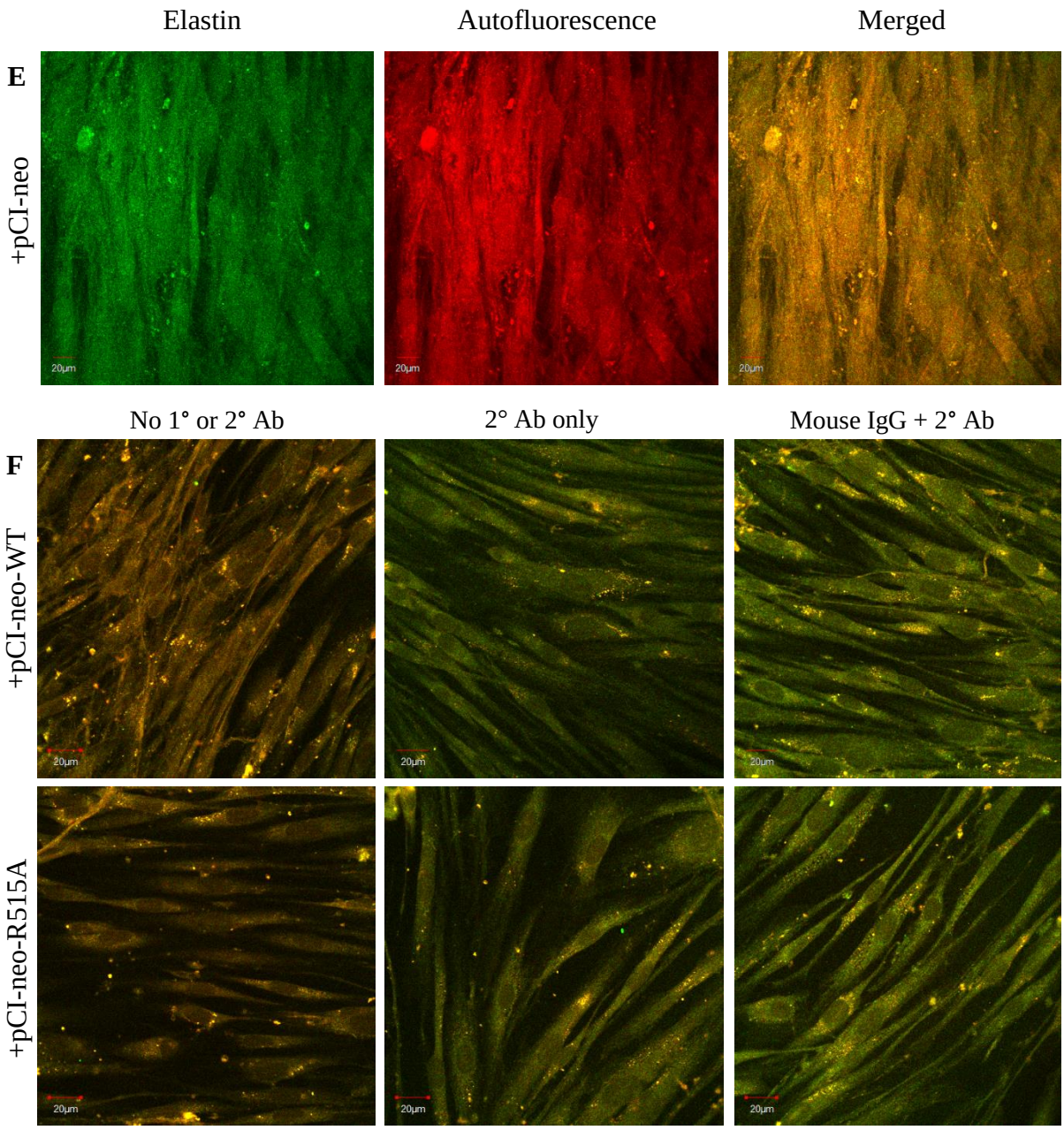

Figure 3.28. Confocal imaging of WT and R515A transfected GM3348 cells stained for elastin with the mouse BA4 and FITC-conjugated anti-mouse antibodies. Images show FITC fluorescence, autofluorescence, and merged channels (A) 1, (B) 4, (C) 7 and (D) 10 days after transfection. Elastic fibres are indicated by arrows in the merged channel. (E) Cells 10 days after transfection with the empty pCI-neo vector. (F) Staining controls: no antibody; FITC-conjugated antibody only; mouse IgG and FITC-

conjugated antibody. Controls show images from merged FITC and autofluorescence channels.

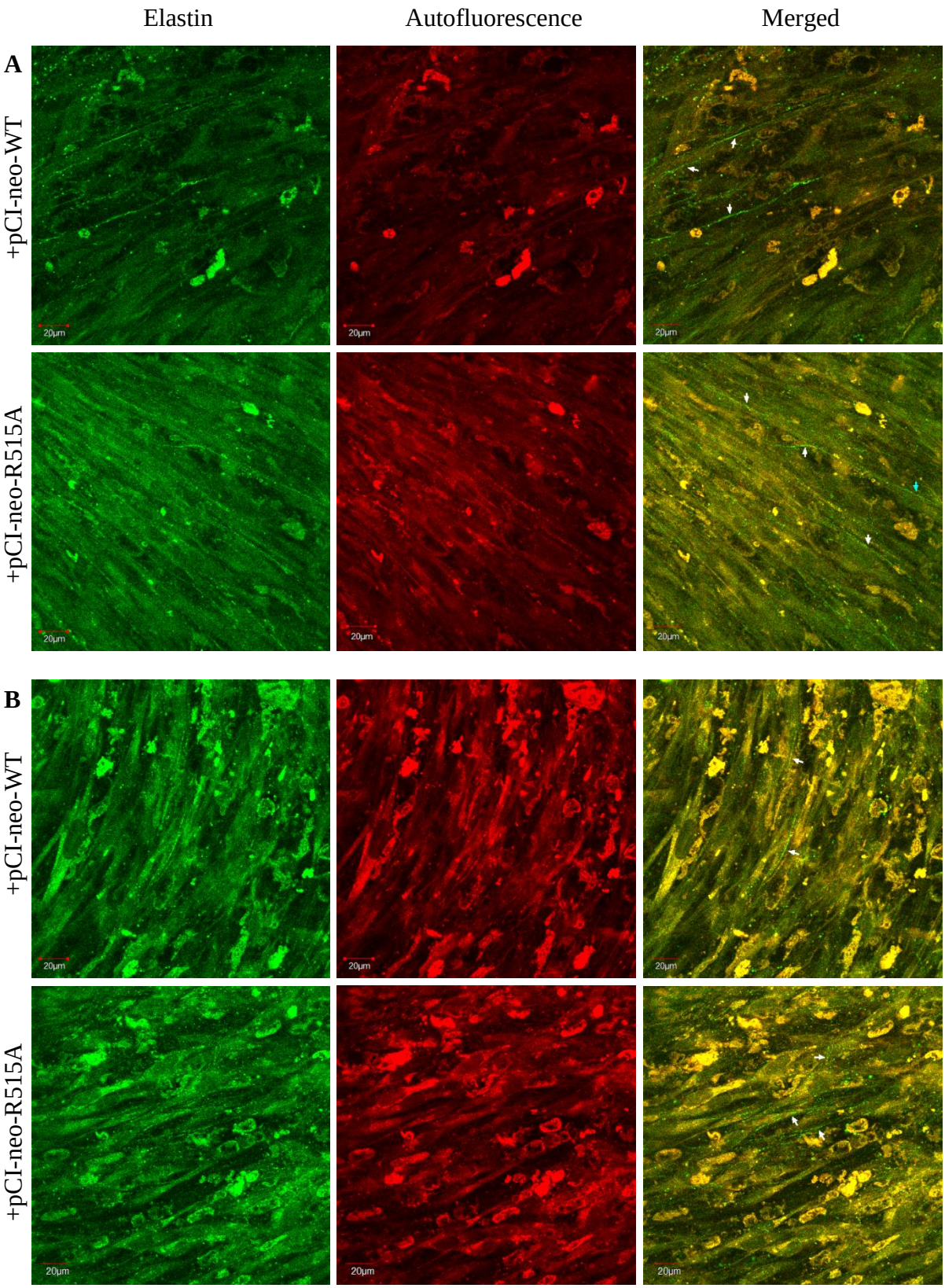
Elastin
Autofluorescence
Merged
A
+pCI-neo-WT
+pCI-neo-R515A
B
+pCI-neo-WT
+pCI-neo-R515A
20µm

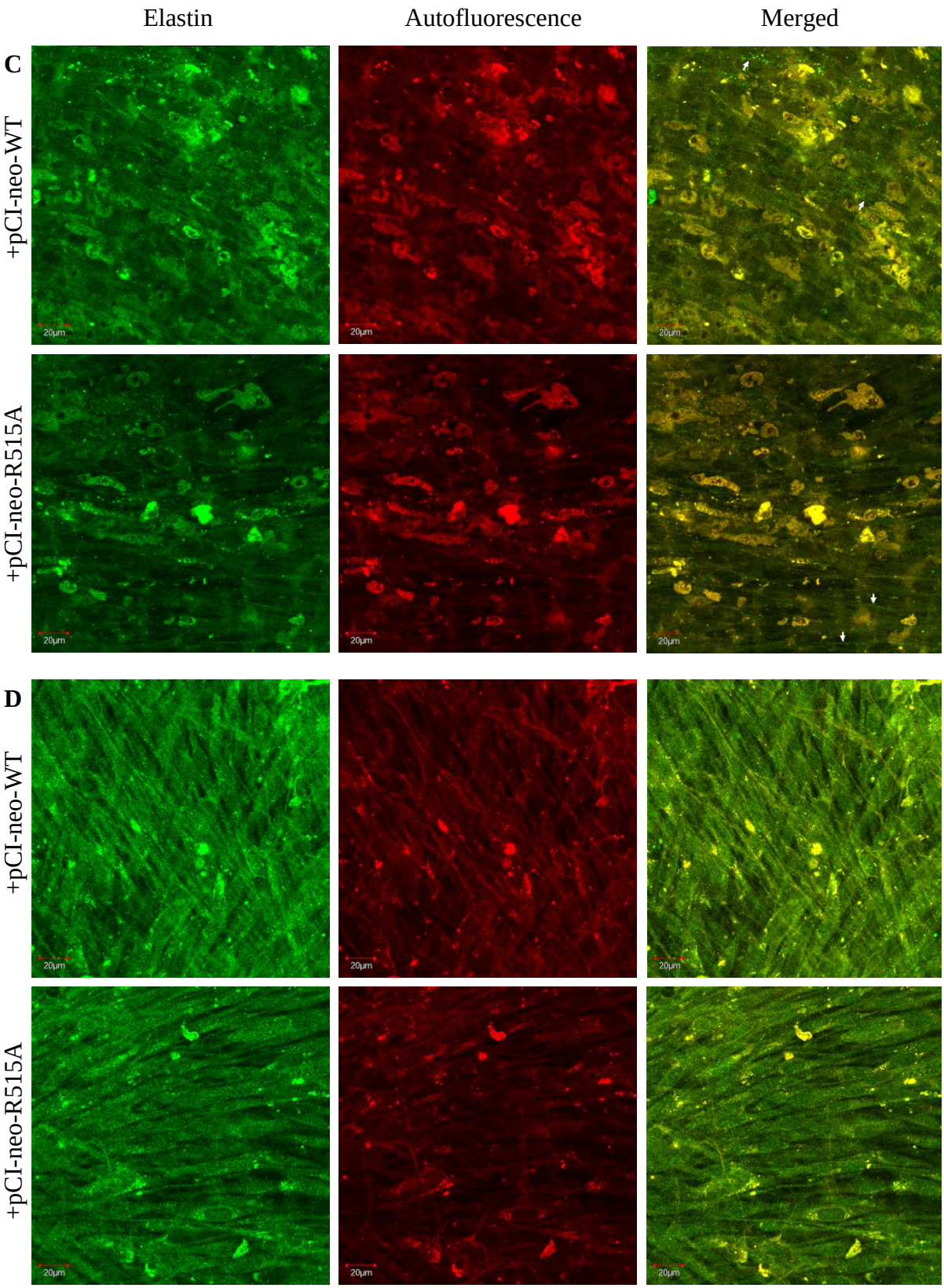
Elastin
Autofluorescence
Merged
C
+pCI-neo-WT
+pCI-neo-R515A
D
+pCI-neo-WT
+pCI-neo-R515A
20µm

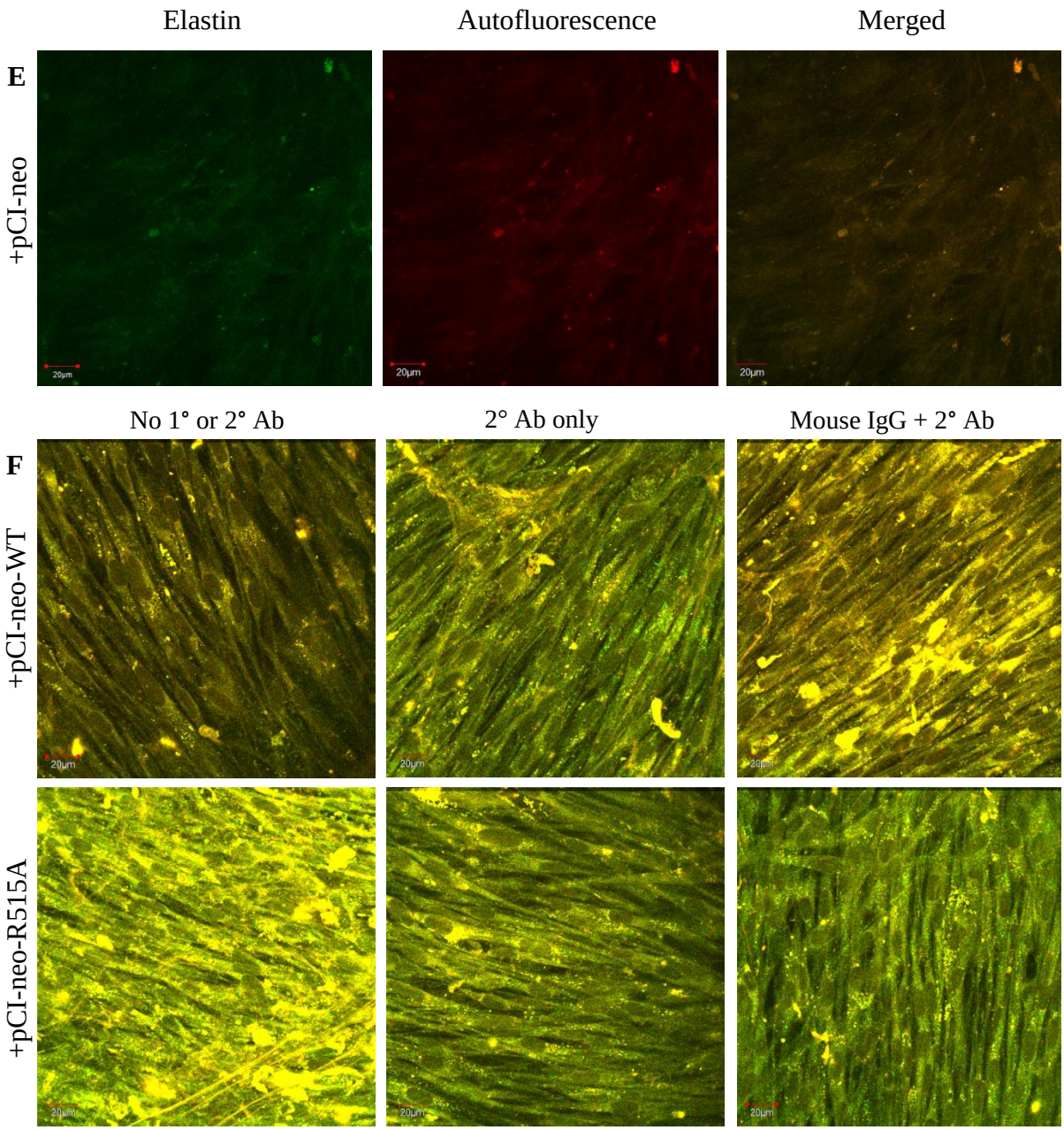

Figure 3.29. Confocal imaging of WT and R515A transfected NHF8909 cells stained for elastin with the mouse BA4 and FITC-conjugated anti-mouse antibodies. Images show FITC fluorescence, autofluorescence, and merged channels (A) 1, (B) 4, (C) 7 and (D) 10 days after transfection. Elastic fibres are indicated by arrows in the merged channel. (E) Cells 10 days after transfection with the empty pCI-neo vector. (F) Staining controls: no antibody; FITC-conjugated antibody only; mouse IgG and FITC-

conjugated antibody. Controls show images from merged FITC and autofluorescence channels.

3.3.4.5 Fluorescence lifetime imaging of elastic fibres

Fluorescence lifetime imaging was utilised to confirm the nature of the fibre structures observed in the transfected fibroblasts at early time points. Fluorescence lifetimes were acquired for distinct regions within the cell and extracellular milieu to establish characteristic profiles of various fluorescent components. These values were compared among untransfected, WT- and R515A- transfected cells, and cells with defined elastic fibres derived from exogenously added tropoelastin.

A single fluorescence lifetime was observed within the DAPI-stained cell nuclei of all samples. This value, averaging 2.7 ns, was not significantly different among the samples (Figure 3.30A).

Background fluorescence lifetimes were then obtained from regions within the extracellular space that did not encompass putative elastic fibres. A number of fluorescence lifetime peaks were recorded, most likely corresponding to different autofluorescent extracellular components. Three distinct fluorescent lifetimes at 1.1-1.2 ns, 1.5-1.6 ns and 1.8-1.9 ns appeared consistently in all samples, with an additional lifetime at 0.9 ns detected in the untransfected sample (Figure 3.30B).

Fluorescence lifetimes were subsequently acquired for extracellular regions containing the previously described fine fibres (Figure 3.30C). Several lifetime peaks were obtained for each sample: 0.9, 1.2, 1.8 and 2.3 ns in WT-transfected cells; 1.1, 1.5, 1.8, 2.2 ns in R515A-transfected cells; and 1.5, 1.9, 2.4 ns in cells with defined elastic fibres. With the exception of the 2.2-2.4 ns peak, the other fluorescence lifetimes could be attributed to non-specific background values. This ~2.3 ns lifetime was not observed in untransfected

cells and has been attributed to elastin [204], supporting identification of the fine fibre structures as elastic fibres.

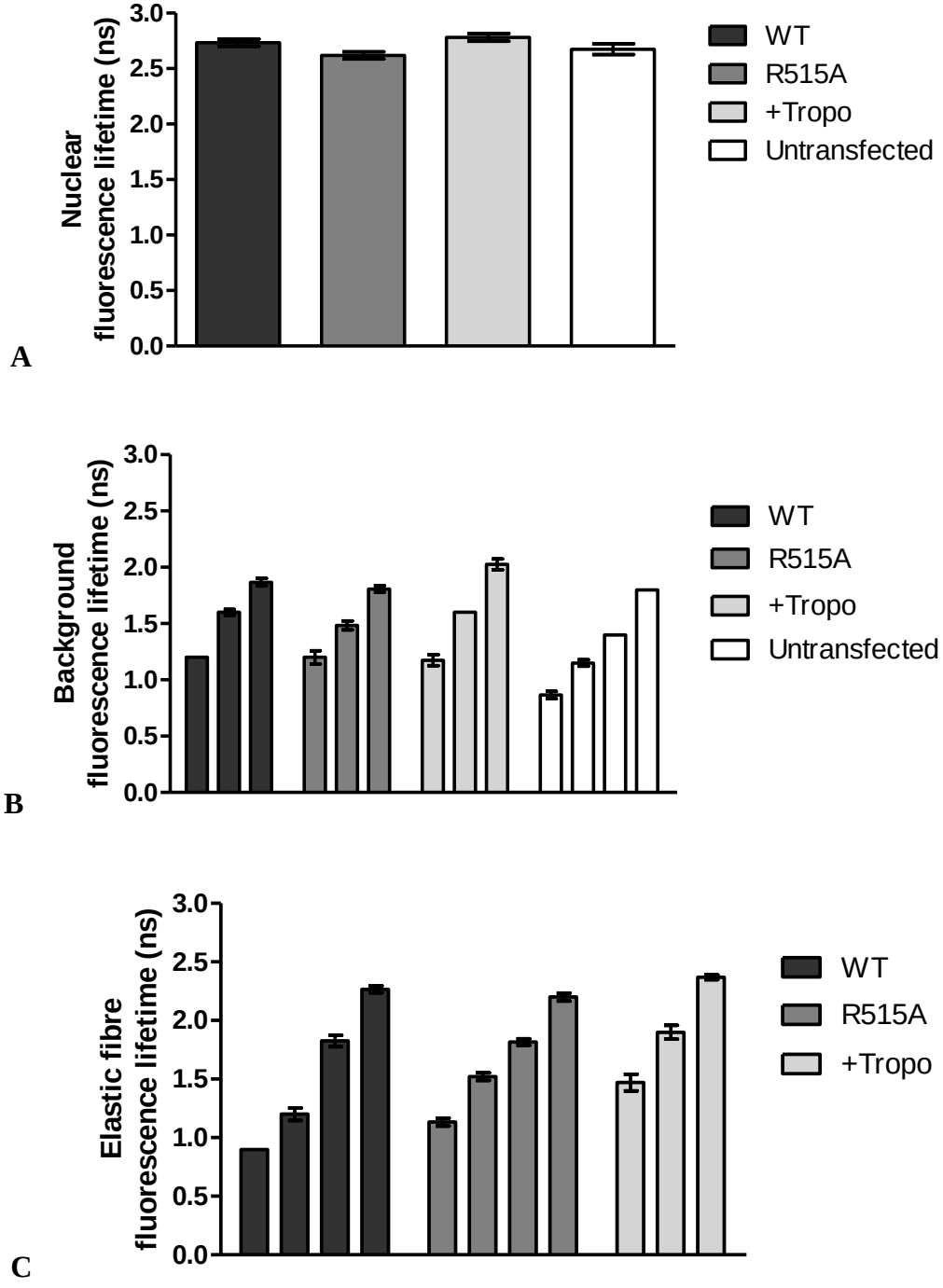

Figure 3.30. Fluorescence lifetime imaging of WT and R515A transfected GM3348 cells. Untransfected cells and cells with tropoelastin added into the culture medium were respectively treated as the negative and positive controls for elastic fibre formation.

Fluorescence lifetimes were acquired from areas containing (A) cell nuclei, (B) extracellular space and (C) elastic fibres.

3.3.5 Addition of tropoelastin to the extracellular matrix of cells

3.3.5.1 Optimisation

Purified WT and R515A tropoelastin constructs were confirmed via SDS-PAGE to be of the expected size (60 kDa) and free from degradation (Figure 3.31).

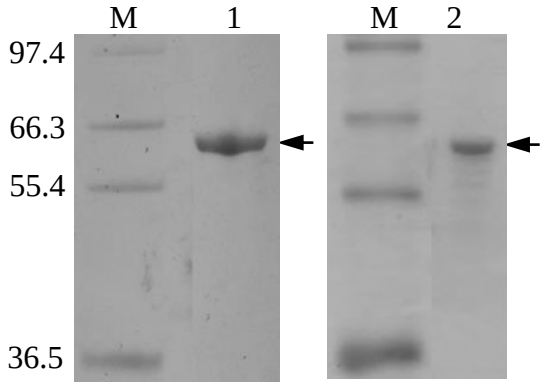

Figure 3.31. SDS-PAGE of purified WT and R515A tropoelastin showing a ~60 kDa band corresponding to the full-length construct. Lanes: M – Mark12 protein standards (kDa); 1 - WT; 2 – R515A.

Elastic fibres formed from WT and R515A tropoelastin monomers added to the cell culture medium were to be detected using an elastin-specific BA4 antibody. The optimum concentration of BA4 required for staining was determined by targeting elastic fibres with increasing dilutions of the antibody. All tested concentrations of BA4 allowed visualisation of WT and R515A elastic fibres; although a 1:600 antibody dilution resulted in noticeably fainter staining, particularly in thinner fibres (Figure 3.32). A 1:500 dilution of BA4 was selected for subsequent elastic fibre detection.

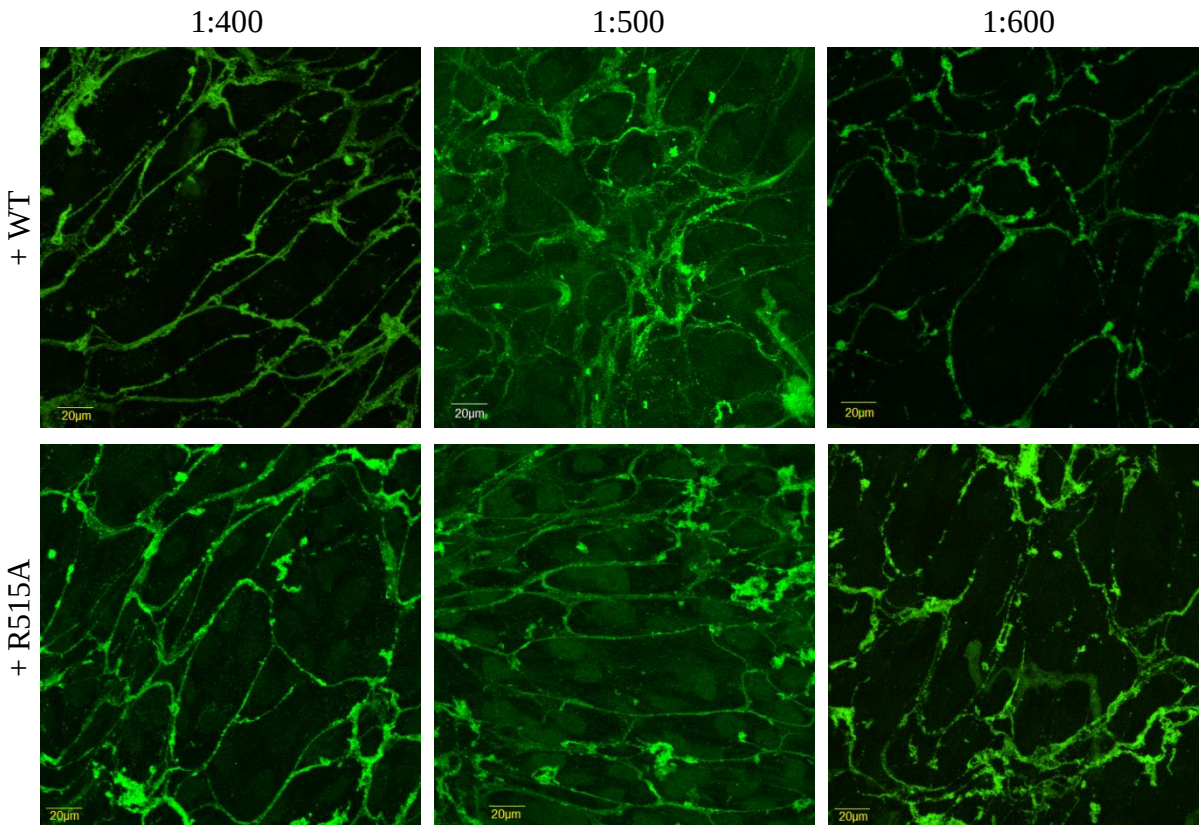

Figure 3.32. Elastic fibres formed by ARPE-19 cells seven days after the addition of 200 µg/mL WT or R515A tropoelastin to the culture medium. The fibres were visualised with 1:400, 1:500 or 1:600 dilutions of the BA4 anti-elastin antibody followed by a 1:500 dilution of FITC-conjugated anti-mouse antibody.

The optimum concentration of tropoelastin to be added to the culture media was determined. The amount of exogenously added WT or R515A directly correlated to the quantity and fluorescence of resulting elastic fibres (Figure 3.33). At the lowest tropoelastin concentration of 4 µg/mL, both WT and R515A fibres were insufficiently defined to allow proper characterisation. A higher tropoelastin concentration of 20 µg/mL was selected for subsequent experiments to magnify potential differences between WT and R515A elastic fibres and allow better comparative analyses of fibre formation.

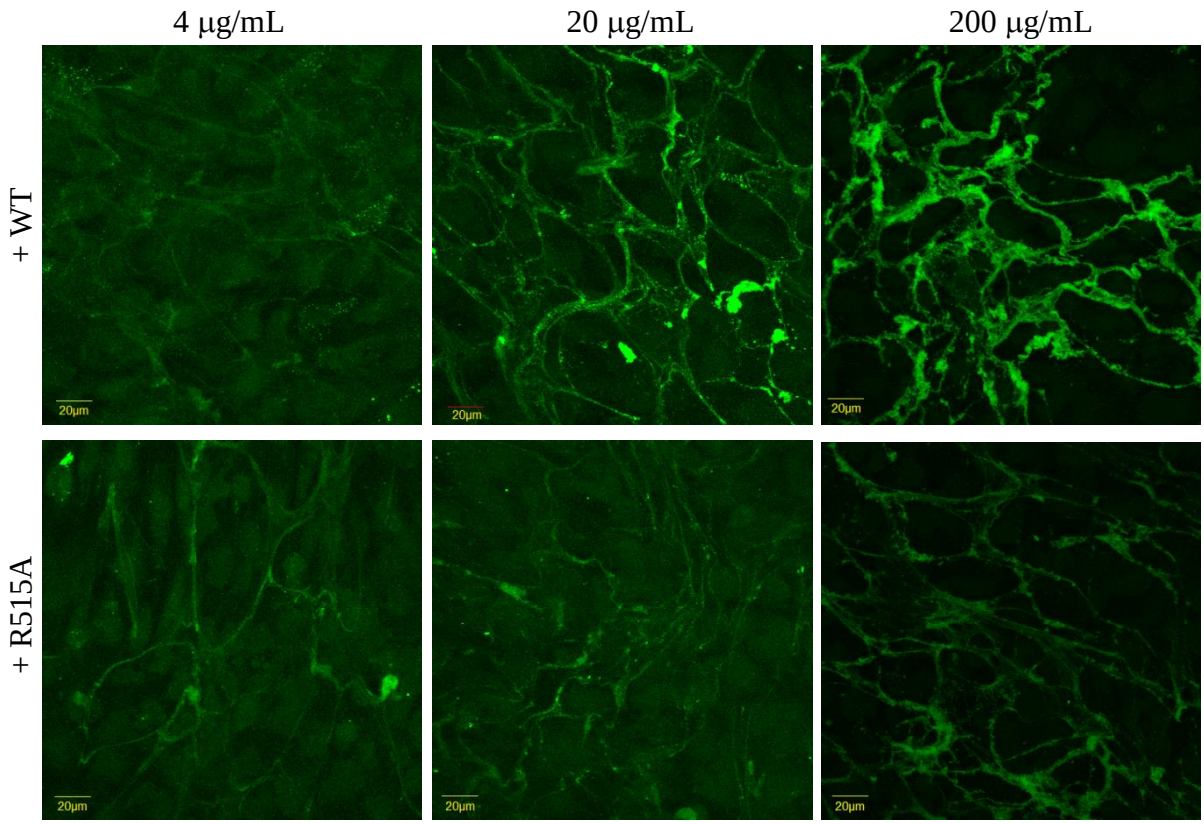

Figure 3.33. Elastic fibres assembled by ARPE-19 cells from 4, 20 or 200 μg/mL of exogenously added WT or R515A. Elastic fibres were visualised 7 days after tropoelastin addition with the BA4 anti-elastin and FITC-conjugated anti-mouse antibodies.

3.3.5.2 Elastic fibre assembly from exogenous tropoelastin

In the presence of an established microfibrillar network, addition of WT or R515A to the culture medium of ARPE-19 cells enabled incorporation of the tropoelastin constructs into elastic fibres (Figure 3.34). However, the time course of fibre formation and the properties of the resulting fibres were significantly different between WT and R515A. One day after tropoelastin addition, WT spherules had arranged linearly while R515A particles remained dispersed across the extracellular environment. By four days, an extensive branched network of WT elastic fibres had formed, which persisted with comparable abundance and a similar morphology through the 10-day experimental period. In contrast, R515A elastic fibres were 34-45% fewer in number, stained 27-36% less intensely, and displayed 24-35% decreased autofluorescence compared to WT fibres (Figure 3.35). This trend was consistent at 4, 7 and 10 days after tropoelastin addition. No elastic fibres were seen when tropoelastin was not added to ARPE-19 cells.

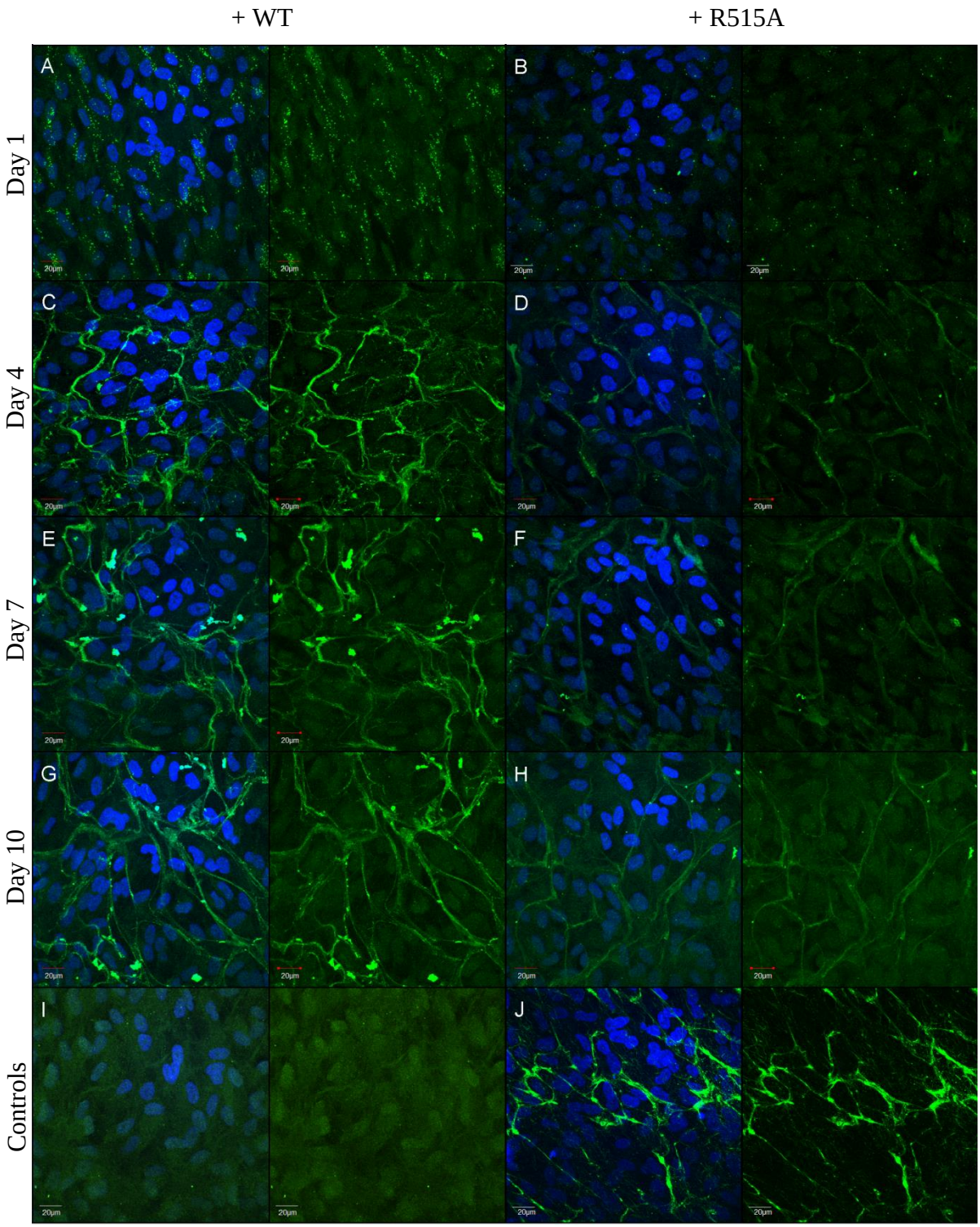

Figure 3.34. (A-H) ARPE-19 cells with 20 µg/mL WT or R515A tropoelastin added to the culture media 14 days post-seeding. The cells were fixed at 1, 4, 7 and 10 days after tropoelastin addition. Elastin fibres were stained with BA4 and FITC-conjugated secondary antibody. Cell nuclei were stained with DAPI. (I) ARPE-19 cells with no

tropoelastin in the culture media. (J) Microfibrils prior to tropoelastin addition, stained with anti-fibrillin-1 and FITC-conjugated secondary antibody. Each pair of images represents the same field of view; the left image shows merged DAPI and FITC channels while the right image shows the FITC channel only.

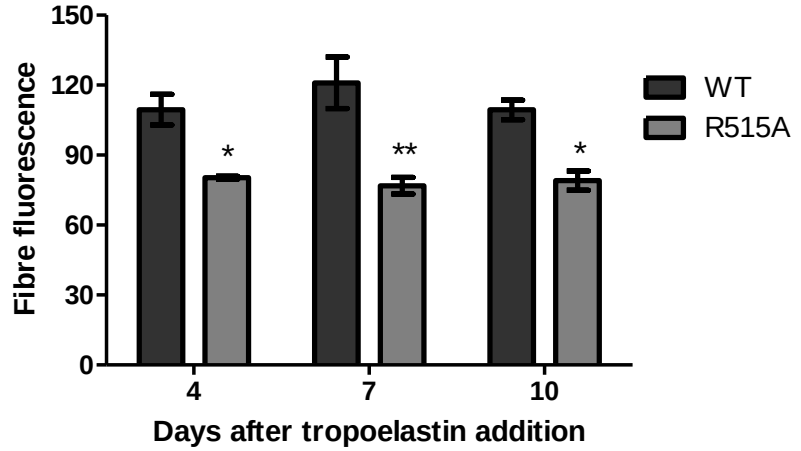

A

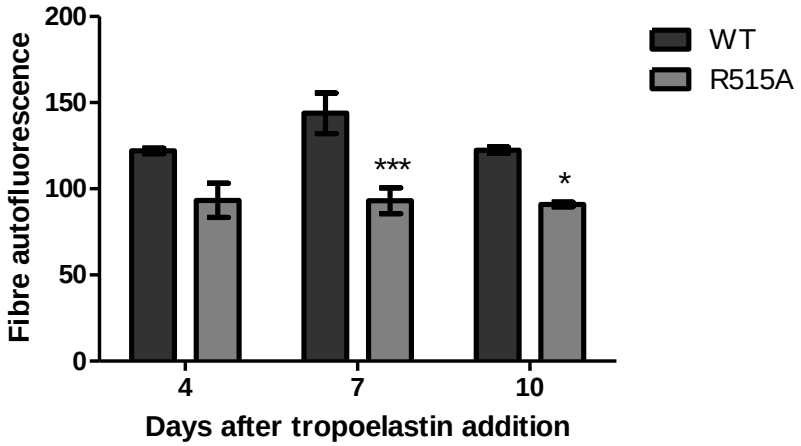

B

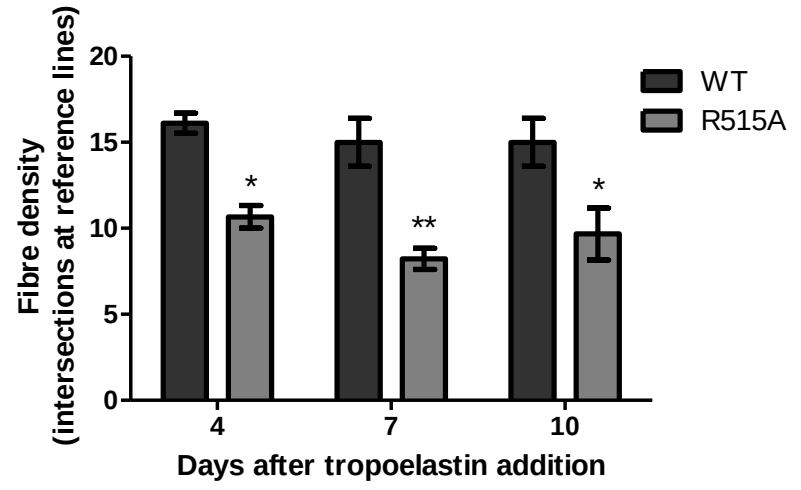

C

Figure 3.35. Characterisation of fluorescence, autofluorescence and density of WT and R515A elastic fibres in ARPE-19.

The differences between WT and R515A elastic fibre formation were magnified in the fibroblast systems. In both GM3348 and NHF8909 cells with developed microfibrils, WT followed the previously described elastogenic time course, with particles organised linearly one day after tropoelastin addition and a well-defined network appearing by four days. Remarkably, R515A remained as punctate species and did not assemble into elastic fibres in GM3348 cells (Figure 3.36), while it formed only faint individual fibres in NHF8909 cells (Figure 3.37).

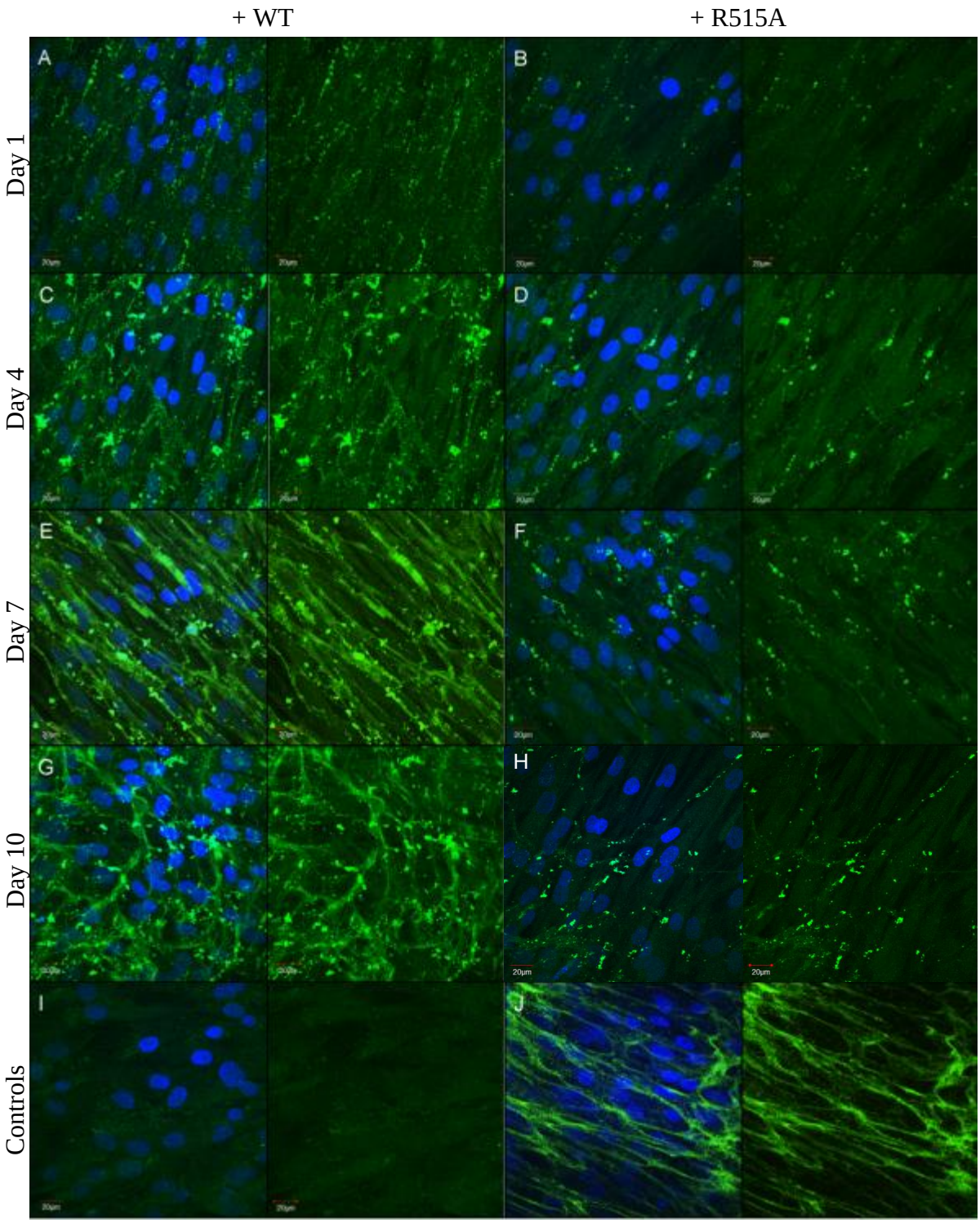

Figure 3.36. (A-H) GM3348 cells with 20 µg/mL WT or R515A tropoelastin added to the culture media 10 days post-seeding. The cells were fixed at 1, 4, 7 and 10 days after tropoelastin addition. Elastin fibres were stained with BA4 and FITC-conjugated secondary antibody. Cell nuclei were stained with DAPI. (I) GM3348 cells with no

tropoelastin in the culture media. (J) Microfibrils prior to tropoelastin addition, stained with anti-fibrillin-1 and FITC-conjugated secondary antibody. Each pair of images represents the same field of view; the left image shows merged DAPI and FITC channels while the right image shows the FITC channel only.

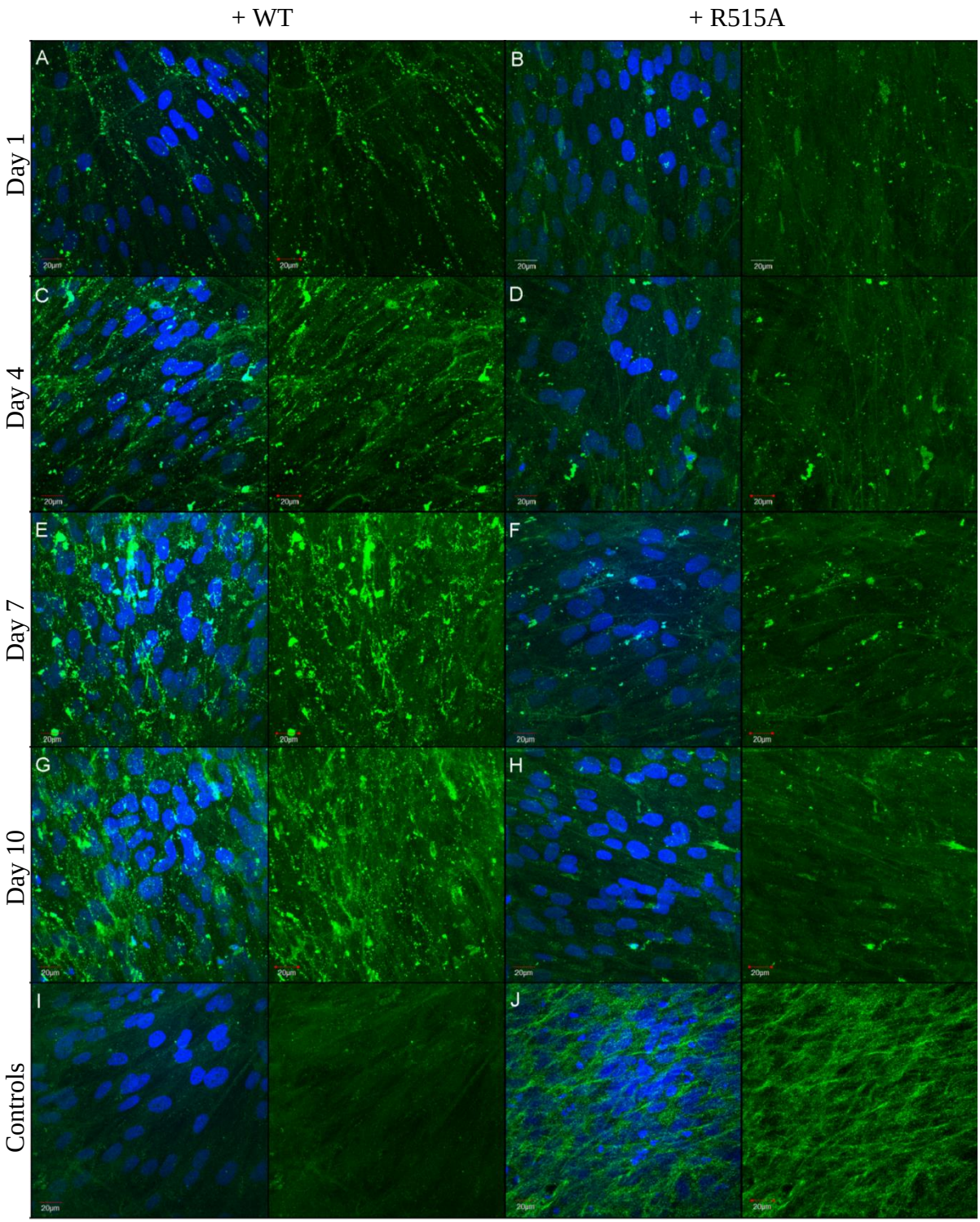

Figure 3.37. (A-H) NHF8909 cells with 20 µg/mL WT or R515A tropoelastin added to the culture media 10 days post-seeding. The cells were fixed at 1, 4, 7 and 10 days after tropoelastin addition. Elastin fibres were stained with BA4 and FITC-conjugated secondary antibody. Cell nuclei were stained with DAPI. (I) NHF8909 cells with no

tropoelastin in the culture media. (J) Microfibrils prior to tropoelastin addition, stained with anti-fibrillin-1 and FITC-conjugated secondary antibody. Each pair of images represents the same field of view; the left image shows merged DAPI and FITC channels while the right image shows the FITC channel only.

Interestingly, when the tropoelastin concentration was maintained throughout the experimental period by addition of fresh WT or R515A during every media change, there were no significant differences between the WT and R515A elastic fibres in ARPE-19 cells (Figure 3.38). An initial lag was observed on the day after the first tropoelastin addition, during which R515A spherules remained disorganised in the extracellular space unlike the linearly arranged WT species. Despite a decreased efficiency in early-stage elastogenesis, the developed R515A fibres exhibited similar fluorescence and density as WT fibres (Figure 3.39).

However, this rescue of elastogenic ability in R515A was not observed in GM3348 fibroblasts (Figure 3.40). Despite the maintained presence of R515A within the extracellular environment, the mutant construct remained as linearly-clustered punctate species and were unable to progress beyond this stage to form defined fibres.

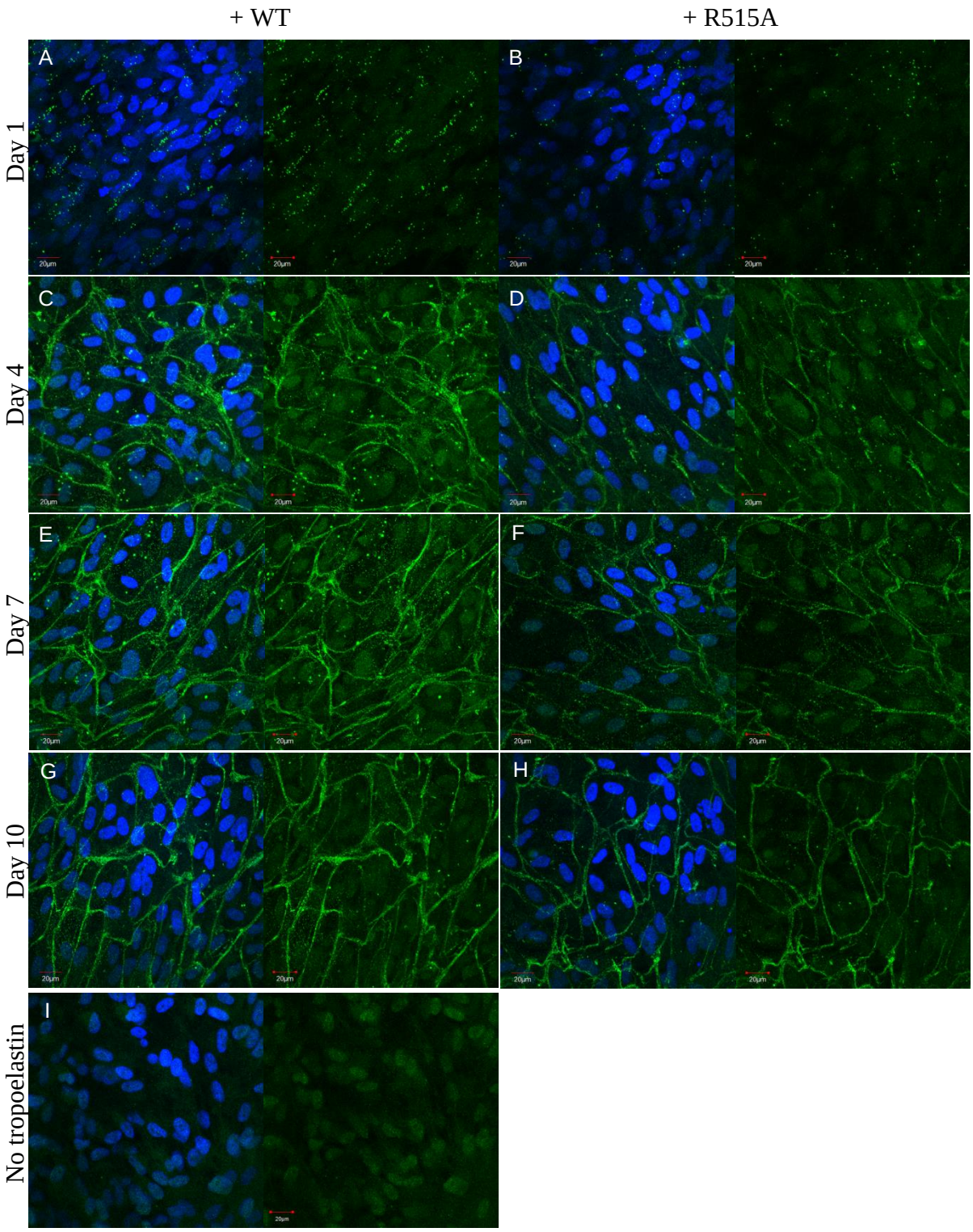

Figure 3.38. (A-H) ARPE-19 cells with 20 µg/mL WT or R515A tropoelastin added to the culture media 14 days post-seeding and supplemented every 2 days. The cells were fixed at 1, 4, 7 and 10 days after the initial tropoelastin addition. (I) ARPE-19 cells with no added tropoelastin. Elastin fibres were stained with BA4 and FITC-conjugated

secondary antibody. Cell nuclei were stained with DAPI. Each pair of images represents the same field of view; the left image shows merged DAPI and FITC channels while the right image shows the FITC channel only.

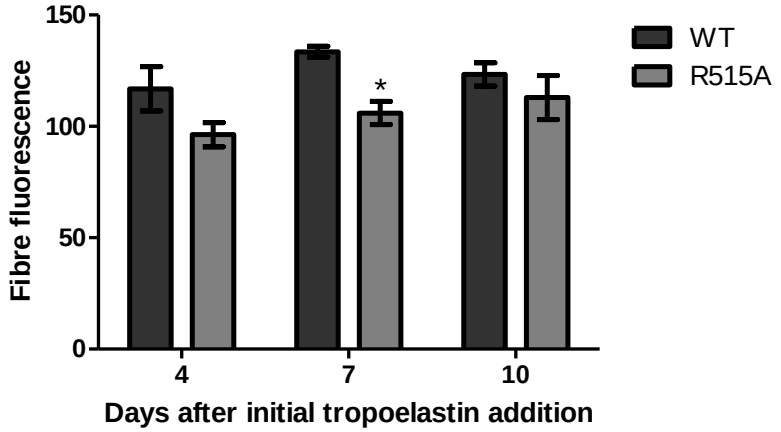

A

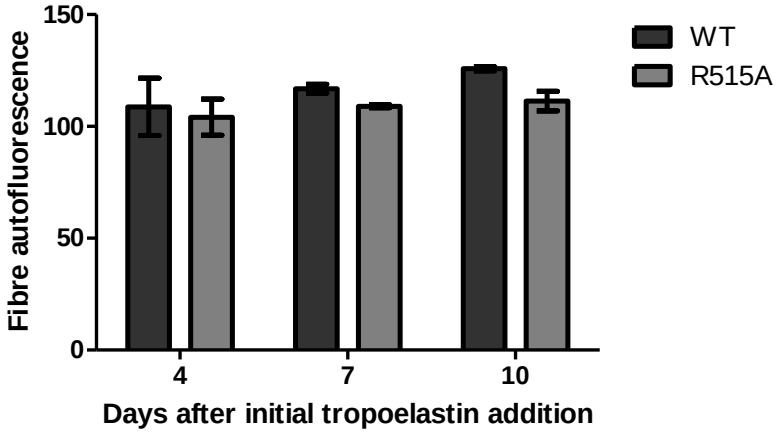

B

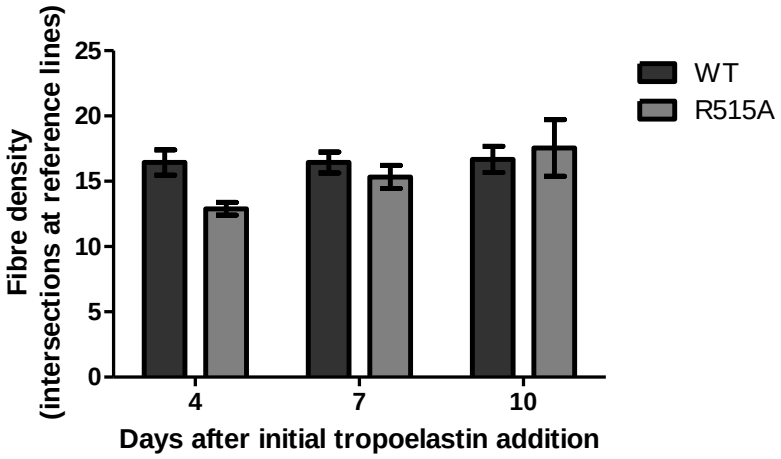

C

Figure 3.39. Characterisation of fluorescence, autofluorescence and density of WT and R515A elastic fibres formed by ARPE-19 cells. Tropoelastin was supplemented every two days after the initial addition.

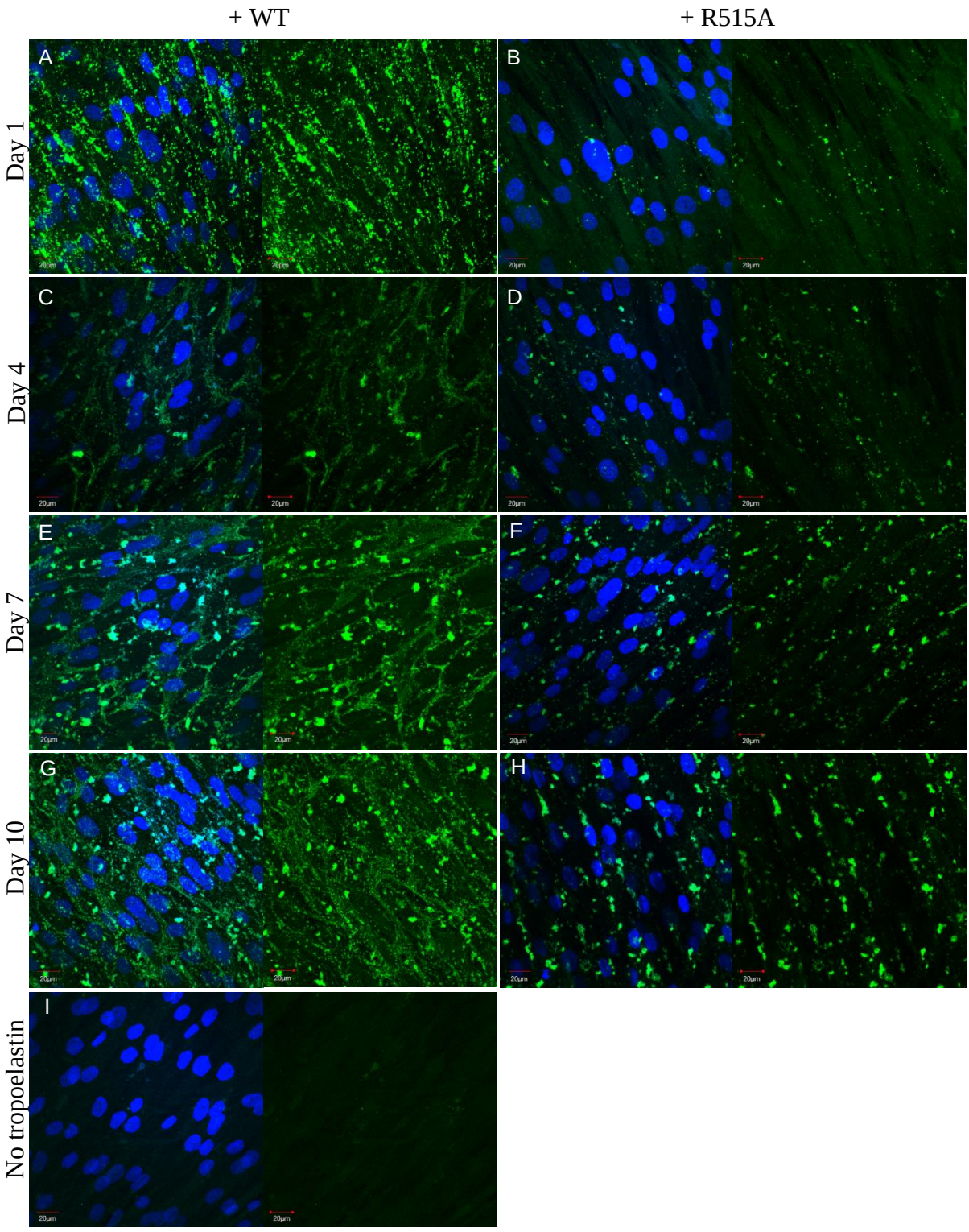

Figure 3.40. (A-H) GM3348 cells with 20 µg/mL WT or R515A tropoelastin added to the culture media 10 days post-seeding and supplemented every 2 days. The cells were fixed at 1, 4, 7 and 10 days after the initial tropoelastin addition. (I) GM3348 cells with no added tropoelastin. Elastin fibres were stained with BA4 and FITC-conjugated

secondary antibody. Cell nuclei were stained with DAPI. Each pair of images represents the same field of view; the left image shows merged DAPI and FITC channels while the right image shows the FITC channel only.

3.4 Discussion

3.4.1 Analysis of potential WT/R515A expression in a human host

The production of WT and R515A elastic fibres in a transfected human host system is reliant on successful expression and synthesis of the tropoelastin species. However, the WT and R515A cDNA sequences had been synthesised for optimal codon usage in *E. coli* [26] and may therefore have a significant number of 'rare' codons that can hamper expression in human cells. The predictive level of WT and R515A expression in a human host was provided by their CAI, which measures the deviation of coding sequences against a reference set of highly-expressed genes [205]. The CAI assumes that highly-expressed genes selectively use codons for tRNA species that are abundant in the cell. The CAI of WT and R515A were identical, implying a similar likelihood of expression in the human system. The CAI of WT/R515A (0.55) was only slightly lower than that calculated for endogenous human tropoelastin (0.68), indicating likely success of WT/R515A expression in human cells.

The WT and R515A sequences contained 12% of codons with a computed value below 30, the threshold set by the algorithm to represent codons with low usage frequency for a given amino acid. The endogenous human tropoelastin transcript also had a small percentage of codons in this category, which may reflect the tightly regulated nature of native tropoelastin expression [80, 81].

In the genome of a number of species including humans, coding sequences are associated with a higher GC content, with sharp changes in GC content observed at the transcription boundaries [206, 207]. The GC contents of the WT and R515A sequences were comparable to that of the endogenous tropoelastin sequence and within the range exhibited by human genes. This supports the potential for heterologous WT and R515A expression in human cells.

3.4.2 Construction of an expression vector containing WT/R515A

The intracellular introduction of WT and R515A tropoelastin into a human system firstly required cloning each sequence into a mammalian cell-specific pCI-neo expression vector.

3.4.2.1 Cohesive-end cloning

The first cloning strategy utilised PCR to engineer distinct restriction sites at the termini of the tropoelastin sequence, which would allow directional ligation into the pCI-neo vector after digestion with corresponding restriction enzymes [208]. The *Eco*RI and *Xba*I restriction sites selected to flank the tropoelastin sequences fulfilled a number of criteria. First, both restriction sites are present in the pCI-neo cloning region to enable ligation of complementary ends of the vector and insert sequences. Second, both sites are not located within the WT and R515A coding sequences, which prevents intragenic cleavage during restriction digestion to produce the cohesive ends for cloning. Third, both sites are recognised by restriction enzymes that exhibit sufficient activity under the same buffer and temperature conditions, in order to facilitate double digestion of vector and insert sequences. Finally, the *Eco*RI and *Xba*I restriction enzymes, unlike most endonucleases [209], are able to cleave at the restriction sites despite a location proximate to the termini of linear sequences.

PCR amplification of the WT and R515A sequences was largely specific, as indicated by a dominant band consistent with the expected size of the tropoelastin template. Subsequent digestion of the tropoelastin insert and pCI-neo vector with *Eco*RI and *Xba*I was also specific, as evidenced by a single product corresponding to the full-length tropoelastin sequence or the linearised vector. The DNA fragments were extracted from the electrophoretic gel, a method that has been demonstrated to increase sample yield while preserving purity for downstream purposes including ligation and transformation [210].

Ligation of the WT or R515A sequence with pCI-neo was expected to proceed directionally due to the preferential annealing of complementary *Eco*RI or *Xba*I cohesive ends. Moreover, re-ligation of the vector should be hindered by the distinct overhanging sequences at both ends. However, screening of bacterial colonies transformed with the ligated constructs showed only the empty pCI-neo vector. This most likely signifies inefficient vector-insert ligation, which may be brought about by incompatible ends due to incomplete restriction digestion or non-functional restriction sites.

3.4.2.2 Direct cloning

To avoid the technical complexities of engineering restriction sites to flank the tropoelastin sequences, a second cloning approach was attempted to directly ligate the PCR-amplified WT or R515A template into the linearised pCI-neo vector. Digestion of pCI-neo by *Sma*I to produce blunt ends appeared to be complete and specific, as indicated by the single band corresponding to the size of the linear plasmid. To prevent spontaneous re-circularisation and re-ligation of the vector DNA, alkaline phosphatase was added to the digest reaction to catalyse the removal of 5′ phosphate groups [211, 212]. However, transformation of electrocompetent bacterial cells with the ligated constructs did not support colony formation on ampicillin selective media. This suggests no uptake of the antibiotic resistance-conferring pCI-neo, which in turn may be due to incomplete ligation of the vector and insert sequences. A likely cause is the non-complementarity of the PCR-amplified tropoelastin sequences with the blunt-ended pCI-neo due to the template-independent terminal transcriptase activity of Taq polymerase [213, 214]. This may have resulted in an overhanging adenosine in the insert sequences that proved incompatible with the linearised vector, despite the accompanying use of a proofreading enzyme with 3′ to 5′ exonuclease activity with the Taq polymerase.

3.4.2.3 Blunt-end cloning

The third cloning method used eliminated the need for PCR amplification of the insert sequences. Instead, the WT and R515A sequences were isolated by restriction digest from the pET-3d bacterial plasmid extracted from transformed *E. coli* stocks. The recessed 3′ ends were filled in using the Klenow fragment of DNA polymerase I [215], a widely-utilised technique to create blunt-ended sequences [216, 217]. The resulting constructs were ligated with the *Sma*I-digested pCI-neo vector. However, screening of the transformed colonies indicated only the presence of the empty vector, indicating unsuccessful incorporation of the WT and R515A sequence. This is consistent with the lower ligation efficiency of blunt-end sequences compared to those with staggered ends [218].

3.4.2.4 Linker-mediated cloning

An alternative cloning strategy employed linker sequences to attach the WT and R515A sequences to the pCI-neo vector. Linker sequences are short oligonucleotides containing recognition sites that can serve as receptors for DNA fragments with compatible cohesive ends [219]. Previous studies have documented the use of two different linker sequences to directionally clone a double-digested insert sequence into another double-digested vector, in which none of the restriction sites are complementary [220, 221]. In this instance, the *Eco*RI site of the pCI-neo vector was ligated to the 5′ *Nco*I site of the tropoelastin insert via an *Eco*RI-*Nco*I linker, while the 3′ *Bam*HI end of the insert was ligated to the *Xba*I cloning site of the vector via a *Bam*HI-*Xba*I linker. The efficiency of linker-mediated cloning was very high, with 100% of WT transformants and 80% of R515A transformants possessing the tropoelastin sequence as confirmed by plasmid restriction analysis and sequencing. The pCI-neo-WT and pCI-neo-R515A expression vectors were successfully constructed from this method.

3.4.3 Stable transfection

3.4.3.1 Validation of the ARPE-19 cell line

Mycoplasma commonly plagues up to 35% of cell cultures, inducing extensive alterations in cell metabolism and physiology without presenting visible morphological changes [222]. It exhibits resistance to most antibiotics and remains visually undetectable under the inverted microscope or by the turbidity of the culture media [223]. Infection can be uncovered using PCR primers that anneal to the evolutionarily conserved 16S rRNA of several mycoplasma species [224]. This method allows identification of mycoplasma at high specificity, sensitivity and accuracy. Through a PCR-based detection method, the ARPE-19 cells used in this study tested negative for mycoplasma contamination.

ARPE-19 is a stable cell line that arose spontaneously from cultured retinal pigmented epithelial cells, and also exhibits similar cellular characteristics to the primary cells [225]. The ARPE-19 cells used in this study had morphological features consistent with previous descriptions of the cell line. Furthermore, the cells showed expression of two retinal pigmented epithelium-specific markers, CRALBP and RPE65, at significantly higher levels than the background expression in control human dermal fibroblast cells. Both marker proteins are involved in the mammalian visual process. CRALBP is a carrier protein for the 11-*cis*-retinol or 11-*cis*-retinaldehyde ligands in visual pigment regeneration [226, 227]. On the other hand, RPE65 modulates the isomerization of 11-*trans* to 11-*cis*-retinol in the visual cycle [228, 229]. While CRALBP was expressed by early ARPE-19 cultures, RPE65 was expressed only by cells that had been cultured for 21 days. This level of expression is supported by previous findings of lower RPE65 expression in ARPE-19 cells compared to primary cultures, most probably due to changes induced by immortalisation and serial passaging of the cells [230]. Furthermore, synthesis of CRALBP and RPE65 is associated with retinal pigmented epithelial cell differentiation, a process that has been observed in

ARPE-19 after 3 weeks in culture [225]. These results indicate that the ARPE-19 cells used in this work display the expected properties of the cell line.

3.4.3.2 Expression of elastogenic components

The assembly of recombinant tropoelastin into elastic fibres in ARPE-19 cells greatly relies on the presence of other extracellular matrix components. ARPE-19 cells expressed essential elastogenic components including fibrillin-1 and lysyl oxidase consistent with previous findings [140, 201]. Fibrillin-1 is the core component of microfibrils [231], which are believed to act as a scaffold for tropoelastin deposition during elastic fibre formation [232]. As evidence, disruption of fibrillin-1 production resulted in the fragmentation and reduction of elastic lamellae in the aortic wall [233]. On the other hand, lysyl oxidase triggers cross-linking between specific tropoelastin lysine residues crucial for elastic fibre maturation [80, 234].

The expression levels of fibrillin-1 and lysyl oxidase in ARPE-19 cells differed from those in an elastogenic cell type such as dermal fibroblasts. Furthermore, minimal fibulin-5 expression was observed in ARPE-19. Fibulin-5 is reportedly located at the interface between elastin and microfibrils [150], and was initially proposed to facilitate adhesion of elastic fibres to the cell surface [125], although it has now been deemed unnecessary for elastogenesis. More recently, fibulin-5 has been shown to regulate tropoelastin deposition on microfibrils [133]. Its decreased presence in ARPE-19 cells may therefore negatively affect elastic fibre formation, although the possibility of functional compensation from other fibulin proteins remains unclear.

No endogenous tropoelastin transcripts were detected in ARPE-19 cells as previously described [140]. This indicates that elastic fibres assembled in this system would

be solely derived from recombinantly expressed or exogenously added tropoelastin, making ARPE-19 cell line useful for comparative studies on WT and R515A elastic fibre formation.

3.4.3.3 Transfection protocol

Transfection of ARPE-19 with pCI-neo-WT or pCI-neo-R515A was performed with Lipofectamine, a 3:1 (w/w) liposome formulation of the polycationic lipid 2,3-dioleyloxy-N-[2(sperminecarboxamido)ethyl]-N,N-dimethyl-1-propanaminium trifluoroacetate (DOSPA) and the neutral lipid dioleoyl phosphatidylethanolamine (DOPE) [235]. The use of cationic lipids for transfection utilises the cell membrane permeability of the lipid subunit and the DNA binding function of the charged unit [236]. The amount of vector DNA and lipid-to-DNA ratio required optimisation for efficient transfection. As was observed, a lower amount of vector DNA would decrease the gene expression of transfected cells, while an excessive amount would inhibit transfection [236]. Similarly, increasing the lipid:DNA ratio would increase transfection efficacy; however, significant toxicity may occur depending on the cell type, duration of exposure to the lipid, and confluency of the cell culture [237]. Transfection efficiency was also increased by pre-complexing the vector DNA with the PLUS reagent enhancer [238]. Under optimal transfection conditions, ARPE-19 exhibited a several million fold increase in tropoelastin expression over untransfected levels.

3.4.3.4 Propagation of transfected cells

Stable maintenance of the WT or R515A sequence within the transfected cells was selected for by culturing the cells in G418-supplemented nutrient media, as antibiotic resistance is conferred by the *neo* gene within pCI-neo [239]. This was demonstrated by the progressive reduction of untransfected cell numbers in contrast to the survival and gradual proliferation of transfected cells over two weeks after G418 addition. However, the

proliferative rate of transfected cells was still dramatically reduced by the presence of G418 in the culture medium, resulting in a lengthy propagation time before sufficient cell numbers could be achieved for downstream experiments. The negative impact of G418 selection on the expansion of *neo*-expressing cultures has been documented [239]. Furthermore, the extent of growth retardation has been correlated with *neo* expression levels, which are in turn dependent on transfection efficiency. Variable transfection efficacies may account for the decreased cell numbers of R515A transfectants compared to the WT or vector-only transformants.

3.4.3.5 Elastic fibre assembly

Elastic fibres were not detected in ARPE-19 cells transfected with WT or R515A. This may be due to the absence of a microfibrillar scaffold on which the secreted tropoelastin can be deposited for cross-linking, which suggests that the cells were assayed too soon after seeding. More significantly, tropoelastin may no longer be expressed by the transfectants, which was confirmed when both WT and R515A expression of the G418-resistant cells were shown to have decreased 300,000-fold to background levels. This unstable expression may be attributed to the unsuccessful chromosomal integration of the tropoelastin sequences.

During transfection, vectors bind to the cell surface via electrostatic interactions between the positively-charged complexes and the negative charges of the cell membrane [240]. DNA uptake normally proceeds via clathrin-mediated endocytosis into the cytoplasm [241]. The DNA molecules possess low mobility and are susceptible to degradation by cytoplasmic exonucleases [240]. It is unlikely that the tropoelastin sequences were degraded at this stage, as an initial spike in tropoelastin expression was observed in the early transfectants. This suggests that the vector DNA had entered the nucleus and was expressed

as an extrachromosomal sequence [242]. Loss of the tropoelastin sequence may have occurred over multiple cycles of cell division, when the DNA is released upon dissolution of the nuclear membrane but not repartitioned after membrane reformation. Unlike the *neo* gene which may have been retained chromosomally, there was no selective advantage for the maintenance of WT/R515A expression.

3.4.4 Transient transfection

The unstable expression of tropoelastin in long-term transfected ARPE-19 cells demonstrated the advantage of studying elastic fibre assembly in a transiently transfected system. Also, since the intracellular uptake and trafficking of vector DNA, and therefore the persistence of recombinant gene expression, are thought to be cell type dependent [243, 244], two other fibroblast cell lines were transfected with WT or R515A to compare elastic fibre formation in an intrinsic elastogenic environment.

3.4.4.1 Expression of elastogenic components

Compared to ARPE-19 cells, GM3348 and NHF8909 fibroblasts were shown to possess similar or higher transcript levels of extracellular matrix proteins involved in elastogenesis, including fibrillin-1, fibulin-4, fibulin-5, and lysyl oxidase family proteins, consistent with their elastogenic phenotype. The interactions between these elastogenic components are thought to be crucial for elastic fibre formation. Fibulin-4 and -5 bind tropoelastin for optimal coacervation and incorporation into fibrillin-rich microfibrils [133, 245]. These molecules also contact lysyl oxidase enzymes to regulate their spatial distribution and substrate specificity [150]. The lysyl oxidase family proteins mediate cross-link formation under different tissue- and development-specific conditions [246], with LOXL1 localising specifically to elastogenic sites [136]. Expression of the major elastogenic components in all three cell lines suggests sufficient capacity for elastic fibre assembly.

Unlike ARPE-19 cells, GM3348 and NHF8909 fibroblasts expressed endogenous tropoelastin. Nevertheless, the detected transcript levels were markedly lower than the expected levels of recombinant tropoelastin mRNA after transfection. Elastic fibres formed in the fibroblast systems are hence expected to be predominantly assembled from the WT or R515A species.

3.4.4.2 Establishment of a microfibrillar network

Microfibrils have consistently been co-localised with elastin in elastic fibres *in vivo*, and are thought to serve as an essential framework for tropoelastin organisation and cross-linking [247-250]. To enable the immediate deposition and assembly of tropoelastin monomers secreted by transfected cells, a microfibrillar network must be established prior to transfection. Based on this rationale, production of the main microfibrillar protein fibrillin-1 by ARPE-19 cells and fibroblasts was tracked to determine the time required for microfibril development.

The GM3348 fibroblasts formed a well-defined network of microfibrils earlier than ARPE-19 cells at 10 days post-seeding. This corresponded to the higher expression of fibrillin-1 in GM3348 as previously described. Nevertheless, ARPE-19 cells exhibited a similar extent of microfibrillar production by 14 days post-seeding. Consistent with previous findings [201], the ARPE-19 microfibrils were observed to be of similar morphology and abundance to those in a natural elastogenic system such as fibroblasts.

3.4.4.3 Elastic fibre assembly

Transient transfection of fibroblasts and ARPE-19 cells were respectively performed on days 10 and 14 after seeding, when an adequate microfibrillar scaffold is expected to have been established. Despite this preparative step, elastic fibres were not detected in ARPE-19 at any tested time point after transfection. On the other hand, very fine fibre structures were observed with WT- and R515A-transfected GM3348 and NHF8909 cells until 7 days after transfection. The size and width of the fibres hindered imaging under typical conditions and compelled the use of a relatively high laser power which also unfavourably magnified background autofluorescence. However, these fibres exhibited elastin-specific immunofluorescent staining that was discernibly more intense than

background autofluorescence. The fibres were also not seen with cells transfected with the empty pCI-neo vector, and in unstained or non-specifically stained samples. In combination, these findings strongly suggest that the observed fibre structures are nascent elastic fibres.

The nature of the fibre structures was subsequently confirmed with fluorescence lifetime imaging microscopy (FLIM). This technique analyses the lifetime of the excited state of a fluorescent molecule and provides a spatially resolved distribution of fluorescence lifetimes within a sample area [251]. As fluorescence lifetimes are characteristic of certain molecules, FLIM can identify the composition of biological tissues [204], such as an extracellular matrix with heterogeneous autofluorescent components [252, 253].

As a control, the fluorescence lifetime of DAPI-stained cell nuclei was compared across all samples. This value, at ~2.7 ns, was similar for transfected and untransfected cells and matched the previously reported two-photon excitation fluorescence lifetime of DAPI-bound DNA [254]. Multiple fluorescence lifetimes were obtained for regions within the extracellular space that did not encompass definitive fibre structures, which is consistent with contributions from various autofluorescent extracellular components. Similar lifetimes were observed across both transfected and untransfected samples, suggesting that elastin is unlikely to be represented within this set of values. Fluorescence lifetimes acquired for extracellular regions containing the fine fibres mostly reflected the background values, except for a ~2.3 ns peak that was observed only in WT- or R515A-transfected cells and in cells with established elastic fibres. Previous studies have also identified the fluorescence lifetime of elastin to be ~2.3 ns when captured within a similar spectral range [204, 255, 256]. This strongly supports the elastic fibre nature of the fibrous structures observed in the transfected fibroblasts.

The formation of elastic fibres by GM3348 and NHF8909 fibroblasts but not by ARPE-19 cells may be accounted for by differences in tropoelastin expression after

transfection. Prior to transfection, expression of native tropoelastin by all cell types was negligible. Post-transfection, WT and R515A expression increased significantly, but rapidly declined after only one day in ARPE-19 cells. Consequently, the levels of secreted tropoelastin may have been insufficient for fibre assembly. On the other hand, WT and R515A transcript levels in fibroblast cells persisted slightly longer until 4 days after transfection, which would have resulted in a higher cumulative amount of tropoelastin monomers in the extracellular environment for elastogenesis. From subsequent experiments with added tropoelastin, four days was required for the monomers to be irreversibly deposited onto the microfibrillar network to form elastic fibres. Furthermore, fibroblasts are known to have a more stable elastogenic phenotype compared to other elastin-producing cells [197]. Nevertheless, elastic fibres were not detected in both GM3348 and NHF8909 fibroblast systems at 10 days after transfection. This suggests that the fine fibres may be unstable and hence inadvertently removed during media washes, while the decrease in tropoelastin expression after 4 days would have precluded formation of new fibres. Alternatively, increased autofluorescence of the elastic fibres associated with cross-link maturation [257, 258] may have masked their elastin-specific staining and made visualisation of the structures difficult.

The overall low extent of elastic fibre formation hindered the characterisation of potential differences between WT and R515A fibres. The high transcript levels of WT and R515A in early transfectants did not translate to the observed quantity of secreted tropoelastin spherules or assembled elastic fibres. This may be due to transcript instability or a tightly-regulated translation step leading to inefficient tropoelastin synthesis.

3.4.5 Addition of exogenous tropoelastin to culture medium

The main challenge with establishing differences between WT and R515A elastic fibre formation has thus far been the *de novo* production of tropoelastin species by cells. To address this, purified WT and R515A constructs were directly added to the culture medium for assembly into elastic fibres. The tropoelastin constructs were confirmed to be full-length, and an optimum tropoelastin concentration was demonstrated to result in distinct fibre formation.

ARPE-19 cells serve as an ideal model for elastic fibre assembly that depends on exogenous tropoelastin since they express the major elastogenic components except for tropoelastin. This is demonstrated by the absence of elastic fibres when tropoelastin was not added to the culture medium. Elastic fibres in ARPE-19 were solely derived from the supplied constructs, as the addition of exogenous tropoelastin does not trigger endogenous tropoelastin expression [140].

In the ARPE-19 system, both WT and R515A were able to form defined and sustained elastic fibres, which supports the ability of the cell line to integrate tropoelastin monomers into cross-linked structures as previously reported [140, 201, 203]. However, R515A particles were less efficient in forming linear clusters than WT in the first day after tropoelastin addition, which may be associated with the reduced propensity of the mutant for self-association [184]. The R515A elastic fibres also displayed significantly lower fluorescence and density than WT fibres. Decreased antibody staining would be expected to result from reduced exposure or number of tropoelastin epitopes in the elastic fibre. Reduced fibre autofluorescence [259] may be correlated to decreased elastin cross-linking [257, 258] that could similarly have arisen from fewer or differently-organised monomers. These results demonstrate the impaired or abnormal elastic fibre assembly of R515A compared to WT.

The decreased elastogenic ability of R515A was magnified in the fibroblast systems, in which the mutant constructs predominantly remained as spherical clusters in GM3348 cells, or formed only very sparse and faint fibres in NHF8909 cells. This sharply contrasted with the extensive WT elastic fibre network observed in both cell lines. The detected elastic fibres were exclusively assembled from exogenously supplied tropoelastin, as evidenced by the lack of fibre formation in untreated fibroblasts. The inability of R515A to form defined elastic fibres may be a compounded effect of decreased self-assembly as well as impaired interactions with fibroblast cells [184] and extracellular matrix components.

The expression of cell-surface receptors such as integrins has been shown to be spatially and temporally regulated [260]. Likewise, lysyl oxidase enzymes [141] and microfibrillar proteins including fibrillins [261-265] and microfibril-associated glycoproteins [266, 267] exhibit tissue- and development-specific expression. Furthermore, certain proteins such as fibrillin-1 have multiple splicing isoforms that are alternatively expressed [268]. The subset of expressed microfibrillar proteins can recruit various lysyl oxidases [150, 269] with different substrate specificities [136]. These strongly support the evolution of tissue- and age-specific elastogenic environments that may select against non-native tropoelastin monomers or assemblies to varying degrees, in compliance with specific functional requirements for the assembled elastic fibre. This would account for differences in the extent of R515A fibre formation between ARPE-19 cells and fibroblasts, and between the GM3348 and NHF8909 fibroblasts.

Interestingly, the impaired elastic fibre assembly of R515A by ARPE-19 was rescued by multiple additions of the construct to the culture medium. In this instance, the immunofluorescence, autofluorescence and abundance of the R515A fibres were indistinguishable from the WT fibres. This suggests that the previously described differences in R515A fibres have mainly stemmed from an inefficient early time course

assembly process. A delay in R515A coacervation, microfibrillar anchorage, or cross-linking may have allowed some monomers to be displaced during media washes, leading to an overall decrease in available molecules for fibre assembly. The supplementation of tropoelastin during each media change would have replenished the lost monomers and allowed elastogenesis to proceed to the same extent as WT. In contrast, multiple tropoelastin additions did not improve R515A fibre formation by GM33348 fibroblasts. This supports a cell-specific bias against R515A fibre assembly that cannot be compensated for by an excess of the mutant construct in the extracellular environment.

These results indicate that the previously documented impaired behaviour of R515A at each major stage of elastogenesis [184] translates to an inadequate ability to form elastic fibres in a cellular environment. The properties of R515A tropoelastin have been associated with a structural deviation originating from the bridge region and encompassing the C-terminal region [184]. R515 may stabilise the tropoelastin bridge region in via charge-based interactions with neighbouring residues. Potential candidates include the negatively-charged E354 or E414 residues in domains 19 and 21, respectively. Consequences of the altered monomer conformation may include not only the functional deficiency of R515A during stages of self-assembly, but also changes in interactions with cells and the extracellular matrix during elastic fibre formation. This study confirms the functional significance of the R515 residue, and the importance of the tropoelastin bridge region in elastogenesis.

4. Characterisation of E345A, E414A and E345A+E414A tropoelastin

4.1 Introduction

4.1.1 Roles of charged tropoelastin residues in elastin assembly

Tropoelastin has a unique domain structure consisting of alternating hydrophobic and hydrophilic regions [4]. The hydrophilic domains are highly basic, and are typically rich in lysines situated near a polyalanine tract or a proline residue [24, 270]. The C-terminus of tropoelastin contains a highly-conserved stretch of positively-charged arginine and lysine residues [183]. The abundance of charged sites in tropoelastin has been associated with distinct roles at various stages of elastic fibre assembly.

In the early stage of elastogenesis after the secretion of tropoelastin into the extracellular space, the monomers are proposed to contact cell-surface glycosaminoglycans (GAGs) such as heparin and chondroitin sulfate B [271]. Interactions are thought to occur between the positive lysine residues in tropoelastin and the negative charge densities in GAGs [91, 93]. The binding of GAGs even at low concentrations neutralises the potentially repulsive charges on tropoelastin molecules [93, 271] and promotes the accumulation and aggregation of nanoparticles into larger-sized assemblies observed on the cell surface [3, 272]. The efficiency of tropoelastin coacervation may be modulated by the subset of bound lysines and the nature of charge densities in GAGs [93].

In addition to an increased intermolecular association, tropoelastin binding to GAGs can facilitate secondary structure changes which are an essential consequence of the coacervation process. Modifications to the lysine residues of tropoelastin can reduce the extended polyproline II helical conformation [271] that is highly favoured in an aqueous environment [58]. Instead, the formation of alpha-helices is promoted, which crucially position lysine residues in close proximity for cross-linking [58, 67]. Circular dichroism

monitoring of tropoelastin during coacervation has similarly demonstrated a transition from an unordered structure to an alpha-helical conformation [273, 274].

The strategic location of positively-charged residues within tropoelastin allows the specific binding of extracellular moieties that promote coacervation. However, the introduction of even a single polar amino acid in its charged state into a hydrophobic sequence increases the solvent accessible surface area and dramatically decreases the propensity of the construct for self-association [112]. This demonstrates how charged residues may regulate tropoelastin coacervation, despite the process being one driven mainly by hydrophobic interactions [275].

The tethering of tropoelastin molecules on the cell surface is also mediated by charged residues. For instance, tropoelastin attachment to the alpha-v-beta-3 integrin on human dermal fibroblasts [179], or to heparan sulfate on smooth muscle cells [83], is predominantly mediated by the C-terminal RKRK cluster. This region is believed to form a charged pocket arising from a disulphide bond between proximal cysteine residues [50]. Masking of the positively-charged structure by oxidising the cysteine residues to negatively-charged sulfonic acid derivatives has been shown to prevent tropoelastin binding to dermal fibroblasts and chondrocytes [83].

The deposition of tropoelastin assemblies onto microfibrils, which act as a scaffold for elastic fibre formation, is likewise proposed to be modulated by electrostatic interactions between the tropoelastin C-terminus and microfibril-associated glycoproteins [45, 50, 102, 276]. This is supported by the detection of glycosaminoglycan components within the elastic fibre [277, 278]. Addition of GAGs to the culture medium has been shown to directly influence the incorporation of tropoelastin monomers into elastic fibres [279]. Following the same principle, tropoelastin molecules that lack the C-terminal region do not assemble into elastic fibres [122, 280, 281].

After tropoelastin deposition onto microfibrils, cross-linking of the monomers is required for the development of mature and stable elastic fibres. Tropoelastin cross-linking directly involves the positively-charged lysine residues within the molecules, as lysyl oxidase enzymes oxidatively deaminate lysine side chains which triggers the formation of bifunctional or tetrafunctional intra- and inter-molecular cross-links [137, 139]. Studies modelling elastin cross-linking with either lysyl oxidase [282] or an amine-reactive chemical linker [143] have reported distinct tropoelastin domains that are enriched in cross-linking sites. Furthermore, within these regions, specific lysine residues are favoured while others remain under-utilised during cross-linking. This is consistent with the specific presentation of a subset of lysine residues when tropoelastin monomers align during coacervation [273, 274].

The involvement of charged tropoelastin residues in elastin assembly may extend beyond simple electrostatic or ionic interactions with elastogenic components, as evidenced by the specificity of the contacts formed. It has been proposed that the recognition of these residues relies heavily on their local conformation [105, 143], which may also be maintained by the charged moieties. KA-rich hydrophilic domains preferentially adopt an alpha-helical secondary structure [283], which are stabilised by negative polar residues at the N-terminus and positive polar residues at the C-terminus [284, 285]. Accordingly, the substitution of an end-capping polar residue with a neutral alanine has been shown to disrupt interactions with the helical dipole and alter the alpha helix structure into a random coil [284].

Charged residues in tropoelastin may also be involved in maintaining the tertiary structure of the protein, as was observed for the R515 residue [184]. The mutation of R515 to an alanine was described in the previous chapter to affect the conformation of the tropoelastin bridge and C-terminal regions, which correlated to a decrease in elastic fibre assembly. While the mechanism by which R515 influences structural stabilisation is unclear,

one hypothesis is via its participation in charge-based interactions. Conceptually, it follows that the positively-charged arginine may be involved in contacts with proximal negatively-charged residue/s.

4.1.2 Negatively-charged residues in tropoelastin

Interestingly, the human tropoelastin sequence [104] contains only three residues with negatively-charged side chains at physiological pH. Despite their relative rarity compared to the abundance of positively-charged lysines and arginines, their significance to tropoelastin structure or function has never been characterised. Two of the three negative residues, glutamate 345 (E345) in domain 19 and glutamate 414 (E414) in domain 21, are predicted to be located in close proximity to R515 and the bridge region based on the tropoelastin nanostructure [72] (Figure 4.1). Therefore, one or both residues may feasibly contact R515 via charge interactions to stabilise this region of tropoelastin.

E345 and E414 may also have functional roles in tropoelastin independent of those of R515, as they reside within domains of known functional or structural importance. Domains 19 and 21 are located within the region spanning domains 19-25 that is enriched for cross-links [143, 282]. In particular, a specific lysine in domain 19 has been reported to participate in cross-linking even at low cross-linker concentrations, which points to this region as the initial point of alignment during tropoelastin coacervation [44]. Consistent with this is the greater propensity of domain 19 for alpha helix formation compared to other hydrophilic domains, which aids the alignment of lysine residues for cross-linking [69, 75]. Specifically, domain 19 has been identified to form cross-links with domain 25 and domain 10 [105], which forms the basis of the head-to-tail model of elastin assembly [72].

Domain 21 is uniquely positioned preceding another hydrophilic domain 23 due to the constitutive splicing of domain 22 in human tropoelastin [33]. The juxtaposition of

domains 21 and 23 is predicted to form a hinge region [74] that has been evidenced by nuclear magnetic resonance [75], SAXS [44] and cross-linking experiments. The hinge region may contribute to the elasticity of the tropoelastin molecule. It is structurally flexible, and fluctuates between open and closed conformations until converging to a hairpin structure [73]. This region is hypothesised to be primarily stabilised by van der Waals interactions, and to a limited extent by a salt bridge between the side chains of E414 and K441. Substitution of the charged groups with neutral residues is predicted to result in significant changes in the hinge structure [73].

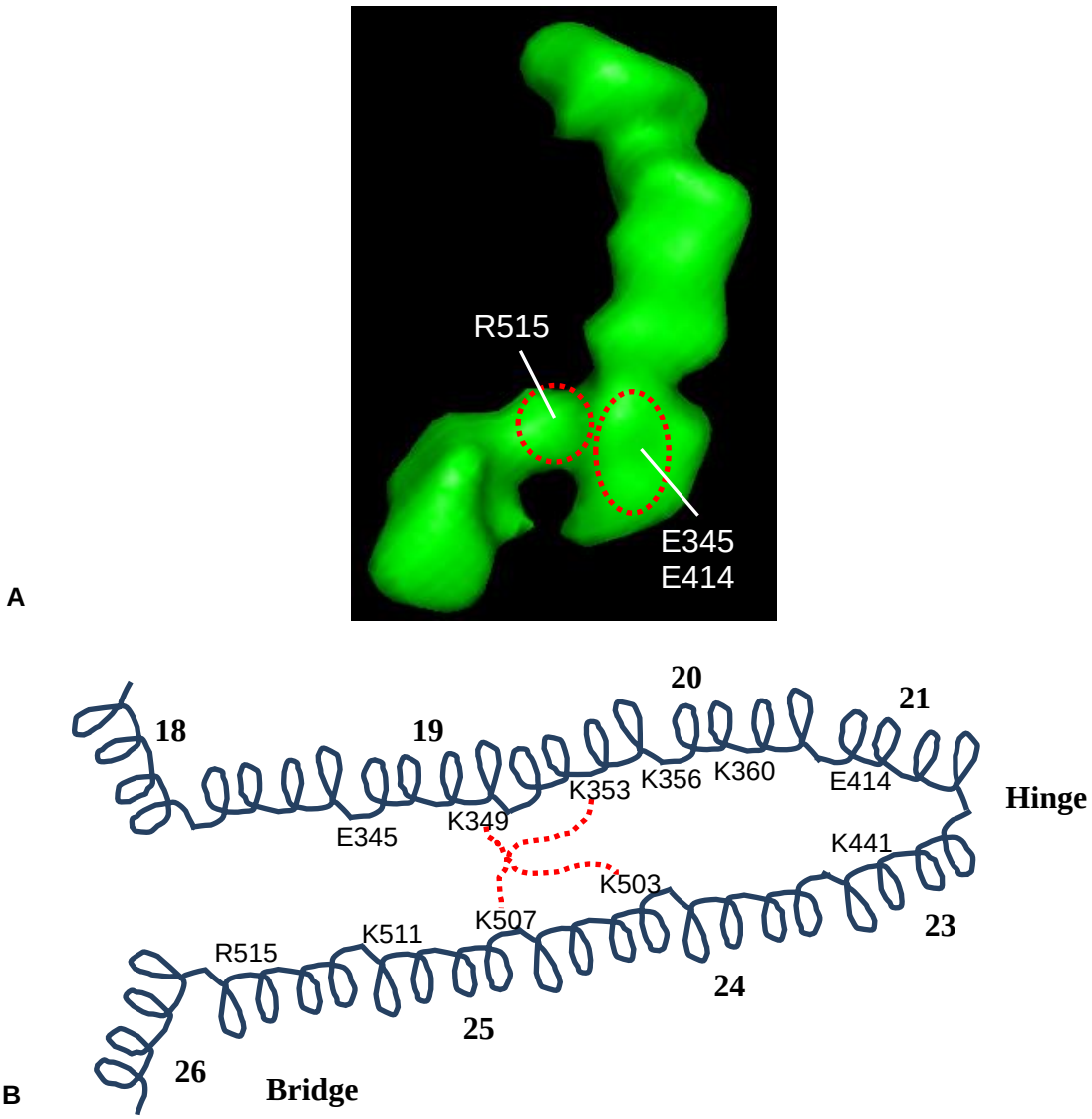

Figure 4.1. (A) Solution structure of wild-type human tropoelastin. The estimated spatial locations of the R515, E345 and E414 residues are indicated. (B) Schematic representation of tropoelastin domains 18-26, adapted from Baldock *et al.* (2011) [72]. A hinge region is formed by domains 21/23. A proposed tetra-functional cross-link occurring between domains 19 and 25 [105] is represented by red dotted lines.

4.1.3 Aims

This chapter aims to explore the functional significance of two negatively-charged tropoelastin residues, E345 and E414, which are spatially situated proximal to the bridge region. Three tropoelastin mutant constructs will be produced: E345A, where the E345 residue has been mutated to an alanine; E414A, where the E414 residue has similarly been replaced with an alanine; and E345A+E414A, where both E345 and E414 residues have been substituted for alanines (Figure 4.2). By comparing the elastogenic properties of these constructs with WT and R515A tropoelastin, the likelihood of R515 binding to one or both glutamate residues will be determined. Additionally, the possibility of E345 and E414 possessing a significance that is unrelated to R515 function will be investigated.

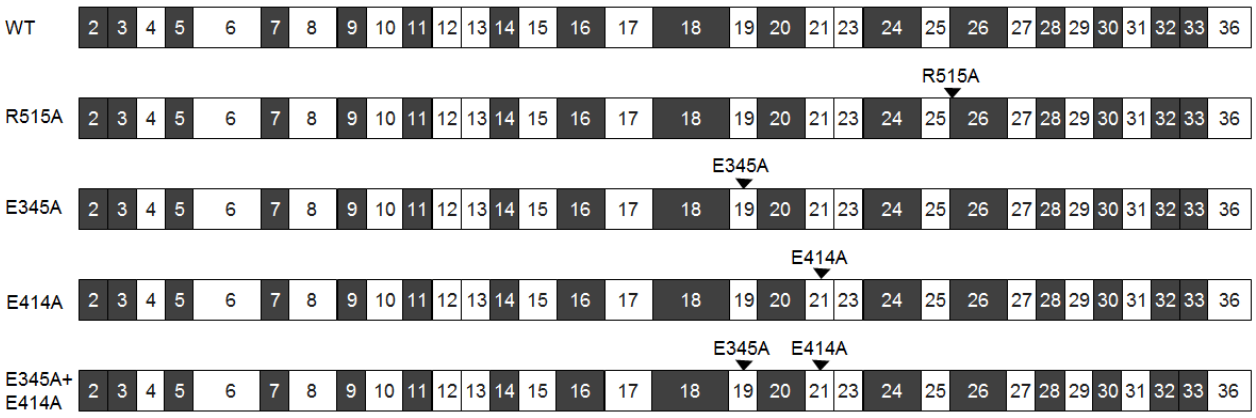

Figure 4.2. Domain structures of the WT, R515A, E345A, E414A, and E345A+E414A tropoelastin constructs. Hydrophobic domains are represented by dark grey boxes, while hydrophilic domains are drawn as white boxes. The domain locations of the mutated residues are indicated.

4.2 Results

4.2.1 Negatively-charged residues in mammalian tropoelastin sequences

Analysis of nine predicted or confirmed mammalian tropoelastin sequences revealed the infrequent occurrence of residues that have negatively-charged side chains at physiological pH (Figure 4.3). All of the surveyed tropoelastin sequences contained four or less such residues. Alignment of the sequences showed that these negatively-charged residues were predominantly located around domain 6 of the N-terminal region or within domains 19-25 of the central hinge and bridge regions. However, the presence of negative residues at the specific 345^{th} and 414^{th} positions was observed only in the primate tropoelastin sequences. The E345 residue in domain 19 was conserved in humans and chimpanzees, while E414 in domain 21 was conserved in humans and baboons. Nevertheless, other mammalian tropoelastin sequences contained negative residues in close proximity to these sites, including two aspartates in domains 17 and 21 of the cow sequence, an aspartate in domain 22 of the dog sequence, an aspartate and a glutamate in domains 22 and 25 of the cat sequence, a glutamate in domain 22 of the pig sequence, an aspartate in domain 25 of the rat sequence, and a glutamate in domain 25 of the baboon sequence. An exception is the mouse sequence, which did not have any negative residues.

```
Dog             MAGLRAAALRPGVLLLLLS-VARPSQPGGVPGAVPG--------GVPGGVYYPGAGIGG- 50
Cat             MAGLRTAALRPGVLLLLLS-IVHPSQPGGVPGAVPG--------AVPGGVYYPGAGLGG- 50
Mouse           MAGLTAVVPQPGVLLILLLNLLHPAQPGGVPGAVPG----GLPGGVPGGVYYPGAGIGGL 56
Rat             MAGLTAAVPQPGVLLILLLNLLHPAQPGGVPGAVPGGVPGGLPGGVPGGVYYPGAGIGG- 59
Cow             MRSLTAAARRPEVLLLLLC-ILQPSQPGGVPGAVPG--------GVPGGVFFPGAGLGG- 50
Pig             MAGLTAAALRPGVLLLLLS-IIHPSQPGGVPGAVPG--------GVPGGVFFPGAGLGG- 50
Human           MAGLTAAAPRPGVLLLLLS-ILHPSRPGGVPGAIPG--------GVPGGVFYPGAGLGA- 50
Chimpanzee      MAGLTAAAPRPGVLLLLLS-ILHPSRPGGVPGAIPG--------GVPGGVFYPGAGLGA- 50
Baboon          ---------------------------GVPGAIPG--------GVPGGVYYPGAGLGG- 23
                                            *****:**        .*****::****:*.

Dog             -LGGGALGPGGKPPKPGAGLLGAFGPGAAGLAGGGPGAG--LGAFPAGAFPGGLVPG--G 105
Cat             -LGGGALGPGGKPPKPGAGLLGAFGPGAGGLAGAGPGAGERLGAFPAGTYPGALVPG--G 107
Mouse           GGGGGALGPGGKPPKPGAGLLGTFGAGPGGLGGAGPGAGA-----------GALVPG--G 103
Rat             GLGGGALGPGGKPPKPGAGLLGAFGAGPGGLGGAGPGAG------------GVLVPG--G 105
Cow             -LGVGGLGPGVKPAKPGVG--GLVGPGLGAEGSALPG-AFP-----------GGFFGAGGG 96
Pig             -LGGGALGPGGKPPKPGVG--GLAGAGLGAGLGAFPAGAFP-----------GALVPG--G 95
Human           -LGGGALGPGGKPLKPVPG--GLAGAGLGAGLGAFPAVTFP-----------GALVPG--G 95
Chimpanzee      -LGGGALAPGVKPLKPVPG--GLVGAGLGAGLGAFPAVTFP-----------GALVPG--G 95
Baboon          -LGGGALGPGGKPLKPGPG--GLAGTGLGAGLGAFPAGAFP-----------GALVPG--G 68
                  * *.*.** ** **  *  *  *.* ..  .. *.              * :. .  *

Dog             VAGAAAAYK-AAKAGAGLG---------------------------GVGGI-GGVGGIGG 136
Cat             VAGAAAAYKAAAKAGAGLG---------------------------GVG-------GIGG 133
Mouse           AAGAAAAYKAAAKAGAGLGGVGGVPGGVGVGGVPGGVGVGGVPGGVGVGGVPGGVGGIGG 163
Rat             GAGAAAAYKAAAKAGAGLG---------GIGGVPGGVGVGGVPGAVGVGGVPGAVGGIGG 156
Cow             AAGAAAAYKAAAKAGAAGL-----------------------------------GVGGIGG 122
Pig             VADAAAAYKAAAKAGAG-------------------------------------LGGVGG 118
Human           VADAAAAYK-AAKAGAGLG-----------------------------------GVPG 117
Chimpanzee      VADAAAAYK-AAKAGAGLG-----------------------------------GVPG 117
Baboon          VADAAAAYK-AAKAGAGLG-----------------------------------GVPG 90
                 *.****** ******.                                      *: *

Dog             VGGLGVSTGAVVPQPGAGVGVGVGAGGKPGKVPGVGLPGVYPGGVLPGTGARFPGVGVLP 196
Cat             VGGLGVSTGAVVPQPGAGVGVGVG--GKPGKVPGVGLPGVYPGGVLPGTGARFPGVGVLP 191
Mouse           IGGLGVSTGAVVPQVGA--GIGAG--GKPGKVPGVGLPGVYPGGVLPGTGARFPGVGVLP 219
Rat             IGGLGVSTGAVVPQLGA--GVGAG--GKPGKVPGVGLPGVYPGGVLPGTGARFPGVGVLP 212
Cow             VGGLGVSTGAVVPQLGA--GVGAG--VKPGKVPGVGLPGVYPGGVLPGAGARFPGIGVLP 178
Pig             VGGLGVSTGAVVPQLGA--GVGAG--AKPGKVPGVGLPGVYPGGVLPGTGARFPGVGVLP 174
Human           VGGLGVSAGAVVPQPGAG--------VKPGKVPGVGLPGVYPGGVLP--GARFPGVGVLP 167
Chimpanzee      VGGLGVSAGAVVPQPGAG--------VKPGKVPGVGLPGVYPGGVLP--GARFPGVGVLP 167
Baboon          VGGLGVSTGAVVPQPGAG--------VKPGKVPGVGLPGVYPGGVLPGTGARFPGVGVLP 142
                :******:****** **          ********************  ******:****

Dog             GVPTGTGVKAKAPGGGG-AFAGIPGVGPFGGQQPGVPLGYPIKAPKLPGGYGLPYSTGKL 255
Cat             GVPTGTGVKAKTPGGGG-AFAGIPGVGPFGGQQPGVPLGYPIKAPKLPGGYGLPYSTGKL 250
Mouse           GVPTGTGVKAKAPGGGG-AFAGIPGVGPFGGQQPGVPLGYPIKAPKLPGGYGLPYTNGKL 278
Rat             GVPTGTGVKAKVPGGGGGAFSGIPGVGPFGGQQPGVPLGYPIKAPKLPGGYGLPYTNGKL 272
Cow             GVPTGAGVKPKAQVGAG-AFAGIPGVGPFGGQQPGLPLGYPIKAPKLPAGYGLPYKTGKL 237
Pig             GVPTGTGVKAKAPGGGG-AFAGIPGVGPFGGQQPGVPLGYPIKAPKLPGGYGLPYSTGKL 233
Human           GVPTGAGVKPKAPGVGG-AFAGIPGVGPFGGPQPGVPLGYPIKAPKLPGGYGLPYTTGKL 226
Chimpanzee      GVPTGAGVKPKAPGVGG-AFAGIPGVGPFGGPQPGVPLGYPIKAPKLPGGYGLPYTTGKL 226
Baboon          GVPTGAGVKPKAPGVGG-AFAGIPGVGPFGVQQPGVPLGYPIKAPKLPGGYGLPYSTGKL 201
                *****:***.*.   .* **:*********  ***:************.******..***

Dog             PYGYGPGGVAGAAGKAGYPTGTGVG---TQAAAAAAKAAKFGAGGAGVLP--GVGGAGIP 310
Cat             PYGYGPGGVAGAAGKAGYPTGTGVG---PQAAAAAAKAAKFGAGGAGVLP--GVGGGGIP 305
Mouse           PYG-----VAGAGGKAGYPTGTGVG---SQAAAAAAKAAKYGAGGAGVLP--GVGGGGIP 328
Rat             PYG-----VAGAGGKAGYPTGTGVG---SQAAVAAAKAAKYGAGGGGVLP--GVGGGGIP 322
Cow             PYGFGPGGVAGSAGKAGYPTGTGVG--PQAAAAAAKAAAKLGAGGAGVLPGVGVGGPGIP 295
Pig             PYGFGPGGVAGAAGKAGYPTGTGVGTQAAAAAAAAKAAAKYGAPGAGVLPGVGVGGVGVP 293
Human           PYGYGPGGVAGAAGKAGYPTGTGVGP-QAAAAAAAKAAAKFGAGAAGVLP--GVGGAGVP 283
Chimpanzee      PYG------------------------------------------------------------ 229
Baboon          PYGYGPGGVAGAAGKAGYPTGTGVGP-QAAAAAAAKAAAKLGAG---VLP--GVGVGGVP 255
                ***
```

```
Dog             GGAGAIPGIGGIAGAGTP---AAAAKAAAKAAKYGAAGGLVPGGP----GFGVPGVGVP- 362
Cat             GGAGAIPGIGGIAGAGTPAAAAAAAKAAAKAAKFGAAGGVVPGGPGFVPGVGVPGVGVP- 364
Mouse           GGAGAIPGIGGIAGAGTP-AAAAAAKAAAKAAKYGAAGGLVPGGP----GVRLPGAGIP- 382
Rat             GGAGAIPGIGGITGAGTP-AAAAAAKAAAKAAKYGAAGGLVPGGP----GVRVPGAGIPG 377
Cow             GAPGAIPGIGGIAGVGAPDA-AAAAAAAAKAAKFGAAGGLP--------GVGVPGVGVPG 346
Pig             GGAGAIPGIGGIAGAGAP----AAAAAAAKAAKYGAAGGLVPGAPGFGPGVGVPGVGVPG 349
Human           GVPGAIPGIGGIAGVGTP-AAAAAAAAAAKAAKYGAAAGLVPGGP----GFGPGVVGVP- 337
Chimpanzee      ----------------------------------AAAGLVPGGP----GFGPGVVGVP- 249
Baboon          GVPGAIPGIGGIAGAGTP-AAAAAAAAAAKAAKYGAAAGLVPGGP----GFGPGVVGVP- 309
                                                 **.*:         *.    .*:*

Dog             ----------GVG-VPGVG-VPGVGVPGVGGPGI---------VGGPGAVSPAAAAKAAA 401
Cat             ----------GVG-VPGVG-VPGVGVPGVGVPGVGVPGVGVPGVGVPGAVSPAAAAKAAA 412
Mouse           ----------GVGGIPGVGGIPGVGGPGIGGPGI---------VGGPGAVSPAAAAKAAA 423
Rat             VGIPGVGGIPGVGGIPGVGGIPGVGGPGIGGPGI---------VGGPGAVSPAAAAKAAA 428
Cow             VGVPGVG-VPGVG-VPGVG-VPGVGVPGVGVPGVGVPGVGVPGVGVPGALSPAATAKAAA 403
Pig             VGVPGVG-VPGVG-VPGVG-VPGVGVPGVGVPGVGVPGVGVPGVGVPGAVSPAAAAKAAA 406
Human           ----------GAG-VPGVG-VPGAGIP--VVPGAGIP-----GAAVPGVVSPEAAAKAAA 378
Chimpanzee      ----------GAG-VPGVG-VPGAGIP--VVPGAGIP-----GAAVPGVVSPEAAAKAAA 290
Baboon          ----------GAG-IPGVG-VPGAGIPGVGVPGAGIPVV--PGAGVPGAVSPAAAAKAAA 355
                          *.* :**** :**.* *    **          .. **.:** *:*****

Dog             KAAKYGARAGVGVGGIPTYGVGVGAGGFPGYGIGAGG------VPGAPLSP-AA-----Q 449
Cat             KAAKYGARAGVGVGGIPTF--GIGAGGFPGYGVGAGVGAVPGAVPGAGLSPAAA-----Q 465
Mouse           KAAKYGARGGVG---IPTY--GVGAGGFPGYGVGAGAG--------------LG-----G 459
Rat             KAAKYGARGGVG---IPTY--GVGAGGFPGYGVGAGAG--------------LG-----G 464
Cow             KAAKFGARGAVGIGGIPTF--GLGPGGFP--GIGDAA------------------------ 436
Pig             KAAKYGARGGVGVGGIPTF--GVGAGGFPGFGVGVGA------------------------ 441
Human           KAAKYGARPGVGVGGIPTY--GVGAGGFPGFGVGVGGIPGVAGVPGVGGVPGVGGVPGVG 436
Chimpanzee      KAAKYGARPGVGVGGIPTY--GVGAGGFPGFGVGVGGIPGVAGVPSVGGVPGVGGVPGVG 348
Baboon          KAAKYGARAGVGVGGIPTF--GVGAGGFPGYGVGVGGIP------GVGGVPGVGGVPGAG 407
                ****:*** .**   ***:  *:*.****  *:* .

Dog             AAAAAQAAAAAKAAKYGAGGVGALGGLVPGVGDGVAG----------VPGTG-----GVP 494
Cat             AAAAAQAAAAAKAAKYGAGGVGGLGGLVPGIGDGVAG----------VPGVG-----GVP 510
Mouse           AS-PAAAAAAAKAAKYGAGGAGALGGLVPGAVPGALPGAVP-----AVPGAG-----GVP 508
Rat             ASQAAAAAAAAKAAKYGAGGAGTLGGLVPGAVPGALPGAVPGALPGAVPGALPGAVPGVP 524
Cow             ---AAPAAAAAKAAKIGAGGVGALGGVVPGAPGAIPG----------LPGVG-----GVP 478
Pig             ---AAQAAAAAKAAKLGAAGAGALGGLVPGAEGAVPG----------VPGAG-----AVP 483
Human           ISPEAQAAAAAKAAKYGAAGAGVLGGLVPGAPGAVPG----------VPGTG-----GVP 481
Chimpanzee      ISP--QAAAAAKAAKY---------GLVP--------------------GVG-----VAP 372
Baboon          ISPEAQAAAAAKAAKYGAAGAGVLGGLVPGAGGIVPG----------VPGVG-----GVP 452
                      *********          *:**                   *.       .*

Dog             GAG--------TPAAAA----------AKAAAKAAQFGLGPGVG----VGPGVGPGVGPG 532
Cat             GVG--------TPAAAA----------AKAAAKAAQFGLGPGIG----VAPGVAPGVAPG 548
Mouse           GAG----TPAAAAAAAA----------AKAAAKAG---LGPGVGG---VPGGVGVGGIPG 548
Rat             GTGGVPGTPAAAAAAAA----------AKAAAKAGQYGLGPGVGG---VPGGVGVGGLPG 571
Cow             GVG--------IPAAAA----------AKAAAKAAQFGLGP------GVGVAPGVGVVPG 514
Pig             GVG--------APAAAA----------AKAAAKAAQFGLGPGIGVAPGVGVAPGVGVAPG 525
Human           GVGTPAAAAAKAAAKAAQFALLNLAGLVPGVGVAPGVGVAPGVGVAPGVGLAPGVGVAPG 541
Chimpanzee      GVG----------------------VAPGVGVAPGVGVAPGVGVAPGVGVAPGVGVAPG 409
Baboon          GVGTPAAAAAKAAAKAAQFG------LVPGVGVAPGVGVAPGVGVAPGVGVAPGVGVAPG 506
                *.*                       . ... *    :.*       *  . . *  **

Dog             -IGPG-----VGPGIGPGIGIGPGGVTGVGTPAAAKAAAKAAAKAQYRAAAGLPAGVPGF 586
Cat             -VAPG-----VAPGIGIGPGGVIGELLRVGTPAAAKAAAKAAAKAQYRAAAGLPAGVPGF 602
Mouse           GVGVGGVPGGVGPGGVTGIGAGPGGLGGAGSPAAAKSAAKAAAKAQYRAAAGLGAGVPGF 608
Rat             GVGPGGVTG-IGTG--PGTGLVPGDLGGAGTPAAAKSAAKAAAKAQYRAAAGLGAGVPGL 628
Cow             -VGVVP-----GVGVAPGIGLGPGGVIGAGVPAAAKSAAKAAAKAQFRAAAGLPAGVPGL 568
Pig             -VGVAP-----GVGVAPGIGIGPGGVIGAGAPAAAKSAAKAAAKAQFQAAAGLPAGVPGF 579
Human           -VGVAP-----GVGVAP--GIGPGGVA-----AAAKSAAKVAAKAQLRAAAGLGAGIPGL 588
Chimpanzee      -VGVAP-----GVGVAP--GIGPGGVA-----AAAKSAAKVAAKAQLRAAAGLGAGIPGL 456
Baboon          -VGVAP-----GVGVAPGVGIGPGGVAGVGAPEAAKSAAKAAAKAQLRAAAGLGA-VPGL 559
                 :.        . *     *   * :       ***:***.***** :***** * :**:
```

```
Dog             GVGAGVPGFGVGAG---------IPGFGVGAGVPGFGAG--------------------- 616
Cat             GVGAGVPGFGVGAG---------VPGFGAGVGVPGFGAG--------------------- 632
Mouse           GAGAGVPGFGAGAGVPGFGAGAGVPGFGAGAGVPGFGAG--------------------- 647
Rat             GVGAGVPGFGAGAG-----------GFGAGAGVPGFGAG--------------------- 656
Cow             GVGAGVPGLGVGAG---------VPGLGVGAGVP--GPG--------------------- 596
Pig             GVGAGVPGFGVGAG---------VPGFGAGA------------------------------ 601
Human           GVGVGVPGLGVGAG---------VPGLGVGAGVPGFGAGADEGVRRSLSPELREGDPSSS 639
Chimpanzee      GVGVGVPGLGVGAG---------VPGLGVGAGVPGFGA--------------------- 485
Baboon          GVGA-VPGLGVGVG---------VPGLGVGAGVPGFGAG--------------------- 588
                *.*. ***:*.*.*           *:*.*.

Dog             ----------AVPGTLAAAKAAKYG--AGG-VGALGGAGVPGGVAGAG------------ 651
Cat             ----------AVPGSLAAAKAAKYG--AAG-VGALGGVGVPG---GAG------------ 664
Mouse           ----------AVPGSLAASKAAKYG--AAGGLGGPGGLGGPGGLGGPGGLGG-------- 687
Rat             ----------AVPGSLAASKAAKYG--AAGGLGGPGGLGGPGGLGGPGGLGGPGGLGGPG 704
Cow             ----------AVPGTLAAAKAAKFGPGGVGALGGVGDLGGAGIPGGVAG----------- 635
Pig             -----------VPGPLAAAKAAKYG--AAGALGGVGDLGGAGIPGGVAG----------- 637
Human           QHLPSTPSSPRVPGALAAAKAAKYGAAVPGVLGGLGALGGVGIPGGVVG----------- 688
Chimpanzee      -----------VPGALAAAKAAKYGAAVPGVLGGLGALGGVGIPGGVVG----------- 523
Baboon          ----------AVPGALAAAKAAKYGAGVPGALGGVGALGGVGIPGGVVG----------- 627
                           ***.***:****:*    * :*. *  *  *   *

Dog             -----------PAASAAAAKAAAKAAQFGLGGAGALGAGGLGAGGAIPG---VGGFGGE- 696
Cat             -----------PAASAAAAKAAAKAAQFGLGGAGALGVGGLGAGGAIPG---VGGFGG-- 708
Mouse           ------AGAAPPAAAAAAAKAAAKAAQYGLGGAGGLGAGGLGAGGLGAGGLGAGGLGAGG 741
Rat             GLGGVPGGVAGAPAAAAAAKAAAKAAQYGLGGAGGLGAGGLGAGGLGAGGLGAGGLGAGG 764
Cow             ----------VVPAAAAAAKAAAKAAQFGLGGVGGLGVGGLGA---VPG---AVGLGG-- 677
Pig             ----------VGP---AAAKAAAKAAQFGVGGVGGLGVGGLGA---VPG---AGAFGG-- 676
Human           ---------AGPAAAAAAAKAAAKAAQFGLVGAAGL--GGLGVGGLG-VPG-VGGLGG-- 733
Chimpanzee      ---------AGPAAAAAAAKAAAKAAQF---GAAGL--GGLGVGGLG-VPG-VGGLAG-- 565
Baboon          ---------AGPAAAAAAAKAAAKAAQFGLGGPAGLGVGGLGVGGLGAVPG-VGGLGG-- 675
                            .   ***********:   * ..*  ****.         . .:..

Dog             ----------------GVSPAAAAKAAKYGATGLGGVLGATRPFQVGGVAARPGFGLSPIY 741
Cat             ----------------VSPAAAAKAAKYGATGLGSVLGATRPFPVGGVAARPGFGLSPIY 752
Mouse           LGAGGLGAGGLGAGGGVSPAAAAKAAKYGAAGLGGVLGA-RPFPG--VAARPGFGLSPIY 798
Rat             LGAGGVIPGAVGLGG-VSPAAAAKAAKYGAAGLGGVLGA-RPFPGGGVAARPGFGLSPIY 822
Cow             ----------------VSPAAAAKAAKFGAAGLGGVLGAGQPFPIG-------------- 707
Pig             ----------------VSPAAAAKAAKYGAAGLGGVLGVTRPFPLGGVAPRPGFGLSPIF 720
Human           ----------------IPPAAAAKAAKYGAAGLGGVLGGAGQFPLGGVAARPGFGLSPIF 777
Chimpanzee      ----------------IPPAAAAKAAKYGAAGLGGVLGGAGQFPLGGVAARPGFGLSPIF 609
Baboon          ----------------VSPAAAAKAAKYGAAGLGGVLGGAGQFPLGGVAARPGFGLSPIF 719
                                :.*********:**:***.***    *

Dog             PGGGAGGLGIGGKPPKPYGGALGALGYQGGACLGKSCGRKRK 783
Cat             PGGGAGGLGIGGKPPKPFGGALGALGYQGGACLGKSCGRKRK 794
Mouse           PGGGAGGLGVGGKPPKPYGGALGALGYQGGGCFGKSCGRKRK 840
Rat             PGGGAGGLGVGGKPPKPYGGALGALGYQGGGCFGKSCGRKRK 864
Cow             --GGAGGLGVGGKPPKPFGGALGALGFPGGACLGKSCGRKRK 747
Pig             PGGGAGGLGIGGKPPKPFGGALGALGYQGGACLGKSCGRKRK 762
Human           PGG----------------------------ACLGKACGRKRK 792
Chimpanzee      PGG----------------------------ACLGKACGRKRK 624
Baboon          PGGGAGGLGVGGKPPKPFGGALGALGYQGAACLGKSCGRKRK 761
                  *                           .*:**:******
```

Figure 4.3. Alignment of mammalian tropoelastin sequences by ClustalW. Identical residues are denoted by "*", conserved residues by ":", and semi-conserved residues by ".". The degree of conservation was based on the similarity score of all residues at

each position, calculated using the Gonnet Pam250 matrix (conserved: score >0.5, semi-conserved: score =<0.5) [286]. With the exception of the signal peptide and the human domain 26A (in greyed out font), all negative residues within the sequences are highlighted. The human tropoelastin E345 and E414 residues are bold underlined. The human (GeneID: 2006), cow (GeneID: 280781), mouse (GeneID: 13717), and rat (GeneID: 25043) tropoelastin sequences are confirmed protein sequences. The dog (NCBI: NC_006589.3), cat (NCBI: XM_003998576.1), pig (Gene Index: TC373476), chimpanzee (NCBI: XM_003318598.2), and baboon (NCBI: XM_003919412.1) sequences are translated from predicted elastin gene sequences.

4.2.2 Production of tropoelastin constructs

4.2.2.1 DNA sequencing

To produce the E345A, E414A and E345A+E414A constructs, *E. coli* cultures were transformed with a pET-3d vector containing the mutant tropoelastin sequence. Sequencing of the 2.1 kb tropoelastin insert within the plasmid following extraction from transformed colonies confirmed the relevant mutation/s at the DNA level (Appendix 8.3-8.5). In the E345A and E414A clones, an alanine-encoding GCA was found at the codon location corresponding to the 345^{th} and 414^{th} tropoelastin residue, respectively. In the E345A+E414A clone, a GCA was located at both codon positions encoding for tropoelastin residues 345 and 414.

4.2.2.2 Mass spectrometry

Comparative mass spectrometry of purified and Lys-C digested WT and E345A showed overlapping peaks within the 4000-6500 mass/charge window, except for a WT-specific peak at 5076.77, labelled B, and an E345A-specific peak at 5018.76, labelled B* (Figure 4.4). Both mass peaks were assigned to the same peptide fragment containing residue 345 (

Table 4.1). The observed mass shift of 58 m/z corresponded to the monoisotopic mass difference between a glutamate and an alanine residue, consistent with an E345A substitution in the mutant construct at the protein level.

Similarly, the mass spectrometry profiles of WT and E414A differed only by a single peak (Figure 4.5). The 5711.01 peak, labelled D in the WT spectrum, was shifted to a 5653.01 peak, labelled D* in the E414A spectrum. Both mass peaks corresponded to the peptide fragment containing residue 414 (

Table 4.1). The peak shift represented the 58 Da mass difference between the wild-type E414 and the mutant A414 residues, and confirmed the presence of an amino acid mutation in the E414A construct.

In the same manner, the WT and E345A+E414A constructs displayed identical mass spectra except in two locations (Figure 4.6). Both the 5076.77 and 5711.01 peaks in the WT profile appeared as 5018.76 and 5653.01 peaks in the E345A+E414A profile, respectively. The first peak was assigned to the tropoelastin peptide containing residue 345, and the second to that containing residue 414. The mass shifts corresponded to the mass difference between glutamate and alanine at both positions, and supported the presence of a double mutation in the E345A+E414A construct.

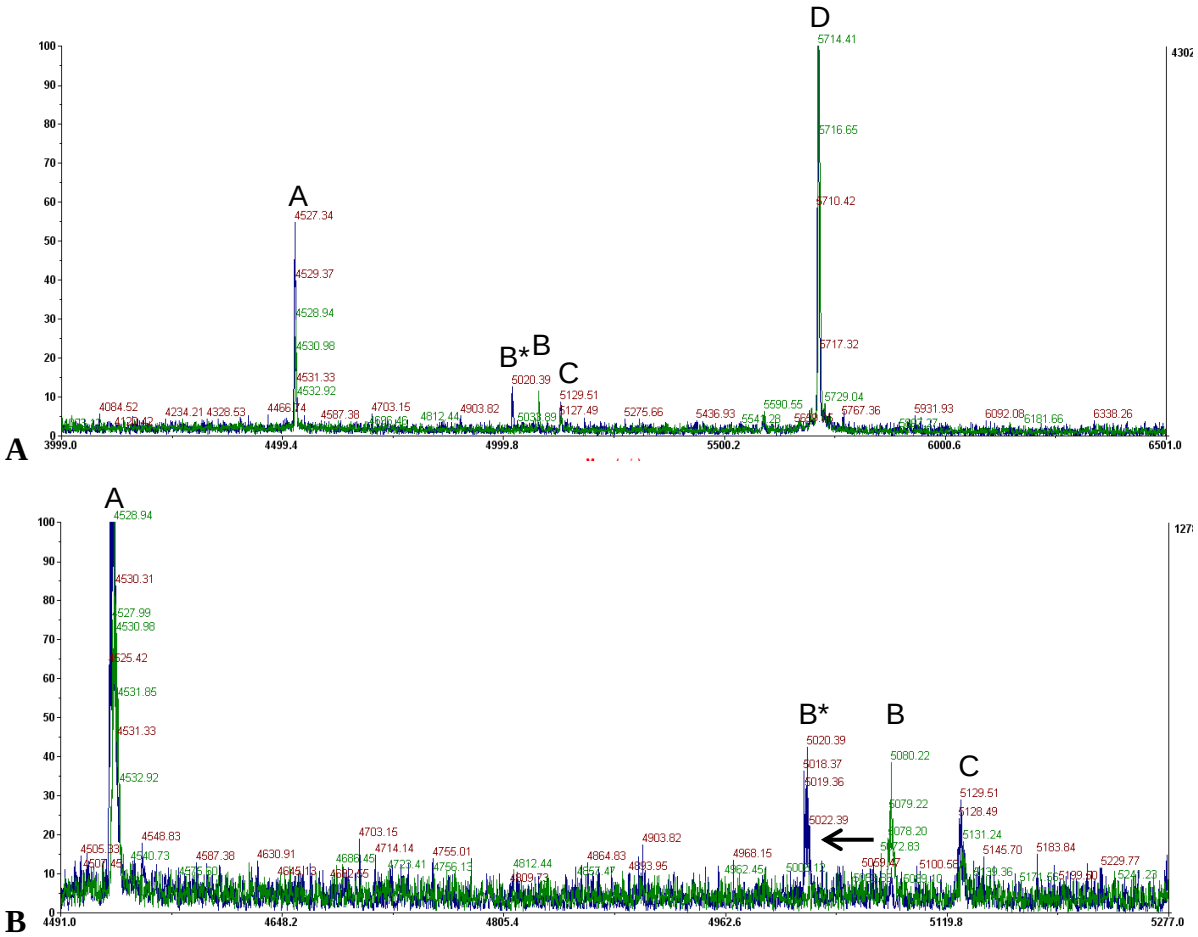

Figure 4.4. Comparative mass spectrometry of WT (green) and E345A (blue) tropoelastin. The peaks within the (A) 4000-6500 and (B) 4490-5280 m/z windows are shown. The 4526.57, 5127.88 and 5711.01 mass peaks, corresponding to peptide sequences common to WT and E345A, were present in both profiles. The 5076.77 peak in the WT spectrum was shifted to a 5018.76 peak in the E345A spectrum (arrow), confirming the mutation at the protein level.

D

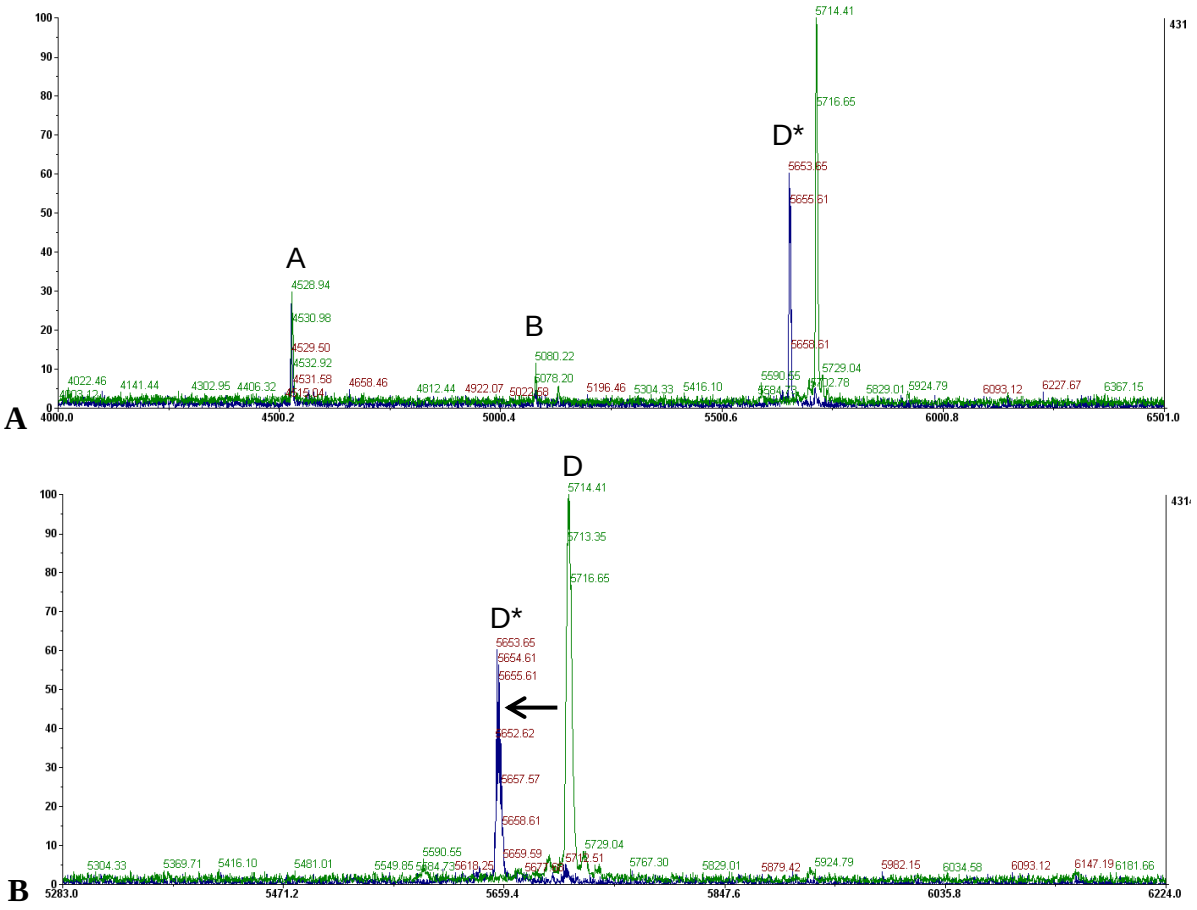

Figure 4.5. Comparative mass spectrometry of WT (green) and E414A (blue) tropoelastin. The peaks within the (A) 4000-6500 and (B) 4490-5280 m/z windows are shown. The 4526.57 and 5076.77, mass peaks, corresponding to peptide sequences common to WT and E414A, were present in both spectra. A mass shift occurred from 5711.01 peak in the WT to the 5653.01 peak in the E414A (arrow), confirming the mutation at the protein level.

D*

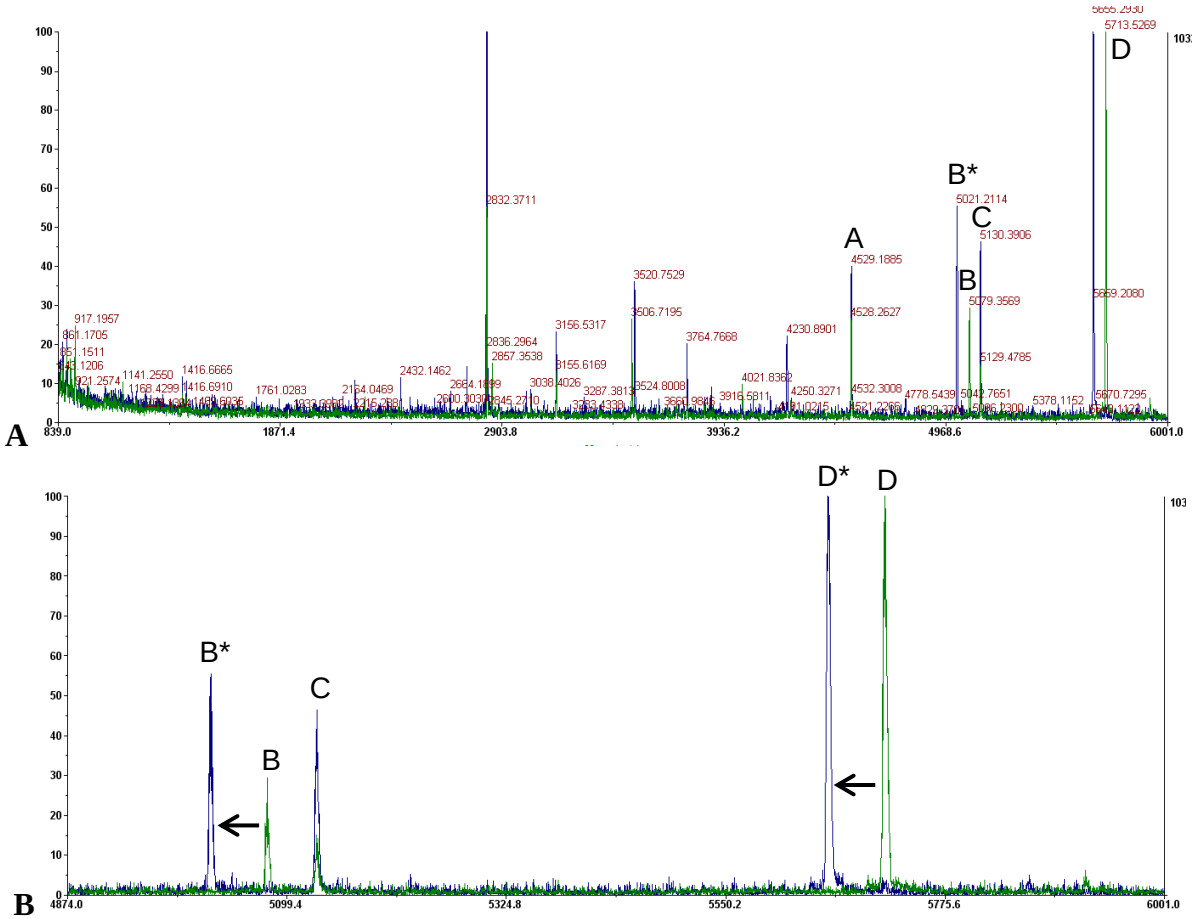

Figure 4.6. Comparative mass spectrometry of WT (green) and E345A+E414A (blue) tropoelastin. The peaks within the (A) 840-6000 and (B) 4875-6000 m/z windows are shown. Within the 4000-6500 m/z range, the 4526.57 and 5127.88 mass peaks, corresponding to peptide sequences common to WT and E345A+E414A, were present in both spectra. The 5076.77 and 5711.01 peaks in the WT profile were shifted to 5018.76 and 5653.01 peaks in the E345A+E414A profile, respectively, confirming the double mutation at the protein level.

Table 4.1. Assignment of peaks from mass spectrometry analyses of Lys-C digested tropoelastin constructs within a mass/charge window of 4000-6500. The residues at positions 345 and 414 are underscored.

Peak	Mass	Residues	Peptide Sequence
A	4526.5720	512-565	AQLRAAAGLGAGIPGLGVGVGVPGLGVGAGVPGLGVGAGVPGF GAVPGALAAAK
B	5076.7671	290-349	YGAAAGLVPGGPGFGPGVVGVPGAGVPGVGVPGAGIPVVPGA GIPGAAVPGVVSP**E**AAAK
B*	5018.7616	290-349	YGAAAGLVPGGPGFGPGVVGVPGAGVPGVGVPGAGIPVVPGA GIPGAAVPGVVSP**A**AAAK
C	5127.8831	442-503	AAQFGLVPGVGVAPGVGVAPGVGVAPGVGLAPGVGVAPGVGV APGVGVAPGIGPGGVAAAAK
D	5711.0130	357-422	YGARPGVGVGGIPTYGVGAGGFPGFGVGVGGIPGVAGVPSVG GVPGVGGVPGVGISP**E**AQAAAAAK
D*	5653.0076	357-422	YGARPGVGVGGIPTYGVGAGGFPGFGVGVGGIPGVAGVPSVG GVPGVGGVPGVGISP**A**AQAAAAAK

4.2.2.3 SDS-PAGE

SDS-PAGE analysis of purified E345A, E414A, and E345A+E414A indicated a ~60 kDa product corresponding to the expected size of the tropoelastin constructs (Figure 4.7). There was no visible contamination with bacterial proteins. The constructs were predominantly full-length with minimal degradation.

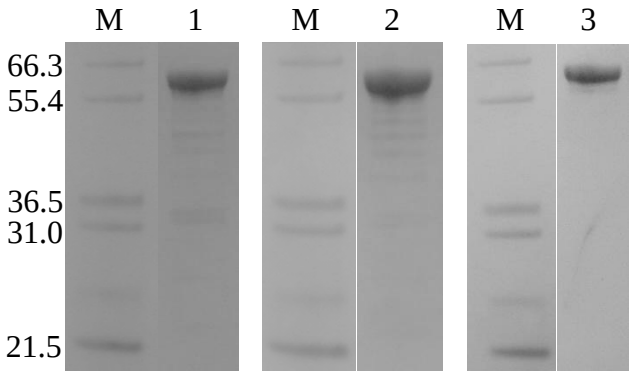

Figure 4.7. SDS-PAGE analysis of purified tropoelastin constructs. Lanes: M – protein standards (kDa); 1 – E345A; 2 – E414A; 3 – E345A+E414A.

4.2.3 Coacervation studies

All tropoelastin constructs displayed temperature-dependent coacervation (**A**

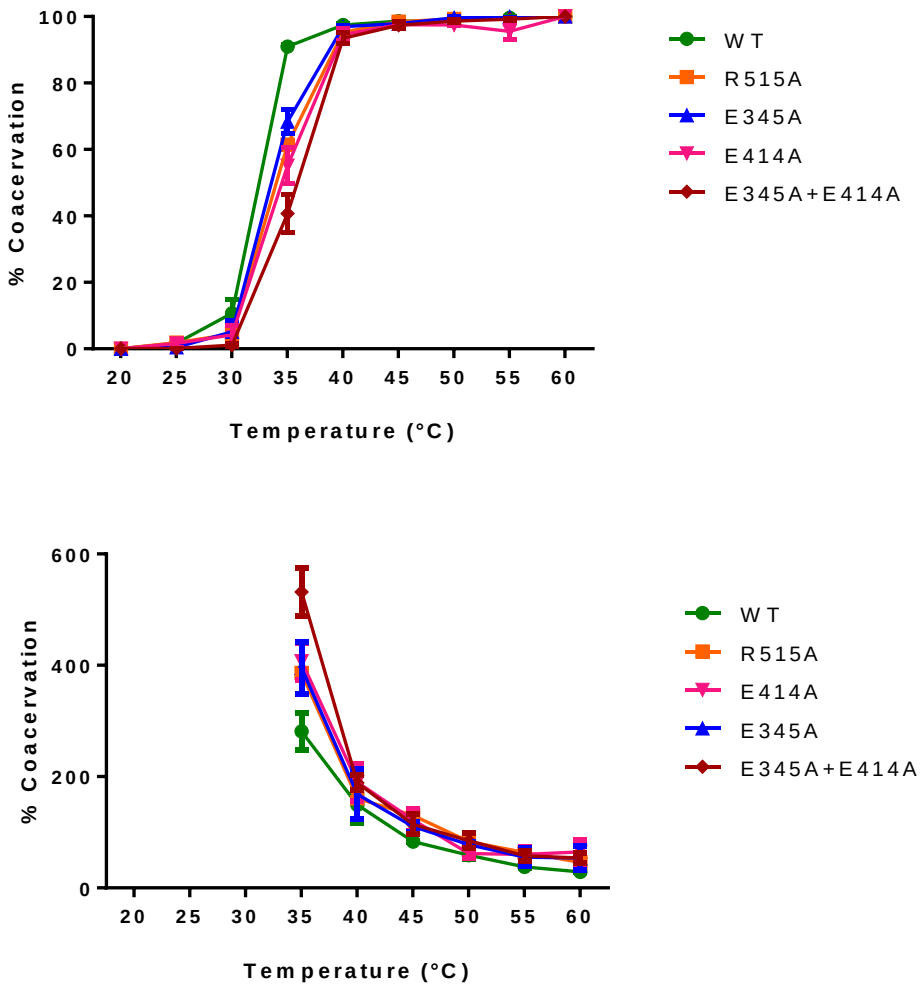

B

Figure 4.8A). As each sample reached a critical temperature, a sharp increase in turbidity was detected and interpreted as a rapid rise in coacervation level. Negligible increases in sample turbidity were observed beyond this transition temperature, which was distinct for each tropoelastin construct. Full coacervation was achieved at 35°C by WT, but only at 40°C by R515A, E345A, E414A and E345A+E41A. At 35°C, the mutant constructs coacervated to variable extents. Both single E to A mutants displayed similar self-association relative to R515A ($p>0.05$), while the E345A+E414A species exhibited significantly reduced coacervation compared to either R515A, E345A or E414A ($p<0.001$).

The time required for full coacervation to occur was also temperature-dependent for all tropoelastin constructs (**A**

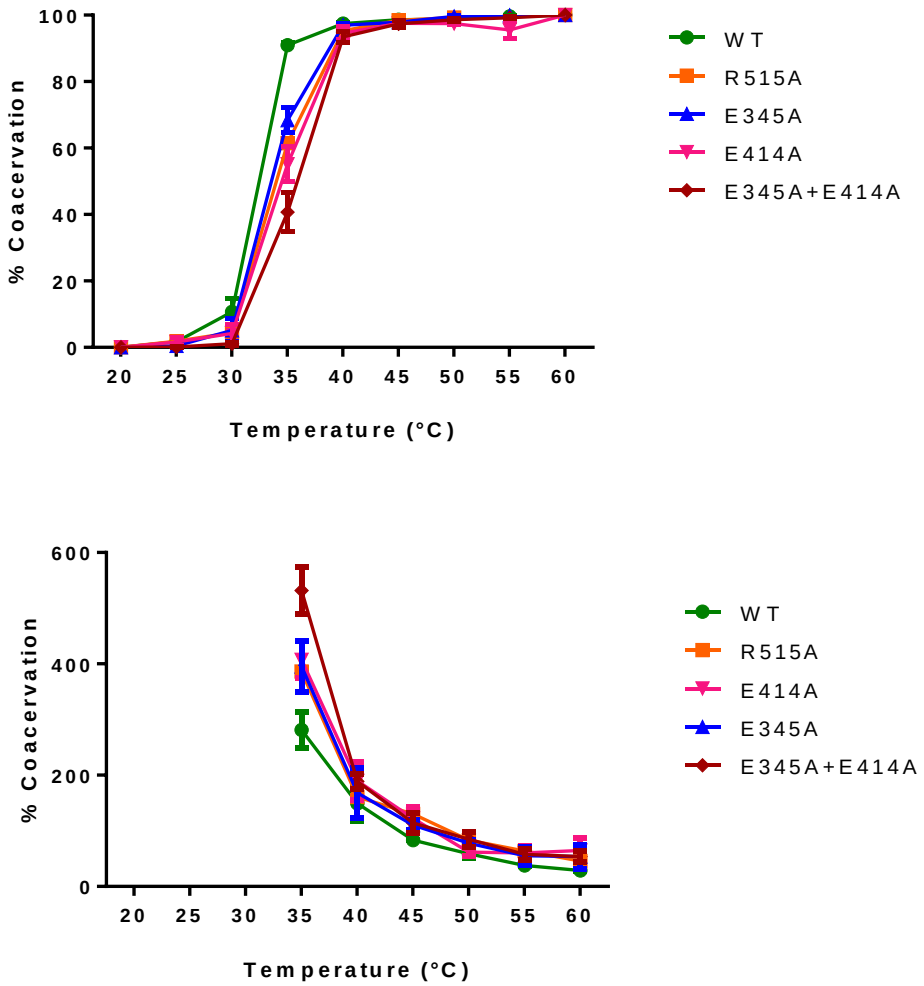

B

Figure 4.8B). Coacervation time decreased exponentially with increasing temperature. A difference in the coacervation time of the constructs was observed below the transition temperature of the mutants at 40°C. Similarly to R515A, the Glu-to-Ala constructs required a significantly longer time to aggregate compared to WT ($p<0.01$). Among the Glu-to-Ala mutants, E345A+E414A coacervated significantly more slowly than either E345A ($p<0.001$) or E414A ($p<0.01$).

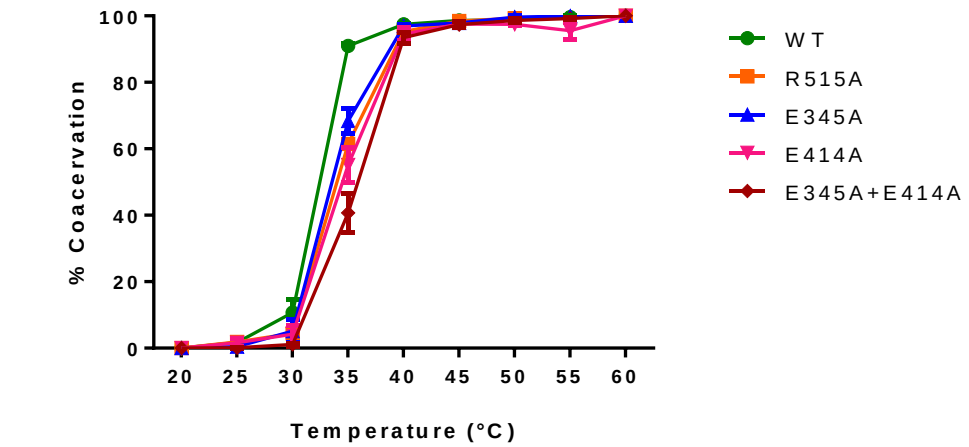

A

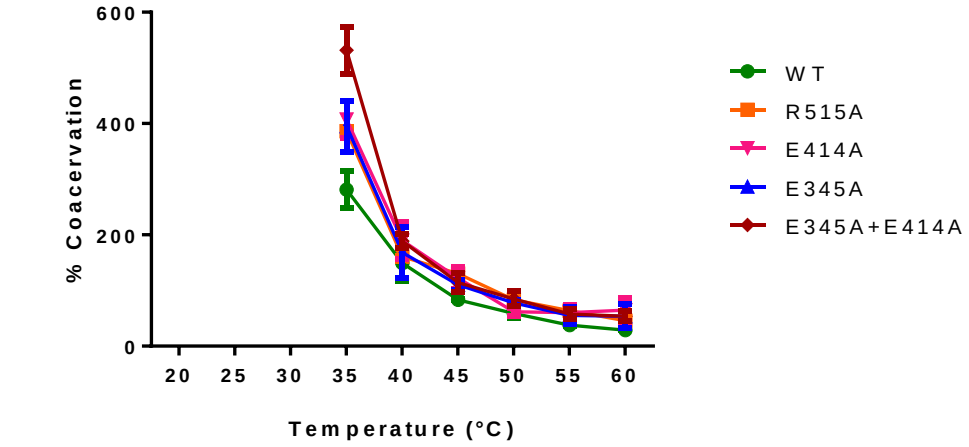

B

Figure 4.8. Coacervation profiles of WT, R515A, E345A, E414A and E345A+E414A tropoelastin. (A) The extent of coacervation at each temperature, expressed as a percentage of the maximum coacervation achieved by each tropoelastin sample. (B) The time taken by each construct to coacervate at each temperature.

The differences in the coacervation profiles of WT and mutant species were confirmed by the analysis of solution particle sizes over a range of temperatures (Figure 4.9). At or below 30°C, all tropoelastin constructs were present as ~10 nm monomers in solution. At 35°C, all WT species had associated into ~400 nm particles, while the mutant species were composed of distinct populations of ~10 nm monomers and aggregates ranging from 800 nm to 3.5 μm. At this temperature, the tropoelastin mutants differed in the extent of coacervation: 32% of R515A, 66% of E345A, 67% of E414A, and 66% of E345A+E414A species remained as monomers. At 40°C, all mutant species had coacervated into 400-500 nm particles similarly to WT. The same trend was observed at 45°C. At 50°C, however, WT tropoelastin had further assembled into ~2 μm aggregates, while the R515A, E345A and E414A constructs formed similar-sized particles only at 55°C. Notably, the E345A+E414A coacervates did not reach this end size even at 55°C.

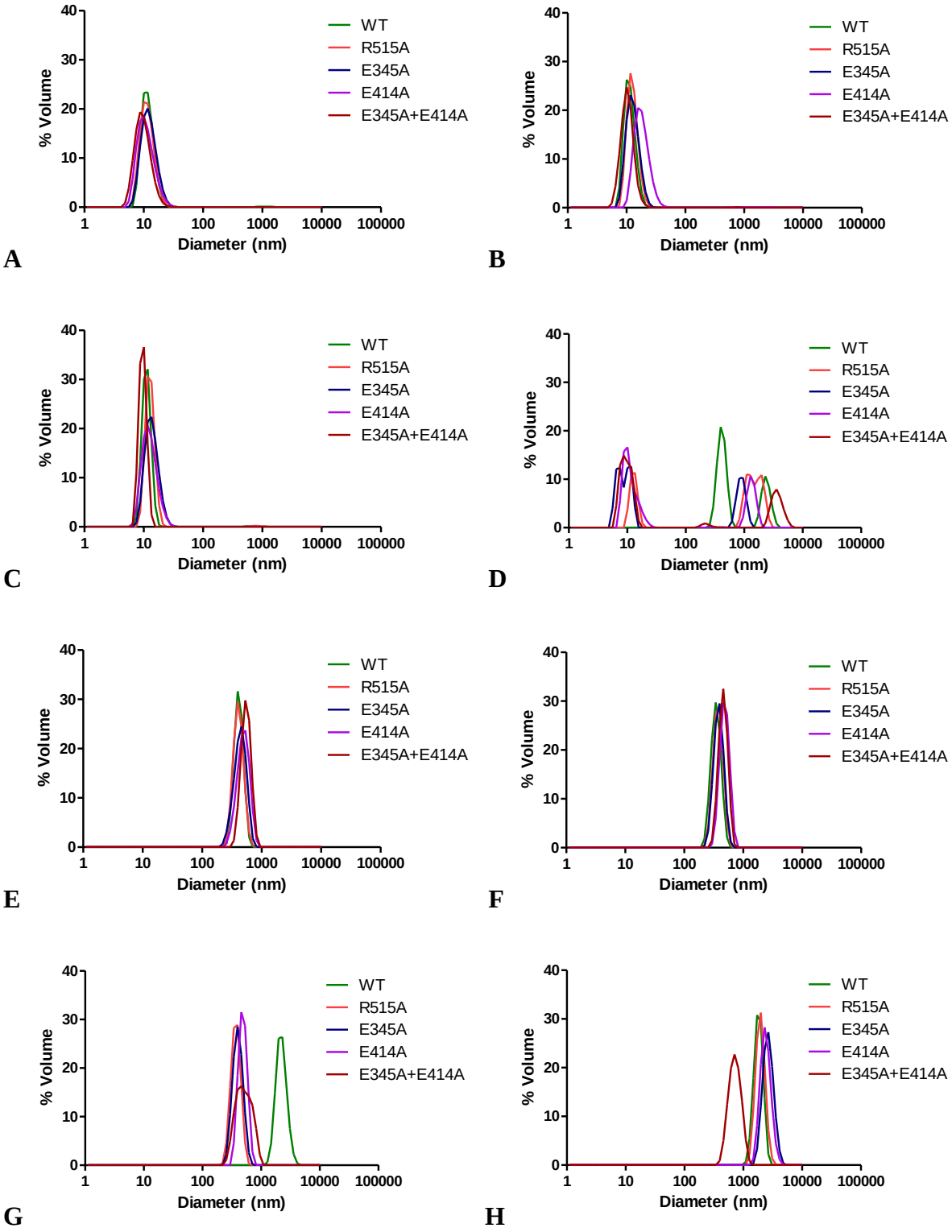

Figure 4.9. Particle sizes of WT, R515A, E345A, E414A and E345A+E414A tropoelastin solutions at (A) 20, (B) 25, (C) 30, (D) 35, (E) 40, (F) 45, (G) 50 and (H) 55°C.

4.2.4 Cross-linking studies

4.2.4.1 Hydrogel construction

Addition of a six-fold molar excess of the chemical cross-linker BS3 to tropoelastin solutions allowed successful production of hydrogels from each tropoelastin construct (Figure 4.10). The hydrogels appeared visually similar with smooth translucent surfaces.

SDS-PAGE analysis of the aqueous solution left after tropoelastin polymerisation revealed the absence of monomer species in all samples (Figure 4.11). This indicated the complete cross-linking of WT and mutant constructs into elastin hydrogels.

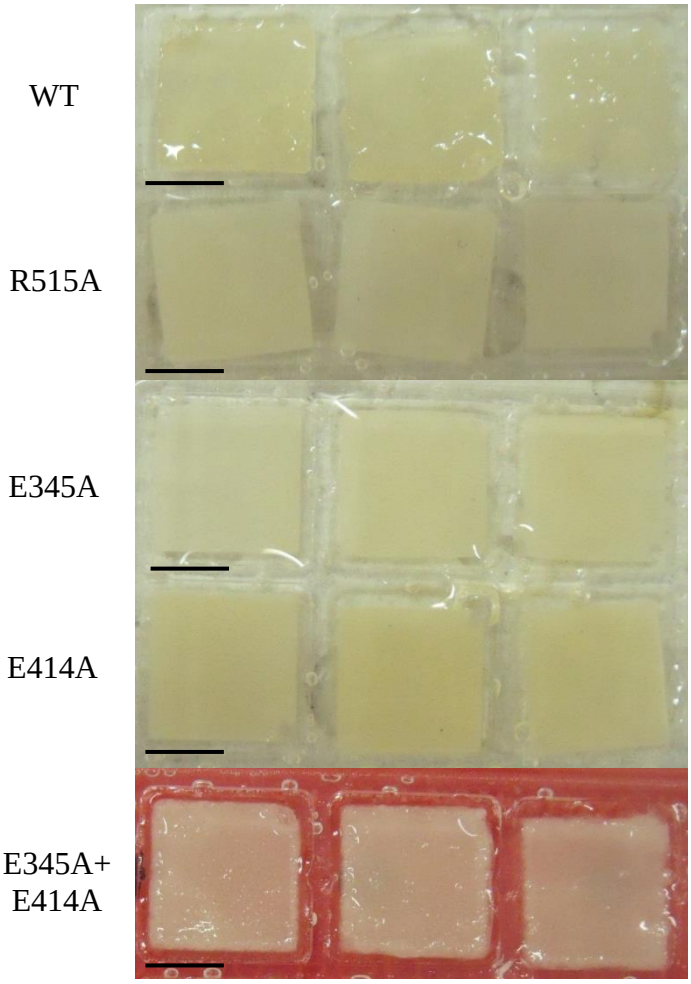

Figure 4.10. Pre-lyophilised hydrogels constructed from the chemical cross-linking of WT, R515A, E345A, E414A and E345A+E414A with BS3. Scale bar: 0.5 cm.

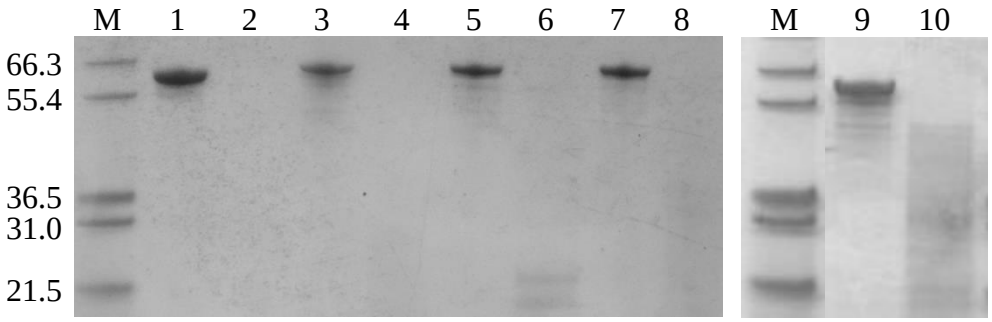

Figure 4.11. SDS-PAGE analysis of the aqueous solution left after tropoelastin cross-linking into hydrogels. Lanes: M – protein standards (kDa); 1 – purified WT; 2 – WT with BS3; 3 – purified R515A; 4 – R515A with BS3; 5 – purified E345A; 6 – E345A with BS3; 7 – purified E414A; 8 – E414A with BS3; 9 – purified E345A+E414A; 10 – E345A+E414A with BS3.

4.2.4.2 Micro-CT of hydrogels

Micro-CT imaging revealed discernible differences in the structural composition of the lyophilised hydrogels (Figure 4.12). The WT hydrogel consisted of a filamentous network interspersed with numerous pores that were visible across the top surface and throughout the cross-section of the material. In contrast, this predominantly porous network structure was not observed in any of the mutant hydrogels.

The mutant species formed hydrogels that were morphologically distinct from each other. The cross-linked R515A hydrogel was composed of compactly-arranged bead-like spherules. The E345A, E414A and E345A+E414A hydrogels also appeared as a dense material; however, the presence of globular structures was not obvious either on the surfaces or within the cross-sections. While the finer structural features of these hydrogels remained largely undefined at this resolution, subtle differences between them could be visibly detected. The E345A hydrogel appeared more compact than the E414A or E345A+E414A constructs, as evidenced by its reduced thickness despite having a mass comparable to the other hydrogels. The E414A hydrogel comprised of more loosely-packed, wispy structures that were easily dislodged during sample handling. The E345A+E414A hydrogel exhibited a fibrous structure reminiscent of the WT material; however, its structure was more compact, with pores significantly smaller than those seen in the WT.

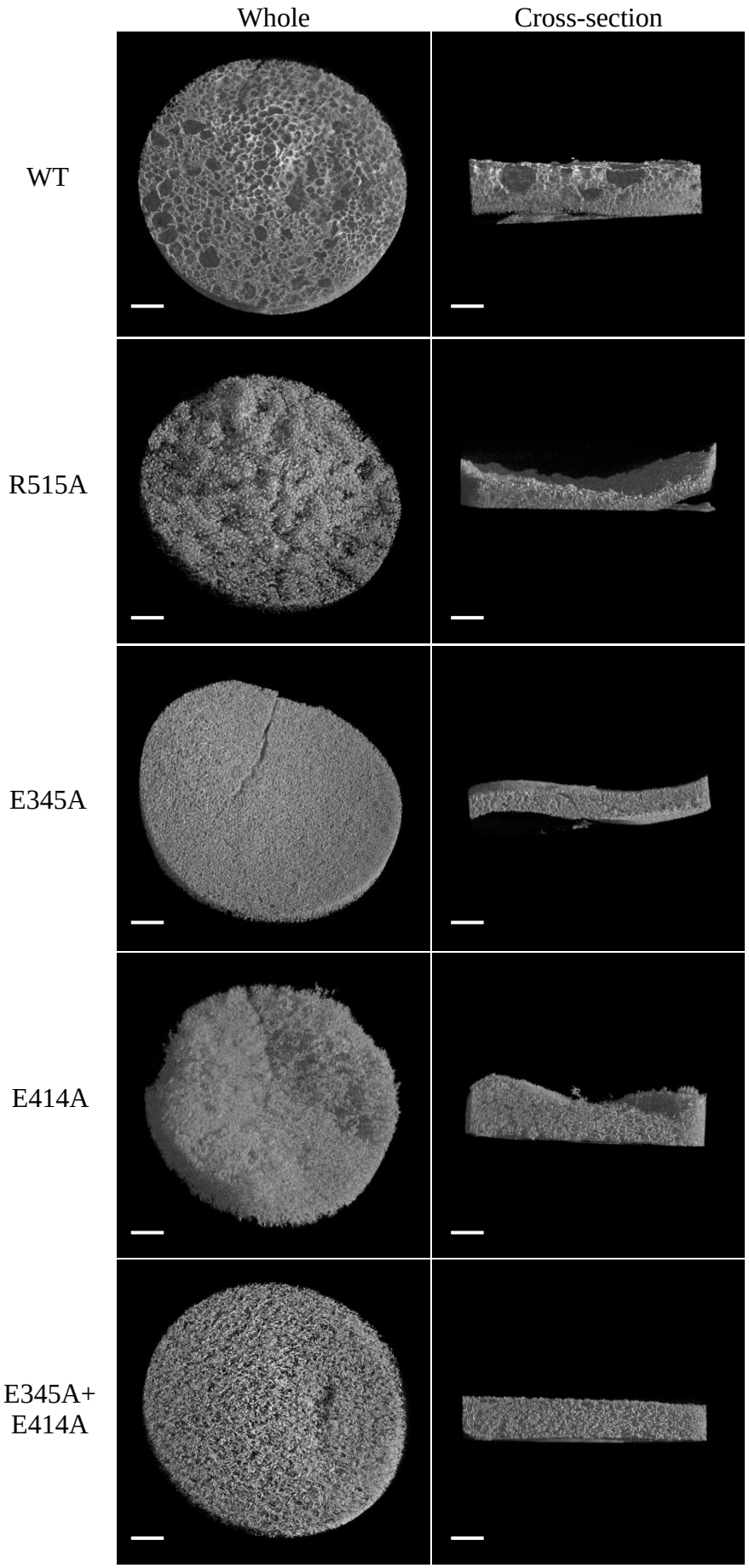
Whole
Cross-section
WT
R515A
E345A
E414A
E345A+
E414A

Figure 4.12. Three-dimensional reconstruction of WT, R515A, E345A, E414A and E345A+E414A hydrogels by micro-CT imaging. For each hydrogel, the whole construct and a cross-section are shown. Scale bar: 0.8 mm.

The most apparent difference between the WT and mutant hydrogels was the abundance of large pore structures in the former that were absent in the mutant constructs. Calculations of hydrogel porosity from micro-CT cross-sections estimated the WT material to be 87% porous and the mutant hydrogels to be significantly denser at 70% porosity for R515A and 76% for E345A, E414A and E345A+E414A (Figure 4.13). There was no statistical difference between the porosities of the mutant hydrogels.

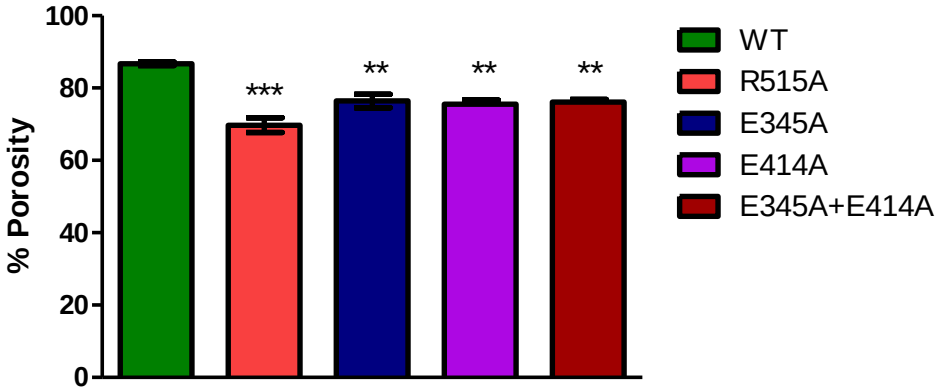

Figure 4.13. Porosity of wild-type and mutant elastin hydrogels calculated from micro-CT analyses.

4.2.4.3 Hydrogel swelling

The elastin hydrogels exhibited profound but differential swelling after being submerged in water for a 24-hr period at various temperatures (Figure 4.14). At the physiological temperature, WT hydrogels absorbed water up to 60 times their dry weight. In contrast, water influx into the mutant hydrogels was significantly reduced. The R515A, E345A, E414A and E345A+E414A hydrogels swelled approximately 8-, 2-, 3- and 5-fold less compared to the WT, respectively. This trend was consistent at each temperature (Figure 4.15). There were no significant differences between the swelling properties of the mutant hydrogels.

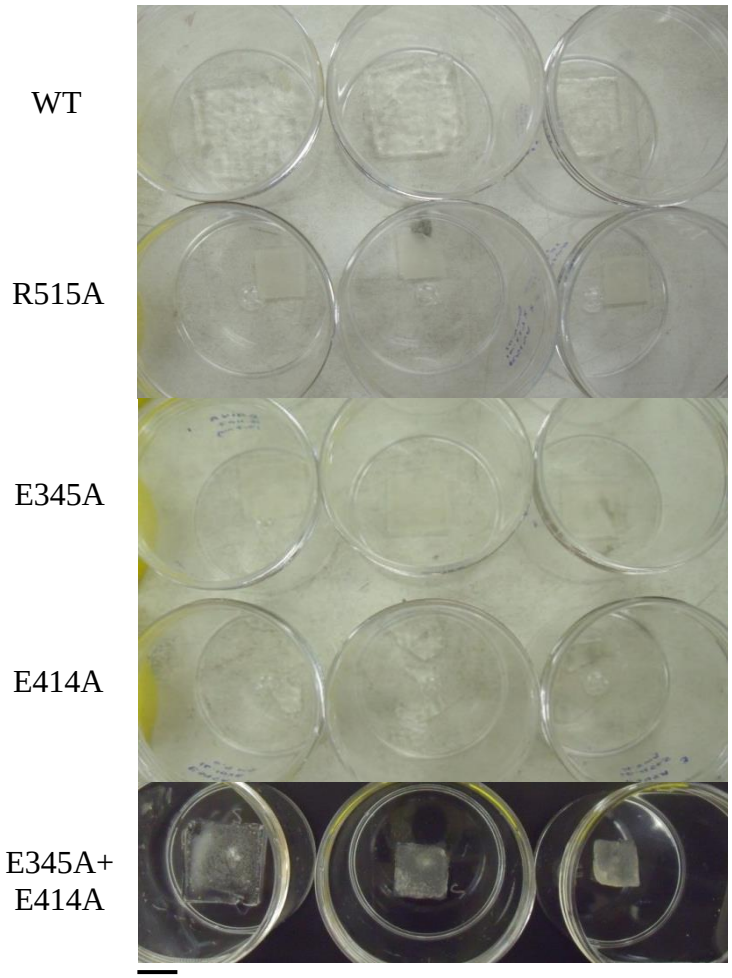

Figure 4.14. WT, R515A, E345A, E414A and E345A+E414A hydrogels swollen in water at 37°C overnight. Triplicate samples are shown. Scale bar: 0.5 cm.

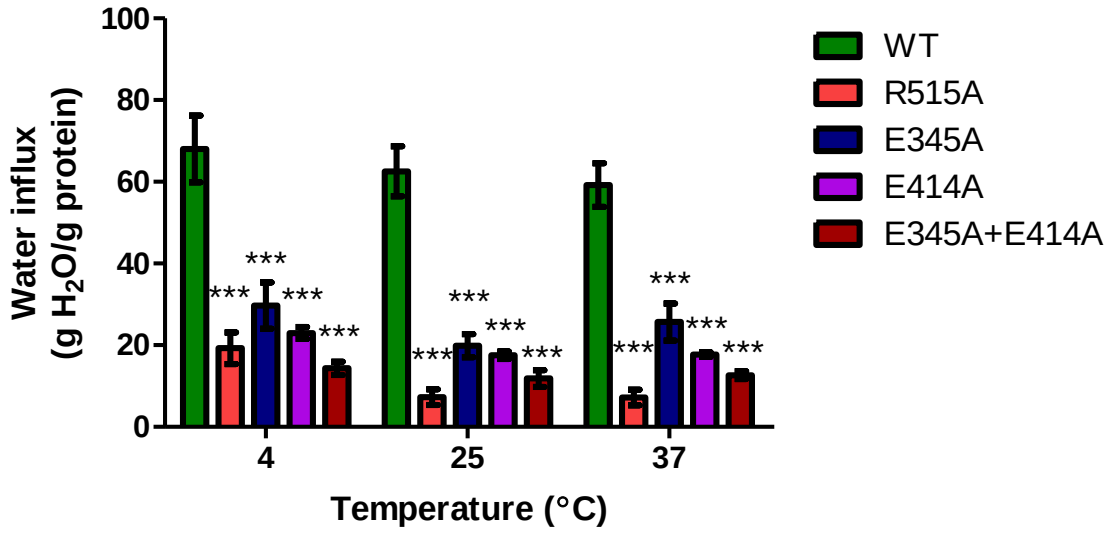

Figure 4.15. Water uptake by hydrogels submerged in water at 4, 25 and 37°C overnight.

4.2.4.4 SEM of hydrogel surfaces

SEM of the hydrogels demonstrated distinct differences in the structural composition of their surfaces (Figure 4.16). The top surface of the WT hydrogel appeared as a flat layer with large pores ~100 μm in size. In contrast, the top surfaces of the R515A, E345A, E414A and E345A+E414A hydrogels were marked by an abundance of ~10 μm globules that were interlinked differently among the mutant hydrogels. In the R515A hydrogel, the globules were clustered to form branching structures across the surface. In the E345A hydrogel, the spherules appeared as discrete entities connected by very fine fibres. In the E414A hydrogel, the particles were interspersed among sheet-like fragments containing a number of ~10 μm pores. In the E345A+E414A hydrogel, the globules were joined by thick fibres that appeared to have arisen from the coalescence of clustered globules themselves. Unlike the top surfaces, the bottom surfaces of the elastin hydrogels shared a similar morphology,

consisting of a smooth sheet-like structure with pores ranging from 20-100 μm in size (Figure 4.17).

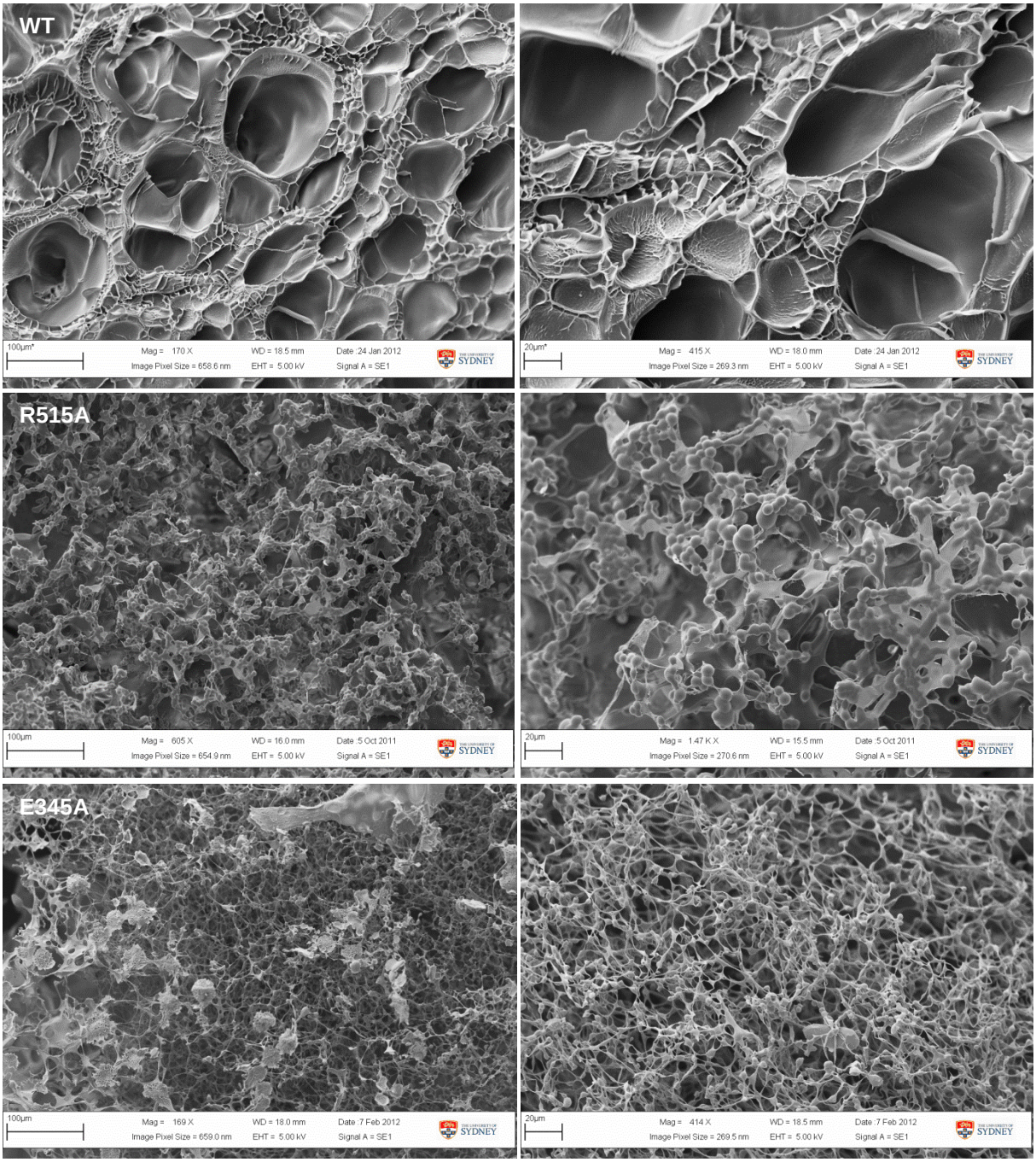

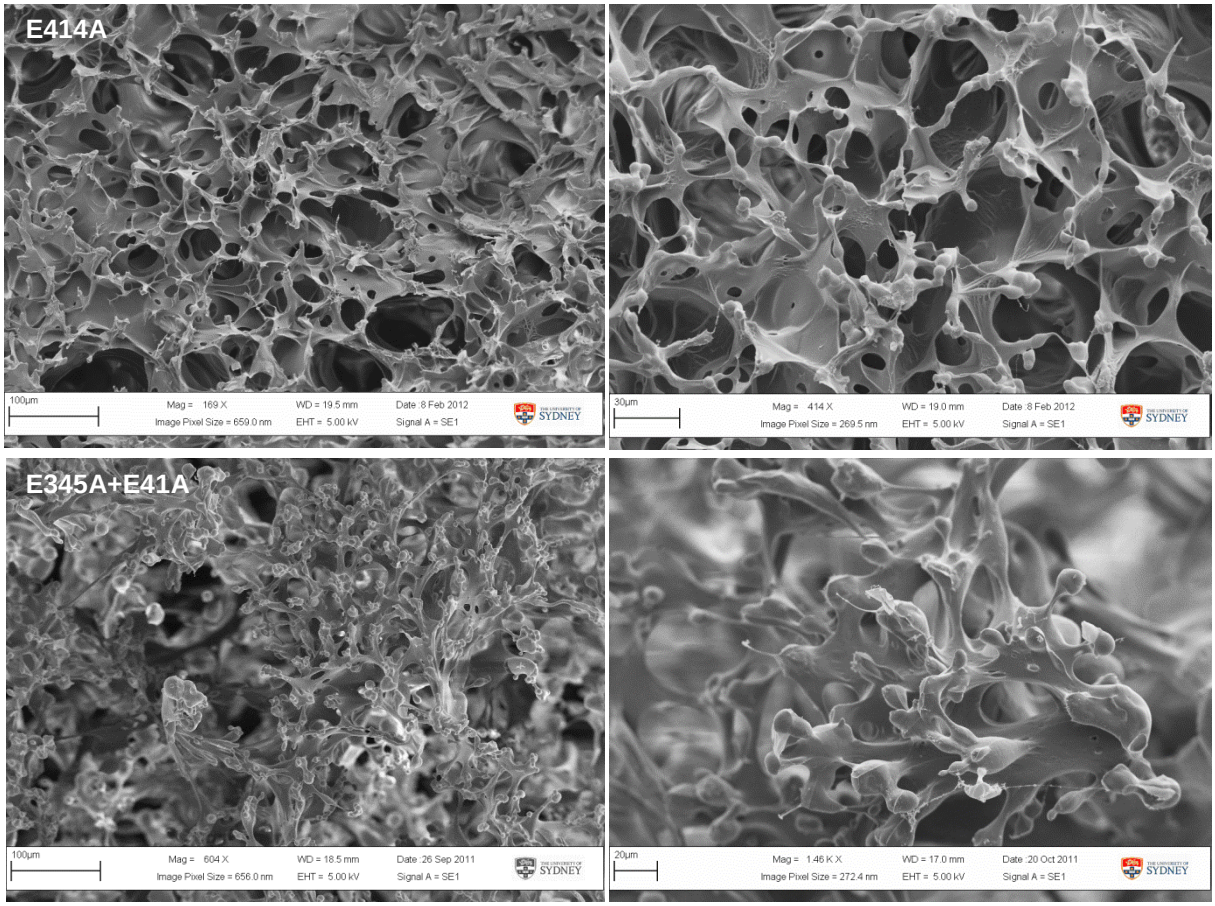

Figure 4.16. SEM imaging of the top surface of hydrogel constructs, shown at low and high magnification.

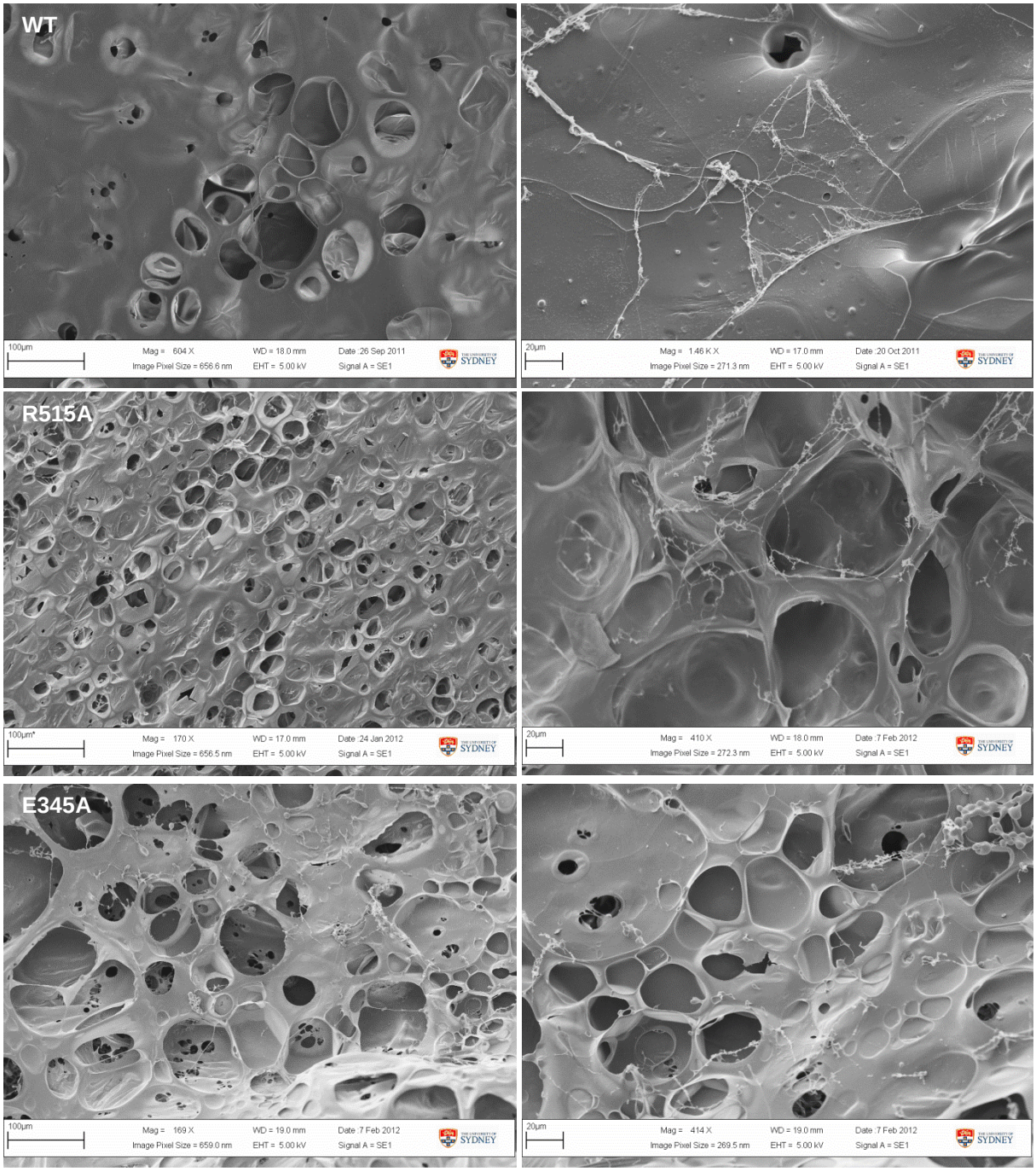
WT
100µm
Mag = 604 X
WD = 18.0 mm
Date :26 Sep 2011
Image Pixel Size = 656.6 nm
EHT = 5.00 kV
Signal A = SE1
20µm
Mag = 1.46 K X
WD = 17.0 mm
Date :20 Oct 2011
Image Pixel Size = 271.3 nm
EHT = 5.00 kV
Signal A = SE1
R515A
100µm*
Mag = 170 X
WD = 17.0 mm
Date :24 Jan 2012
Image Pixel Size = 656.5 nm
EHT = 5.00 kV
Signal A = SE1
20µm
Mag = 410 X
WD = 18.0 mm
Date :7 Feb 2012
Image Pixel Size = 272.3 nm
EHT = 5.00 kV
Signal A = SE1
E345A
100µm
Mag = 169 X
WD = 19.0 mm
Date :7 Feb 2012
Image Pixel Size = 659.0 nm
EHT = 5.00 kV
Signal A = SE1
20µm
Mag = 414 X
WD = 19.0 mm
Date :7 Feb 2012
Image Pixel Size = 269.5 nm
EHT = 5.00 kV
Signal A = SE1

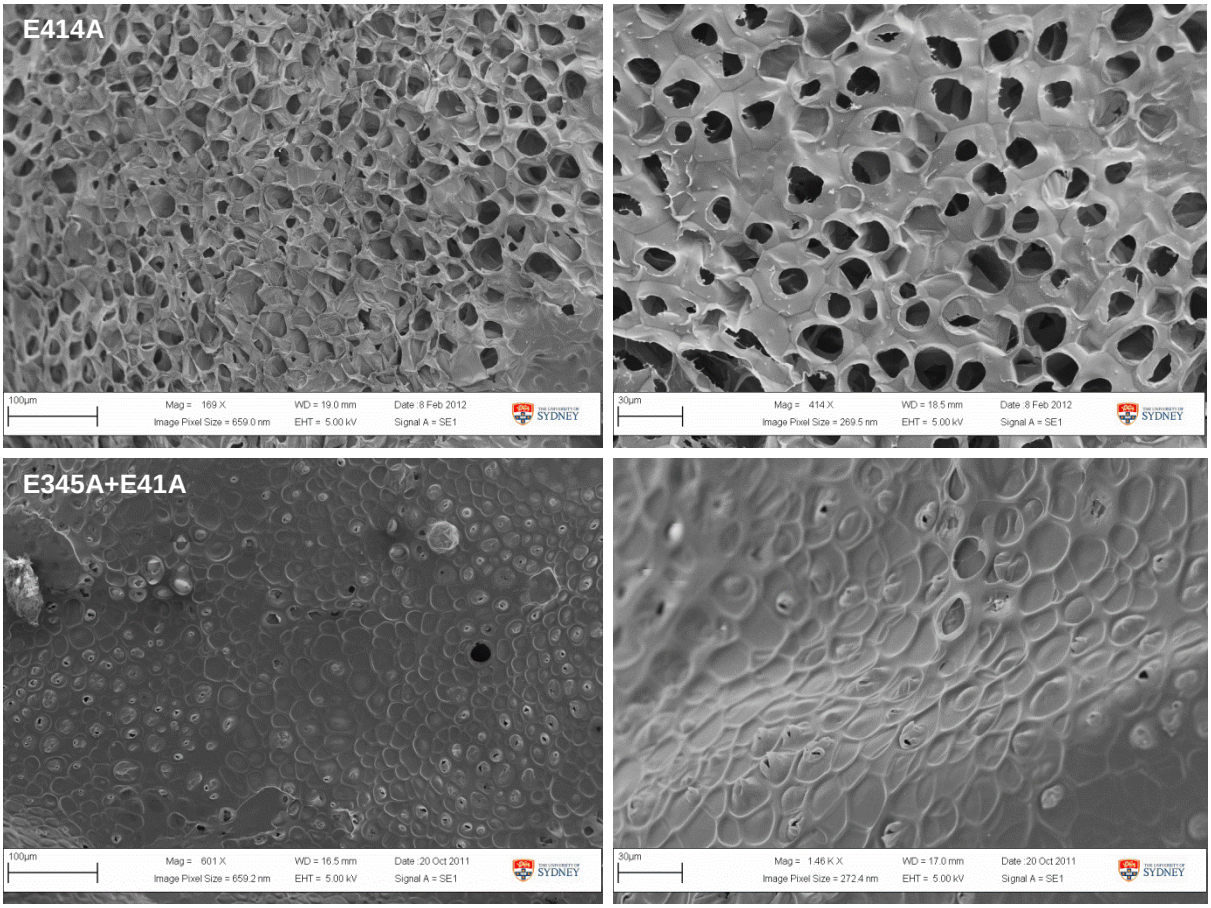

Figure 4.17. SEM imaging of the bottom surface of hydrogel constructs, shown at low and high magnification.

4.2.5 Cell attachment

Tissue culture wells coated with the tropoelastin constructs supported attachment of human dermal fibroblasts in a dose-dependent manner until saturation at ~10 μg/mL tropoelastin

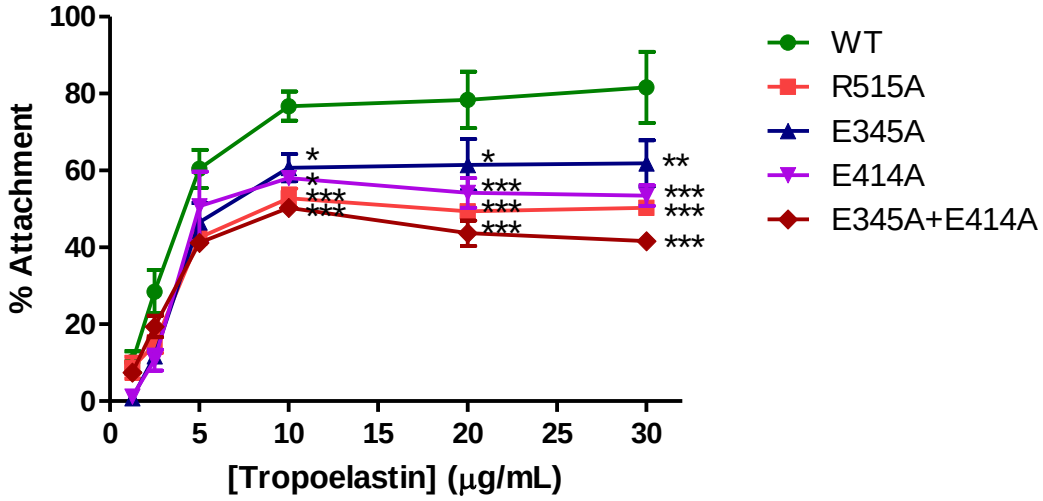

(Figure 4.18). At tropoelastin concentrations supporting maximum cell attachment, WT allowed the adhesion of up to 80% of seeded cells. In contrast, all mutant constructs were associated with significantly reduced cell interactions. Compared to the WT construct, R515A, E345A, E414A and E345A+E414A supported the attachment of 53%, 61%, 58% and 50% of seeded cells, respectively. There was no statistical difference between cell adhesion to the tropoelastin mutants.

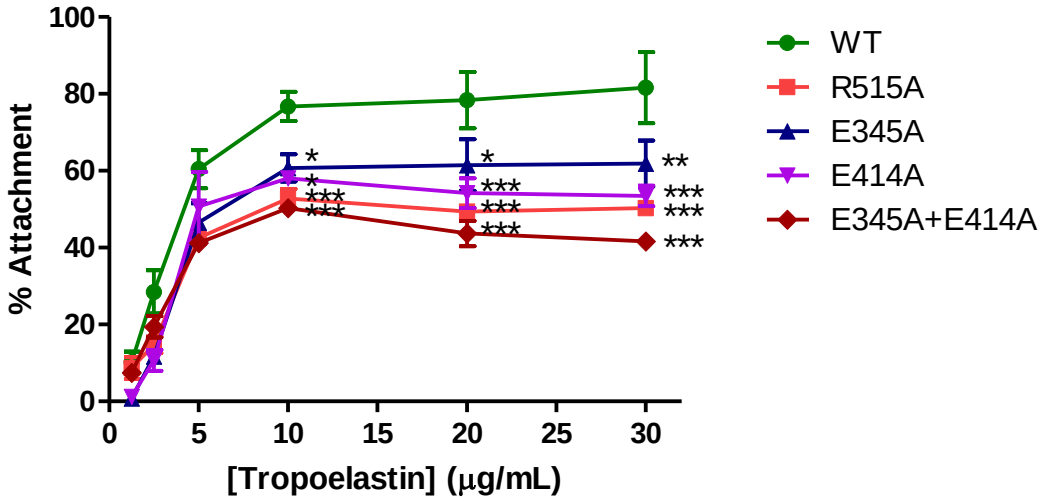

Figure 4.18. Attachment of GM3348 human dermal fibroblasts to WT, R515A, E345A, E414A and E345A+E414A tropoelastin.

4.2.6 Detection of tropoelastin by ELISA

To elucidate the observed differences in fibroblast attachment to the tropoelastin constructs, the coating of WT and mutant species on cell culture wells was characterised by ELISA.

The amount of bound tropoelastin detected by the BA4 anti-elastin antibody increased proportionally to the coating concentration until saturation at ~10 μg/mL tropoelastin (Figure 4.19A). At excess concentrations of tropoelastin, similar levels of WT, R515A, E345A, E414A and E345A+E414A were detected.

The accessibility of the tropoelastin C-terminus on the surface-bound constructs was compared using an antibody directed against domain 36 of tropoelastin (Figure 4.19B). The specificity of the antibody was confirmed with the low levels of epitope detection in the M155n construct, which is truncated after domain 25 and therefore does not contain the tropoelastin C-terminus. At the maximum tropoelastin coating concentration, a significantly decreased amount of C-termini was detected in all mutant constructs compared to WT. At most, only 55%, 79%, 66% and 75% of R515A, E345A, E414A and E345A+E414A domain 36 was accessible to the antibody, respectively.

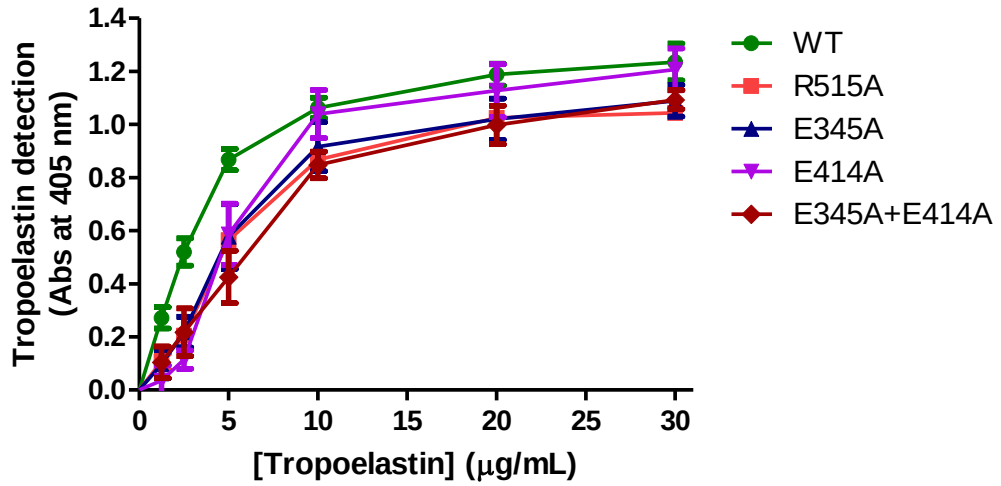

A

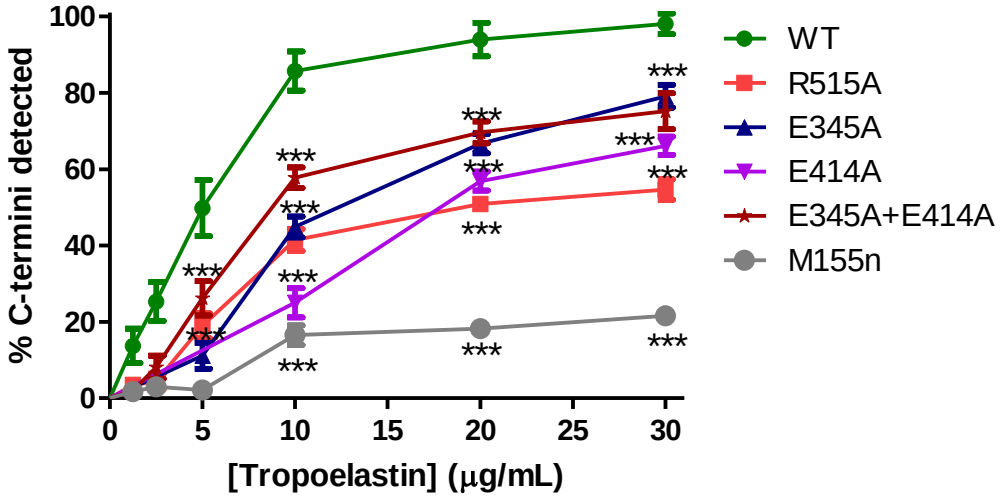

B

Figure 4.19. Detection of tropoelastin bound on tissue culture wells by the (A) BA4 anti-elastin antibody and (B) anti-C-terminus antibody.

4.2.7 Elastic fibre assembly

The ability of the tropoelastin constructs to form elastic fibres in a cellular environment was determined by the addition of WT, R515A, E345A, E414A and E345A+E414A to the culture medium of human dermal fibroblasts (Figure 4.20). One day after tropoelastin addition, WT spherules were arranged in a linear fibre-like morphology. In contrast, the mutant species remained randomly dispersed or were clustered in a globular organisation in the extracellular space. By day four, fine well-defined WT elastic fibres were visible. Elastic fibre structures were likewise observed in the R515A, E414A and E345A+E414A samples. However, these fibres respectively displayed a 26%, 21% and 23% reduction in immunofluorescence, and were 27%, 65% and 37%% less abundant than WT fibres despite comparable cell numbers in all samples

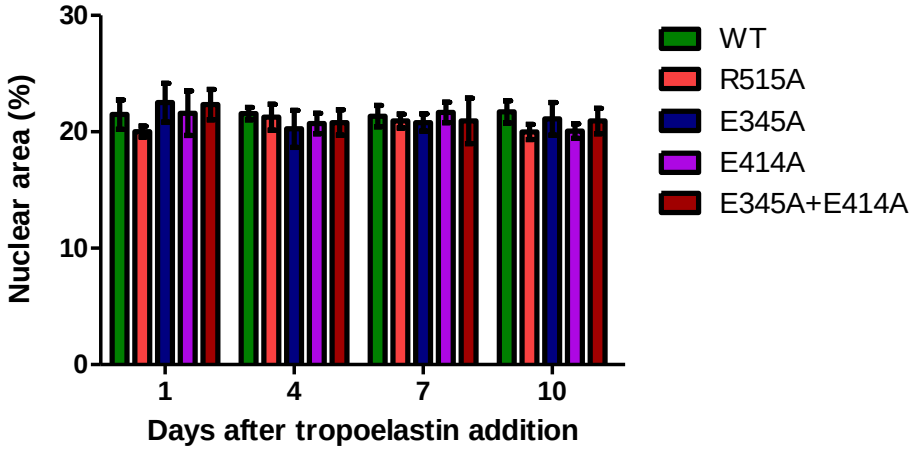

(Figure 4.21). Remarkably, the E345A construct remained as punctate species and did not form definitive elastic fibres. These differences in the elastogenic ability of the tropoelastin constructs were consistently observed at seven and ten days after tropoelastin addition, although the number of E414A fibres eventually increased to levels comparable with the E345A+E414A fibres. No elastic fibres were detected when tropoelastin was not added to the culture medium of cells. The faintly fluorescent fibres observed in the staining controls are due to elastin autofluorescence.

Day 1

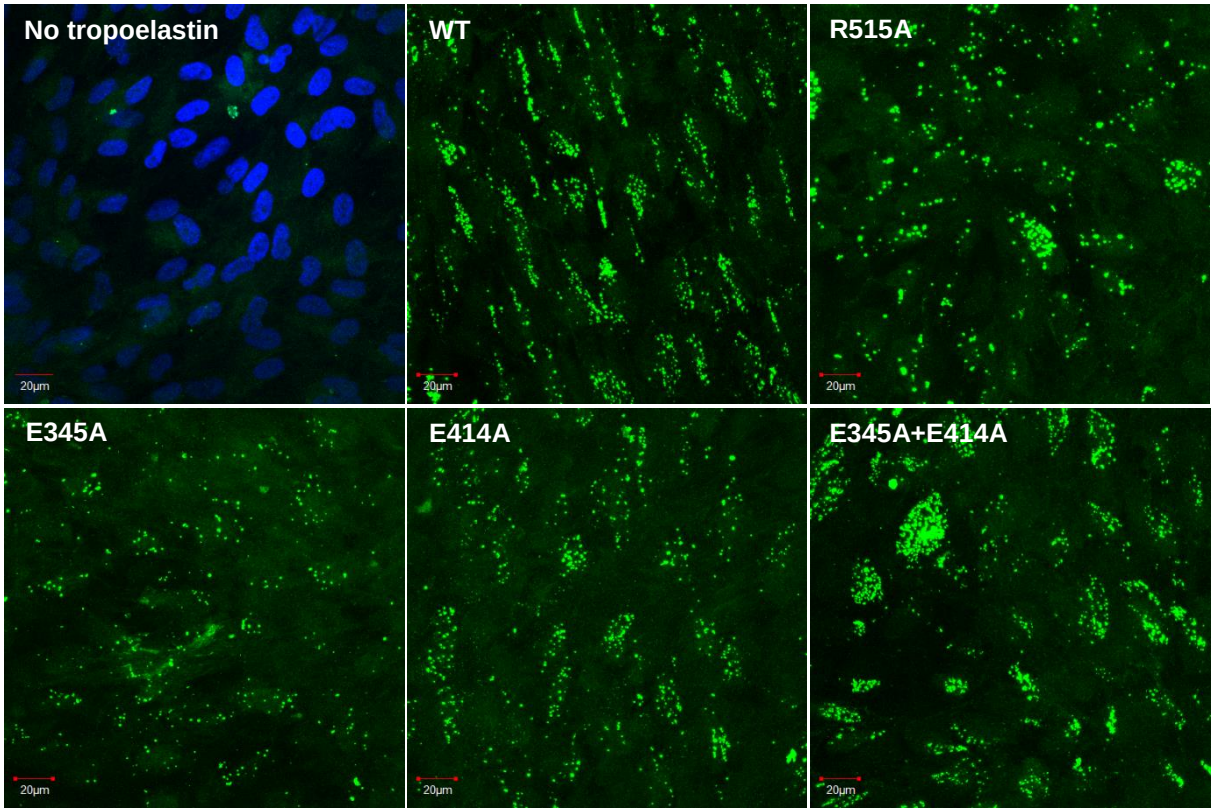
No tropoelastin
WT
R515A
E345A
E414A
E345A+E414A
20µm

Day 4

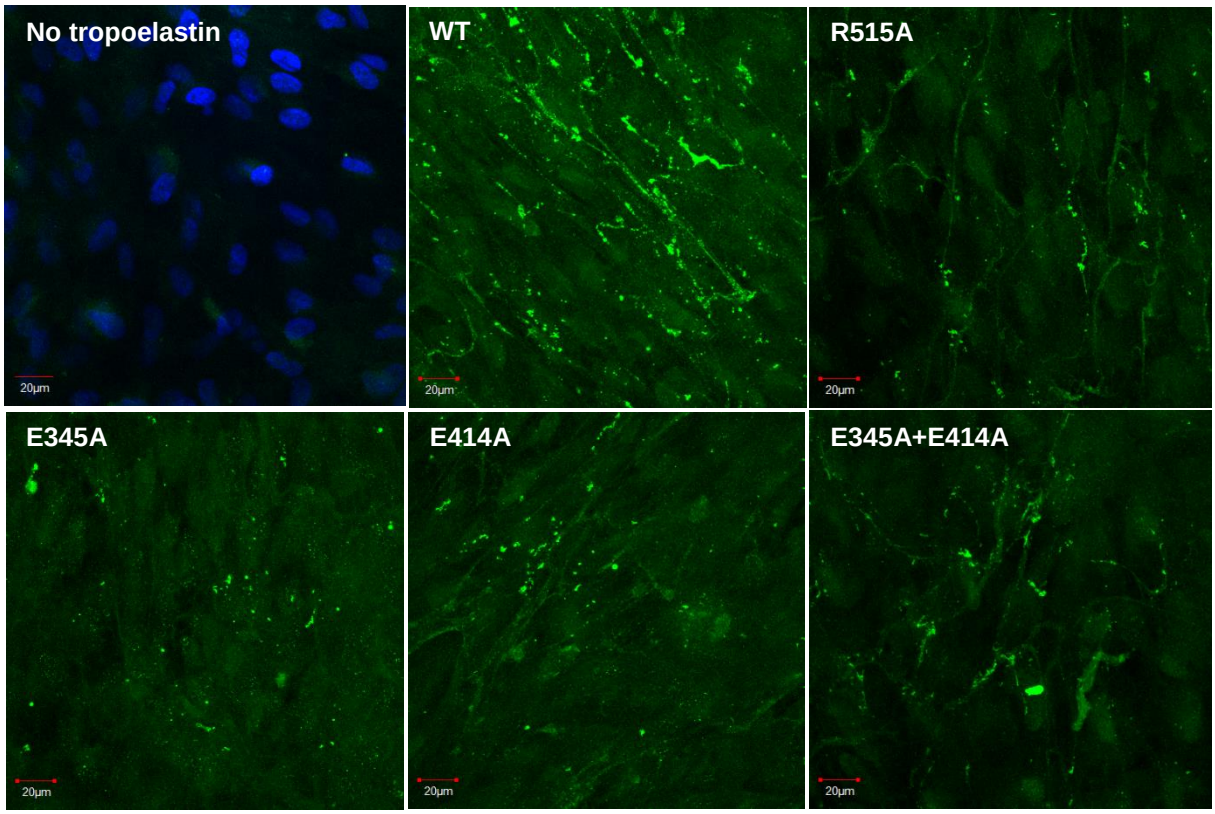
No tropoelastin
WT
R515A
E345A
E414A
E345A+E414A
20µm

Day 7

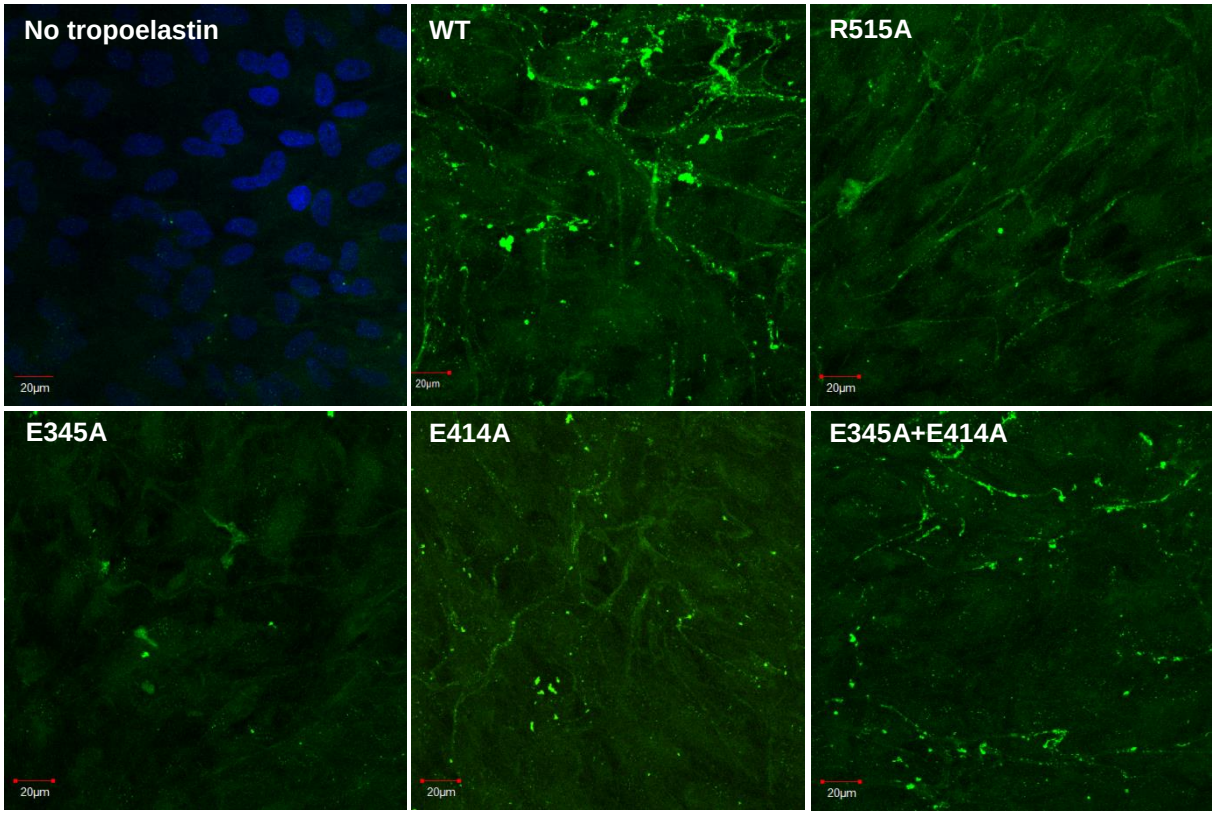
No tropoelastin
WT
R515A
E345A
E414A
E345A+E414A
20µm

Day 10

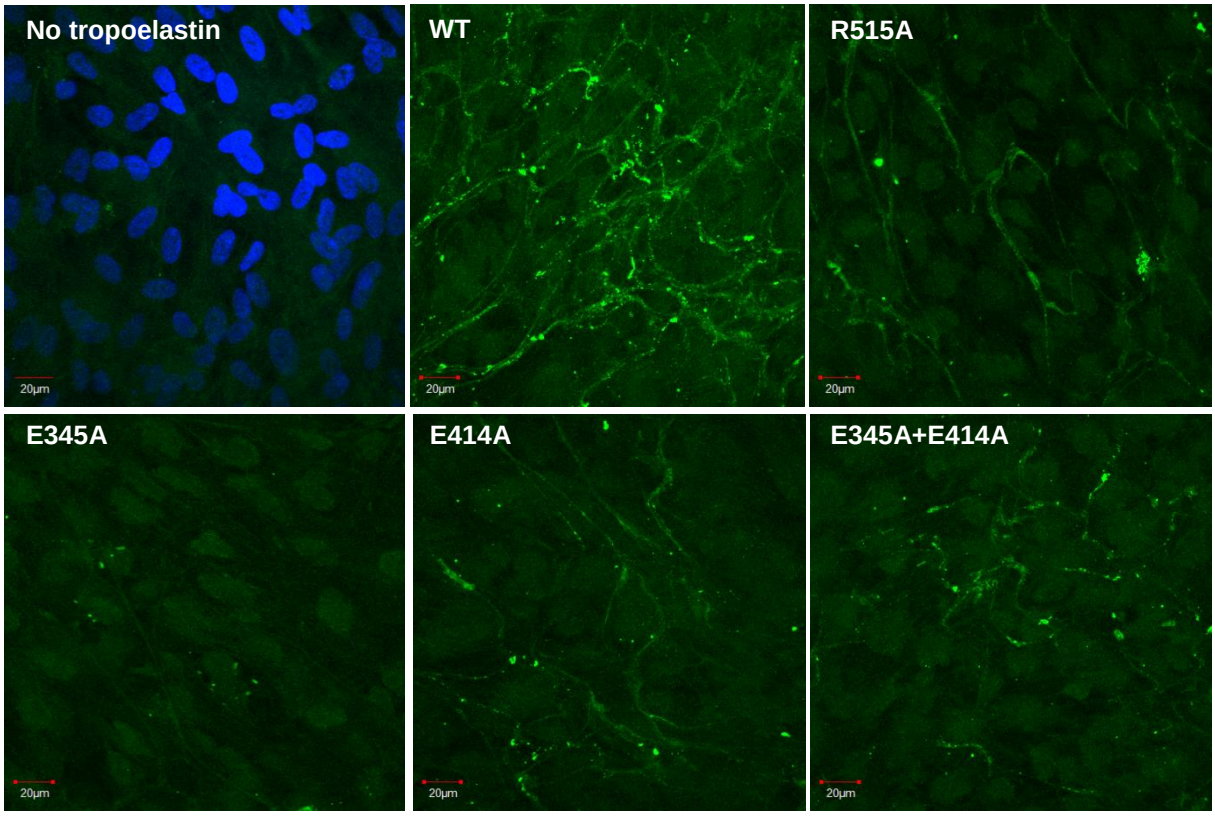
No tropoelastin
WT
R515A
E345A
E414A
E345A+E414A
20µm

Controls

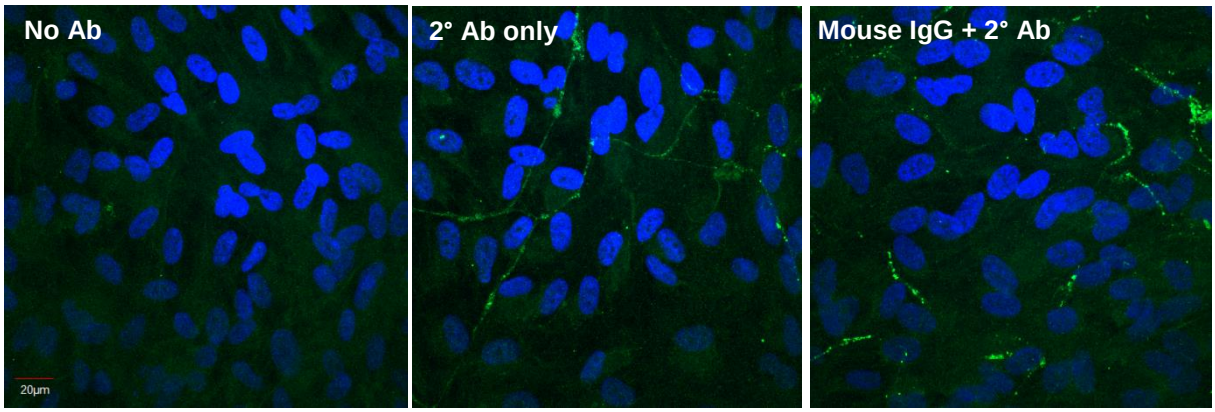

Figure 4.20. Elastic fibre assembly by GM3348 human dermal fibroblasts at 1, 4, 7 and 10 days after addition of 20 µg/mL WT, R515A, E345A, E414A or E345A+E414A tropoelastin into the culture medium. Elastic fibres were stained with the mouse BA4 anti-elastin antibody and a FITC-conjugated anti-mouse antibody. Staining controls consist of samples to which WT tropoelastin was added, but were treated with no antibody, with the secondary antibody only, or with a non-specific primary antibody and the secondary antibody. Cell nuclei were stained with DAPI.

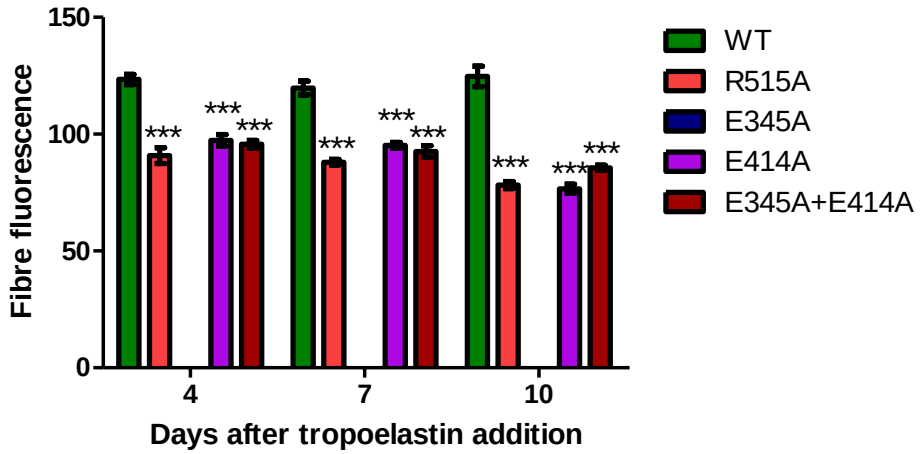

A

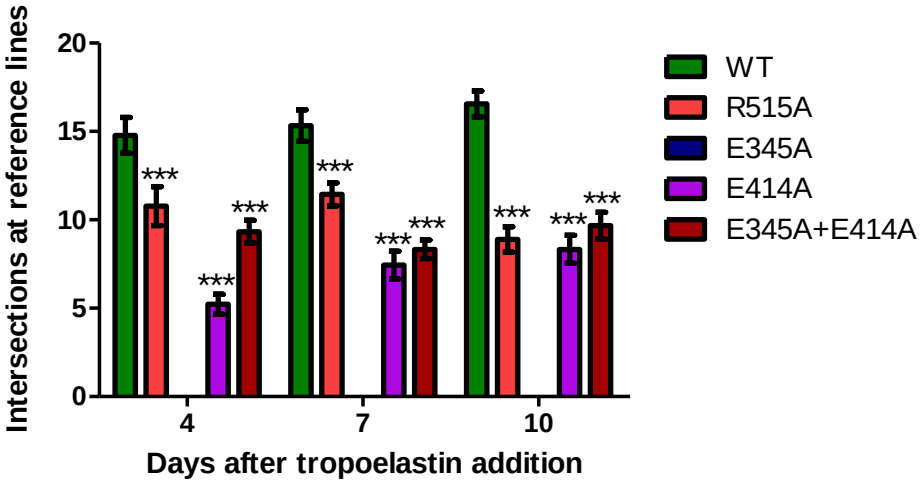

B

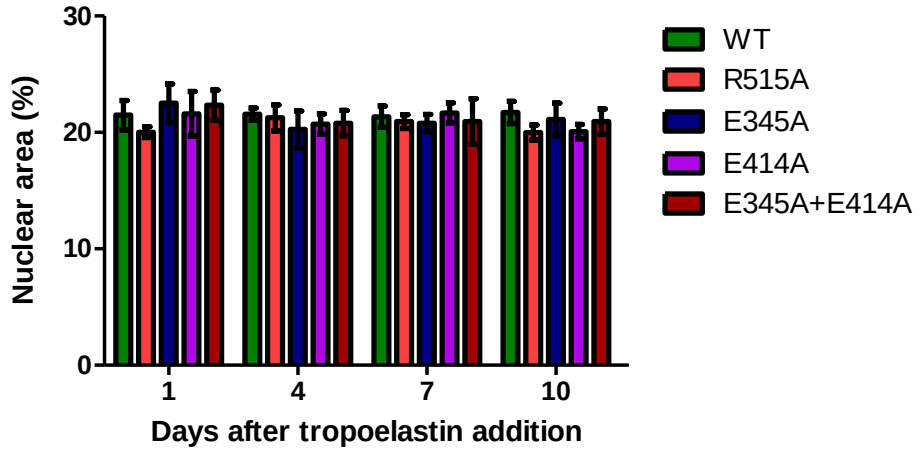

C

Figure 4.21. (A) Elastin-specific fluorescence and (B) density of elastic fibres. (C) Cell numbers as measured by the area occupied by cell nuclei per field of view.

4.2.8 Structural studies

4.2.8.1 Far-UV CD

Far-UV CD analysis indicated that the tropoelastin constructs possessed comparable spectral features, including a negative minimum at 200 nm and a slight shoulder at 220 nm (Figure 4.22). This computationally translated to a similar secondary structure composition of the constructs, consisting predominantly of unordered regions (49%), with a small percentage of alpha-helices (10%), beta-sheets (19%), turns (12%), and polyproline-2 helices (9%).

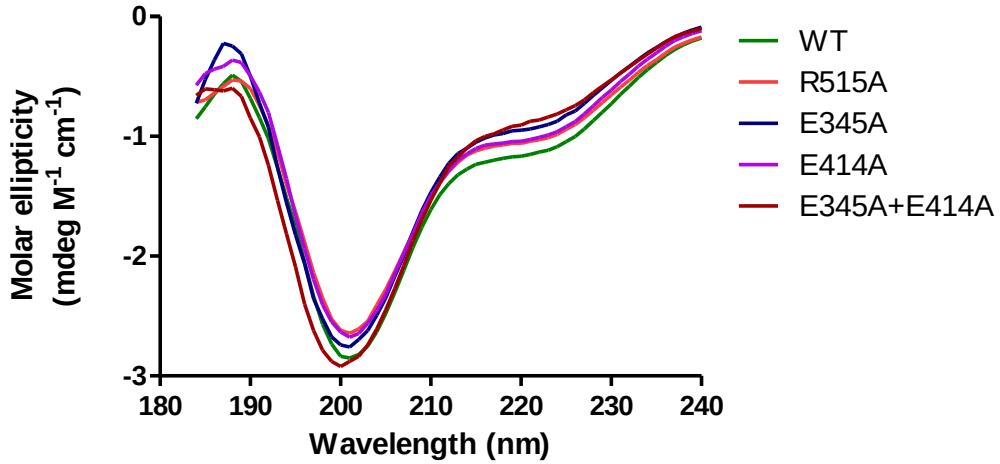

A

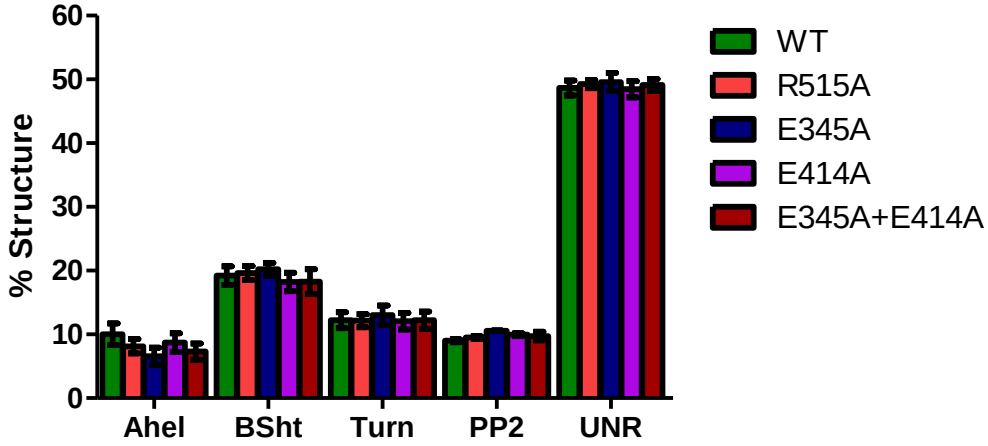

B

Figure 4.22. (A) CD spectra and (B) secondary structure composition of WT, R515A, E345A, E414A and E345A+E414A tropoelastin constructs. Ahel: alpha-helix; BSht: beta-sheet; PP2: polyproline-2 helix; UNR: unordered.

4.2.8.2 SAXS

SAXS analysis of the E345A, E414A and E345A+E414A mutant constructs revealed solution structures that exhibited the same characteristic features as WT tropoelastin (Figure 4.23). Each structure possessed an N-terminal coil region connected to a C-terminal foot region by a bridge region. Overlaying the WT and mutant nanostructures indicated an aligned N-terminal region. However, structural divergence began to occur around the hinge region downstream of the N-terminal coil, leading to conformational differences in the bridge and C-terminal regions. For instance, the E345A model displayed a longer N-terminus-to-hinge distance and a highly contracted bridge which increased the proximity of the C-terminus to the central axis of the molecule. In contrast, E414A showed a mass-dense hinge region and an elongated bridge and C-terminus. On the other hand, the double E345A+E414A mutant structure exhibited an enlarged but shortened hinge region with no dramatic change in either the length of the bridge region or the distance of the C-terminus from the central axis of the molecule. The distance between the hinge and C-terminal foot regions, taken to be an estimate of the bridge length, was measured to be 8.0, 6.9, 10.0 and 8.2 nm for WT, E345A, E414A and E345A+E414A, respectively.

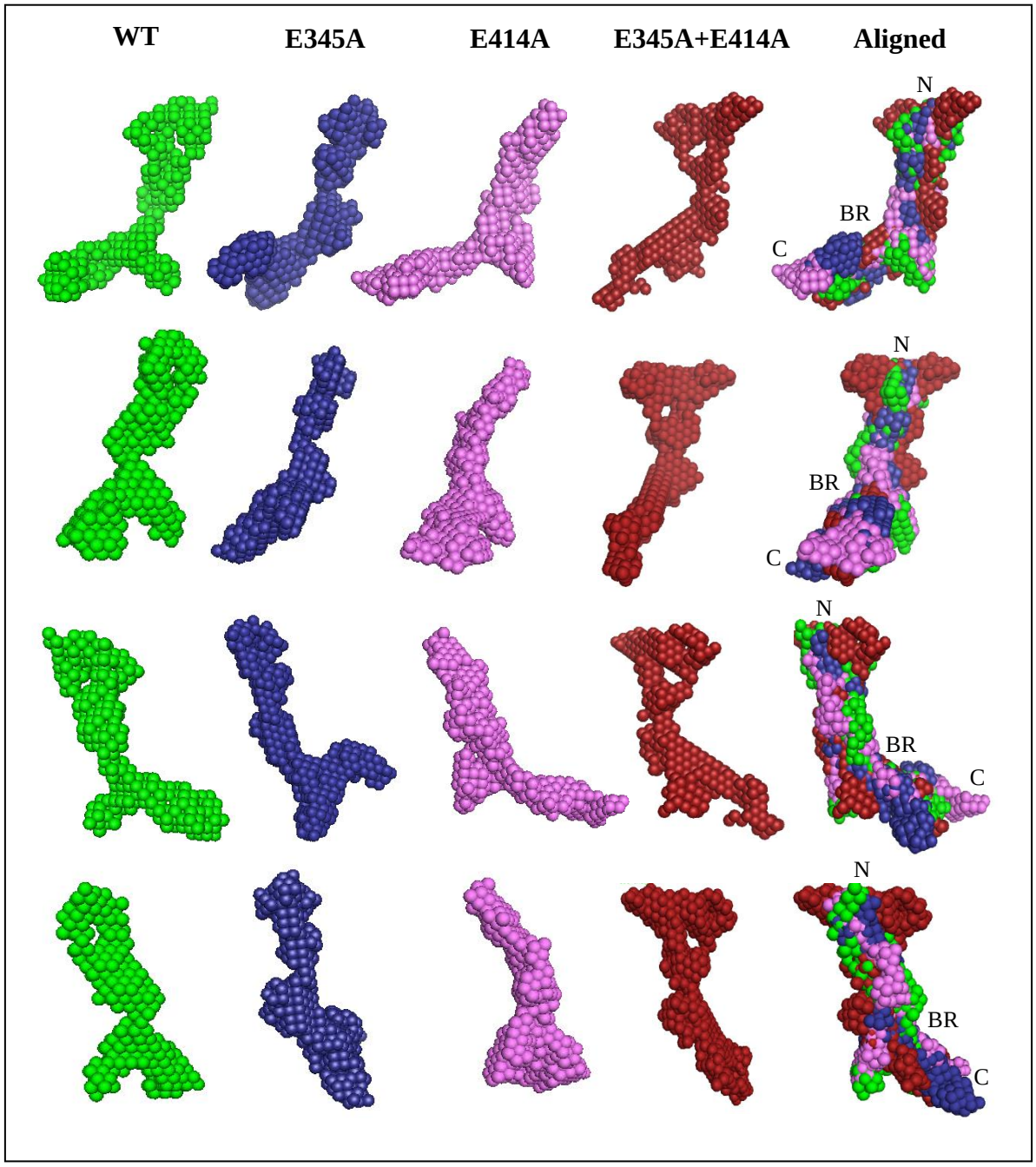

Figure 4.23. Solution structures of WT, E345A, E414A and E345A+E414A tropoelastin constructs obtained from SAXS. N: N-terminus; BR: bridge region; C: C-terminus. The rows indicate different views of the models as they are rotated clockwise around the vertical axis.

4.3 Discussion

4.3.1 Negatively-charged residues in tropoelastin

Examination of nine mammalian tropoelastin sequences confirmed that residues with negatively-charged side chains at physiological pH appear infrequently, occurring on the average at three positions within each sequence. These residues did not seem to be randomly scattered throughout the sequence; instead, they were clustered either in domain 6 or in the segment spanning domains 19-25. This chapter focused on the negative residues within the central regions of tropoelastin, which in the human sequence corresponded to the E345 in domain 19 and the E414 in domain 21.

Both sites are located in hydrophilic domains, which typically display a higher extent of sequence conservation among different species compared to hydrophobic regions [27, 47]. This was supported by the conservation of residues flanking the E345 and E414 sites in the aligned mammalian tropoelastin sequences. However, the E345 and E414 residues themselves were not conserved among all mammalian sequences. These positions were occupied by an alanine residue in most sequences. The E345 appeared only in human and chimpanzee tropoelastin, while E414 was present only in human and baboon tropoelastin. This suggests a primate-specific divergence resulting from at least three mutation events in the evolutionary tree (Figure 4.24). In the absence of sequence data from other primates, the simplest scenario would involve either an A345E or an A414E mutation in the nearest common ancestor of humans, chimpanzees and baboons. In the first case, an A414E would then be hypothesised to occur independently in the human and baboon sequences. In the second case, an A345E mutation could then have arisen in the nearest common ancestor of humans and chimpanzees, followed by a loss of the A414 in the chimpanzee sequence. The lineage-specific evolutionary activity surrounding these sites may be suggestive of their significance in primate tropoelastin.

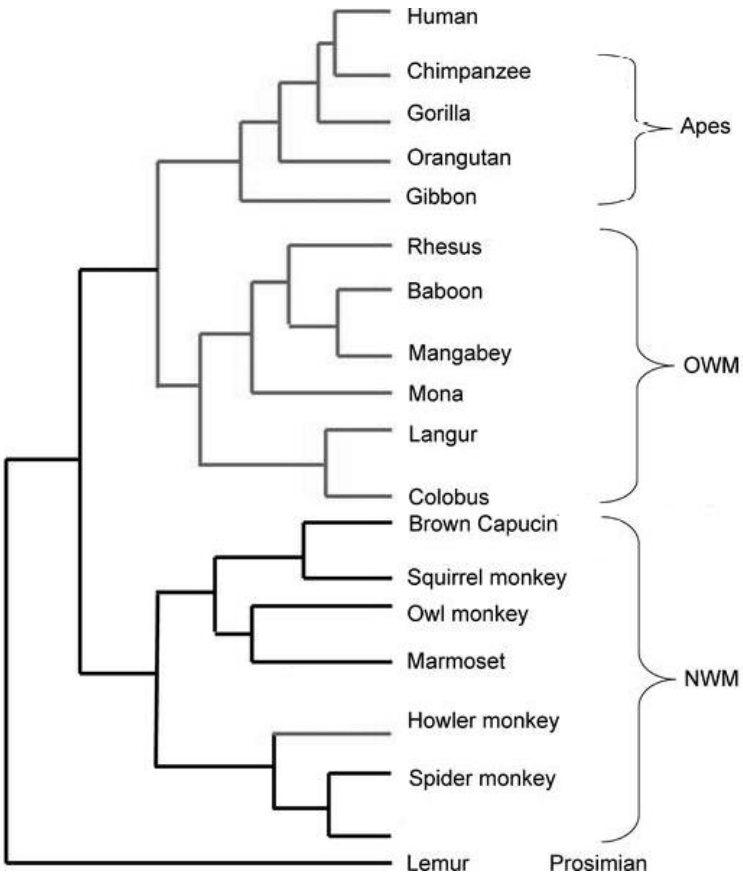

Figure 4.24. Phylogenetic tree of primates, adapted from Gilad *et al.* (2004) [287]. OWM: Old World Monkeys; NWM: New World Monkeys.

Interestingly, negatively-charged glutamate and aspartate residues were also found in other mammalian tropoelastin sequences in close proximity to the 345 and 414 positions. Such residues were located at different sites in the sequences of mammals belonging to distinct evolutionary clades [288], which suggests the convergent evolution of select negative moieties within the domain 19-25 cluster. Coupled with the association of this region to tropoelastin coacervation [44], cross-linking [105, 178], and structure [74], this posits a functional importance to the presence of negative residues in this region of tropoelastin.

4.3.2 Production of E345A, E414A, and E345A+E414A tropoelastin

To explore the role of the E345 and E414 residues in human tropoelastin, mutant constructs in which one or both sites were replaced with an alanine were recombinantly produced using an established small-scale bacterial expression system [153]. The purified constructs were shown by SDS-PAGE analysis to be predominantly full-length with an expected molecular weight of ~60 kDa. The presence of an E345A and/or E414A mutation in the constructs was verified by sequencing the tropoelastin insert within plasmid DNA extracted from transformed *E. coli* stocks. In the E345A, E414A and E345A+E414A clones, an alanine-coding GCA had replaced the wild-type glutamate-coding GAA at the codon positions corresponding to the residue 345, residue 414, and residues 345 and 414, respectively.

Comparative mass spectrometry of E345A, E414A and E345A+E414A against WT tropoelastin further confirmed the mutations at the protein level. Lys-C, which specifically cleaves at the carboxyl side of lysine residues, was used to digest the constructs as it would generate large peptides for analysis owing to a maximum of 35 cleavage sites in tropoelastin [143]. Within the examined mass window, only peaks assigned to peptide fragments containing the mutated residues displayed a mass shift between the WT and mutant species. Each shift corresponded to the mass difference between glutamate and alanine. The mass spectrometry profiles of the mutant constructs supported the presence of a glutamate-to-alanine substitution at the 345, 414, or 345 and 414 positions.

4.3.3 Coacervation

The capacity of the tropoelastin constructs for coacervation was examined as this process represents the first crucial stage in elastogenesis and greatly impacts upon their assembly into elastic fibres [101]. Following previous studies [93, 153, 275], coacervation was modelled *in vitro* in salt and pH conditions approximating the extracellular environment. All tropoelastin species displayed a sharp transition from the monomer to coacervate stage over a narrow temperature range (within 10°C), which has consistently been observed in similar assays of various tropoelastin isoforms [70, 108, 275]. However the temperature at which this transition occurred varied among the tropoelastin constructs. WT achieved full coacervation at physiological temperatures, which was consistent with previous findings for recombinant human tropoelastin [93]. In contrast, E345A, E414A and E345A+E414A coacervated fully at a higher temperature of 40°C similar to R515A.

The coacervation temperature of tropoelastin corresponds to the endothermic energy required to disrupt the hydrogen bonds in the clathrate water shielding hydrophobic domains, which leads to the exposure and interaction of hydrophobic segments [62, 289]. The stability of the clathrate water has been proposed to be influenced by protein hydrophobicity. Accordingly, studies have shown a strong inverse correlation between coacervation temperature and the number of hydrophobic domains in tropoelastin [62, 97, 99, 186, 289]. However, this model does not explain the higher transition temperature of the tropoelastin mutants compared to WT, as all the constructs possess the same number of hydrophobic domains. Furthermore, the substitution of charged glutamate residues with neutral alanines in E345A/E414A/E345A+E414A would theoretically increase protein hydrophobicity and therefore decrease coacervation temperature. This is supported by studies describing the reduced hydrophilic surface area of a Glu-containing elastin-like peptide at low pH when the Glu residues have no net charge [112]. Conversely, at pH 7, the presence of charged

functional groups increased the transition temperature and disrupted the conformation of the coacervated peptides. The unexpected increase in the coacervation temperature of the E345A/E414A/E345A+E414A mutants conceptually reflects a higher energy requirement for the disruption of bound water, which indicates an increase in protein hydration [185, 186]. As was the case for R515A, this may be due to structural differences between the WT and Glu-to-Ala constructs. The varying levels of coacervation by each mutant at 35°C further suggest a distinct conformation for each species.

Potential mechanistic differences in the coacervation of WT and mutant tropoelastin were explored by analysing solution particle sizes over a temperature range, as this would illustrate the presence of static species including stable intermediates. Below 35°C, all WT and mutant constructs were in a ~10 nm monomer form consistent with the lack of sample turbidity observed at these temperatures. At 35°C, all WT species shifted from the monomer to a ~400 nm aggregate state, while only one-third of the R515A and two-thirds of the E345A/E414A/E345A+E414A populations exhibited this phase transition. These results mirrored the full and partial coacervation observed respectively in WT and mutant tropoelastin solutions during light spectrophotometry assays at this temperature. At 40°C, all mutant species formed similar-sized particles as WT, reflecting their previously described maximum coacervation at this temperature. Apart from the disparity in the monomer-to-polymer transition temperature of WT and E345A/E414A/E345A+E414A, a difference was also observed in the temperature at which end-sized ~2 μm coacervates were formed. This occurred at 50°C for WT and at 55°C for R515A, E345A and E414A, but not within the tested temperature range for E345A+E414A. This is consistent with the impaired self-association of the Glu-to-Ala constructs, and indicates a more severe phenotype of the double E345A+E414A mutant compared to the single E345A or E414A mutants.

Despite these differences, common features were observed in the coacervation of WT and mutant tropoelastin constructs. First, the shift from monomer to polymer was rapid and corresponded to the sharp increase in sample turbidity seen in light spectrophotometric assays. This is reflective of the coacervation process being driven mainly by hydrophobic interactions [101]. Second, all constructs appeared to initially form ~500 nm intermediates prior to forming full-sized coacervates. Third, the coacervates of all constructs did not exceed ~2 μm, indicating an upper size threshold similar to previously reported values [11]. These observations suggest that although the coacervation of the mutant species had a higher energy requirement, it proceeds in a similar manner to that of WT tropoelastin.

In addition to the thermodynamic differences, kinetic differences were also observed in the coacervation of WT and mutant constructs. In all constructs, the temporal requirement for coacervation was directly related to temperature, which was consistent with previous findings [275]. At physiological temperatures, mutant species coacervated more slowly than WT to varying degrees (WT>R515A>E345A>E414A>E345A+E414A). The rate of coacervation has likewise been linked to protein hydrophobicity, as greater cooperativity among a larger number of hydrophobic segments would hasten coacervation [70]. However, this model again does not account for the variable coacervation times of the WT and mutant tropoelastin constructs. This may suggest a possible structural change in the E345A, E414A and E345A+E414A tropoelastin that displaces hydrophobic domains and results in decreased cooperative interactions during coacervation. Because the differences in coacervation time were minimised once the transition temperature of the mutant constructs was reached, the initial delay in coacervation may also be due to the inadequate removal of bound water surrounding hydrophobic regions.

Based on the impaired coacervation properties of the E345A, E414A and E345A+E414A constructs, both the E345 and E414 residues appear to have significant roles

in tropoelastin function. It is unlikely that the residues play a direct role in coacervation, as the process is known to be driven by hydrophobic interactions. More probably, both residues, either independently or in tandem, may be involved in maintaining the local tropoelastin structure. Mutation of these sites may have resulted in conformational changes which can alter the nature of protein-bound water and displace hydrophobic domains, leading to the observed increase in coacervation temperature and time.

4.3.4 Cross-linking

The ability of tropoelastin to be cross-linked strongly reflects its propensity to be incorporated into stable elastic fibres. Cross-linking of the tropoelastin constructs was modelled in extracellular temperature, pH and salt conditions with BS3, a primary amine-reactive homobifunctional chemical cross-linker targeted to lysine residues within a maximum distance of 11.4 Å [290]. This identifies regions aligned by coacervation [44] and approximates *in vivo* cross-linking by lysyl oxidase [143], as demonstrated by the similarities between BS3-cross-linked and native elastin [1]. Consistent with previous findings, a six-fold molar excess of BS3 [20] allowed the incorporation of all WT and mutant monomer constructs into the cross-linked hydrogel material.

The hydrogels displayed strikingly different morphological and functional properties. Micro-CT reconstruction of the WT material showed a fibrous and porous network similar to microscopic images of previously-characterised elastin hydrogels [20] and consistent with the filamentous nature of natural elastin [8, 13, 14]. This markedly contrasted with the compressed structures of the mutant hydrogels. The E345A, E414A and E345A+E414A hydrogels did not possess the bead-like granules evident on the R515A surface. Hydrogels produced from the three E→A constructs also differed in appearance. Surprisingly, the double E345A+E414A mutant hydrogel resembled the WT material most closely, albeit with visibly smaller channels. The compositional heterogeneity between WT and mutant hydrogels, and among the mutant hydrogels, suggest differences in the cross-linking of each tropoelastin construct.

The compact nature of the mutant hydrogels was reflected in their decreased porosities compared to the WT material. The porosity of polymers such as hydrogels is thought to be determined by the separation kinetics of the homogeneous multi-component system into polymer-rich and polymer-lean phases [291]. This may be influenced by various

mechanical techniques during biomaterial construction [292]. Since the WT and mutant hydrogels were formed in the same manner, variations in their phase separation, and therefore in hydrogel porosity, are most likely due to differences in the polymerisation phase, which would have arisen from differences in the cross-linking process.

Cross-linking differences may also account for the differential swelling properties of WT and mutant hydrogels in water. Water absorption by WT hydrogels amounted to ~60 times the protein mass, consistent with the established swelling ability of cross-linked elastin [293, 294] and elastin-mimetic peptides [295]. In contrast, the mutant hydrogels exhibited a comparable decrease in water intake, which reflects their reduced porosities compared to the WT construct. Hydrogel swelling is defined by interactions between the solvent and the polymer. The influx of solvent stretches the junctions of the hydrogel [188, 189] and decreases the mobility of the flexible hydrophobic segments within the rigid cross-linked domains [28]. This is balanced by the entropic increase associated with the mixing of solvent and bound water within the polymer [189]. The reduced water absorption of mutant hydrogels may therefore be due to changes in polymer-associated hydration brought about by a non-native conformation of the cross-linked assemblies. Hydrogel swelling is also conventionally thought to be inversely related to cross-link density [1, 188, 190, 191], which suggests probable differences in the abundance or nature of cross-links formed in the mutant hydrogels compared to WT.

The surfaces of the swollen hydrogels were analysed at a higher resolution with SEM. While the bottom surfaces were similar between constructs, the top surfaces showed distinct structural morphologies. The porous sheet-like structure of the WT surface was similar to that observed in the micro-CT studies and existing SEM images of synthetic elastin [20], indicating the structural consistency of the cross-linked WT material. In contrast, the upper surface of the R515A hydrogel consisted entirely of globular clusters similar to previous

findings [184]. The spheres have sizes consistent with those of partially cross-linked nascent elastin prior to their condensation into fibrous structures [11, 94]. Based on the assumption that the globules represent precursors of mature fibrous or sheet-like structures [296], cross-linking of the E345A, E414A and E345A+E414A constructs appeared to have progressed further than R515A. While the top surfaces of these hydrogels retained the presence of the globules, they were linked by coalesced structures to form closed networks. This differs from the open-link clusters on the R515A surface. Among the Glu-to-Ala mutants, however, the elastin spheres were connected by morphologically distinct assemblies – fine fibrils in E345A, sheet-like fragments in E414A, and thick fibers which seemed intermediate between a fibrillar and a flat structure in E345A+E414A. These are indicative of differences in the extent and/or nature of cross-linking among the tropoelastin constructs. The presence of nascent elastin globules particularly suggests that E345A, E414A and E345A+E414A, like R515A, have a decreased ability to form mature cross-linked structures characteristic of normal elastin.

The aberrant or incomplete cross-linking of E345A, E414A and E345A+E414A is unlikely to be directly due to the elimination of negatively-charged residue/s, as cross-linking involves specific lysine residues [143] that remain present in the mutant constructs. It is also unlikely to be caused by inadequate coacervation at the cross-linking temperature, since no monomer species were left in the aqueous phase after hydrogel formation. Possibly, some regions within the mutant coacervate are misaligned, which may displace contacting sites and detrimentally affect the formation of cross-links [44]. This would again be consistent with structural modifications in the mutant constructs that shift or block important cross-linking domains in the molecule.

4.3.5 Cell and antibody interactions

The tropoelastin constructs promoted the attachment of human dermal fibroblasts in a saturable manner similar to previous observations [45, 179]. Cell attachment to each construct plateaued at tropoelastin concentrations at or above 10 μg/mL, which most likely represents full coverage of the cell culture wells by the protein molecules. At these concentrations, the majority of the seeded cells bound to WT tropoelastin, while 31%, 21%, 24% and 34% fewer cells adhered to the R515A, E345A, E414A and E345A+E414A constructs, respectively.

Previous studies have demonstrated that fibroblasts bind via the $\alpha_v\beta_3$ adhesion receptor to the tropoelastin C-terminus [297], specifically the terminal GRKRK residues [179]. In all the tropoelastin mutants, the altered residues are located distally from the C-terminus, indicating that the observed decrease in cell attachment is not due to the mutational disruption of cell binding sites. The decreased fibroblast attachment of E345A, E414A and E345A+E414A therefore suggests a limited accessibility of their C-termini to fibroblast adhesion receptors when the constructs are physisorbed on a surface. This hypothesis was confirmed via antibody detection of the C-terminal domain 36 on surface-coated tropoelastin constructs. Antibody specificity was indicated by the low level of detection in M155n tropoelastin, which is truncated after domain 25 and therefore does not contain the C-terminus [153]. With each construct, the amount of detected C-termini increased directly with the coating concentration and corresponded to the extent of fibroblast attachment. At excess tropoelastin concentrations, 44%, 19%, 33% and 23% fewer C-termini were observed in R515A, E345A, E414A and E345A+E414A, respectively. This decrease reflects a comparable magnitude of reduction in the cell attachment of the mutant species, suggesting that a less exposed C-terminus is the likely reason for their decreased fibroblast attachment.

The decreased C-terminal availability of the mutant species was not due to the reduced adsorption of the constructs to the tissue culture wells, as evidenced by the comparable protein levels detected by the anti-elastin BA4 antibody. The BA4 antibody is known to predominantly target the hydrophobic VGVAPG pentapeptide in domain 24 [298], and to some extent, other similar sequences with a xGxxPG or xGxPGx motif [299]. These sequences were unmodified in the WT and mutant tropoelastin species, which allows the extent of BA4 antibody binding to be correlated to protein concentration. This confirms that the detection of fewer C-termini in the mutant constructs was due to reduced exposure rather than a decrease in the number of surface-bound tropoelastin molecules. This supports a non-localised structural modification in the E345A, E414A and E345A+E414A tropoelastin species that involves a spatial displacement or partial obscuring of the C-terminal region.

The mechanisms by which other cell types bind to tropoelastin are not yet fully understood. While integrins are the major adhesion receptors for most extracellular matrix components, other cell-surface receptors including glycosaminoglycans such as heparin sulfate and chondroitin sulfate may also mediate attachment to tropoelastin [18]. These molecules are also thought to interact with tropoelastin at or near its C-terminus [45]. The importance of this region to cell interactions is consistent with its high sequence conservation among tropoelastin sequences of various species [21, 49]. The decreased accessibility of the E345A, E414A and E345A+E414A C-terminus therefore implies similarly reduced interactions with other cell types that utilise this region as a receptor ligand.

Interactions between cells and tropoelastin molecules are believed to be important in the assembly of elastic fibres. For instance, tropoelastin coacervation is thought to occur at specific cell-surface sites on which newly synthesised molecules are deposited [3, 45]. Weak cellular binding of mutant constructs may hence allow for the easy detachment of monomers

from the cell surface and preclude their incorporation into elastic fibres [18]. In support of this, a previously described tropoelastin mutant that supported minimal cell attachment also exhibited a profoundly reduced ability to assemble into elastic fibres [172]. In addition, tropoelastin-cell interactions may be involved in the anchorage of the elastic network [179], and the regulation of tissue-specific elastic fibre architecture by mechanical manipulation of cell-surface elastin [3, 6, 94]. Consequently, the decreased adhesion of fibroblasts to the mutant tropoelastin constructs may lead to reduced elastic fibre assembly, and/or the formation of fibres with non-native morphology.

4.3.6 Elastic fibre assembly

To determine the ability of the different tropoelastin species to form elastic fibres in a cellular environment, purified constructs were added to the culture medium of cells following previous approaches [184, 202, 203]. Consistent with findings reported in the previous chapter, WT tropoelastin added to cultured GM3348 fibroblasts assembled into a linear morphology after one day, while the R515A species remained dispersed in the extracellular space. The E345A, E414A and E345A+E414A constructs displayed a similar lack of linear organisation; however, the E414A and E345A+E414A spherules appeared to cluster in a globular arrangement in contrast to the more random placement of the E345A species. These differences in the early-stage assembly of WT and mutant tropoelastin, and those among the mutant constructs, again suggest a differential presentation of interacting domains most likely arising from inherent conformational changes within each molecule.

By four days after tropoelastin addition, the WT, R515A, E414A and E345A+E414A constructs had formed visible elastic fibres. The fibres shared a similar general branched structure consistent with the known architecture of the skin elastic network [3, 4], which supports the cell-specific shaping of elastic fibre morphology [6]. However, relative to the WT fibres, the E414A and E345A+E414A fibres, like R515A, exhibited significantly reduced immunofluorescence and abundance. The elastic fibres detected by immunostaining represent those formed solely from exogenous tropoelastin, as evidenced by the absence of visible fibres in control samples with no added constructs. The decreased staining of mutant elastic fibres by BA4 contrasts against the comparable antibody detection of all WT and mutant constructs previously observed in ELISA experiments. This strongly suggests that the BA4 epitopes, predominantly in domain 24, are equally accessible in the surface-bound monomers, but become differentially exposed in the assembled elastic fibres. This implies that the E414A and E345A+E414A constructs may be arranged in an atypical manner within

the elastic fibre. Abnormal association of the mutant species, which is supported by the non-native morphology of their cross-linked hydrogels, may also hinder the expansion of the elastic fibre network and account for the markedly reduced number of mutant fibres compared to WT. It is also possible that the early-stage assembly of the mutant species is inefficient, as extrapolated from their longer coacervation time even at high monomer concentrations at physiological temperature. Compounded with their decreased binding to fibroblasts, these may contribute to the loss of mutant tropoelastin constructs during cell culture media changes prior to their incorporation into stable fibres, leading to the observed scarcity of E414A and E345A+E414A elastic fibres.

While most of the mutant tropoelastin constructs displayed only subtle differences in elastogenic ability, E345A did not form defined elastic fibres in GM3348 fibroblasts. This was unexpected in light of its comparable functionality with the other mutants in assays simulating the various stages of elastin assembly. The absence of E345A elastic fibres is unlikely to be caused by a lack of other elastogenic components in the cellular environment, as a similar number of cells passaged from the same stock were present in all samples. This then suggests impaired interactions of E345A with extracellular matrix components such as microfibrillar proteins and lysyl oxidase enzymes that are necessary for elastic fibre formation. Possibly, the E345A may also self-associate in a manner that is incompatible with the elastic fibre structure of dermal fibroblasts. The assembly of tropoelastin monomers into a fibrillar morphology is proposed to involve intra- and intermolecular contacts between specific domains in the N-terminal and C-terminal regions [72, 105]. Accordingly, structural changes in the E345A C-terminus as suggested by ELISA experiments may inhibit the specific head-to-tail assembly process crucial for fibre formation.

The inability of the Glu-to-Ala tropoelastin mutants to form wild-type elastic fibres strongly indicates the importance of the E345 and E414 residues in elastin assembly.

Counter-intuitively, the E345A+E414A construct did not possess the same or greater degree of elastogenic impairment as E345A. Furthermore, the double mutant formed significantly more fibres than E414A at the early stages of fibre assembly. This interestingly suggests that the abolishment of both E345 and E414 is more conducive to elastic fibre formation than the removal of either site alone. Structurally, this may be reflected by a closer resemblance of the E345A+E414A conformation to that of WT compared to either E345A or E414A.

4.3.7 Structural analysis

CD analysis of WT and mutant tropoelastin showed similar spectra consisting of a large negative peak at ~200 nm, which corresponds to disordered hydrophobic regions, and a negative shoulder at ~220 nm, which is assigned to the alpha-helical structure of cross-linking domains [109, 110, 273]. The CD profiles of the tropoelastin constructs are consistent with those previously observed in bovine tropoelastin [300], α-elastin [273], κ-elastin [301], elastin polypeptides [302] and recombinant human tropoelastin [275], indicating the presence of the same types of secondary structure.

The secondary structure of the tropoelastin constructs was estimated from the CD spectra using established algorithms [173]. As expected, all WT and mutant species showed similar structural composition, consisting mainly of unordered regions and a small percentage of alpha-helices, beta-sheets, turns, and polyproline-2 helices. This trend was comparable to results obtained from nuclear magnetic resonance [53] and Raman spectroscopic data [303, 304]. The high amount of unordered regions and the contrasting low level of helical structures in the tropoelastin constructs were previously observed in hydrolysed elastin peptides [274], and consistent with a monomer form. After coacervation, the helical content of tropoelastin can increase to 50% following the increased ordering of monomer species [110]. On the other hand, the presence of β-turns is thought to occur in hydrophobic domains and is proposed to be responsible for the elasticity of the elastin polymer in a hydrated environment [305].

The CD results suggest that conformational modifications in the E345A, E414A and E345A+E414A constructs are unlikely to be due to changes in their secondary structures. For instance, the tropoelastin domain 19 which contains E345 has been shown to have the greatest propensity for helix formation in an aqueous solution than any other cross-linking domain [69, 75]. Since charged residues are known to stabilise helical structures [284], the

substitution of E345 with a neutral alanine can potentially disrupt helix formation and affect the molecular structure. There was, however, no evidence of significant changes in the secondary structure composition of all mutant constructs.

In light of this, the solution structures of the WT and mutant tropoelastin species were determined by SAXS analyses. The constructs showed structural features similar to those previously described in recombinant wild-type human tropoelastin, including an elastic coil region thought to span the N-terminus to around domain 18, a turn/hinge region containing domains 21/23, a bridge region from domains 25-26, and a cell-interactive C-terminal foot region [72].

Comparison of the WT and E345A structures demonstrated a slight elongation of the hinge region accompanied by a significant shortening of the bridge region and a contraction of the C-terminus towards the central mass of the molecule. Due to a proposed turn formed by the adjoining hydrophilic domains 21 and 23 [74], a conformational symmetry occurs around this region that positions domain 19 in close proximity with domain 25 (Figure 4.25). This supports the formation of a well-characterised intra-molecular cross-link between the two domains [105]. This conformation also potentially allows the E345 residue to contact one of several positively-charged residues in domains 25 and 26, such as K507, K511 or R515. (The charged group in K507, however, may be modified by its participation in cross-linking [143]; hence, contact with E345 is unlikely if interactions should persist in cross-linked elastin.) Removal of the E345 site in the E345A mutant may therefore enable the free lysine or arginine to bind to an alternative site, possibly the E414 residue. This would result in an apparent lengthening of the hinge region and a dramatic contraction of the bridge region similar to the observed structure of E345A tropoelastin. Apart from the obvious repositioning of the C-terminus, such a conformational change may also displace or obscure the large hydrophobic domains within the region, such as domains 20, 24 and 26, as well as

the essential cross-linking domains 19 and 25. This would lead to the observed impairment of E345A coacervation and cross-linking. Furthermore, the shortening of the bridge region may sterically prevent the head-to-tail assembly of E345A monomers, which may account for the described lack of elastic fibre formation in fibroblast cultures.

In marked contrast to E345A, the nanostructure of the E414A construct displayed an enlarged hinge and an extended bridge region. The tropoelastin hinge, formed by the adjacent domains 21 and 23, is proposed to undergo a number of fluctuations between open and closed states prior to converging into a hairpin structure [73]. This structure is predicted to be stabilised by a salt bridge between the E414 residue within domain 21 and the K441 residue within domain 23 (Figure 4.25). Abolishment of the E414 site may therefore disrupt the stability of the hinge and contribute to a structural change in this region as observed in the E414A construct. This is supported by the altered hairpin shape of a mutant sequence in which both E414 and K441 were mutated to a glutamine and a leucine, respectively [73]. In addition, the positively-charged residue normally bound to E414 may then interact with an upstream negative site such as E345, which is consistent with the high flexibility of this region [44, 54]. This would result in the elongation of the bridge region as seen in the E414A SAXS structure. Such a conformational shift may likewise mask or alter the native positions of the proximal hydrophobic and hydrophilic domains, as well as that of the C-terminal foot, resulting in the decreased assembly and cell binding of E414A.

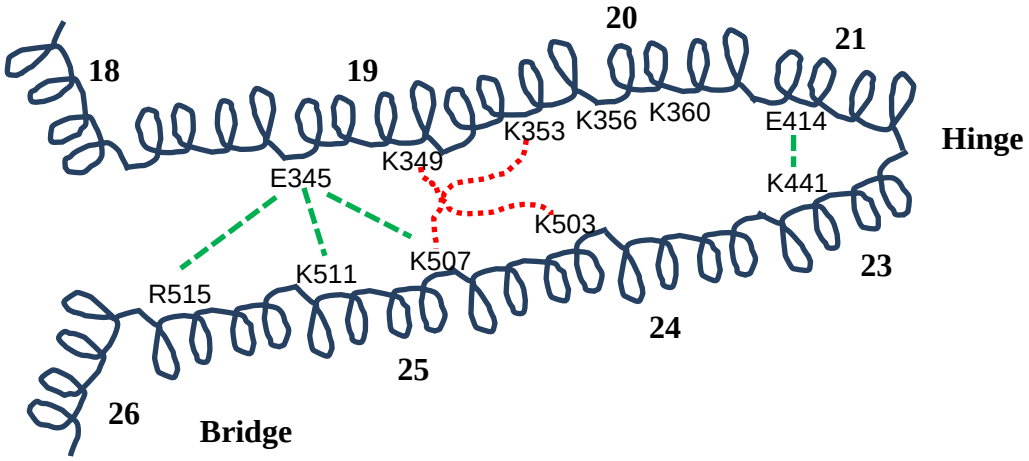

Figure 4.25. Schematic representation of tropoelastin domains 18-26, adapted from Baldock *et al.* (2011) [72]. A hinge region is formed by domains 21/23. A proposed tetra-functional cross-link occurring between domains 19 and 25 [105] is represented by red dotted lines. Potential contacts formed by the E345 and E414 residues are indicated by green dashed lines.

Interestingly, the structure of the E345A+E414A construct also exhibited a bulkier hinge region but showed no significant changes in the length of the bridge region and the distance of the C-terminus from the vertical axis. In the absence of both the E345 and E414 residues, the available positively-charged sites can remain unbound without forming aberrant local structures that contract or extend the bridge region. However, the elimination of stabilising interactions within the tropoelastin hinge may increase the torsional flexibility of this region and/or modify its equilibrated conformation [73], resulting in the enlarged hinge structure observed in the E345A+E414A shape. This may similarly contribute to the spatial dislocation of coacervation and cross-linking regions within domains 18-26, as well as steric hindrances during monomer self-association and fibre assembly. Specific cell receptor binding sites in the C-terminal foot may also be oriented differently to those in WT tropoelastin, resulting in reduced cell and antibody binding properties.

These findings support a model wherein the central tropoelastin domains 19-25 are positioned symmetrically from the hinge region formed by domains 21/23. This large loop area may be stabilised by charge interactions involving the E345 and E414 residues and proximal lysines or arginines. E345 appears closely positioned to K507 and K511 in domain 25, and to R515 in domain 26. However, the participation of K507 in cross-linking, and the observed differences between the functional and structural properties of the E345A and R515A species suggest that binding of E345 to either K507 or R515 is less probable. On the other hand, E414 most likely contacts the K441 in domain 23. Removal of a glutamate residue at either the 345 or 414 positions may enable non-native interactions to occur between the free positively-charged side chain and the remaining negatively-charged site. This may alter the length of the adjoining bridge which consequently affects the position of the C-terminal region. The abolishment of both E345 and E414 may preclude the formation of abnormal charge interactions and preserve the bridge length. Similarly, the charge abolishment of one or both pairs of potentially interacting residues (E345/K511 or E414/K441) would prevent uncompensated charges and theoretically maintain the bridge distance. However, any resulting destabilisation of the loop region can result in conformational changes to the tropoelastin hinge and bridge regions. This model strongly suggests the importance of both E345 and E414 residues in maintaining the structure of the central tropoelastin region, which in turn is essential for functional tropoelastin assembly.

5. Characterisation of tropoelastin with domain 22

5.1 Introduction

5.1.1 Sequence diversity of the tropoelastin gene

The human *ELN* gene that codes for tropoelastin [21] represents a dynamically evolving genomic region [183]. It is susceptible to mutation events, as evidenced by a number of polymorphisms associated with the tropoelastin sequence [306-308]. These polymorphisms may occur at a single nucleotide position, or may involve the deletion or insertion of longer gene segments. The altered coding sequences can translate to amino acid substitutions [172], truncations [155, 158], or frame shift mutations [121, 168, 170] in the expressed protein. While the majority of changes to the tropoelastin sequence pose no phenotypic consequences, several are associated with clinical diseases such as supravalvular aortic stenosis [309, 310], Williams-Beuren syndrome [311] and cutis laxa [33, 162].

Other tropoelastin gene mutations may occur at a species or lineage level, such as the loss of exons 34 and 35 at the 3′ end of the human *ELN* gene [312]. This was thought to be facilitated by downstream Alu-repeat mediated recombination events [21, 24, 312], due to selective advantages conferred by functional changes in the arterial wall [312] during the evolutionary divergence of primates in the last 70 million years [313]. Since then, the human *ELN* has undergone further sequence modifications [32, 33]. Alignment of the human tropoelastin gene with orthologous sequences has revealed numerous exonic insertions and deletions, which provide species-specific characteristics while preserving the overall properties of the protein [183].

5.1.2 Alternative splicing of tropoelastin

Apart from genetic mutations, another main contributor to the diversity of the tropoelastin protein sequences is the extensive but tightly-regulated alternative splicing of tropoelastin transcripts at well-conserved and functionally-equivalent splice junctions [21, 24, 29, 31, 38, 104, 270, 314]. The exon:intron ratio of tropoelastin at approximately 1:19 [270] is unusually low for a GC-rich sequence [315]. Out of 34 exons in the human tropoelastin transcript, six exons including exons 22, 23, 24, 26A, 32 and 33 have been reported to be spliced with varying frequencies [24, 31, 314, 316]. Exon 26A, for instance, is constitutively spliced out [29] except in aged [4] or diseased [37] states. Conceptually, the alternate usage of exons enables the production of functionally diverse tropoelastin isoforms from a single gene sequence, which is supported by the tight regulation of the splicing process [38]. The tropoelastin splice variants may be secreted in specific cellular environments to accommodate the different functional and structural requirements of the elastic fibre network in various tissues [55].

Interestingly, exon 22 appears to be always spliced out in human tropoelastin transcripts [31-35]. It is absent in all 13 human tropoelastin isoforms currently recorded in the UniProt database. The retention of exon 22 in the human *ELN* gene [183] is unexpected considering its disuse in the mature transcript. The constitutive post-transcriptional splicing of exon 22 may have evolved relatively recently in the mammalian lineage, since exon 22 remains expressed in bovine [317], mouse [33] and rat [318, 319] tropoelastin mRNA obtained from various tissues.

5.1.3 Effects of domain 22 splicing

5.1.3.1 The tropoelastin hinge region

Exon 22 codes for a short hydrophobic sequence, GAAGAGVLGGLVPGAPGAVPG VPGTGGVP, in the central region of tropoelastin [44]. Exclusion of domain 22 interrupts the highly-conserved structure of alternating hydrophobic and hydrophilic domains in tropoelastin [4]. The resultant adjoining hydrophilic domains 21 and 23 contain a central GVGTP peptide, which was computationally predicted to form a flexible turn or hinge region [74]. The presence of a tropoelastin hinge was subsequently empirically confirmed by SAXS [320] and nuclear magnetic resonance analyses [75].

The hinge sequence is unstructured with neither alpha-helical or beta-sheet content [74, 75, 321], and is hence postulated to contribute substantially to the structural flexibility of the tropoelastin molecule [178]. In support of this, molecular dynamic studies have demonstrated that the hinge region can adopt a closed conformation in which the flanking helical segments are in an anti-parallel arrangement, or an open structure where the neighbouring regions are parallel and extended [73]. The hinge region is proposed to oscillate between these models before converging into a closed hairpin structure (Figure 5.1). This conformational equilibration is consistent with the broad spatial distribution accessed by elastin peptides [322] and the significant motions exhibited by hydrated elastin [323, 324]. Accordingly, an elastin-like peptide corresponding to domains 21/23 has been reported to display a more rigid structure and less mobility upon alanine substitution of the central turn sequence [325]. These findings support the involvement of the hinge region in tropoelastin elasticity.

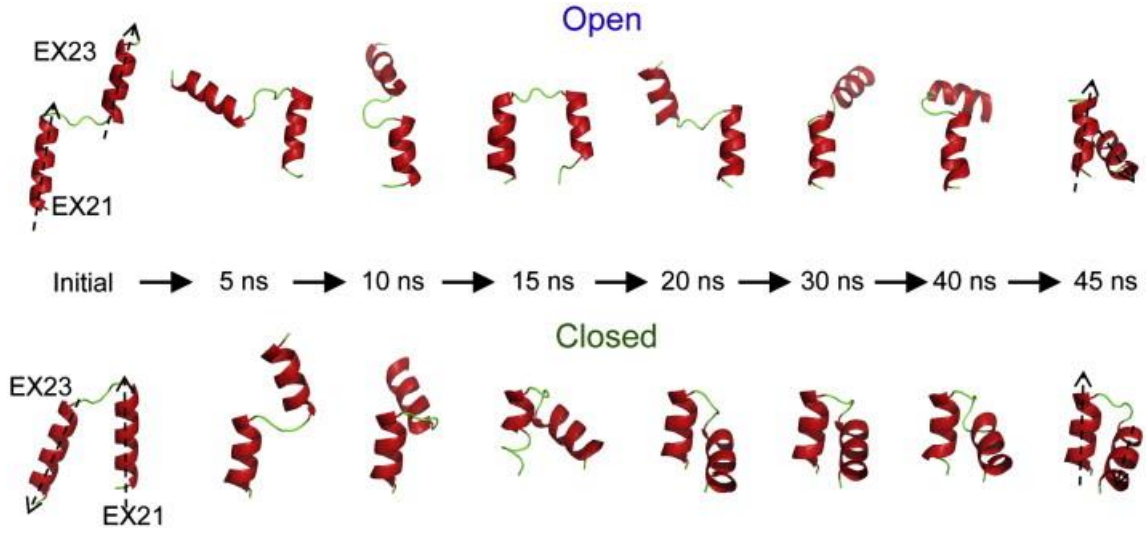

Figure 5.1. Ribbon structures showing the converging trajectories of the domain 21/23 hinge region with an initial open or closed conformation. This figure is obtained from Djajamuliadi *et al*. (2009) [73].

The conformational flexibility of the hinge region appears to be intricately linked with tropoelastin function during elastic fibre assembly. The hinge structure may contribute to the position and dynamics of hydrophobic regions involved in coacervation [325]. The hinge also lies within a stretch of domains enriched in cross-linking sites [143, 282]. The geometry adopted by this region is proposed to enable inter- and intra-molecular contacts between lysine residues, allowing spontaneous condensation into cross-links upon modification by lysyl oxidase [178].

5.1.3.2 Human-specific elastic fibre properties

The specific exclusion of domain 22 in human tropoelastin, which is particularly well-documented in samples obtained from dermal fibroblasts [31], suggests unique properties of human skin elastic fibres distinct from those in other species that may express domain 22. Skin biopsies from 13 different animals showed that human skin contains the

highest percentage of desmosine, approximately 2- to 106-fold higher than any other animal skin [326]. For example, humans have 2-, 3- and 32-fold more desmosine per area of skin compared to the pig, cow and mouse, respectively, which express exon 22 in their tropoelastin. As desmosines are direct products of cross-linking, this suggests a higher elastin content in human skin compared to skin from other species [327]. This is supported by the uniform distribution of elastic fibres across the entire dermis in human skin [326]. In contrast, elastic fibres in most animals were consistently confined to the upper dermis near the follicle area and pili muscle attachment. It has been proposed that while elastic fibres in human skin originate from dermal fibroblasts [328], those in most mammalian skin are solely derived from epithelial-like cells lining the hair follicles [329]. Significantly, the elastic fibre architecture in human skin differs markedly from that in other animals [326]. Human dermal elastic fibres are predominantly long, straight and aligned in organised sheets. In avian skin, elastic fibres are heavier and highly-branched. In sheep, rabbit and other mammalian skin, elastic fibres associated with the follicle area are long and thick with very fine radiating fibrils. The unique properties of human skin elastic fibres are not common to other primates, as non-human primate skin samples retained the features observed in other animals.

Differences in the skin elastic fibres of various species conceivably reflect differences in their functional requirements [326]. In birds, elastic fibres anchor feather follicles to smooth muscle bundles and transmit signals for movement. In most animals, the organisation of skin elastic fibres are likely modified to meet the reduced obligation for mechanical performance. Nevertheless, the elastic fibres similarly attach hair follicles to pili muscles for movement and hair placement. In humans, however, skin elastic fibres are not limited to areas of hair follicles and muscle tissue, but are located throughout the dermis, suggesting a primary role in the maintenance of skin integrity rather than movement. This

change in the functional requirement of elastic fibres in human skin may be associated with the unique loss of domain 22 in human tropoelastin.

5.1.4 Aims

This chapter explores the functional significance of exon 22 splicing in human tropoelastin. This study describes the properties of an EX22 tropoelastin variant in which domain 22 is inserted between domains 21 and 23 (Figure 5.2). The elastogenic potential and nanostructure of the EX22 construct will be compared against WT tropoelastin, allowing the development of a model for the selective advantage of domain 22 exclusion in human tropoelastin.

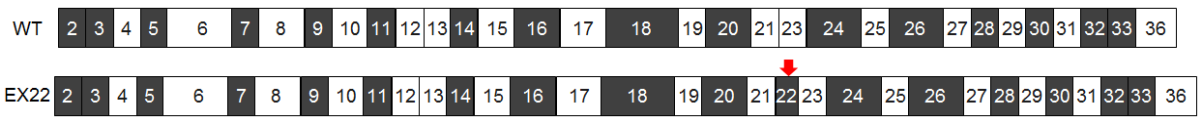

Figure 5.2. Domain structure of WT and EX22 tropoelastin. The placement of domain 22 is indicated. Hydrophobic and cross-linking domains are indicated by grey and white boxes, respectively.

5.2 Results

5.2.1 Analysis of splicing sequences for exons 21-23

Analysis of the genomic sequence encompassing exons 21 to 23 of human tropoelastin indicated the potential splice signals utilised during mRNA processing to determine the expression of exonic segments (

Table 5.1). The algorithm used by the Human Splicing Finder tool evaluated the similarity of the splice signals, including donor and acceptor splice sites and the branch point, to the consensus sequences. In human transcription/translation systems, the donor and acceptor sties typically follow the [C/A]AGGTRAGT [330] and YYTTYYYYYYNCAGG motifs [331], respectively; while the branch point sequence consists of YNYCRAY [332], where Y is a pyrimidine (T/C), R is a purine (A/G) and N is any nucleotide.

The acceptor splice site and branch point sequences that determine the inclusion of exons 21 and 23 in the mature transcript have high similarity to the consensus sites (consensus values >80), and are therefore predicted to be highly expressed in human tropoelastin. However, the acceptor splice site and branch point sequences of exon 22 have lower consensus values than those of the neighbouring exons 21 and 23. Accordingly, exon 22 is predicted to have decreased recognition by the splicing machinery, which may be a contributing factor in its exclusion from the mature human tropoelastin transcript.

Furthermore, in the human *ELN*, the distance of the branch point from the 3′ splice site is greater in exon 22 (62 bases) than for either of its neighbors exon 21 (28 bases) and exon 23 (24 bases). Branch points are optimally located 16-25 bases and typically within 40 bases from the acceptor splice site, with those situated further upstream often associated with skipped exons [333, 334].

Table 5.1. Splice site and branch point sequences of human tropoelastin exons 21-23 predicted by the Human Splicing Finder tool [330]. Their position within the human tropoelastin gene (NCBI reference: NG_009261.1) and similarity to the consensus sequence (consensus values 0-100) are indicated.

Exon	Splice signal	Position	Sequence	Consensus
21	Donor splice site	33337-33345	CCCGTGAGC	80.9
	Branch point	33541-33547	TTCTGAG	87.4
	Acceptor splice site	33564-33577	GTTTCCTTGTAGCC	82.9
22	Donor splice site	33615-33623	ACGGTAAGT	94.3
	Branch point	34231-34237	CACCCAC	84.1
	Acceptor splice site	34274-34287	CCACTCCCCGAGGT	80.7
23	Donor splice site	34370-34378	CAGGTGAGC	96.7
	Branch point	34516-34522	CTCTCAC	96.6
	Acceptor splice site	34532-34545	TCACACCTCCAGGA	90.4

5.2.2 Production and validation of EX22 tropoelastin

5.2.2.1 Exon 22 sequence design

The exon 22 sequence was derived from the reverse translation of the human domain 22 sequence GAAGAGVLGGLVPGAPGAVPGVPGTGGVP and optimised for *E. coli* codon usage. The majority of the utilised codons represented that with the highest usage frequency for each amino acid. To improve translational efficiency, a percentage of such codons for glycine and alanine, which account for 55% of the exon 22 sequence, were substituted with synonymous codons with the second highest usage frequency.

The exon 22 sequence designed for optimal *E. coli* expression was as follows:

5′- GGT GCG GCG GGT GCG GGT GTT CTG GGT GGC CTG GTT CCG GGT GCG CCG GGC GCG GTT CCG GGT GTG CCG GGT ACC GGC GGT GTT CCG -3′

The exon 22 sequence was inserted between exons 21 and 23 of the wild-type tropoelastin gene via site-directed mutagenesis (GenScript, USA) to create the EX22 tropoelastin DNA construct.

5.2.2.2 Plasmid sequencing

E. coli was successfully transformed with the pET-3d plasmid containing the EX22 tropoelastin gene. Plasmid DNA extracted from the transformed bacterial colonies was sequenced, which confirmed the insertion of exon 22 between exons 21 and 23 of the tropoelastin sequence (Appendix 8.6).

5.2.2.3 Mass spectrometry

The EX22 tropoelastin construct was produced via a small-scale *E. coli* expression system following the same methods previously described for other tropoelastin mutants. Comparative mass spectrometry of Lys-C-digested WT and EX22 indicated similar peak profiles, except for a shift from the 1077 m/z peak in the WT spectrum, labeled A, to a 3367 m/z peak in the EX22 spectrum, labeled D (Figure 5.3). Both peaks were assigned to a peptide fragment containing the junction of exons 21 and 23. The mass increase of the peak in the EX22 spectrum corresponded to the cumulative mass of the 25 residues comprising domain 22 (

Table 5.2) and confirmed the presence of the domain 22 insert between domains 21 and 23 in the mutant construct.

Within the 3134-3500 m/z window, two additional peaks assigned to peptide regions common to WT and EX22 tropoelastin (labeled B and C) were detected in both spectra. Salt adducts of peptides were also visible as secondary peaks with a increased m/z of 23 relative to the main peaks.

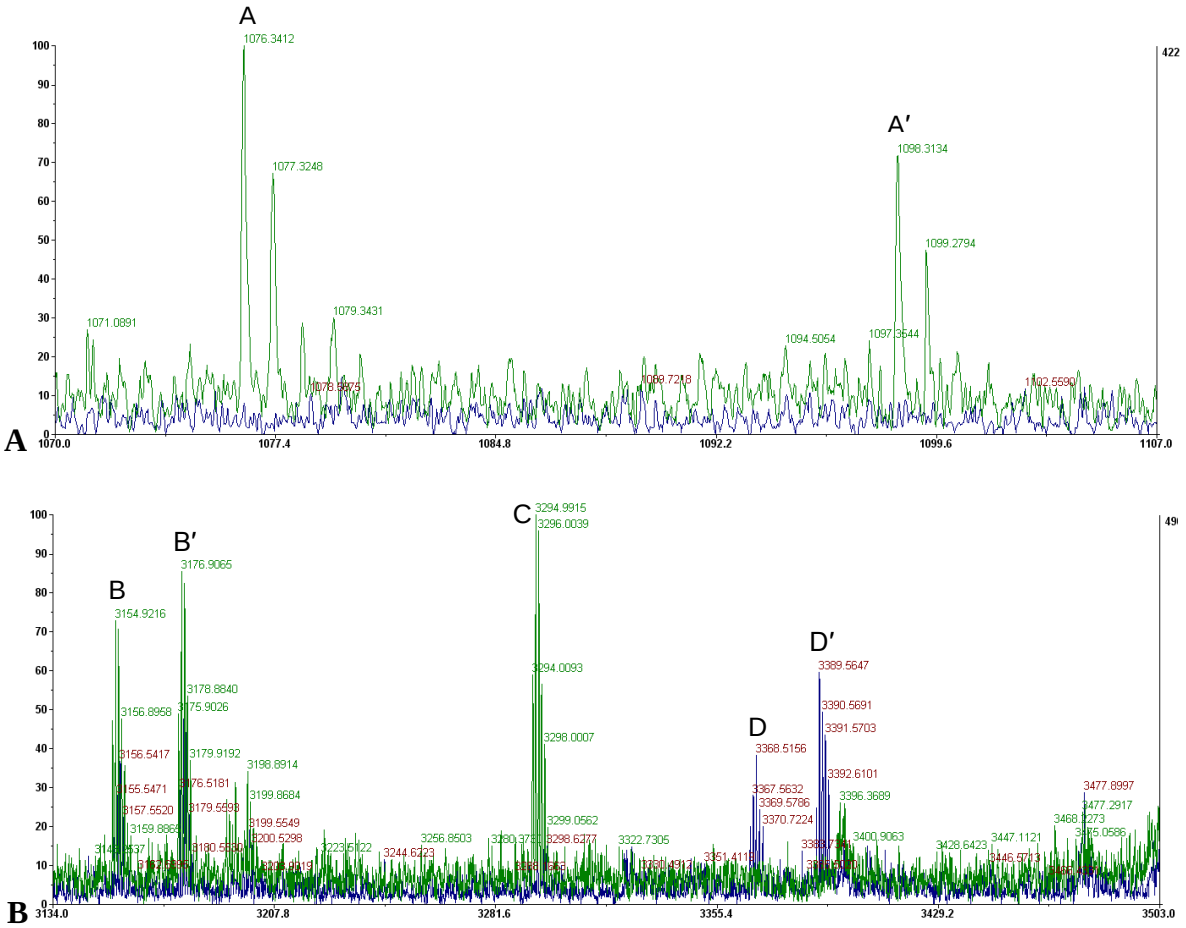

Figure 5.3. Comparative mass spectrometry of WT (green) and EX22 (blue) tropoelastin showing overlaid profiles. (A) The 1077 m/z peak in the WT spectrum, labeled A, is absent in the EX22 spectrum. (B) The 3367 m/z peak, labeled D, only present in the EX22 spectrum. Other peaks are seen in both spectra. Salt adducts are indicated by a prime symbol after the label.

Table 5.2. Assignment of peaks in the mass spectra of WT and EX22 tropoelastin. The domain 22 sequence is underlined.

Peak	Mass	Residues	Sequence
A	1076.6	426-437	YGVGTPAAAAAK
B	3154.8	610-647	AAQFGLVGAAGLGGLGVGGLGVPGVGGLGGIPPAAAAK
C	3294.9	115-150	VPGVGLPGVYPGGVLPGARFPGVGVLPGVPTGAGVK
D	3366.8	426-466	YGAAGAGVLGGLVPGAPGAVPGVPGTGGVPGVGTPAAAAAK

5.2.2.4 SDS-PAGE analysis

SDS-PAGE analysis of purified WT and EX22 tropoelastin showed bands consistent with the expected size of WT (60 kDa) and EX22 (62 kDa) (Figure 5.4). The constructs appeared to be fully intact. There was no evidence of degradation or contamination with bacterial proteins.

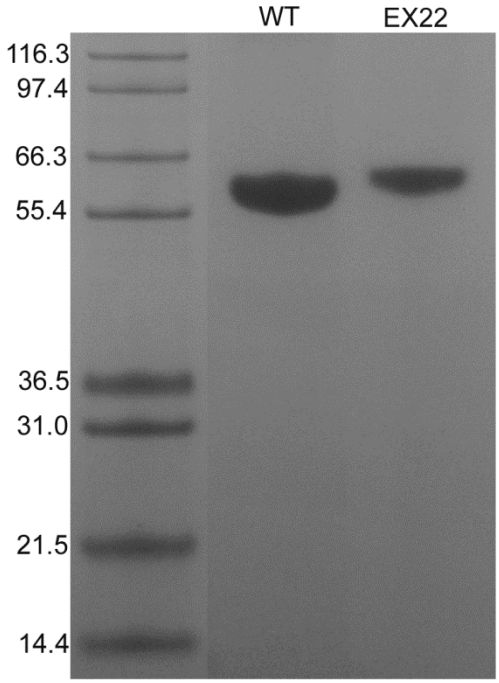

Figure 5.4. SDS-PAGE of purified WT and EX22. The bands correspond to the expected size of the full-length constructs (WT: 60 kDa, EX22: 62kDa). Sizes of the protein standards are indicated in kDa.

5.2.3 Coacervation

5.2.3.1 Light spectrophotometry

WT and EX22 tropoelastin exhibited similar temperature-dependent coacervation profiles (Figure 5.5A). WT and EX22 solutions remained clear under UV light spectrophotometry below 30°C, but both underwent a rapid increase and subsequent plateau in turbidity at and above 35°C. The critical temperature at which WT and EX22 tropoelastin displayed maximum coacervation was identified at 35°C and was identical for both constructs.

WT and EX22 differed slightly in the time required to achieve full coacervation at each temperature (Figure 5.5B). Between 35 to 45°C, EX22 coacervated almost twice as rapidly compared to WT. However, the differences in coacervation time decreased with increasing temperature and converged above 45°C.

5.2.3.2 Particle size analysis

Analysis of the particle sizes within WT and EX22 tropoelastin solutions at various temperatures revealed an identical process of self-association (Figure 5.6). At 30°C and below, WT and EX22 molecules were predominantly in a ~10 nm monomer form. At 35°C, both WT and EX22 had rapidly aggregated into 600-700 nm assemblies. Similarly-sized coacervates were also observed at higher temperatures, with no evidence of further association into larger coacervates.

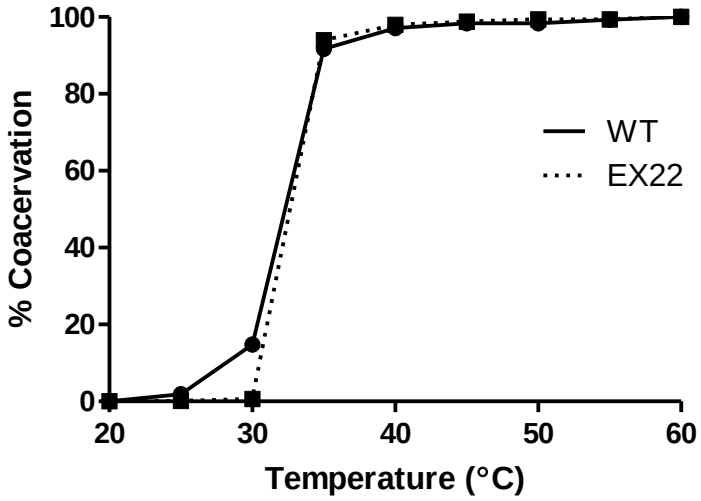

A

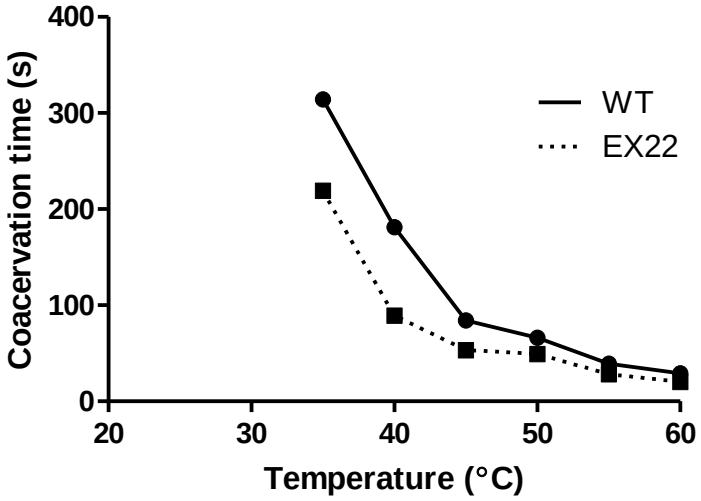

B

Figure 5.5. Coacervation properties of WT and EX22 tropoelastin. (A) The extent of tropoelastin coacervation at each temperature. (B) The time taken by each construct to reach maximum coacervation at each temperature.

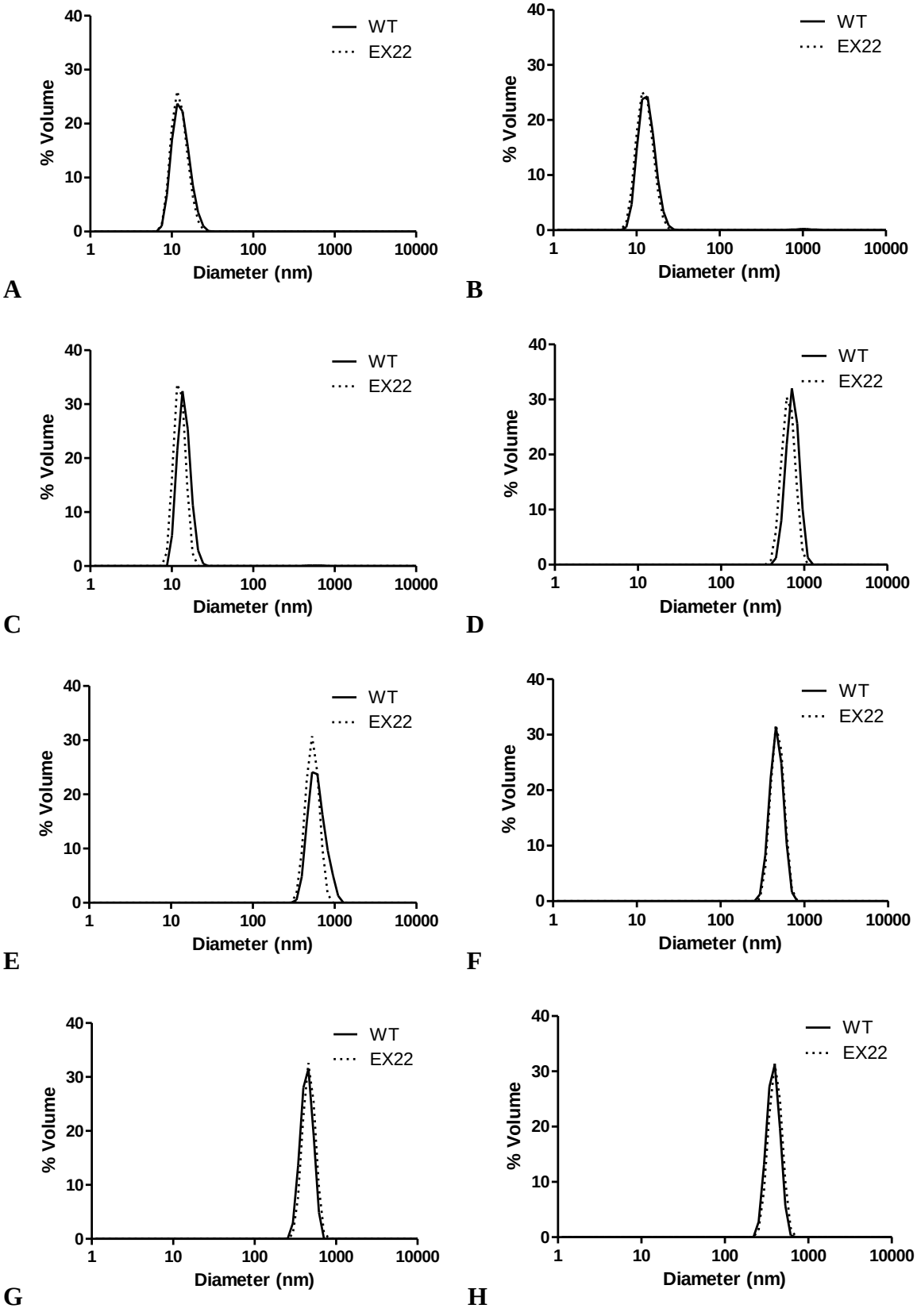

Figure 5.6. Analysis of particle sizes in WT and EX22 tropoelastin solutions at (A) 20, (B) 25, (C) 30, (D) 35, (E) 40, (F) 45, (G) 50 and (H) 55°C.

5.2.4 Cross-linking

5.2.4.1 Hydrogel construction

WT and EX22 tropoelastin formed elastin hydrogels after incubation with an amine-reactive bi-functional BS3 cross-linker at physiological temperature, salt and pH conditions (Figure 5.7). The EX22 hydrogels showed decreased thickness but possessed a similarly pliable texture compared to WT hydrogels.

Cross-linking of the WT and EX22 constructs with BS3 proceeded to completion. SDS-PAGE analysis of the aqueous solution left after WT and EX22 hydrogel formation showed the absence of monomer species, indicating complete incorporation into the cross-linked material (Figure 5.8).

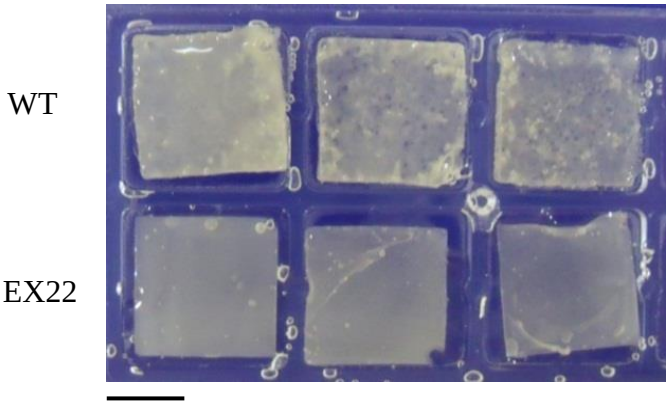

Figure 5.7. Hydrogels constructed from WT and EX22 tropoelastin cross-linked with 10 mM BS3. Scale bar: 0.5 cm.

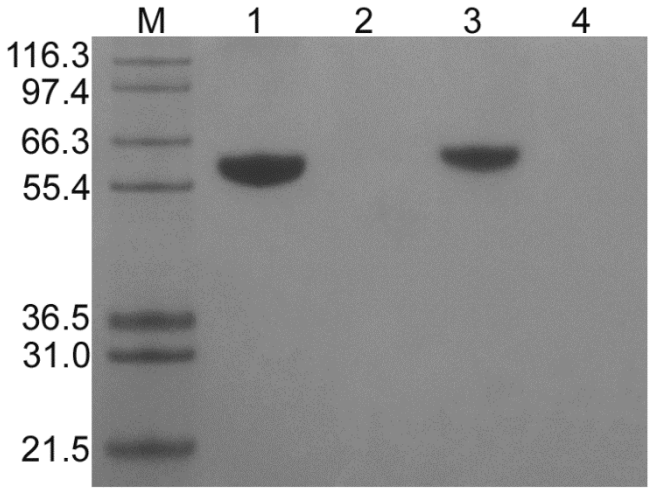

Figure 5.8. SDS-PAGE analysis of the extent of WT and EX22 cross-linking. Lanes: M – Mark12 protein standards (kDa); 1 – WT; 2 – WT + 10 mM BS3; 3 – EX22; 4 – EX22 + 10 mM BS3.

5.2.4.2 Micro-CT of hydrogels

Micro-CT imaging of WT and EX22 hydrogels enabled a 3-D reconstruction of the cross-linked products (Figure 5.9). The WT hydrogel had a fibrous and extensively porous composition that was maintained across the entire thickness of the material. In contrast, the EX22 hydrogel appeared to be highly compact, with a thickness 2.5-5.5 times less than that of the WT hydrogel of a similar mass. Consistent with the dense structure was the absence of fibrous structures or discernible channels on or within the EX22 hydrogel.

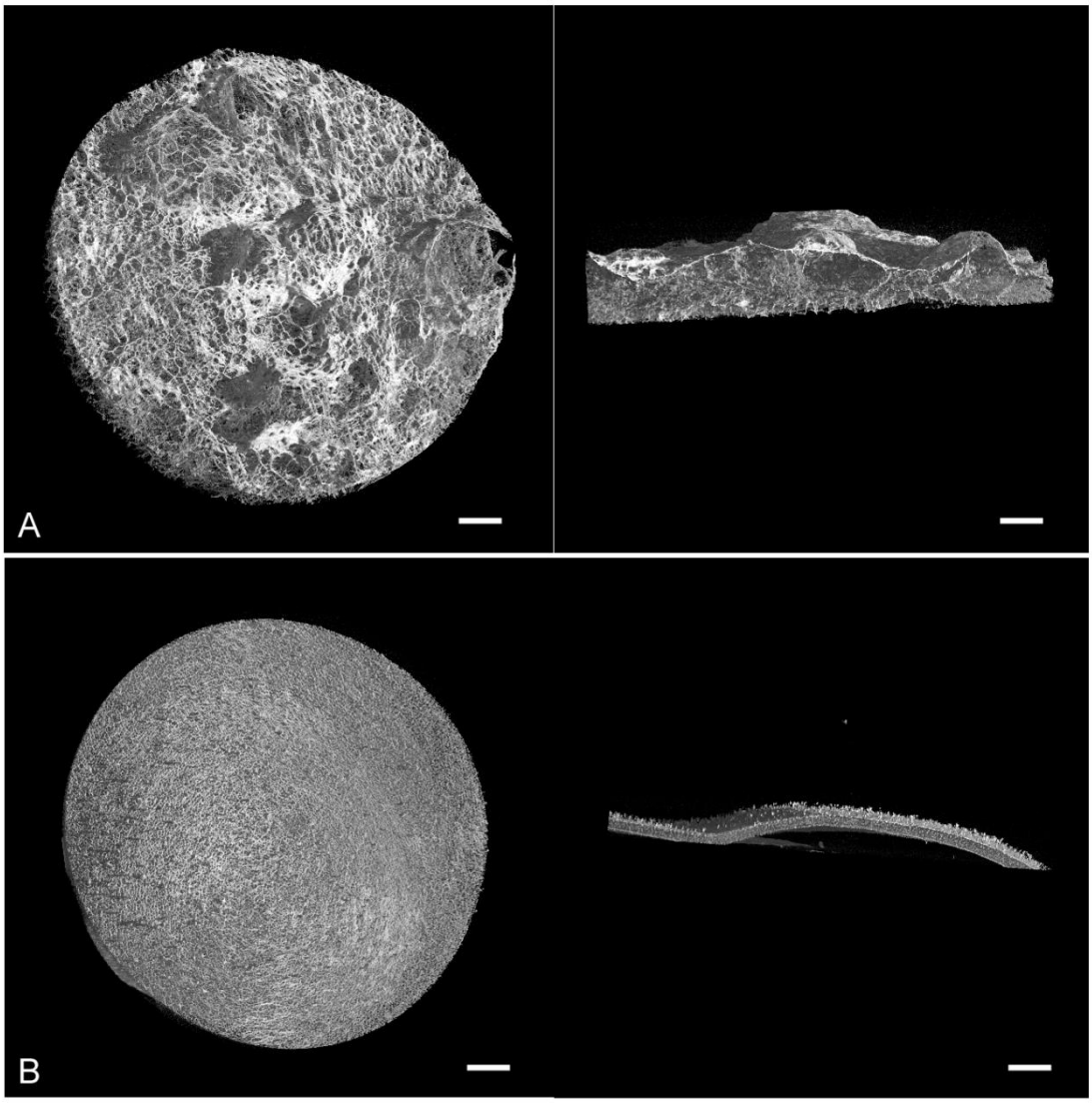

Figure 5.9. Micro-CT reconstruction of (A) WT and (B) EX22 hydrogels. Each panel shows the top (left) and cross-section (right) views of the hydrogel. Scale bar: 0.5 mm.

Automated analyses of each slice of the hydrogel reconstructions allowed calculation of the overall porosity of the materials (Figure 5.10). The EX22 hydrogel was estimated to be 23% less porous than the WT, which represented a significant decrease in open channel formation in the mutant construct during cross-linking.

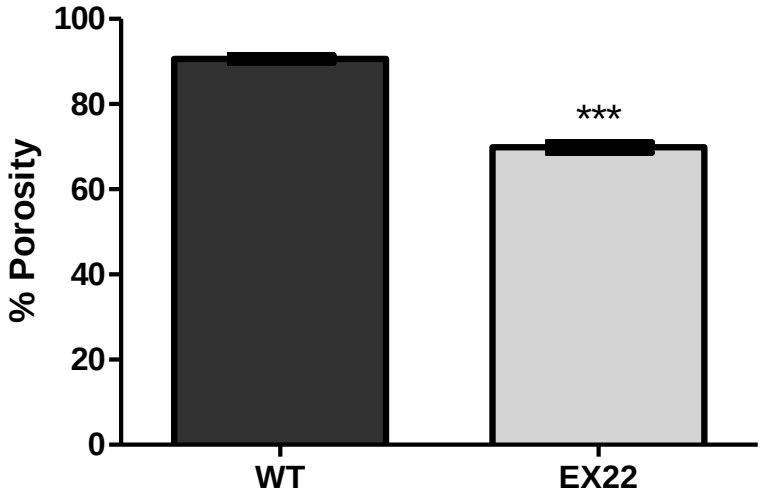

Figure 5.10. Porosity of WT and EX22 hydrogels calculated by automated analyses of micro-CT cross-sectional images.

5.2.4.3 Hydrogel swelling

Both WT and EX22 hydrogels displayed remarkable expansion when submerged in water, although the extent of swelling was significantly different between the wild-type and mutant constructs (Figure 5.11). WT hydrogels underwent a 17- to 24-fold increase in volume, while EX22 hydrogels showed a narrower 6- to 7-fold increase compared to pre-swelling volumes.

Differences between the post-swelling volumes of WT and EX22 hydrogels could be accounted for by differences in fluid influx into the cross-linked materials (Figure 5.12). At 4, 25 and 37°C, water intake by EX22 hydrogels was consistently less than WT hydrogels. While WT hydrogels absorbed 73-110 g of water per gram of protein, EX22 hydrogels absorbed only 24-26 g of water per gram of protein. This represented a 67-76% decrease in water intake by the EX22 mutant hydrogels compared to the wild-type.

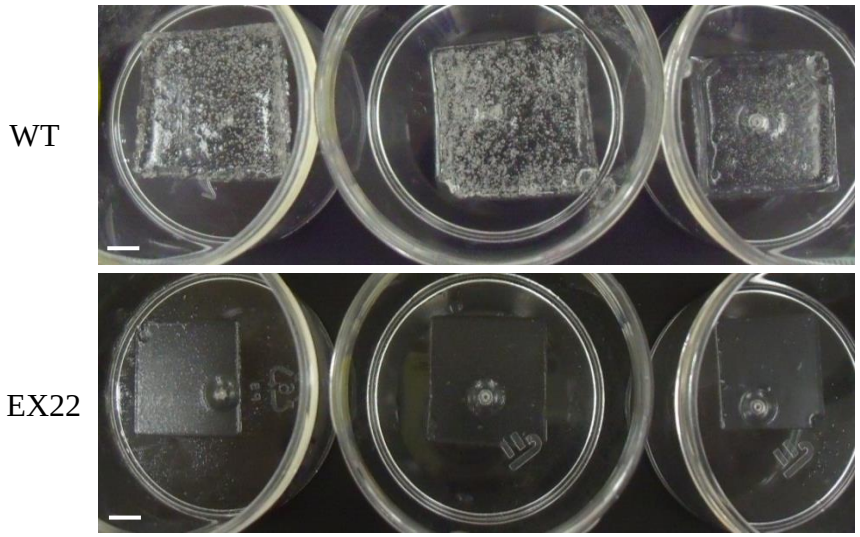

Figure 5.11. WT and EX22 hydrogels swollen in water for 24 hrs at 37°C. Triplicate samples are shown. Scale bar: 0.5 cm.

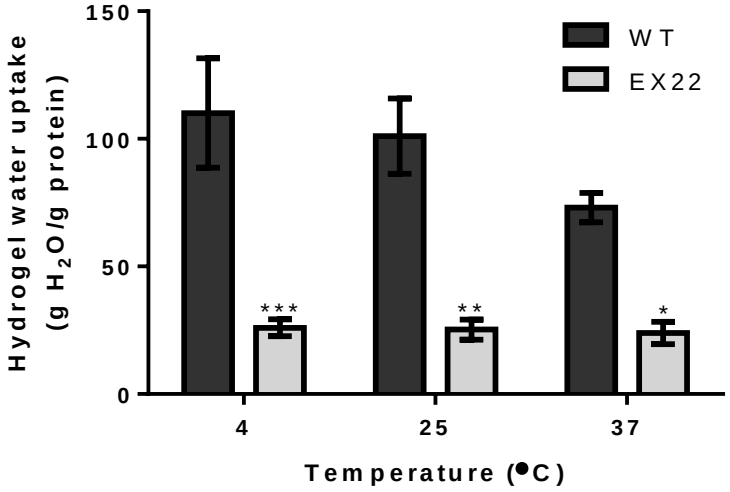

Figure 5.12. Swelling of WT and EX22 hydrogels in water at 4, 25 and 37 °C.

5.2.4.4 SEM of hydrogels

Scanning electron microscopy of WT and EX22 hydrogels demonstrated distinct differences in their surface morphology (Figure 5.13). The top surface of the WT hydrogel was characterised by a highly porous network with open channels ranging from ~80-120 μm in diameter. In contrast, the EX22 hydrogel top surface was composed of a dense, solid sheet to which fragments of shard-like or fibrous structures are attached. Pores on this surface were also markedly smaller, with an average diameter of ~10 μm.

The bottom surfaces of WT and EX22 hydrogels were comparatively devoid of features. Both consisted of a smooth and flat layer in which majority of pores had coalesced together.

The edges of the hydrogels clearly highlighted prominent differences in the cross-linked structures of the WT and EX22 constructs. The WT hydrogel appeared inflated, with open channels traversing across the thickness of the material. In contrast, the EX22 hydrogel was likely formed from closely-stacked layers of sheet-like structures, which gave rise to a highly compact polymer.

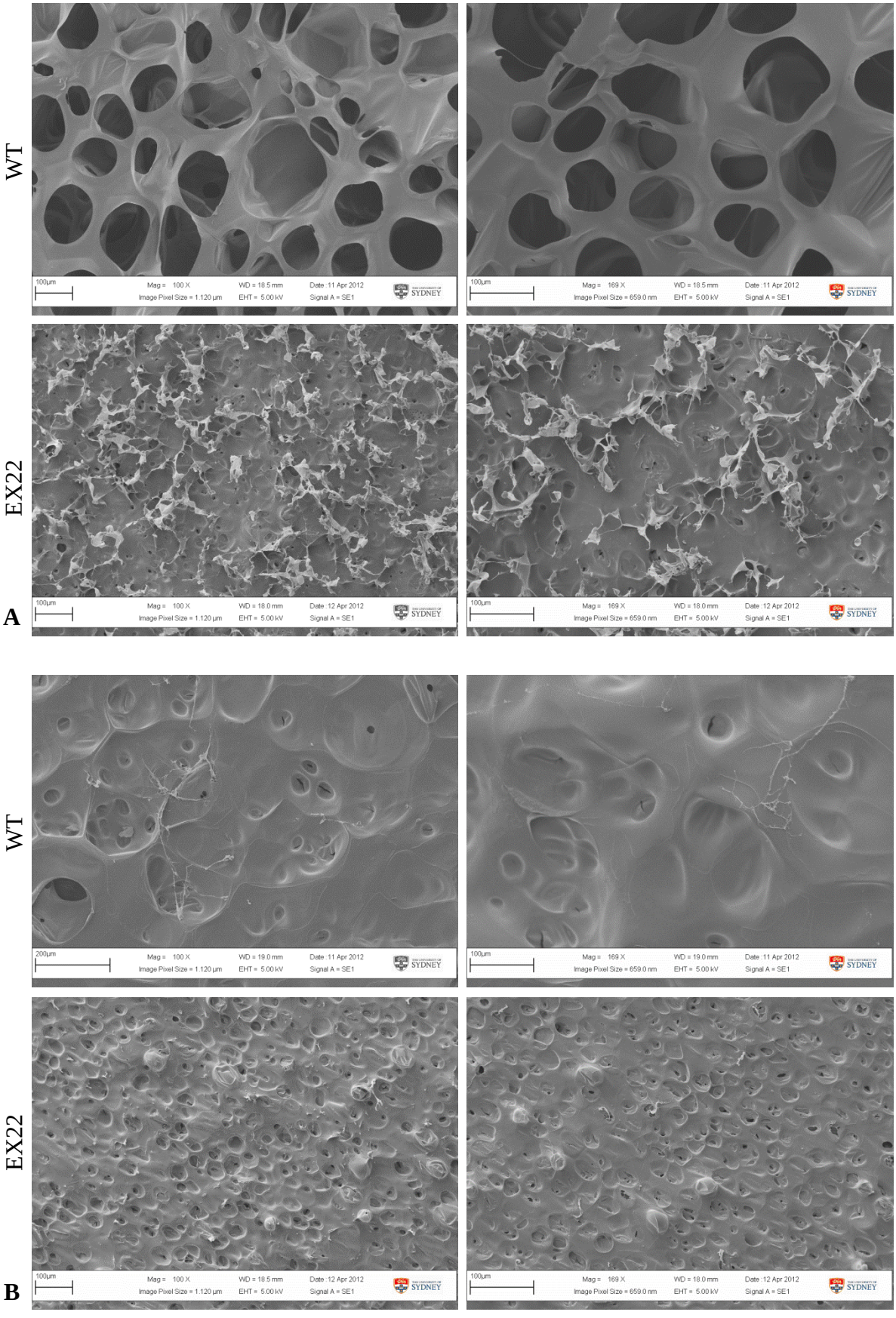
WT
EX22
A
WT
EX22
B

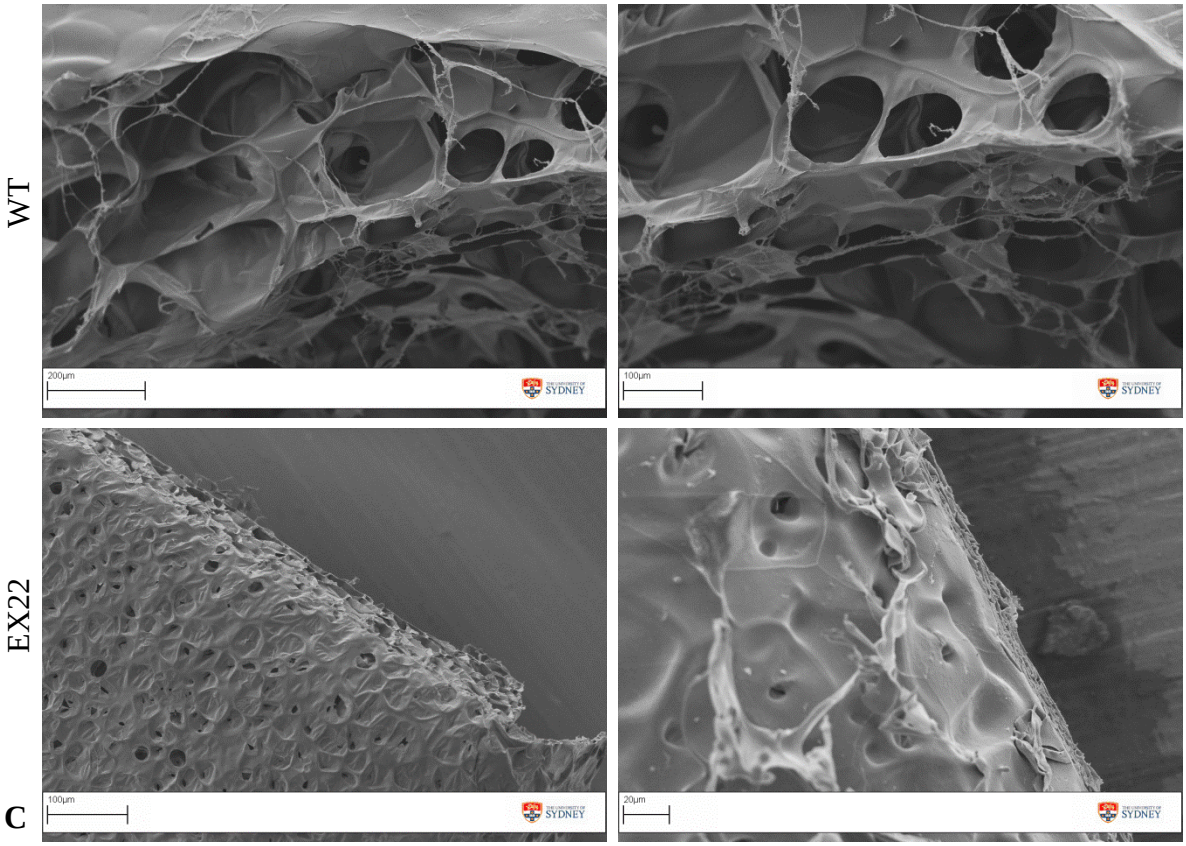

Figure 5.13. Scanning electron microscope images of WT and EX22 hydrogels. The (A) top, (B) bottom and (C) edge of each hydrogel are shown at low (left) and high (right) magnifications.

5.2.5 Cell attachment

WT and EX22 tropoelastin coated on tissue culture wells supported the attachment of GM3348 human dermal fibroblasts in a concentration-dependent manner (Figure 5.14). Increasing amounts of surface-bound tropoelastin allowed adhesion of a greater percentage of seeded cells, until saturation at 5 μg/mL tropoelastin. At tropoelastin concentrations enabling maximum cell attachment, up to 80% of seeded cells adhered to both the WT and EX22 constructs. There was no perceived difference in the ability of either species to interact with dermal fibroblast cells.

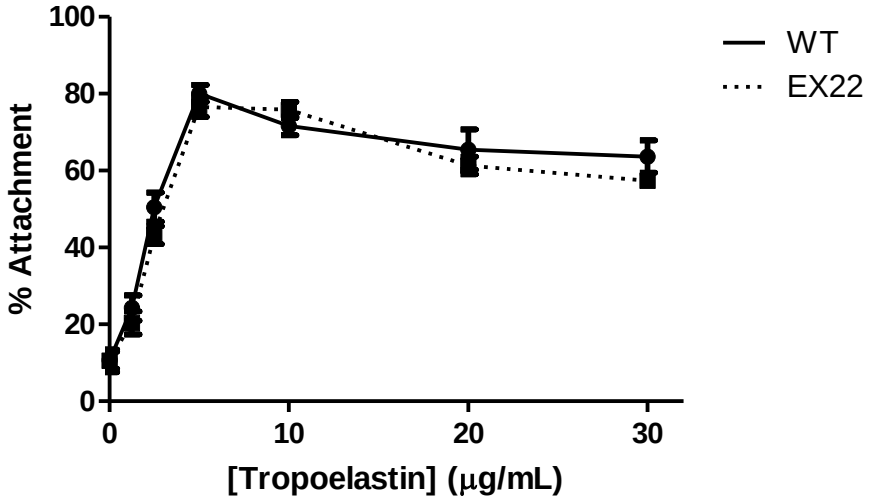

Figure 5.14. Attachment of GM3348 human dermal fibroblasts to tissue culture wells coated with increasing concentrations of WT and EX22 tropoelastin.

5.2.6 Antibody detection

Antibodies targeted against epitopes situated across the tropoelastin molecule were used to compare the exposure of specific regions in the WT and EX22 constructs (Figure 5.15). The antibody against domain 6 detected equivalent levels of the epitope on both WT and EX22, indicating similar exposure of the N-terminal segment of both constructs. However, the BA4 antibody, which primarily recognizes a sequence in domain 24, bound ~15% less to EX22 than to WT. This suggested a slightly reduced exposure of the central region of EX22. Additionally, the antibody against domain 36 also detected ~30% fewer epitopes in EX22 compared to WT, indicating decreased accessibility of the C-terminus in EX22 tropoelastin.

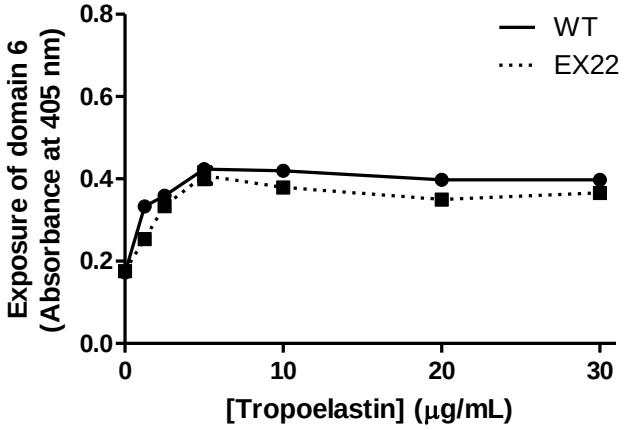

A

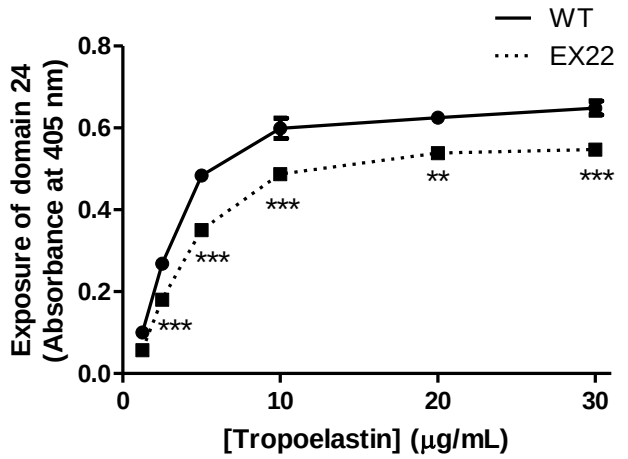

B

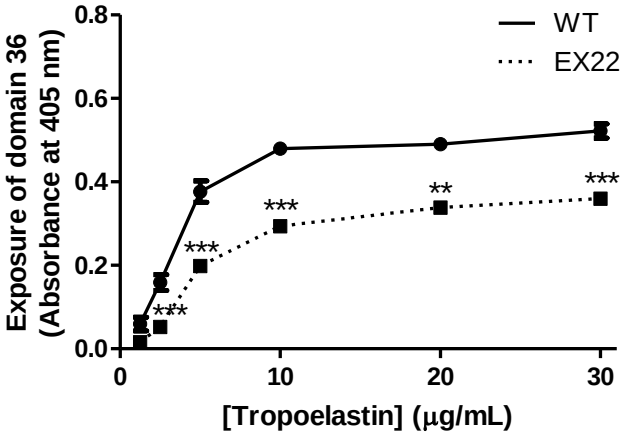

C

Figure 5.15. Enzyme-linked immunosorbent assay of WT and EX22 tropoelastin. The primary antibody used was targeted against (A) domain 6, (B) domain 24, or (C) domain 36.

5.2.7 Elastic fibre assembly

5.2.7.1 By GM3348 dermal fibroblasts

The elastogenic ability of WT and EX22 tropoelastin with GM3348 human dermal fibroblasts was determined by the addition of purified constructs to the culture media of cells. At a lower concentration of exogenous tropoelastin (20 μg/mL), WT monomers had begun to assemble linearly after one day, and progressively formed long branched fibres within 4-10 days (Figure 5.16). These WT elastic fibres displayed characteristic autofluorescence which intensified over time. In stark contrast, EX22 tropoelastin did not assemble into elastic fibres. The mutant species remained as dispersed spherules in the extracellular space even after 10 days.

At a higher concentration of added tropoelastin (200 μg/mL), WT species followed the same elastogenic process, but formed a more extensive elastic fibre network (Figure 5.17). Interestingly, EX22 tropoelastin was also able to form elastic fibres, which, however, appeared as close clusters of punctate species rather than as continuous structures. This was most prominent until 7 days after tropoelastin addition. The EX22 fibres were also less abundant and stained significantly less than the WT fibres, although the autofluorescence of both types of fibres were comparable (Figure 5.18). Differences in the properties of WT and EX22 elastic fibres were not due to differences in cell numbers.

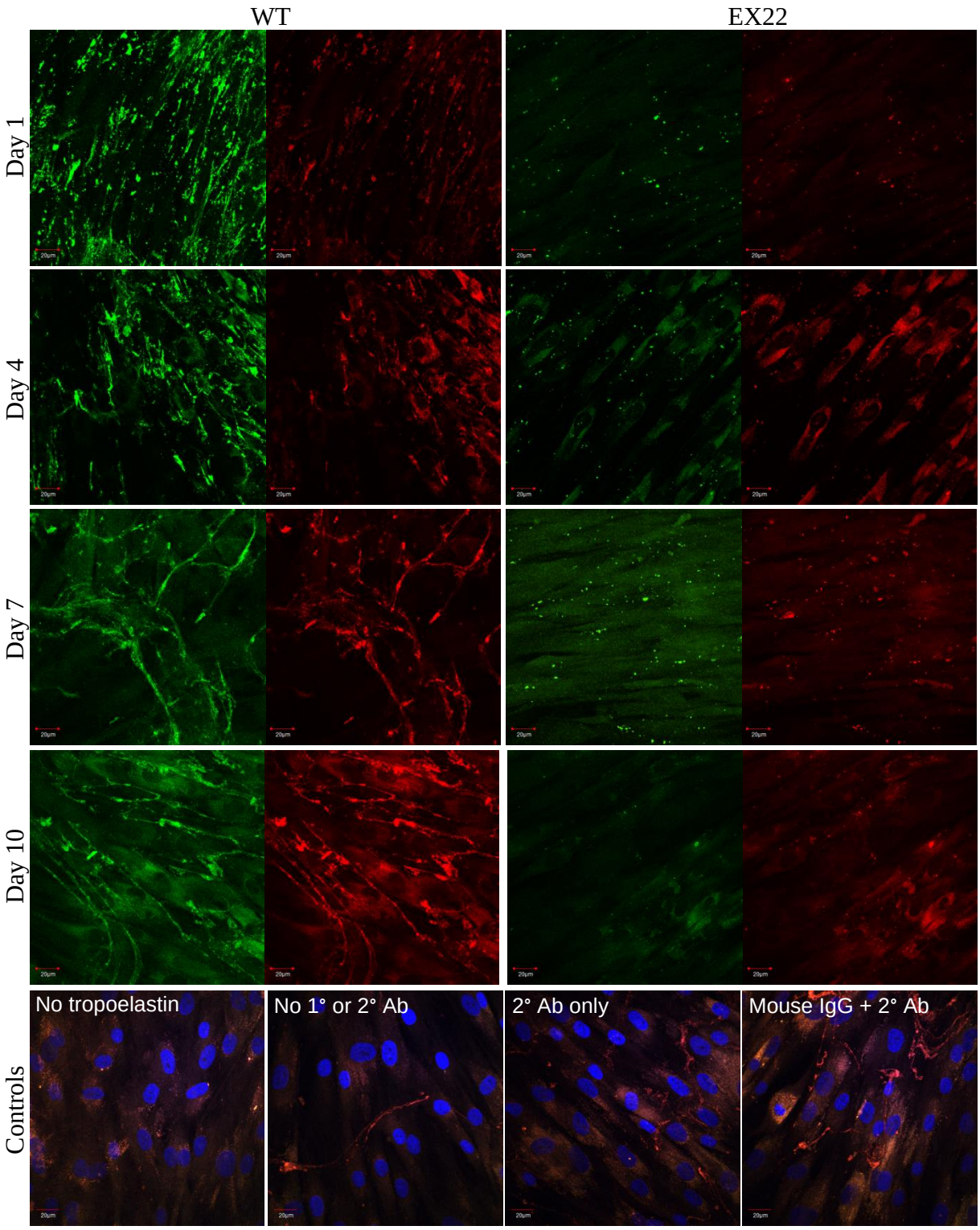

Figure 5.16. Confocal microscope images of WT and EX22 elastic fibres formed from 20 μg/mL tropoelastin by GM3348 human dermal fibroblasts. Samples were fixed and stained with a mouse anti-elastin antibody and a FITC-conjugated anti-mouse antibody at 1, 4, 7 and 10 days after tropoelastin addition. Elastin-specific

immunofluorescence (green) and autofluorescence (red) of the elastic fibres are shown. Controls include a no tropoelastin sample, and samples with added WT but with no antibody, with the secondary antibody only, or with a non-specific mouse antibody and the secondary antibody. Controls show merged fluorescence images with DAPI-stained cell nuclei.

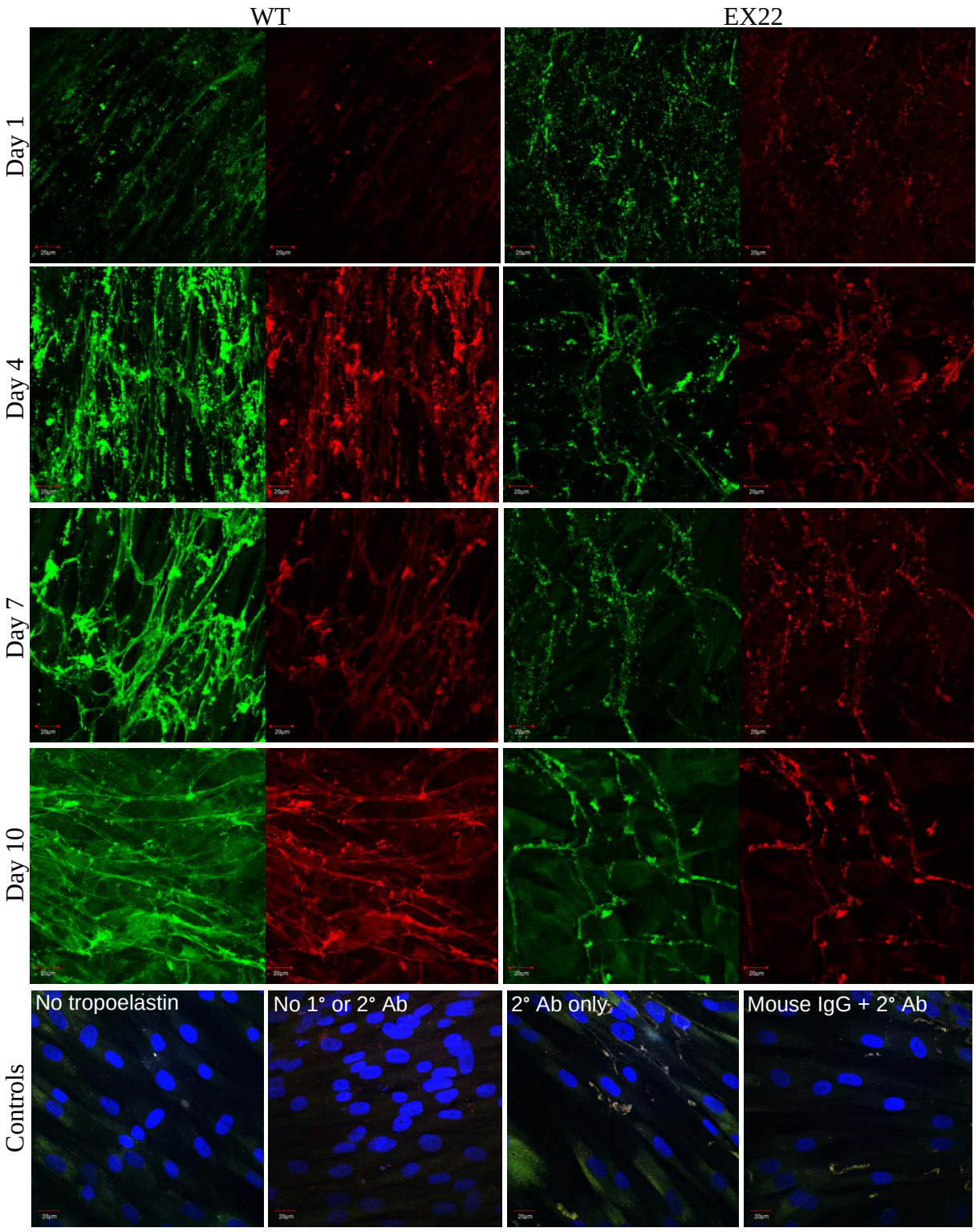

Figure 5.17. Confocal microscope images of WT and EX22 elastic fibres formed from 200 μg/mL tropoelastin by GM3348 human dermal fibroblasts. Samples were fixed and stained with a mouse anti-elastin antibody and a FITC-conjugated anti-mouse antibody at 1, 4, 7 and 10 days after tropoelastin addition. Elastin-specific

immunofluorescence (green) and autofluorescence (red) of the elastic fibres are shown. Controls include a no tropoelastin sample, and samples with added WT but with no antibody, with the secondary antibody only, or with a non-specific mouse antibody and the secondary antibody. Controls show merged fluorescence images with DAPI-stained cell nuclei.

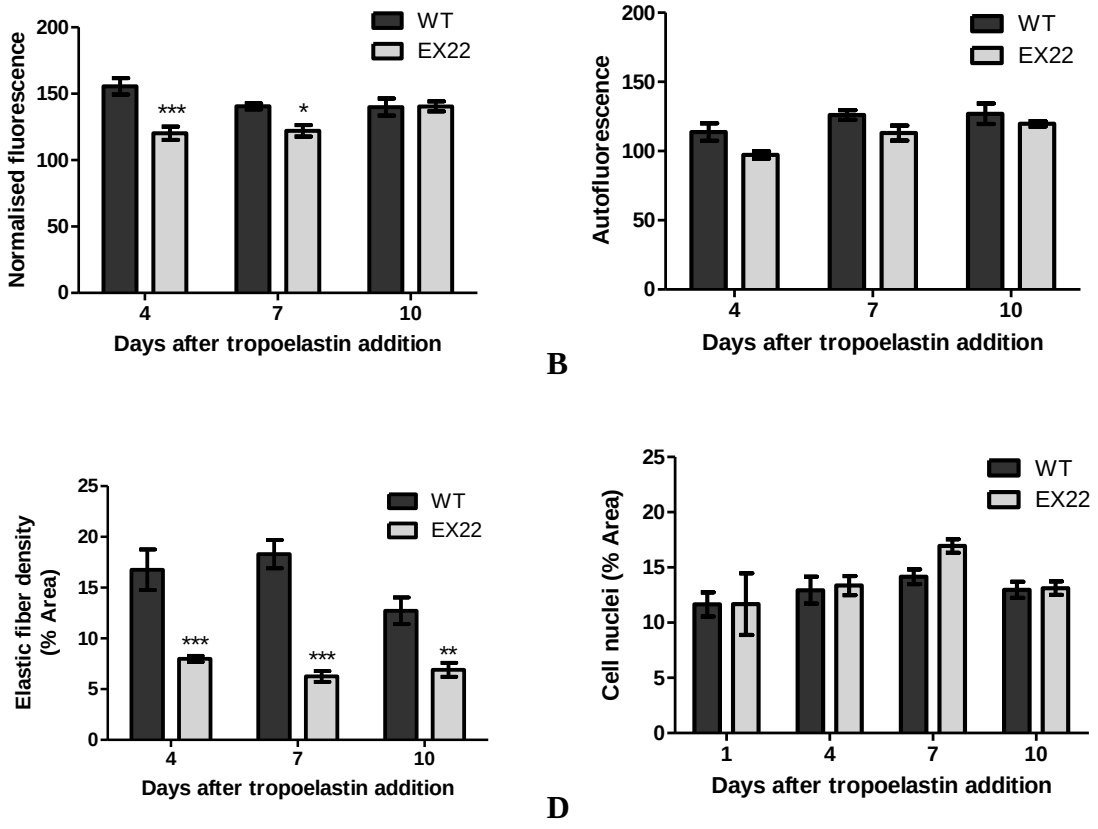

Figure 5.18. Comparative (A) immunofluorescence, (B) autofluorescence and (C) abundance of WT and EX22 elastic fibres produced from 200 μg/mL exogenous tropoelastin in GM3348 cells. (D) Cell numbers as indicated by the area occupied by cell nuclei per field of view.

5.2.7.2 By ARPE-19 cells

The ability of WT and EX22 to form elastic fibres with human retinal pigmented cells was also determined by the addition of exogenous tropoelastin to the cellular environment. At low concentrations of added tropoelastin (20 μg/mL), elastic fibres were successfully established from both WT and EX22, although the elastogenic time course and elastic fibre characteristics differed between both constructs (Figure 5.19). One day after tropoelastin addition, WT spherules had organised linearly while EX22 species remained randomly distributed across the extracellular environment. By 4 days, a well-defined network of WT elastic fibres had developed, which stably persisted throughout the experimental period. While EX22 also formed visible fibres within this time frame, they were significantly fewer in number and exhibited markedly reduced immunofluorescence and autofluorescence (Figure 5.20). Moreover, the EX22 fibres appeared as dispersed rather than defined structures, which was represented by an increased average fibre width relative to the WT (Figure 5.21).

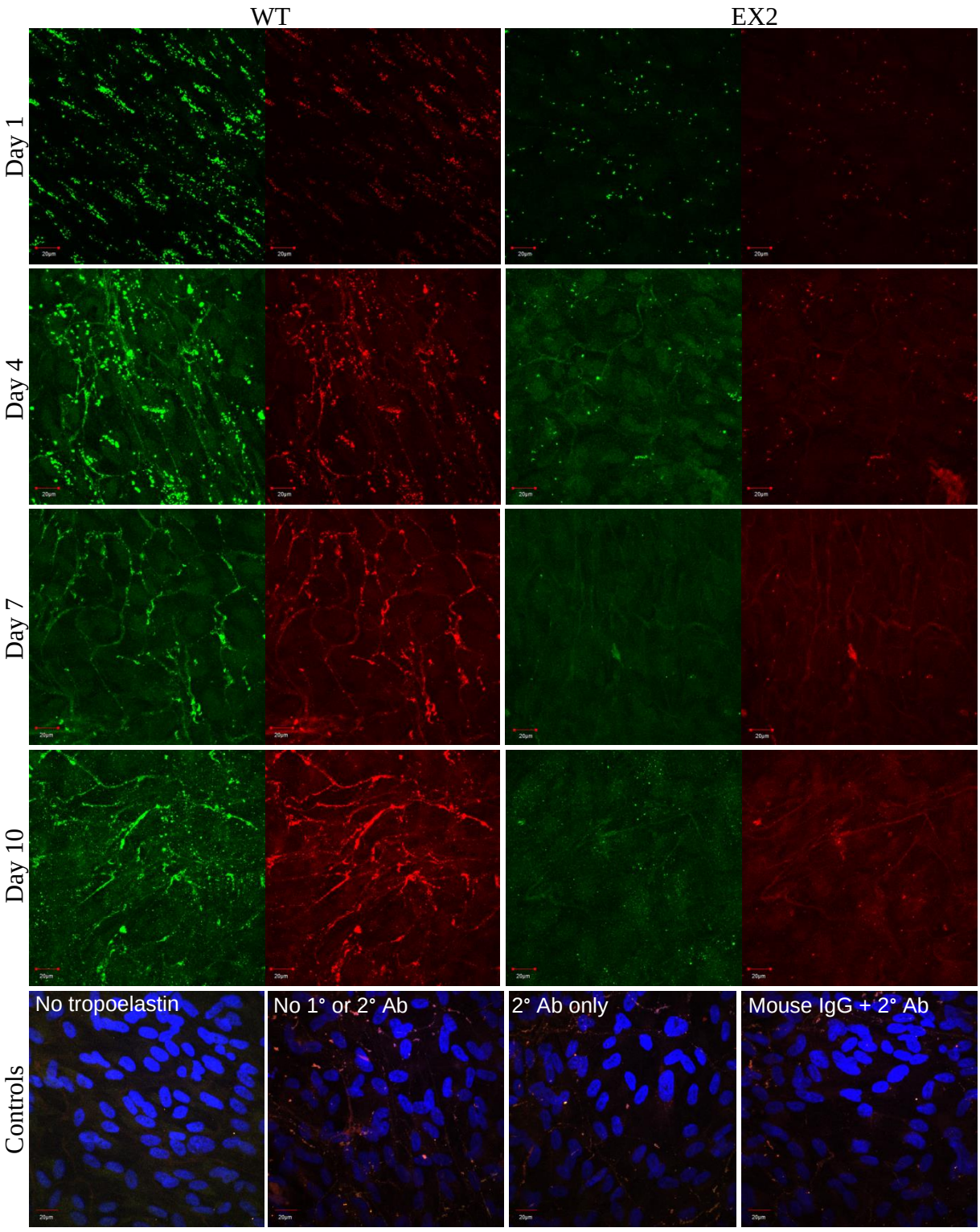

Figure 5.19. Confocal microscope images of WT and EX22 elastic fibres formed from 20 μg/mL tropoelastin by ARPE-19 cells. Samples were fixed and stained with a mouse anti-elastin antibody and a FITC-conjugated anti-mouse antibody at 1, 4, 7 and 10 days after tropoelastin addition. Elastin-specific immunofluorescence (green) and

autofluorescence (red) of the elastic fibres are shown. Controls include a no tropoelastin sample, and samples with added WT but with no antibody, with the secondary antibody only, or with a non-specific mouse antibody and the secondary antibody. Controls show merged fluorescence images with DAPI-stained cell nuclei.

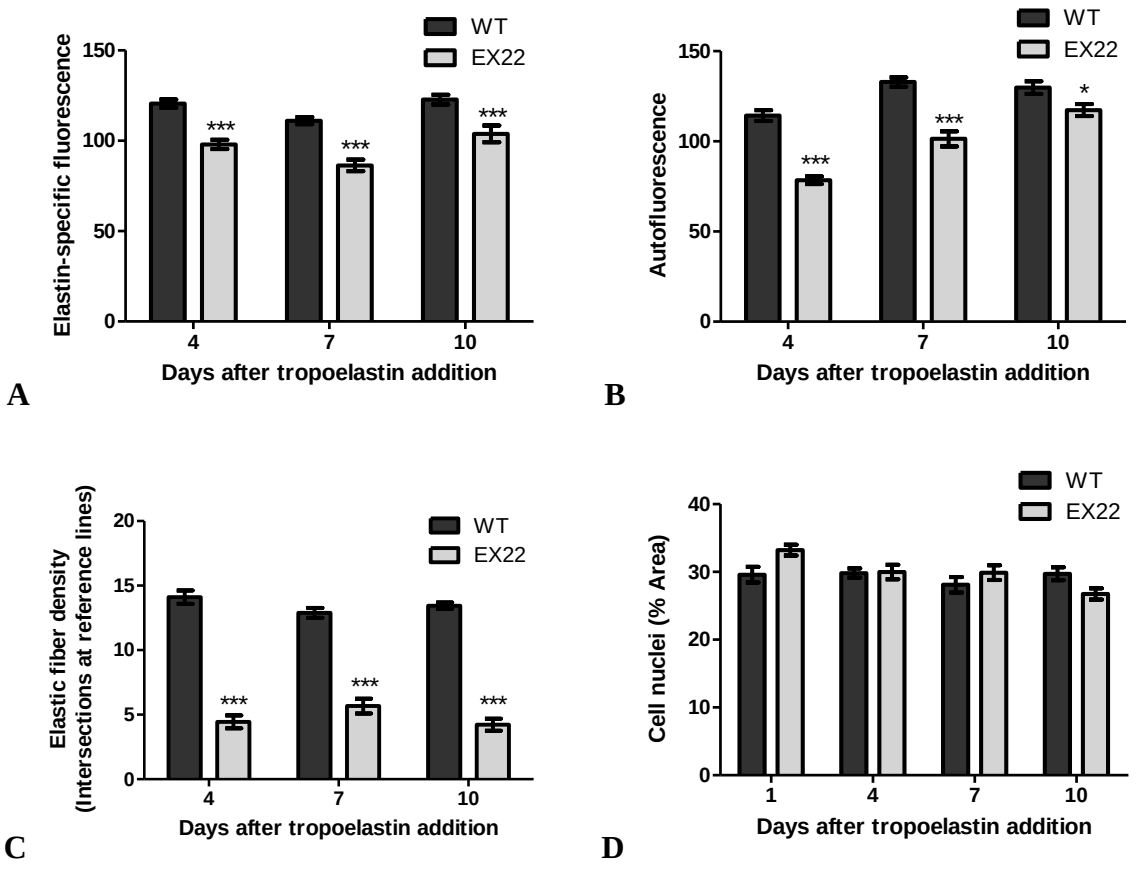

Figure 5.20. Comparative (A) immunofluorescence, (B) autofluorescence and (C) abundance of WT and EX22 elastic fibres produced from 20 μg/mL exogenous tropoelastin in ARPE-19 cells. (D) Cell numbers as indicated by the area occupied by cell nuclei per field of view.

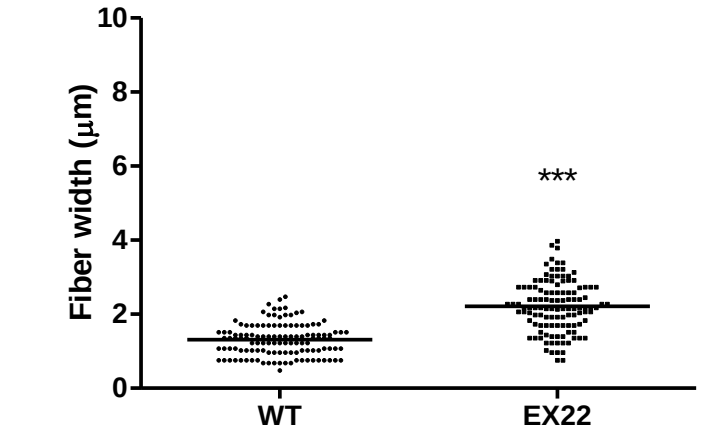

A

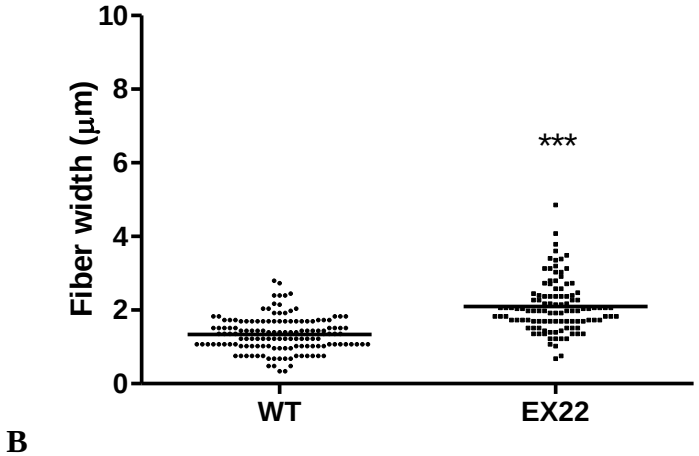

B

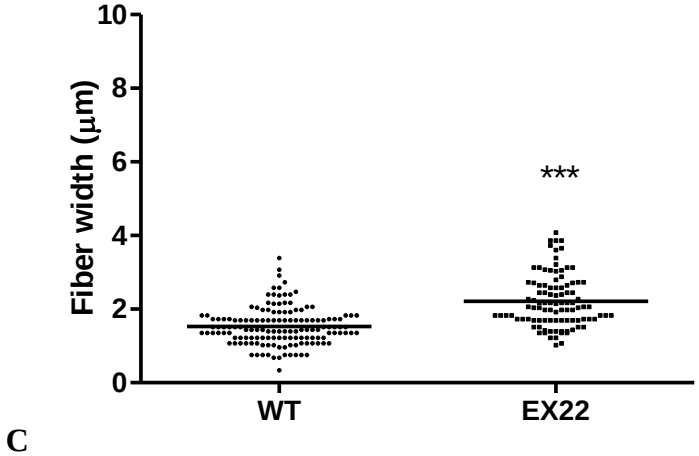

C

Figure 5.21. Width of WT and EX22 elastic fibres formed from the addition of 20 μg/mL tropoelastin by ARPE-19 cells. The fibres were measured (A) 4, (B) 7 and (C) 10 days after tropoelastin addition.

At a higher concentration of exogenous tropoelastin (200 μg/mL), both WT and EX22 constructs established a more extensive system of elastic fibres (Figure 5.22). However, the same differences were observed between WT and EX22 fibre formation. An initial lag in EX22 elastogenesis was evident after one day, wherein short WT fibrils were already visible while EX22 globules remained as separate clusters. The EX22 fibres that subsequently formed after 4 days were, as previously described, significantly less abundant and displayed dramatically decreased fluorescence compared to WT fibres (Figure 5.23). The average width of EX22 fibres was also consistently greater than that of WT fibres (Figure 5.24).

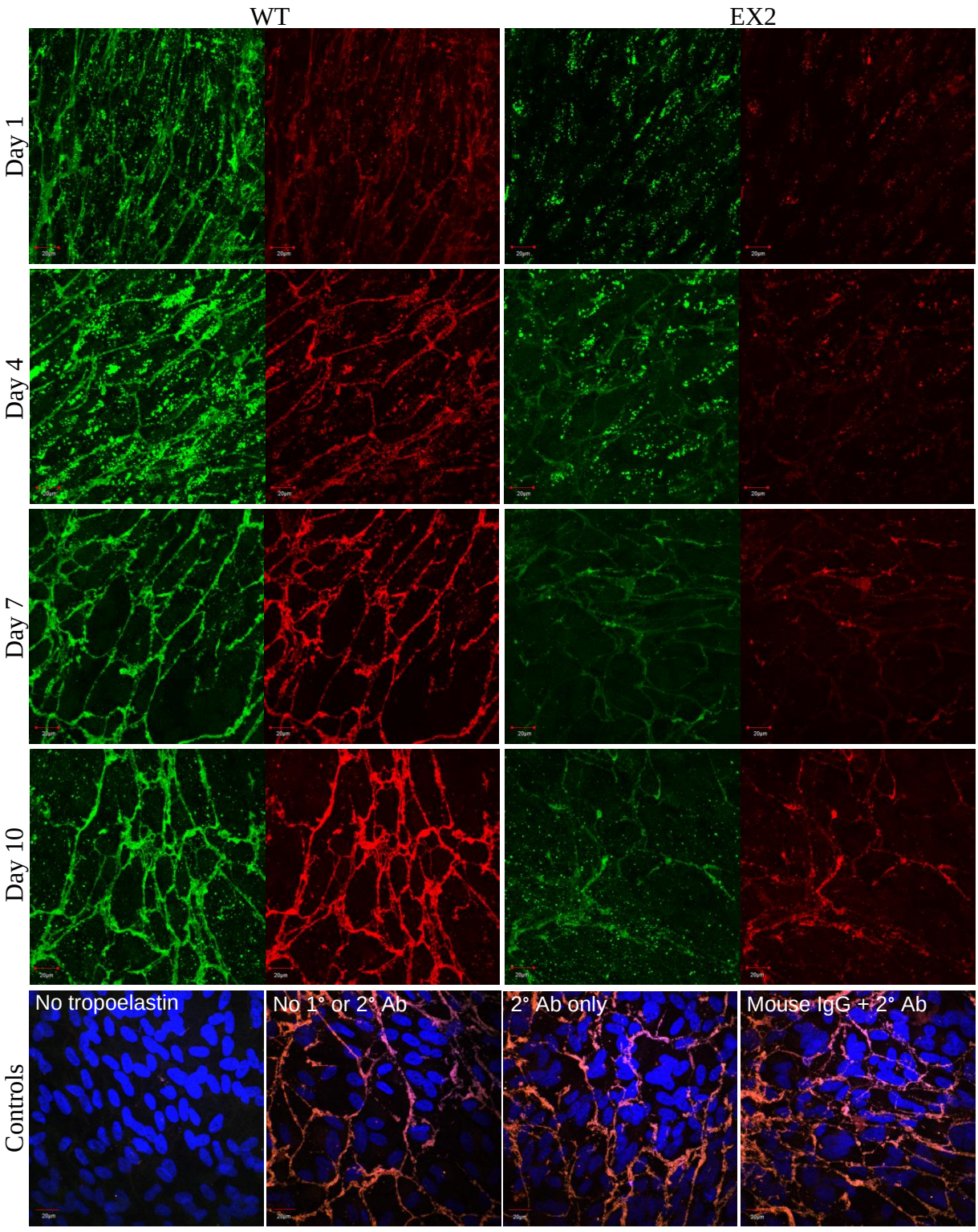

Figure 5.22. Confocal microscope images of WT and EX22 elastic fibres formed from 200 μg/mL tropoelastin by ARPE-19 cells. Samples were fixed and stained with a mouse anti-elastin antibody and a FITC-conjugated anti-mouse antibody at 1, 4, 7 and 10 days after tropoelastin addition. Elastin-specific immunofluorescence (green) and

autofluorescence (red) of the elastic fibres are shown. Controls include a no tropoelastin sample, and samples with added WT but with no antibody, with the secondary antibody only, or with a non-specific mouse antibody and the secondary antibody. Controls show merged fluorescence images with DAPI-stained cell nuclei.

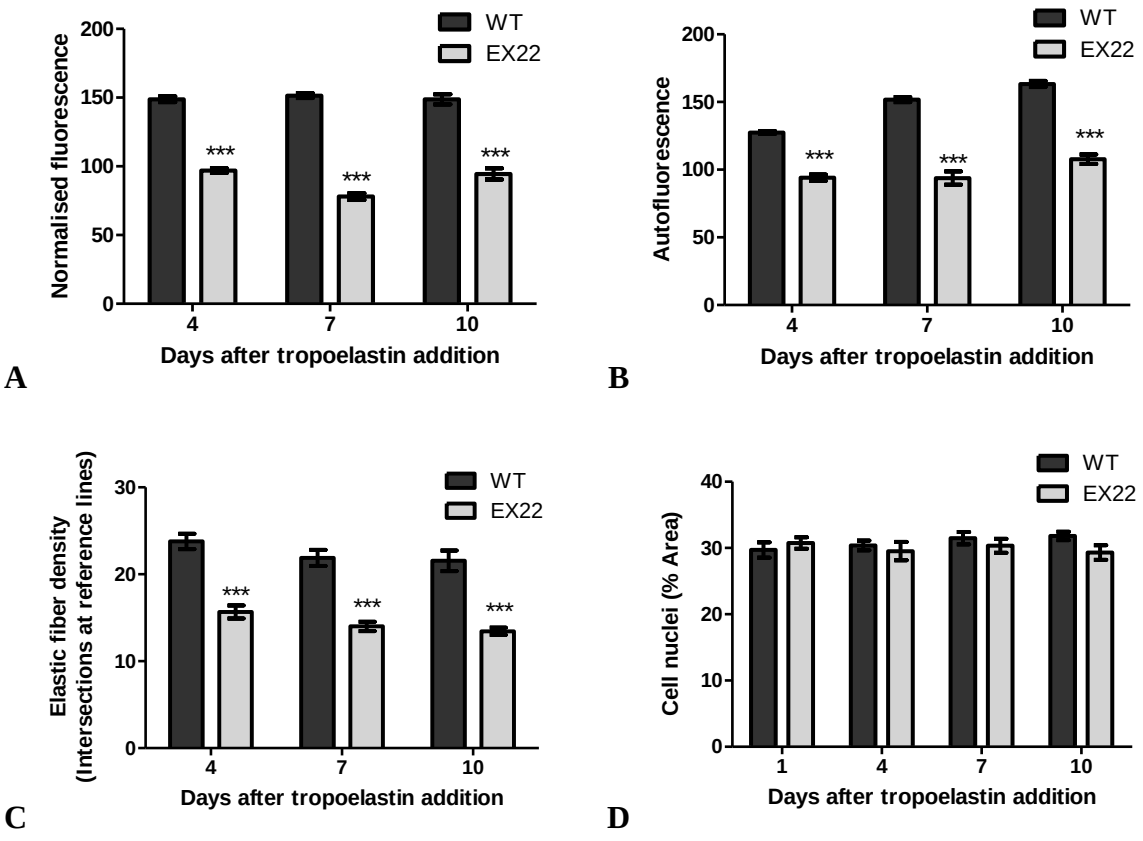

Figure 5.23. Comparative (A) immunofluorescence, (B) autofluorescence and (C) abundance of WT and EX22 elastic fibres produced from 200 μg/mL exogenous tropoelastin in ARPE-19 cells. (D) Cell numbers as indicated by the area occupied by cell nuclei per field of view.

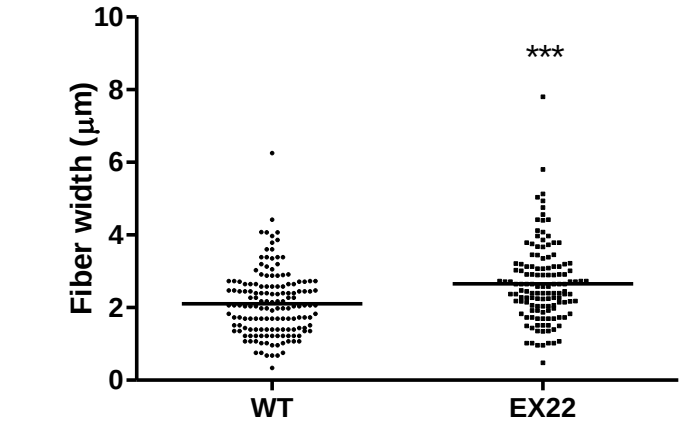

A

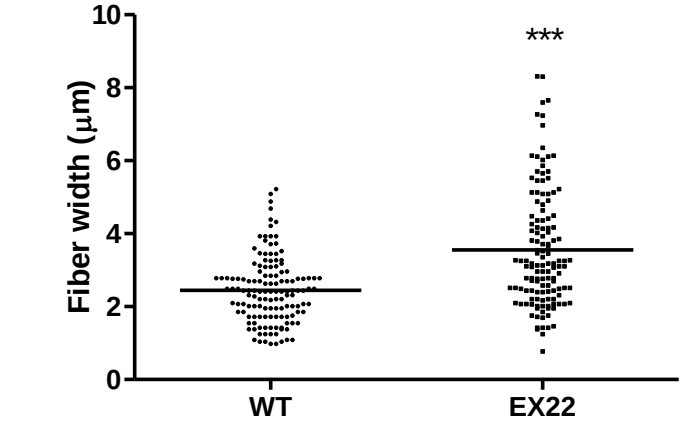

B

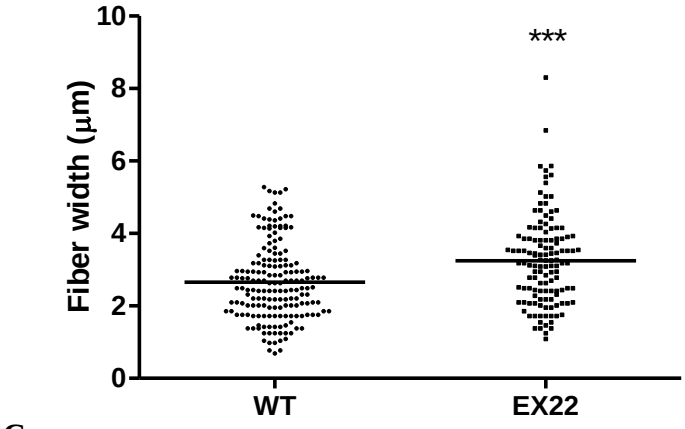

C

Figure 5.24. Width of WT and EX22 elastic fibres formed from the addition of 200 μg/mL tropoelastin by ARPE-19 cells. The fibres were measured (A) 4, (B) 7 and (C) 10 days after tropoelastin addition.

5.2.8 Structural studies

5.2.8.1 Far-UV CD

The CD spectra of WT and EX22 possessed similar features, including a minimum at ~200 nm and a negative shoulder at ~220 nm (Figure 5.25). From the CD spectra, the secondary structure composition of both WT and EX22 were calculated to be similar, comprising predominantly of unordered structure (49-50%) and a small percentage of alpha-helix (9-10%), beta-sheet (19%), turn (12%) and polyproline II helix (9%) structures.

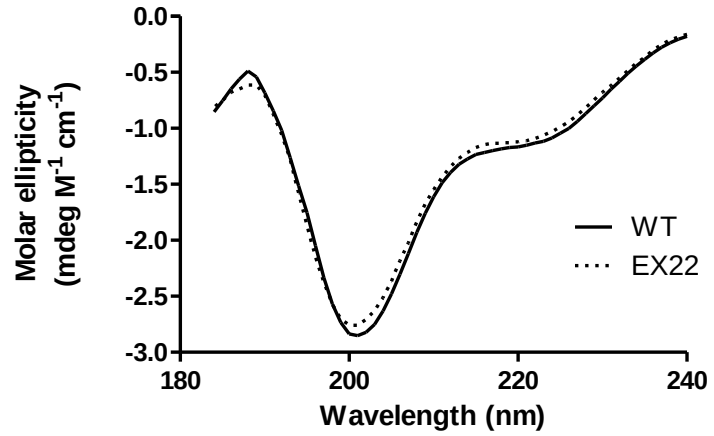

A

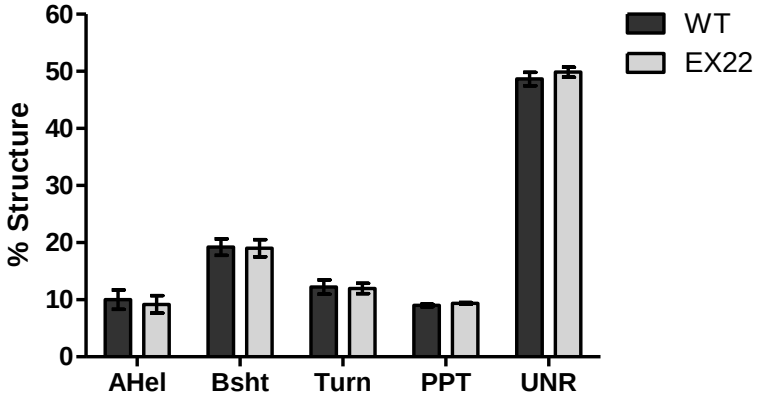

B

Figure 5.25. Circular dichroism analysis showing the (A) CD spectra and (B) secondary structure composition of WT and EX22 tropoelastin. The percentages of alpha-helix (AHel), beta-sheet (BSht), turn, polyproline II helix (PPT) and unordered (UNR) structures are indicated.

5.2.8.2 SAXS

Structural analysis of EX22 by SAXS indicated a nanostructure with similar length along the central axis (~14 nm) and similar general features to the WT shape, including an elastic coil region spanning the N-terminal segment, a hinge/turn connected to the central bridge region, and a C-terminal foot region (Figure 5.26). However, overlaying the WT and EX22 shapes revealed an increased mass in the area assigned to the hinge and bridge regions of the EX22 structure, consistent with the expected placement of the additional 29 residues comprising domain 22. This conformational change around the EX22 bridge region also resulted in a slight spatial deviation of the C-terminus.

The WT and EX22 structures were separately fitted together in a head-to-tail model to simulate the assembly of tropoelastin monomers during elastogenesis (Figure 5.27). This approach highlighted potential differences in the self-assembly of the WT and EX22 constructs. The buried surface area between contacting EX22 molecules, calculated to be 6693.754 $Å^2$, was substantially greater than the 1743.191 $Å^2$ calculated between a WT pair. In addition, the helical structure produced by the assembled EX22 molecules displayed a different periodicity to the WT model. Three EX22 monomers, but only two WT monomers, were required per full turn of the helix.

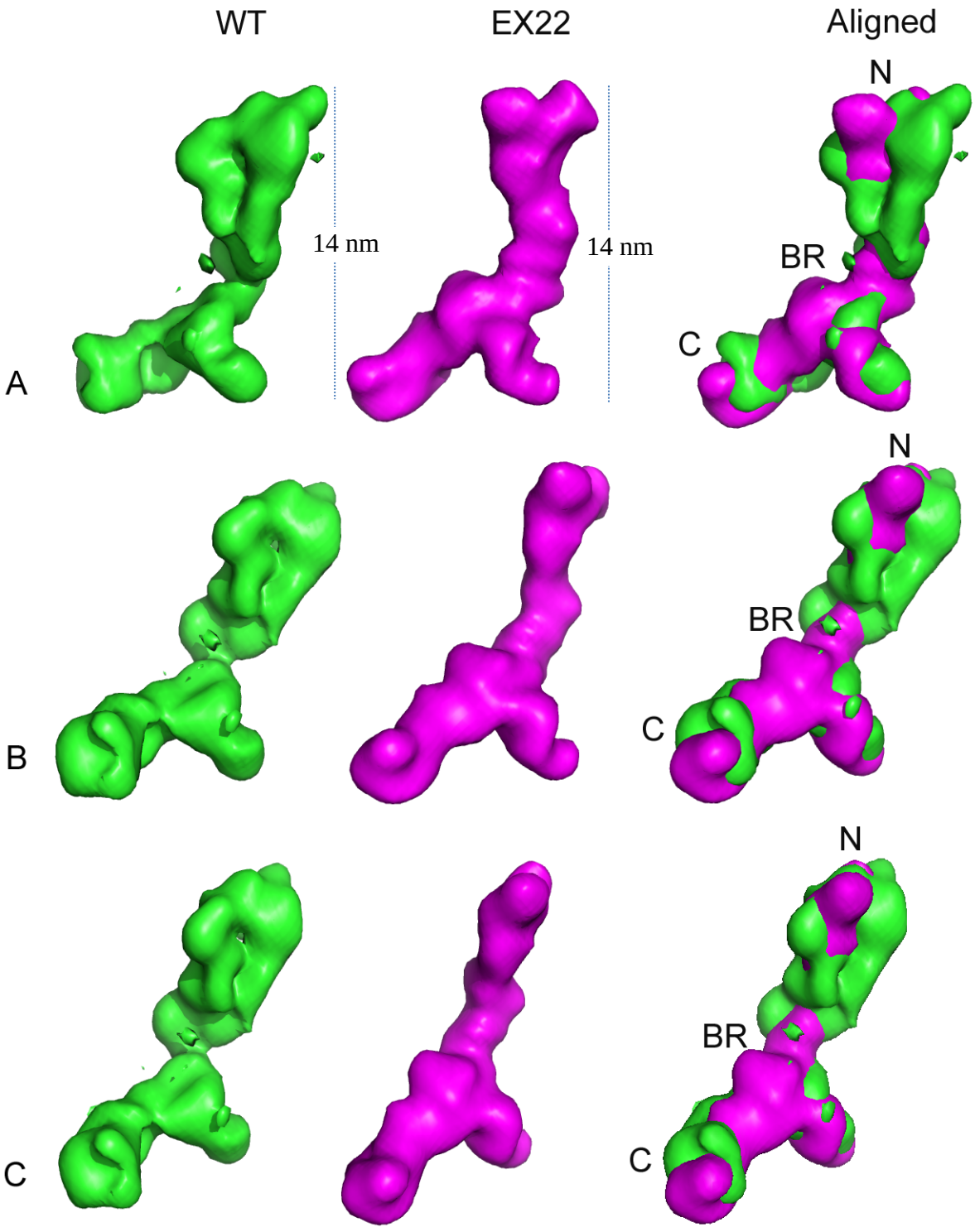

Figure 5.26. Solution structures of WT and EX22 tropoelastin obtained from SAXS studies. Panels show the WT (green), EX22 (magenta) and merged structures rotated laterally. The tropoelastin N-terminus (N), bridge region (BR) and C-terminus (C) are indicated.

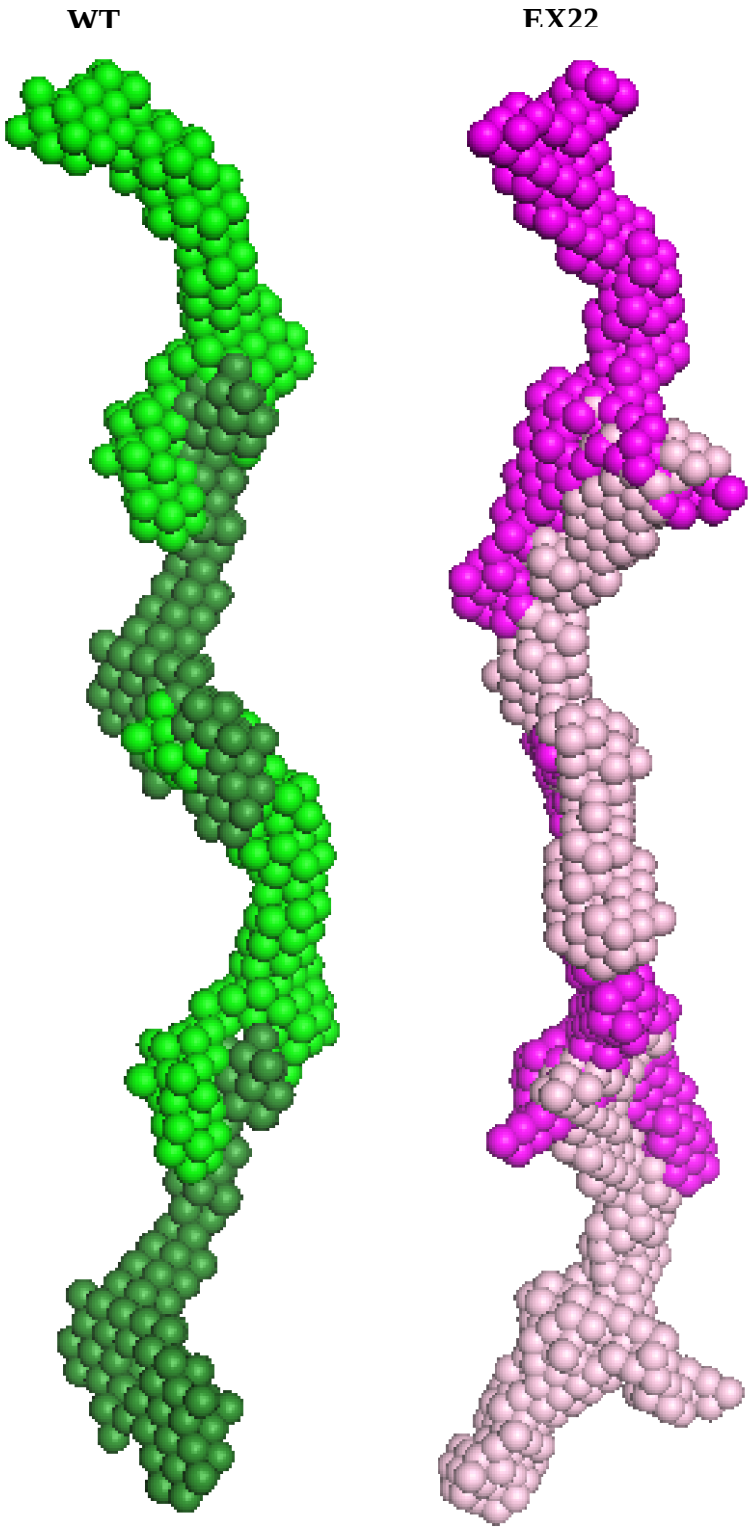

Figure 5.27. Model showing the head-to-tail tandem assembly of WT (green) and EX22 (magenta) molecules. WT and EX22 monomers were not drawn to scale.

5.3 Discussion

5.3.1 Analysis of splicing signals

The lack of exon 22 in mature human tropoelastin transcripts [33], despite its presence in the tropoelastin gene [183], indicates that the sequence is likely removed during pre-mRNA processing. Exon 22 has been identified as one of the six tropoelastin exons subject to alternative splicing [31, 314].

Splicing typically occurs via a series of spliceosome-catalysed reactions at specific sequences within the intron separating the two exons [335]. These sequences include a donor site at the 5′ end of the intron, an acceptor site at the 3′ end, and a branch point up to 50 bases upstream of the acceptor site. Analysis of the potential splice sequences associated with exons 21-23 of human tropoelastin revealed a high similarity of all donor splice sites to the consensus sequence, which strongly suggests that exon 22 skipping is not due to a weak 5′ splice site. This is not surprising, given that the site may also regulate the splicing of exon 23 to exon 21. However, the acceptor splice site and branch point sequences of exon 22 have lower consensus values compared to exons 21 and 23. Disruptions to these motifs are known to decrease splicing efficiency [334, 336, 337] and increase the usage of alternative sites [338]. In particular, mutations to the branch site can allow the formation of lariats that encompass an exon and lead to its exclusion from the final transcript [334]. Similarly, exon 22 skipping may result from inferior spliceosomal recognition of the acceptor splice and branch sites due to their increased divergence from consensus sequences. In such cases, alternative sequences, i.e. those of exon 23, are utilised instead.

Moreover, the distance of the branch point from the 3′ splice site is greater in exon 22 (62 bp) compared to that in exon 21 (28 bp) or exon 23 (24 bp). Branch points are optimally located 16-25 bp from the acceptor splice site, with those situated further upstream

often associated with skipped exons [334]. A distal branch point relative to the acceptor splice site may also have contributed to the poor splicing of exon 22.

Since the tropoelastin exon 22 does not appear to be expressed in humans, there may be no impetus for its preservation in the tropoelastin gene. Similar to the circumstances leading to the deletion of exon 35 from the human tropoelastin sequence [312], the loss of constitutive splice signals for exon 22 may likewise herald its eventual loss from the genome.

5.3.2 Production of EX22 tropoelastin

Expression of the native human exon 22 in *E. coli* may be hindered by differences in the codon usage pattern of the two organisms. For this reason, a strategy was adopted following the design of the synthetic wild-type human elastin gene [26], in which the exon 22 sequence of the EX22 gene was backtranslated from domain 22 of human tropoelastin using codons optimised for high-level expression in *E. coli*. This avoids the occurrence of 'rare' codons which can reduce protein yield and lead to aberrant constructs [339]. However, the resulting sequence was extremely biased towards codons that represented the most frequently occurring for each amino acid in *E. coli* genes. The sequence was therefore refined by utilising all highly-used codons for the two most repeated residues in domain 22, glycine and alanine.

The synthetic exon 22 sequence was incorporated into the wild-type tropoelastin gene to give rise to the EX22 gene construct. DNA sequencing of plasmids from transformed colonies confirmed the correct placement of exon 22 between exons 21 and 23. The expressed protein was subsequently confirmed by comparative mass spectrometry against WT to possess a mass spectrum consistent with the presence of domain 22. SDS-PAGE analysis further indicated that the EX22 tropoelastin was pure and full-length.

5.3.3 Coacervation studies

As the first essential stage of elastogenesis [101, 187], the coacervation of tropoelastin species directly determines their ability to assemble into elastic fibres. Following previous studies on recombinant human tropoelastin [153, 275], the coacervation of WT and EX22 was modelled *in vitro* under extracellular salt and pH conditions, in which sample turbidity was directly correlated to the extent of self-association [340].

WT and EX22 possessed similar temperature-dependent coacervation profiles. Both samples exhibited rapid aggregation over a narrow temperature range (30-35°C), similar to previous observations on the coacervation of various tropoelastin isoforms [70, 108, 275] and consistent with the entropic nature of the process [4]. Maximum coacervation was reached by both constructs at physiological temperatures. This critical temperature is reproducible for a given tropoelastin or elastin-like polypeptide [131], as it reflects the energy required to disrupt the clathrate water shielding hydrophobic domains from self-interactions [62, 97, 185, 341]. As such, coacervation temperature is greatly dependent on the number [186] and contextual arrangement [62, 108, 342] of hydrophobic domains in tropoelastin. Interestingly, the presence of a hydrophobic domain 22 in EX22 did not affect its coacervation temperature. This may be interpreted as a lack of significant change in overall protein hydration, due to a minimal increase in protein hydropathy, or to conformational changes eclipsing the potential hydration effects of the additional hydrophobic domain. The latter scenario may feasibly arise from the placement of domain 22 within the tropoelastin hinge, as disruptions to this region have been associated with local changes in secondary structure [74].

Analysis of the particle sizes in the tropoelastin solutions confirmed the similar coacervation behaviour of WT and EX22. Both constructs existed in the ~10 nm monomer form at 30 °C and below, but sharply transited into the ~1 μm coacervate phase at 35°C and

remained as similar sized aggregates until 55°C. These results were identical to the pattern of temperature-dependent turbidity increase previously observed during light spectrophotometry of WT and EX22 solutions. The rapid shift from monomer to polymer was consistent with coacervation being driven mainly by hydrophobic associations [11, 101]. Furthermore, the establishment of a stable end size for the WT and EX22 assemblies indicates a cessation of tropoelastin aggregation, which is thought to be regulated by the organisation of monomers at the coacervate surface [115]. From these results, there appears to be no mechanistic differences between WT and EX22 coacervation.

While the thermodynamic requirements for WT and EX22 coacervation are similar, temperature-dependent kinetic differences were observed. EX22 coacervated more rapidly than WT below 45 °C, although the coacervation time of both constructs decreased and converged at higher temperatures. The rate of coacervation relates to the cooperativity of interactions among hydrophobic regions [70]. Addition of the hydrophobic domain 22 may have contributed to a higher coacervation rate of EX22 by increasing potential hydrophobic contacts or altering the relative positions of existing contacts to favour self-association. In particular, the insertion of domain 22 may interrupt the native conformation of the hinge region formed by the adjoining hydrophilic domains 21 and 23. Studies on elastin-like polypeptides focused on this region have found that disruptions to the central turn between domains 21 and 23 can affect the dynamics of proximal hydrophobic domains and promote coacervation [74, 325].

The ability of EX22 to coacervate comparably to WT in an *in vitro* environment represents an intrinsic property of tropoelastin that is not abolished or hampered by the inclusion of domain 22. This is not surprising, since domain 22 is expressed in the tropoelastin of non-human mammals such as cows and rats [33, 39]. The evolutionary reasons for the exclusion of domain 22 in human tropoelastin may be more apparent in a

heterogeneous cellular environment, where a number of matrix components are known to interact with tropoelastin monomers to facilitate and regulate their assembly into higher order structures [125, 127, 128, 276]. These proteins and proteoglycans, including fibrillins, fibulins and matrix-associated glycoproteins, can affect the rate, but not temperature, of tropoelastin coacervation [131]. The level of control afforded by matrix proteins is suited to subtler differences in coacervation properties, such as those observed between WT and EX22.

5.3.4 Cross-linking studies

Tropoelastin crosslinking, mediated by lysyl oxidase enzymes *in vivo* [136, 137], occurs between specific lysine residues [143, 282] to form intra- and intermolecular linkages that give rise to mature and insoluble elastic fibres. Cross-linking of WT and EX22 was modelled *in vitro* with BS3, an amine-reactive homobifunctional cross-linker [343] targeted to lysine residues at most 11.4 Å apart [290]. Addition of a six-fold molar excess of BS3 allowed complete incorporation of both WT and EX22 into the hydrogel material, indicating that the inclusion of domain 22 in human tropoelastin does not inhibit the formation of cross-links. This was also expected given the functionality of non-human tropoelastin isoforms in which domain 22 is present.

Despite the similar propensity of WT and EX22 constructs for BS3 cross-linking, micro-CT imaging of the resulting hydrogels revealed remarkable differences in their structural composition (Fig 4). The WT hydrogel comprised of interwoven fibres interspersed with large pores that spanned the surface and cross-section of the sample. This morphology is consistent with the filamentous nature of natural elastin [8, 13, 14] and similar to previous descriptions of synthetic elastin hydrogels [20]. In contrast, the EX22 hydrogel appeared as a dense material with no visible channels. This was quantifiably reflected in the decreased porosity calculated for the EX22 hydrogel compared to the WT. Hydrogel porosity is defined by the separation kinetics of the initially homogenous system into polymer and aqueous phases, followed by the removal of the latter phase [291]. While hydrogel porosity can be influenced by mechanical techniques [344] or the addition of extrinsic components that increase viscosity [345, 346], variations in phase separation in a two-component system of BS3 and tropoelastin alone are most likely due to differences in the cross-linking process.

The compositional dissimilarities between the WT and EX22 hydrogels may account for their functional differences. Elastin hydrogels characteristically swell in an aqueous environment [190, 295, 345], as demonstrated by the ability of WT and EX22 hydrogels to support the intake of water multiple fold their dry weight. However, in accordance with their reduced porosity, EX22 hydrogels consistently swelled significantly less than WT hydrogels. Hydrogel swelling is dictated by interactions between the polymer and the solvent. Solvent influx extends the network junctions of the hydrogel and constrains the flexible hydrophobic segments within rigid cross-linked regions [188]. This is balanced by the entropic increase associated with the mixing of solvent and hydration water within the polymer [189]. The extent of hydrogel swelling is conventionally thought to be inversely related to cross-link density [188, 190, 191]. This suggests that EX22 hydrogels may have more extensive cross-links than the WT material.

Scanning electron microscopy confirmed distinct structural differences in the WT and EX22 hydrogel surfaces. The WT hydrogel showed a highly porous and fibrous network top surface that appeared to have coalesced into a sheet-like layer on the bottom surface. This is similar to previous findings [20, 296, 347], demonstrating the structural consistency of synthetic elastin hydrogel constructs. In contrast, the EX22 hydrogel, except for several short fibrous structures on the top surface, was mainly composed of a compact sheet on both top and bottom surfaces. The edges of the WT and EX22 hydrogels clearly demonstrated these compositional differences. A large open network of fibres was visible across the full thickness of the WT hydrogel, while compressed sheet-like layers comprised the EX22 hydrogel. These results strongly suggest a difference in the organisation of EX22 molecules during cross-linking into higher-order structures.

The compositional differences between the cross-linked WT and EX22 material reflect the morphological differences in the native elastic fibres produced by species that

differentially express domain 22 in tropoelastin. Like the highly porous nature of WT hydrogels, human dermal elastic fibres are long and branched. In contrast, sheep, rabbit and other mammalian skin have elastic fibres that are thick with only very fine radiating fibrils [327] that appear to simulate the compactness of EX22 hydrogels.

The effect of domain 22 inclusion on tropoelastin cross-linking may arise from differences in the arrangement of EX22 molecules during coacervation. Since cross-link formation relies greatly on the proximity of specific lysine residues that are aligned during tropoelastin self-association [44, 60, 67, 100, 119], slight variations in the coacervate structure can affect the number or nature of cross-links. In addition, the placement of domain 22 within the cross-link enriched domains 19-25 [143, 282] increases the probability of altering the relative positions of lysine residues important in native cross-linking. The hinge region, in particular, is thought to adopt open and closed conformations that determine the formation of intra-molecular and intermolecular contacts, respectively [178]. Disrupting the tropoelastin hinge region, a possible consequence of domain 22 inclusion, is associated with an increased local structure [74], which may then impact upon the distribution of cross-links within the tropoelastin monomer and between contacting molecules. These differences in cross-linking are manifested by the formation of EX22 hydrogels that are structurally and functionally dissimilar to the WT elastin polymer.

5.3.5 Cell and antibody interactions

Cells interact with tropoelastin throughout the elastogenic process, from the coacervation of monomers on cell surface receptors [3] to the instigation of cellular responses as a component of the extracellular matrix [348]. WT and EX22 tropoelastin coated on cell culture wells supported the adhesion of human dermal fibroblasts in a saturable manner [45, 179], and to the same extent. At coating concentrations allowing maximum cell attachment, up to 80% of seeded cells adhered to both species. Fibroblasts are known to bind via the $\alpha_v\beta_3$ integrin to the tropoelastin C-terminus [18, 83, 297], primarily the terminal RKRK residues [179]. The equivalent level of fibroblast attachment on WT and EX22 suggests comparable accessibility of fibroblast binding site/s on the C-terminal region of both constructs.

To perceive conformational changes within the tropoelastin molecule caused by the addition of domain 22, surface-bound WT and EX22 were probed using antibodies targeted against specific tropoelastin domains. The antibody against tropoelastin domain 6 detected equivalent levels of the epitope on both WT and EX22, indicating similar exposure of the N-terminal segment of both constructs. However, the BA4 antibody, which predominantly recognizes the hydrophobic hexapeptide VGVAPG in tropoelastin domain 24 [298], showed decreased binding to EX22 than to WT. This suggests a reduced exposure of the central hinge/bridge region of EX22, which coincides with the expected location of domain 22, and is likely due to a conformational change in this region.

Interestingly, the hydrophobic sequences recognised by the BA4 antibody have been shown to be ligands of the elastin binding protein (EBP) [299]. This implies that EX22 tropoelastin may also show decreased binding to EBP. EBP has been proposed to facilitate the intracellular transport of tropoelastin to specific cell-surface sites [349]. Additionally, as part of the elastin receptor complex, it can mediate a number of cellular responses including

chemotaxis [350, 351], adhesion [352], proliferation [353], and vasodilation [354]. Decreased interactions with either EBP or the elastin receptor may therefore lead to an inefficient transit through the secretory pathway [299] and reduced biological activity.

In addition, the antibody against the tropoelastin C-terminus also detected fewer epitopes in EX22 than WT. This implies a partially inaccessible C-terminus in EX22 that may have been displaced or obscured by an upstream conformational change. While this was initially unexpected given the similar extent of fibroblast attachment to both constructs, fibroblasts and the anti-domain 36 antibody may recognise different sequence motifs within the C-terminus. Moreover, fibroblasts may bind to secondary sites independent of the RKRK sequence in domain 36 (Lee *et al*., in preparation). The reduced exposure of specific C-terminal sites in EX22 may affect its ability to form elastic fibres, as this highly-conserved region [183] has been implicated in contacting microfibrillar proteins crucial for tropoelastin incorporation into elastic fibres [276, 355, 356]. Other studies have also demonstrated that certain structural changes to the C-terminus do not affect fibroblast $\alpha_v\beta_3$ integrin binding [297] but can affect tropoelastin assembly [356].

5.3.6 Elastic fibre assembly

To determine the elastogenic potential of the WT and EX22 tropoelastin, purified constructs were added to cultured human cells with an established microfibrillar network, as this acts as an essential scaffold for elastin deposition [94, 249]. Elastic fibres were formed by dermal fibroblasts even from low concentrations of exogenous WT tropoelastin, while EX22 species remained as spherules and only assembled into elastic fibres at high concentrations within the extracellular environment. The stark contrast between the elastogenic capacity of WT and EX22 was not reflective of their relative functionality in previous tropoelastin-focused assays. This suggests some selectivity against the non-native EX22 isoform on a cellular level, similar in principle to the observed bias against the incorporation of a cutis laxa-associated tropoelastin mutant into vascular elastic fibres [33]. The decreased efficiency of EX22 fibre assembly was only partially compensated by an excess of added monomers, as evidenced by the early lag in the EX22 elastogenic time course and the formation of significantly fewer fibres than WT. Furthermore, the diffused, weakly-stained nature of EX22 fibres, in contrast to the continuous, highly-fluorescent WT fibres, suggests an irregular distribution of the mutant species on microfibrils [33] plausibly due to aberrant interactions with microfibrillar proteins and/or differential packing of monomers within the elastic fibre. However, the autofluorescence of EX22 fibres was similar to that of WT fibres. Since elastin autofluorescence has been attributed to its cross-linked structure [257, 258], this implies that EX22 and WT fibres undergo a similar extent of maturation over time.

The elastogenic capability of EX22 was tested in another model system using human retinal pigmented epithelial cells, a cell line that naturally expresses the major elastogenic components except tropoelastin [140]. At low and high concentrations of supplied tropoelastin, WT established an elastic fibre network similar to that described in the

fibroblast environment. In contrast to fibroblasts, EX22 fibres were formed even at low concentrations by ARPE-19 cells. This demonstrates a tissue-specific tolerance for EX22 that is higher in ARPE-19 cells compared to GM3348 fibroblasts. Interestingly, the dermal elastic fibres of mammals which produce tropoelastin with domain 22 are proposed to originate from hair follicular cells, which have an epithelial lineage similar to ARPE-19 cells [326, 329]. In contrast, dermal elastic fibres of humans are known to be derived from fibroblastic cells [328]. This may account for the differential fibre assembly of EX22 in the GM3348 and ARPE-19 cellular environments.

EX22 fibres, while present in ARPE-19 cells, were significantly fewer in number, confirming a decreased efficiency of EX22 incorporation into the elastic matrix. The reduced immunofluorescence and autofluorescence of EX22 elastic fibres likewise suggest a non-native organisation of monomers within the assembled fibre, and/or impaired interactions with elastogenic proteins including cross-linking enzymes within the ARPE-19 environment. The increased average width of EX22 fibres further confirms the propensity of EX22 to form morphologically different elastic fibres, consistent with reports that sequence polymorphisms in tropoelastin can alter the architecture of resulting elastic fibres [55]. The thicker EX22 fibres reflect a characteristic of skin elastic fibres in mammals which express tropoelastin with domain 22 [326]. This morphology is most likely linked to the primary function of such elastic fibres for movement, in contrast to that of hair placement or the maintenance of skin integrity in humans [326].

The presence of domain 22 in human tropoelastin severely impacts upon its elastogenic ability, perhaps due to slight structural changes within the monomer that affect the arrangement of assembled molecules and their interaction with extracellular matrix components essential for fibre formation. This leads to a fibre morphology that deviates from the wild-type, and which, accordingly, may be functionally inferior [55].

5.3.7 Structural analysis

The far-UV CD spectra of WT and EX22 tropoelastin showed characteristic features, including a large negative peak at 200 nm associated with the disordered nature of hydrophobic domains, and a minor negative peak at 220 nm associated with the limited alpha-helical structure of cross-linking domains [117, 274]. Calculation of the secondary structure composition from the WT and EX22 CD spectra using a number of algorithms [173] consistently indicated no difference between the constructs. In tropoelastin species containing domain 22, this hydrophobic region is predicted to form a coil structure [44]. Previous studies on an elastin mimetic focused on domains 20-21-23-24 indicated that disrupting the hinge between domains 21 and 23 significantly changes the alpha-helical content of the peptide [73, 325]. While the addition of domain 22 in tropoelastin may disturb the hinge region, the local changes in secondary structure may not be detected as changes in the overall percentage of coil or alpha-helical structures in the EX22 molecule.

The solution structure of human tropoelastin consists of an elastic coil region spanning the N-terminus to domain 18, continuing to the hinge region in domains 21/23, then a bridge region around domain 25-26, which connects to the C-terminal foot region [72]. SAXS analysis of WT and EX22 produced nanostructures that possess these characteristic features. However, the EX22 structure exhibited an increased mass in the hinge and bridge regions corresponding to the expected location of domain 22. The conformational change around the EX22 bridge region was also associated with a slight protrusion of the C-terminus, consistent with the role of the tropoelastin bridge in orienting the C-terminal region [184]. The structural changes around the central and C-terminal domains supported the previously described differential exposure of antibody epitopes in these areas.

The domain 21/23 hinge in tropoelastin represents a highly flexible region, which can adopt a range of conformations wherein the flanking helical segments are either looped or extended [73]. In a hydrated environment, the hinge is thought to fluctuate between closed and open states until converging via van der Waals interactions to a hairpin structure that is stabilised by a salt bridge. The proposed motions of the hinge region may contribute to the broad conformational distribution of the tropoelastin molecule [322-324], which plays an important role in biological elasticity [28]. Sequence alterations to the hinge have been shown to introduce steric constraints that interfere with its native configuration [322] and increase the rigidity of the structure [325]. Consequently, the addition of domain 22 in the EX22 hinge region may likewise decrease the number of conformations accessible to the molecule.

While the conformational changes in EX22 were not linked to any discernible difference in the overall secondary structure composition of the WT and EX22 constructs, local conformational differences were modeled by replica exchange molecular dynamics, an accelerated structure prediction algorithm (Tarakanova, A. and Buehler, M., pers. comm.). The WT hinge displayed a high presence of helices, while the EX22 hinge had a high beta sheet content with significantly reduced helical content (Figure 5.28). Coil and turn composition did not vary significantly between the constructs. Representative structures of the EX22 construct displayed a high propensity for double beta strand formation between amorphous domains, which may be essential in stabilising the hinge region. A reduced flexibility of the hinge supports the observed limited exposure of the central and C-terminal regions in EX22.

A

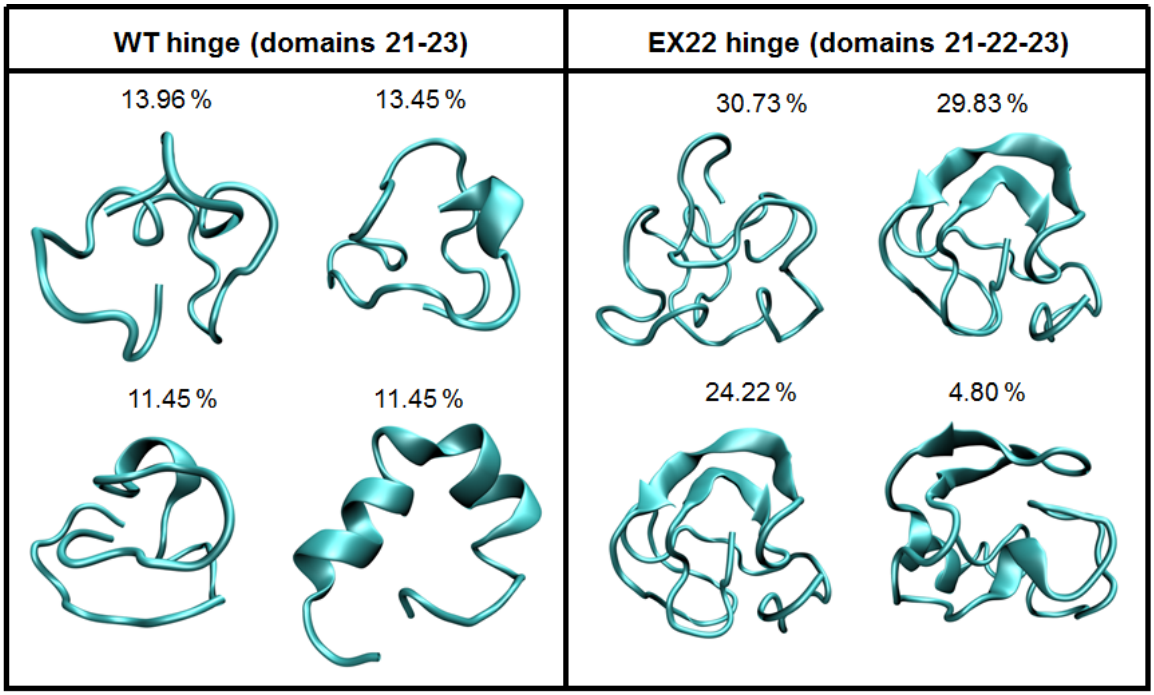

B

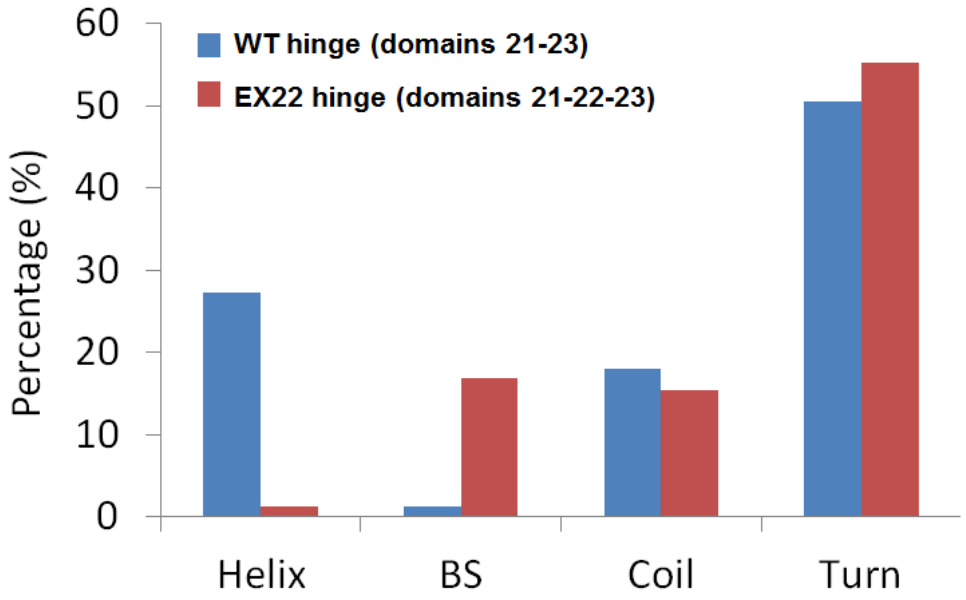

Figure 5.28. (A) Representative structures of WT and EX22 hinge region. Percentages indicate significance of cluster from which the lowest energy representative conformation is extracted. (B) Secondary structure content [helix, beta strand (BS), coil, turn] compared for molecular models of the hinge regions of WT and EX22 constructs.

Possible consequences of the altered EX22 structure were manifested by modelling monomer assembly according to the proposed head-to-tail mechanism of elastin microfibre formation [72]. In this model, domains 19 and 25 bracketing the hinge region of one molecule were juxtaposed with the N-terminal domain 10 from a second molecule to allow the formation of a well-defined cross-link [105]. WT and EX22 molecules fitted to this model produced different coil structures, in which the buried surface area between two EX22 monomers was greater than that between a WT pair. This indicates potential variations in intermolecular contacts between WT and EX22 monomers during elastin assembly. These properties may account for the differences in WT and EX22 tropoelastin incorporation during elastogenesis, as well as the organisation of molecules within the elastic fibre structure.

This chapter helps to shed light on the evolutionary impetus behind the exclusion of domain 22 in human tropoelastin, by demonstrating that the inclusion of domain 22 greatly impacts upon the native assembly of tropoelastin into higher order structures, including hydrogels in cross-linking assays, or elastic fibres in model cellular environments. These properties may be attributed to conformational changes affecting the hinge, bridge and C-terminal regions of tropoelastin, which potentially translate into differences in intermolecular interactions and supramolecular structure during assembly. These results support a strong functional advantage for the maintenance of the native hinge structure in human tropoelastin, as inserting domain 22 markedly disrupts the hinge and reduces the efficiency of tropoelastin to assemble into an abundant elastic fiber system such as that found in the human dermis.

6. Characterisation of the D72A tropoelastin construct

6.1 Introduction

6.1.1 The tropoelastin N-terminal region

The solution structure of human tropoelastin comprises a distinct narrow (2-3 nm), elongated segment that persists for ~11 nm before branching into the bridge and foot regions [72]. Structural comparison of the full-length species with constructs truncated at various distances from the N-terminus allowed the assignment of this linear section to the tropoelastin N-terminal region encompassing domains 2-18. This spring-like coil region is proposed to account for tropoelastin elasticity, which is characterised by the ability of the single molecule to reversibly extend to 8 times its resting length [72]. The N-terminal region displays the typical structural motif of the tropoelastin molecule comprising of alternating hydrophobic and hydrophilic domains [357]. Mechanistically, the elasticity of tropoelastin molecules arises from the substantial entropy associated with the flexibility of hydrophobic domains in the relaxed state [77, 78]. Extending the monomer increases order by restricting the range of accessible conformations [358]. Furthermore, the increased solvent exposure of hydrophobic regions induces local ordering of water molecules and contributes to a decrease in entropy. The spontaneous recoil manifested by tropoelastin after release of the stretching force is driven by the return to a more favourable disordered state [76].

Previous studies on the functional significance of specific tropoelastin domains in elastogenesis have primarily implicated the central and C-terminal regions in the coacervation, microfibrillar deposition and cross-linking stages of elastic fibre assembly [44, 70, 122, 143, 276]. However, the N-terminal region may also play important but less well-characterised roles in elastin assembly. For instance, it likely contributes to the overall structure of the coacervate, as evidenced by the conformational transition from beta-strand to alpha-helix displayed by the isolated domain 2-7 peptide upon an increase in ambient

hydropathy between different solvents [357]. The N-terminal segment may also facilitate tropoelastin integration into the microfibrillar scaffold. While fibrillin-1, the most abundant microfibrillar protein, binds multiple sites within tropoelastin, its primary point of contact is localised within the N-terminal domain 4 of tropoelastin [135]. Several N-terminal domains may also participate in cross-linking. Studies have observed the presence of at least three intra-molecular lysinonorleucine links in the region spanning domains 6-15, including contacts between domains 6 and 8, domains 12 and 13, and domains 14 and 15 [282]. Intermolecular cross-links may likewise exist between the N-terminal region of one monomer and the central or C-terminal regions of another. In particular, interactions are proposed to occur between domains 6 and 36, domains 8 and 23, domains 12 and 21/23, domains 13 and 19, domains 13 and 23, and domains 15 and 23 [143, 282]. A major cross-linking site in elastin is formed through the association of domains 10, 19 and 25, in which the domain 10 sequence of one tropoelastin strand bridges the desmosine-linked domains 19 and 25 of a second molecule via two lysinonorleucine links [105]. The importance of the tropoelastin N-terminal region in elastogenesis is supported by the association of a P211S mutation in domain 12 with an autosomal recessive cutis laxa phenotype [35] that is characterised by deficient dermal elastic fibres [359, 360].

6.1.2 The N-terminal D72 site

A number of assembly and structural properties of tropoelastin are modulated by charged residues within the molecule. The attachment of secreted tropoelastin monomers on the cell surface is predominantly mediated by the basic C-terminal RKRK cluster [83, 179]. The efficiency of coacervation may be regulated via the neutralisation of repulsive lysine charges by negatively-charged groups in cell-surface GAGs [93]. These transient interactions can also promote the formation of alpha-helical secondary structure which crucially positions lysines in close proximity for cross-linking [58, 67]. Tropoelastin deposition onto microfibrils is likewise proposed to be facilitated by electrostatic interactions with microfibril-associated glycoproteins [45, 50, 102, 276]. Cross-linking reactions that stabilise the nascent elastic fibre directly involve the positively-charged lysine residues within tropoelastin [137, 139]. Charged residues may also be involved in maintaining the tertiary structure of the protein, as demonstrated by the conformational changes exhibited by tropoelastin constructs with mutations at the R515, E345 and E414 sites.

In contrast to the more recognised roles of the positively-charged residues in tropoelastin function, little has been described of the rarely occurring negatively-charged residues. The significance of two of three such residues located in the central hinge and bridge regions has been explored in a previous chapter. The third negatively-charged residue in tropoelastin is an aspartate (D72) in the hydrophilic KA-rich cross-linking domain 6 of the N-terminal region. This region within the tropoelastin gene may have undergone remodelling events during evolution, as demonstrated by the relative sequence divergence [183]. Such circumstances are rare in the hydrophilic domains, which are typically conserved to maintain the primary and spatial structure required for cross-linking, unlike hydrophobic regions which generally tolerate mutations if overall hydrophobicity is

preserved [183]. The human tropoelastin domain 6 is also susceptible to degradation by matrix metalloproteinases (MMP) such as MMP-7, MMP-9 and MMP-12 [361-363]. This supports the solvent exposure of the region and its accessibility to potential interactions with other tropoelastin monomers and extracellular matrix proteins during assembly, which may be mediated by the negatively-charged D72 site.

6.1.3 Aims

This chapter investigates the significance of the D72 residue to tropoelastin structure and function. A tropoelastin construct with an alanine substitution at the D72 site (D72A) (Figure 6.1) was produced and assayed for its propensity for coacervation, cross-linking, cell interaction, and elastic fibre assembly in comparison to the wild-type isoform (WT). The solution structures of WT and D72A were compared to identify variations in monomer conformation that may account for differences in assembly properties. These results may help indicate the evolutionary benefits gained by the presence of a negatively-charged D72 site in the N-terminal region of human tropoelastin, and further our understanding of the role of this under-characterised region in tropoelastin function.

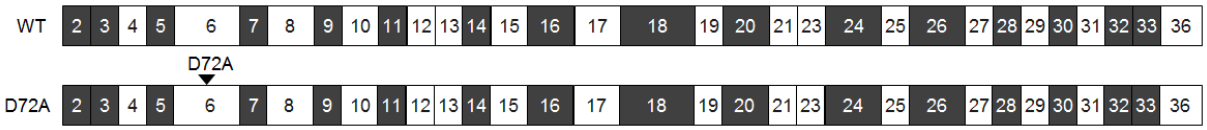

Figure 6.1. Domain structures of WT and D72A tropoelastin. Hydrophobic and hydrophilic domains are represented by grey and white boxes, respectively.

6.2 Results

6.2.1 Conservation of D72 in mammalian tropoelastin sequences

Alignment of domains 2-6 of mammalian tropoelastin sequences indicated the common presence of an N-terminal negatively-charged site in the majority of the sequences (Figure 6.2). The D72 site itself is conserved in human, chimpanzee, baboon and pig tropoelastin. Although both cat and cow tropoelastin do not possess the D72 residue, a negatively-charged glutamate lies upstream of this site within the same domain. The rodent sequences do not contain a negatively-charged residue in the N-terminal region.

In the tropoelastin sequences that maintain a glutamate or aspartate in domain 6, preservation of such a site appears to have occurred despite greater sequence deviation within this domain compared to neighbouring regions.

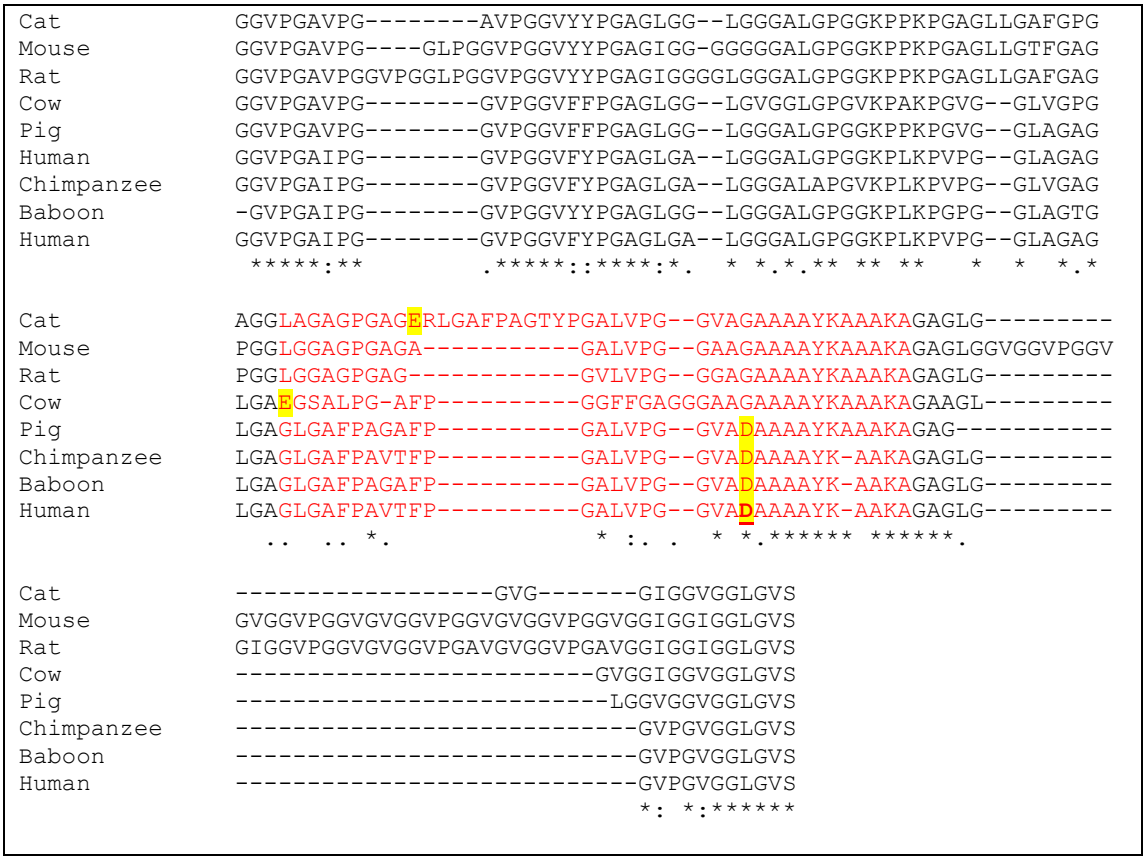

Figure 6.2. Alignment of domains 2-7 of mammalian tropoelastin sequences using ClustalW. Identical residues are denoted by "*", conserved residues by ":", and semi-conserved residues by ".". The degree of conservation was based on the similarity score of all residues at each position, calculated using the Gonnet Pam250 matrix (conserved: score >0.5, semi-conserved: score =<0.5) [286]. Domain 6 is in red font. Negatively-charged residues are highlighted in yellow. The human tropoelastin D72 residue is bold underlined. The human (GeneID: 2006), cow (GeneID: 280781), mouse (GeneID: 13717), and rat (GeneID: 25043) tropoelastin sequences are confirmed protein sequences. The cat (NCBI: XM_003998576.1), pig (Gene Index: TC373476), chimpanzee (NCBI: XM_003318598.2), and baboon (NCBI: XM_003919412.1) sequences are translated from predicted elastin gene sequences.

6.2.2 Production and confirmation of D72A tropoelastin

6.2.2.1 DNA sequencing

Plasmid DNA extracted from transformed *E. coli* colonies was sequenced to confirm the presence of the D72A mutation in the tropoelastin gene. The resulting sequence indicated an alanine-encoding GCA codon at the position encoding residue 72 of tropoelastin, confirming the mutation at the DNA level (Appendix 8.7).

6.2.2.2 Mass spectrometry

Comparative mass spectrometry of purified WT and D72A tropoelastin that had been digested with Lys-C showed two peaks within the 5000-6800 m/z window common to both species (Figure 6.3). These 5076.8 and 5711.0 m/z peaks, labelled A and B respectively, were assigned to peptide fragments that lie outside the mutated region (Table 6.1). However, the 6713.6 m/z peak labelled C was present only in the WT spectrum, while the 6669.7 m/z peak labelled C* was present only in the D72A spectrum. Both peaks corresponded to the same peptide encompassing residues 1-78 of tropoelastin, with the mass shift between the peaks coinciding with the mass difference between an aspartate and an alanine residue. These results were consistent with a D72A mutation in the mutant tropoelastin construct at the protein level.

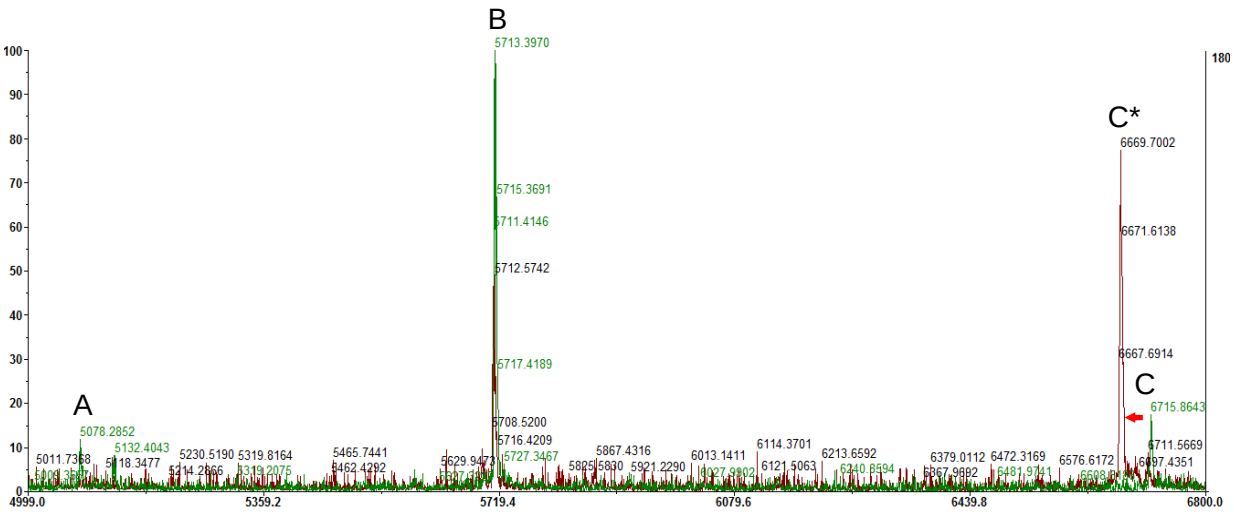

Figure 6.3. Comparative mass spectrometry of WT (green) and D72A (red) tropoelastin showing the peaks within the 5000-6800 m/z window.

Table 6.1. Assignment of mass spectrometry peaks of WT and D72A tropoelastin observed within the 5000-6800 m/z window. Residue 72 is underlined.

Peak	Mass	Residues	Sequence
A	5076.8	290-349	YGAAAGLVPGGPGFGPGVVGVPGAGVPGVGVPGAGIPVV PGAGIPGAAVPGVVSPEAAAK
B	5711.0	357-422	YGARPGVGVGGIPTYGVGAGGFPGFGVGVGGIPGVAGVP SVGGVPGVGGVPGVGISPEAQAAAAAK
C*	6669.7	1-78	GGVPGAIPGGVPGGVFYPGAGLGALGGGALGPGGKPLKP VPGGLAGAGLGAGLGAFPAVTFPGALVPGGVAAAAAAYK
C	6713.6	1-78	GGVPGAIPGGVPGGVFYPGAGLGALGGGALGPGGKPLKP VPGGLAGAGLGAGLGAFPAVTFPGALVPGGVADAAAAYK

6.2.2.3 SDS-PAGE

SDS-PAGE analysis of purified WT and D72A tropoelastin indicated bands corresponding to constructs of the expected size (~60 kDa) (Figure 6.4). Moreover, the samples were full-length, non-degraded, and free from protein contaminants from the bacterial expression and purification process.

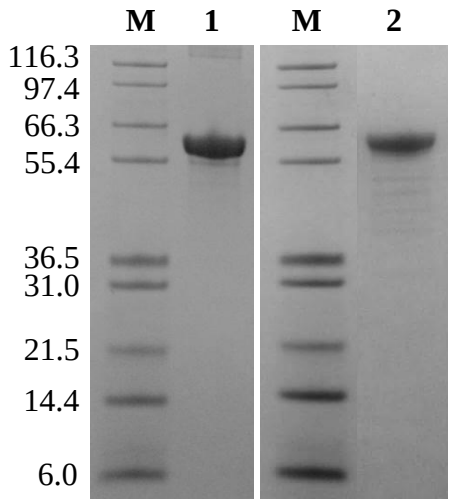

Figure 6.4. SDS-PAGE of purified WT and D72A tropoelastin. Lanes: M – protein standards in kDa; 1 – WT; 2 – D72A.

6.2.3 Coacervation studies

6.2.3.1 Light spectrophotometry

Solutions of WT and D72A tropoelastin were analysed spectrophotometrically to determine light absorbance, which was used as a measure of the extent of coacervation. WT tropoelastin achieved full coacervation at 35°C, beyond which no further increase in sample turbidity was observed (Figure 6.5A). In contrast, the D72A mutant displayed only partial aggregation at 35°C, and attained maximum coacervation at a higher temperature of 40°C. Both tropoelastin species also differed in the time taken to coacervate at each temperature, particularly within the physiologically relevant temperature range of 35-40°C (Figure 6.5B). At these temperatures, D72A coacervated substantially more slowly than WT. Differences between the coacervation times of the constructs decreased with increasing temperatures.

6.2.3.2 Particle size analysis

To confirm differences in the coacervation behaviour of WT and D72A, the particle sizes of the tropoelastin solutions were assessed over a temperature range via dynamic light scattering (Figure 6.6). At 20-25°C, both WT and D72A species were in the 10-15 nm monomer form. At 30°C, 43% of WT tropoelastin had aggregated while all D72A species remained as monomers. At 35°C, all of WT but only 76% of D72A constructs had assembled into coacervates. At 40°C, all of the D72A species had fully coacervated, but the diameter of the mutant assemblies (~0.5 μm) is significantly smaller that of the WT (~2.3 μm). This difference between the WT and D72A coacervate sizes was observed even at higher temperatures up to 55°C.

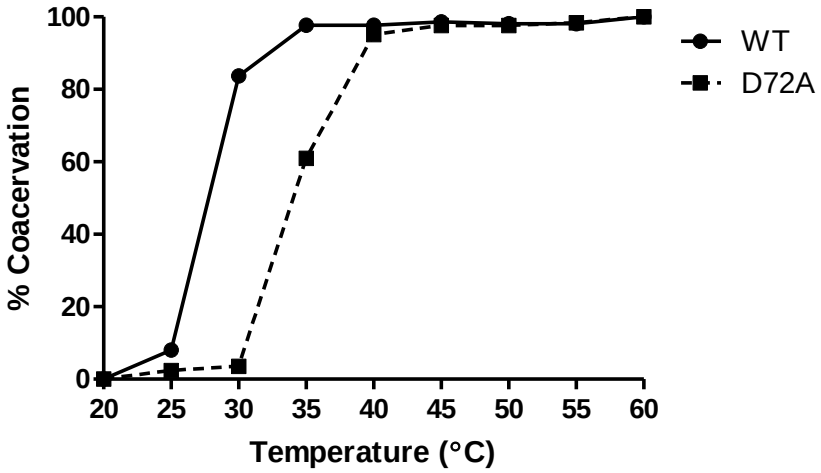

A

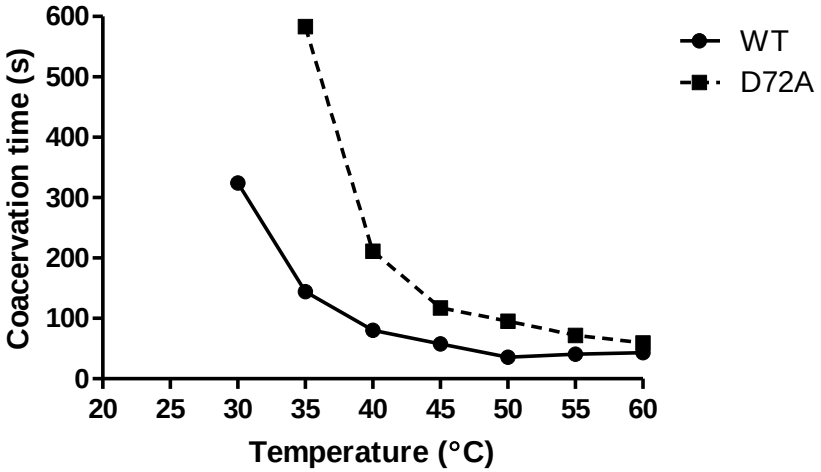

B

Figure 6.5. Coacervation profiles of WT and D72A tropoelastin. (A) The extent of coacervation at each temperature indicated by relative sample turbidity. (B) The time required to achieve maximum coacervation at each temperature.

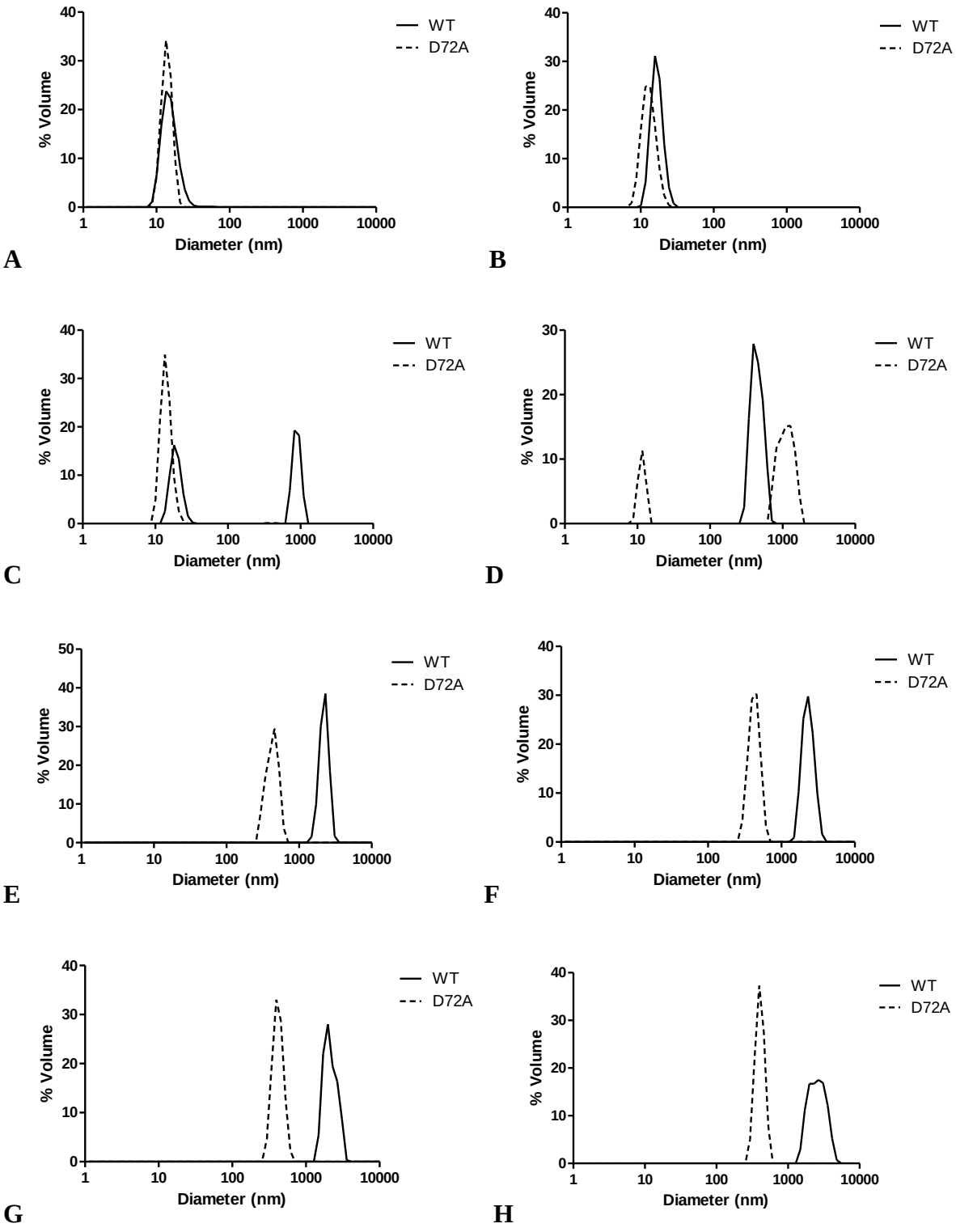

Figure 6.6. Particle sizes of WT and D72A tropoelastin solutions at (A) 20, (B) 25, (C) 30, (D) 35, (E) 40, (F) 45, (G) 50 and (H) 55°C.

6.2.4 Cross-linking studies

6.2.4.1 Hydrogel construction

WT and D72A tropoelastin cross-linked with 10 mM BS3 for 16 hrs produced hydrogels as illustrated in Figure 6.7. All WT and D72A species polymerised under these conditions, as evidenced by the absence of tropoelastin monomers in the aqueous solution left after hydrogel formation (Figure 6.8).

6.2.4.2 Micro-CT of hydrogels

Micro-CT reconstruction of the WT and D72A hydrogels indicated distinct structural differences between the constructs (Figure 6.9). The D72A hydrogel was composed of discrete thin layers of material which were stacked to form an overall dense and compact structure. This morphology contrasted greatly with the open fibrous network that spanned the entire thickness of the WT hydrogel. Analysis of the x-ray projection slices across the z-axis of the hydrogels confirmed visual observations that the WT material had a significantly higher porosity at 90.2 ± 0.6% than the D72A material at 59.4 ± 1.3% (Figure 6.10).

6.2.4.3 Hydrogel swelling

The WT and D72A hydrogels also exhibited differences in swelling behaviour. When submerged in water for 24hrs, the mutant hydrogels visibly expanded less than the WT constructs (Figure 6.11). Consistent with this smaller volume increase, the amount of water absorption by D72A hydrogels was 58-62% less than that by WT hydrogels. This significant decrease in swelling by mutant hydrogels was observed consistently at three different temperatures.

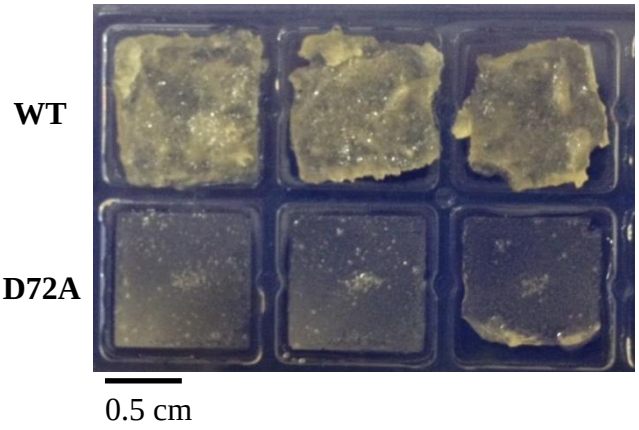

Figure 6.7. Hydrogels constructed from cross-linking of WT and D72A tropoelastin with 10 mM BS3 for 16 hr at 37°C.

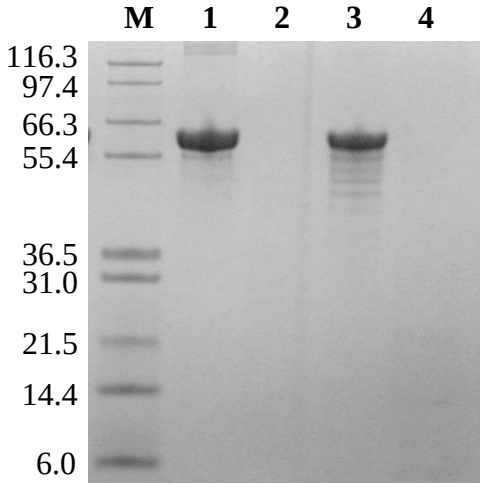

Figure 6.8. SDS-PAGE of the aqueous layer left after tropoelastin cross-linking with BS3 into hydrogels. Lanes: M – protein standards in kDa; 1 – WT; 2 – WT + 10 mM BS3; 3 – D72A; 4 – D72A + 10 mM BS3.

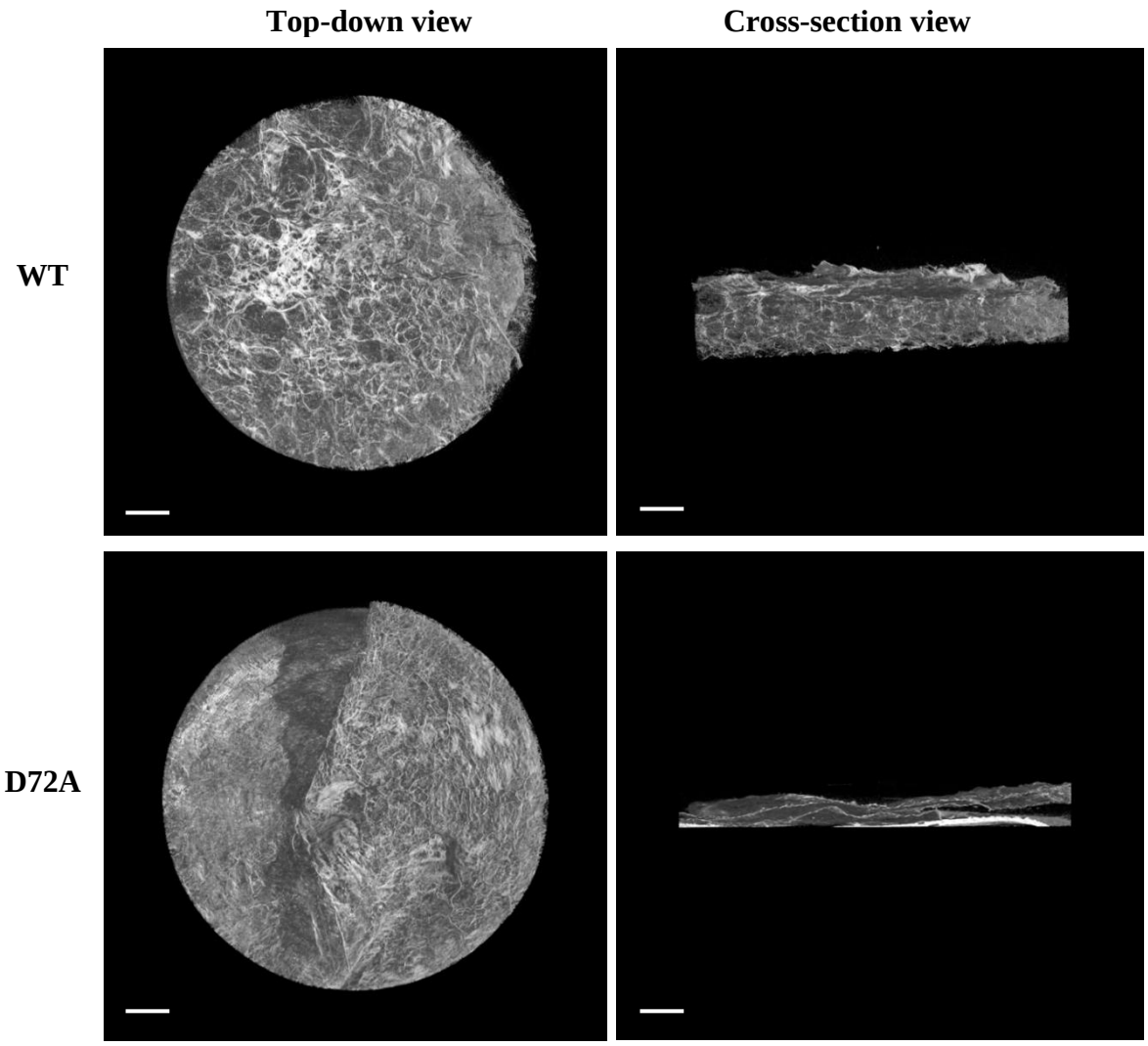

Figure 6.9. Micro-CT reconstruction of WT and D72A hydrogels. Scale bar: 0.5 mm.

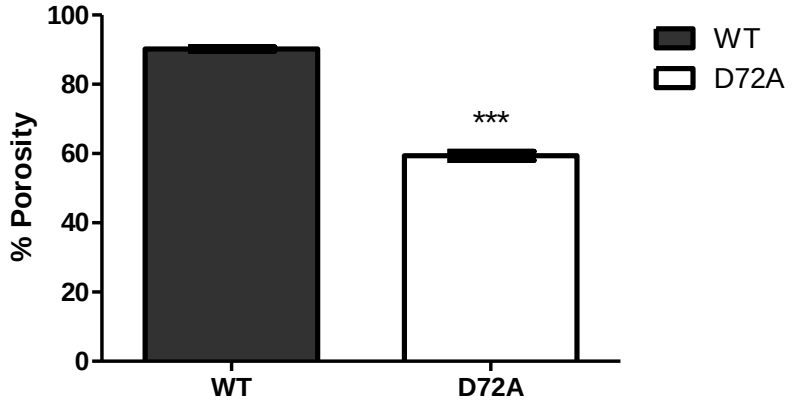

Figure 6.10. Porosity of WT and D72A hydrogels calculated from micro-CT cross-sectional images.

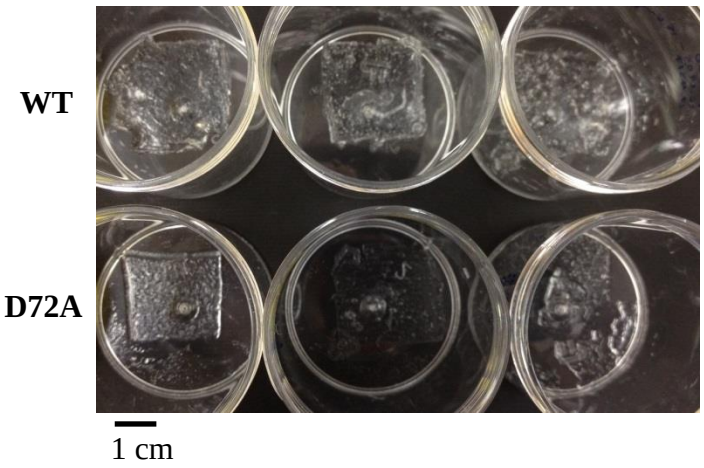

Figure 6.11. Representative image of WT and D72A hydrogels swollen in water for 24 hrs at 37°C. Triplicate samples are shown. Scale bar: 1 cm.

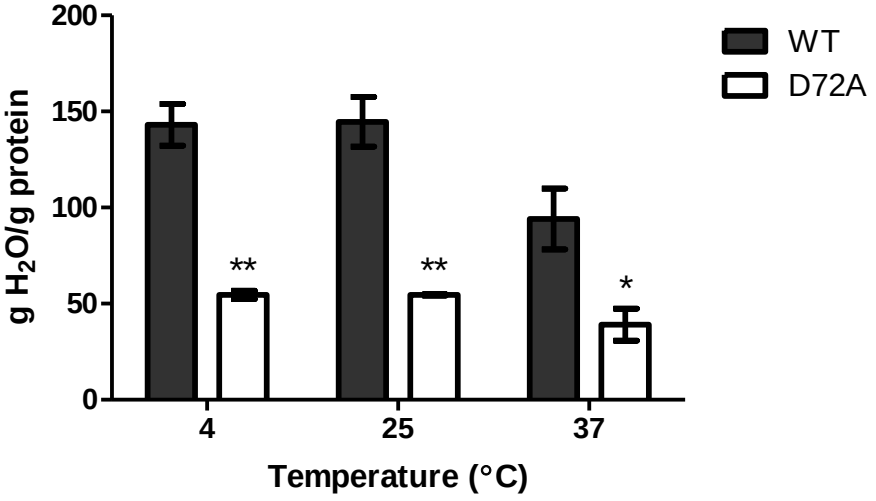

Figure 6.12. Swelling of WT and D72A hydrogels in water at 4, 25 and 37°C. The amount of water absorbed is expressed as a ratio to hydrogel mass.

6.2.4.4 SEM of hydrogels

SEM imaging of the hydrogels revealed differences between the surface structures of the WT and D72A constructs at high resolution. While the top surface of the WT hydrogel showed a highly porous, honeycomb-like network with open channels approximating 150-200 μm in diameter, the top surface of the D72A hydrogel comprised a solid sheet with fewer and smaller pores averaging 20-40 μm (Figure 6.13). Thin fibres were present on the D72A hydrogel surface, which appeared to be in the process of coalescing into the surface layer. The top surface of the D72A hydrogel reflected a similar morphology to the bottom surfaces of both WT and D72A cross-linked constructs, which were characterised by a smooth dense sheet with rarely-occurring pores ~20 μm in size (Figure 6.14).

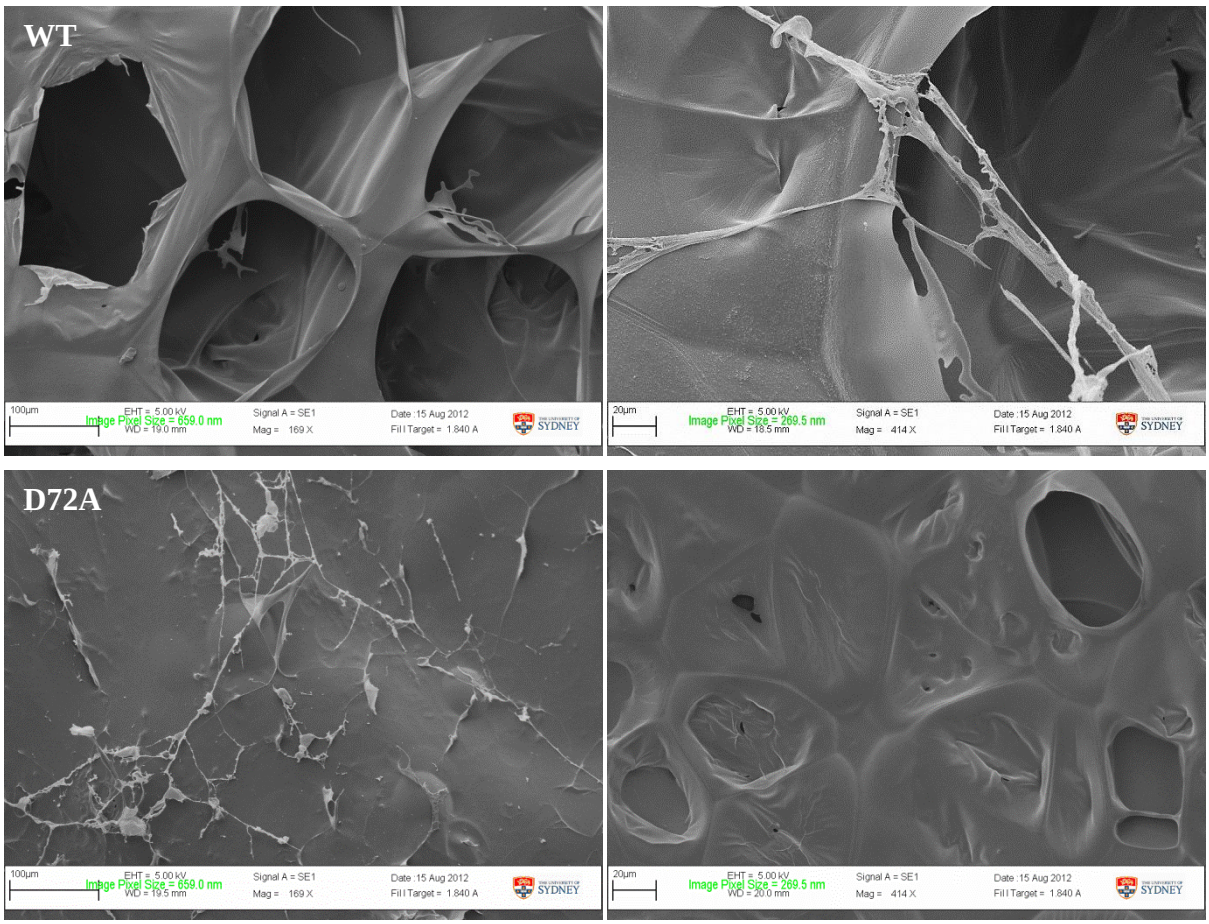

Figure 6.13. SEM images of the top surface of WT and D72A hydrogels under two magnifications.

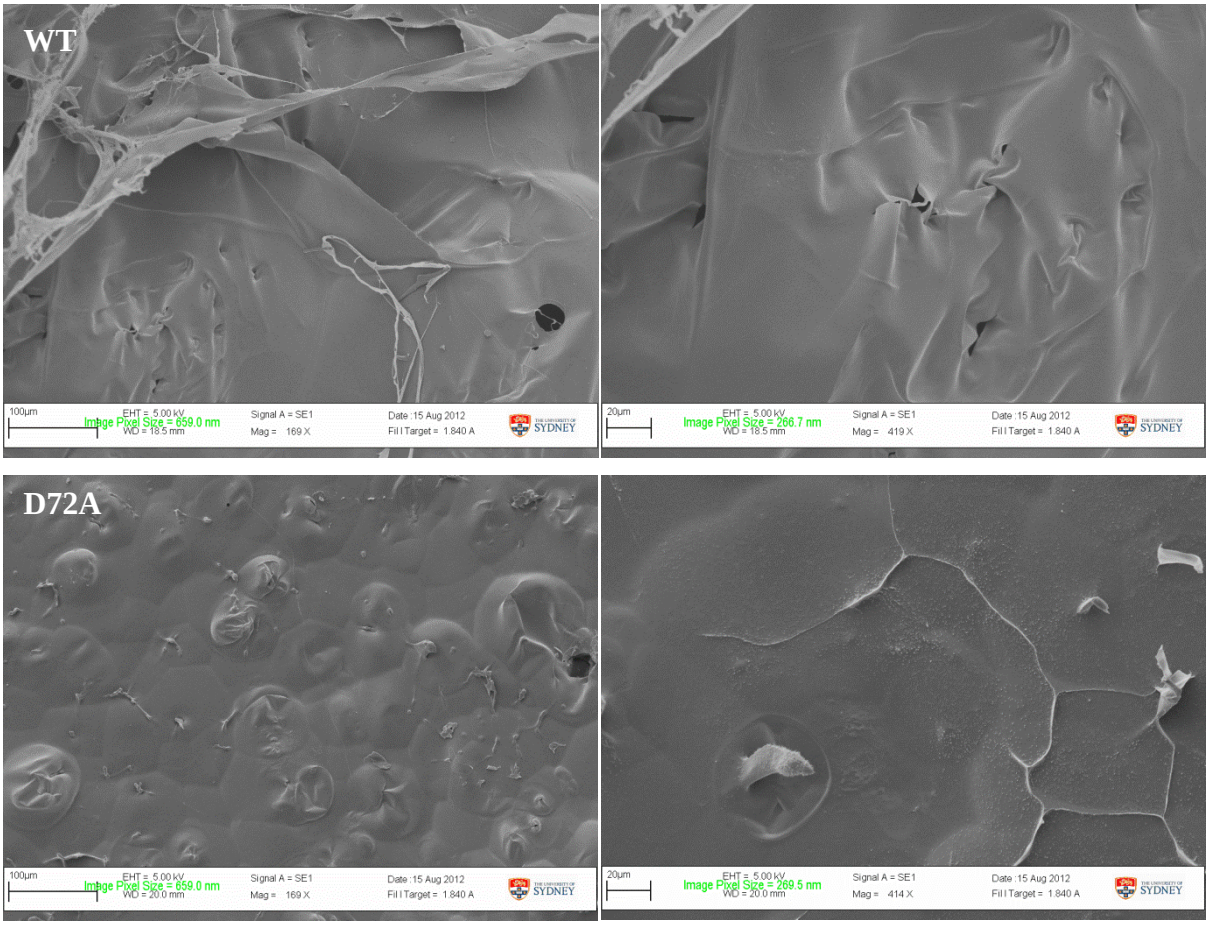

Figure 6.14. SEM images of the bottom surface of WT and D72A hydrogels under two magnifications.

6.2.5 Cell attachment

Both WT and D72A tropoelastin exhibited no significant difference in their ability to support the attachment of human dermal fibroblasts (Figure 6.15). Cell adhesion to WT- or D72A-coated tissue culture plastic increased dependently on tropoelastin concentration until a plateau at ~5 μg/mL. At saturation levels of tropoelastin coating, ~75% of seeded cells attached to WT and D72A.

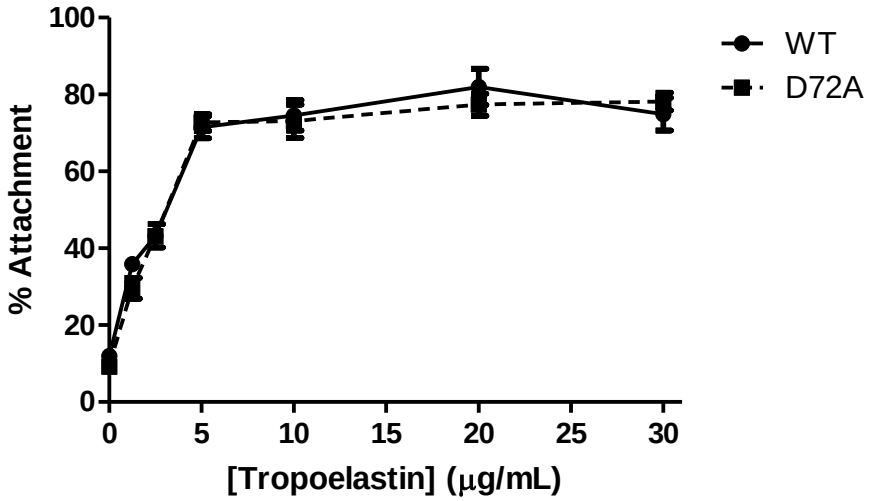

Figure 6.15. Attachment of GM3348 human dermal fibroblasts to WT and D72A tropoelastin.

6.2.6 Elastic fibre assembly

6.2.6.1 By GM3348 fibroblasts

WT and D72A tropoelastin showed markedly different capacities for elastic fibre formation when added to the culture medium of GM3348 human dermal fibroblasts (Figure 6.16). One day after tropoelastin addition, WT globules were clustered linearly as a precursor step to fibre development. In contrast, D72A particles assembled into few visible spherules, which were dispersed across the extracellular medium. The tropoelastin species excited at 488 and 559 nm were detected in the 515-545 nm channel due to FITC-conjugated immunostaining, as well as in the 563-610 nm channel due to autofluorescence. Four days after tropoelastin addition, a branched network of WT elastic fibres was visible, but no D72A spherules or fibres were present. The same trend was observed seven and ten days after tropoelastin addition. Control samples without exogenous tropoelastin showed no elastic fibre formation. Staining controls containing WT tropoelastin but with missing or non-specific antibodies showed faintly visible elastic fibres mainly due to elastin autofluorescence.

Day 1

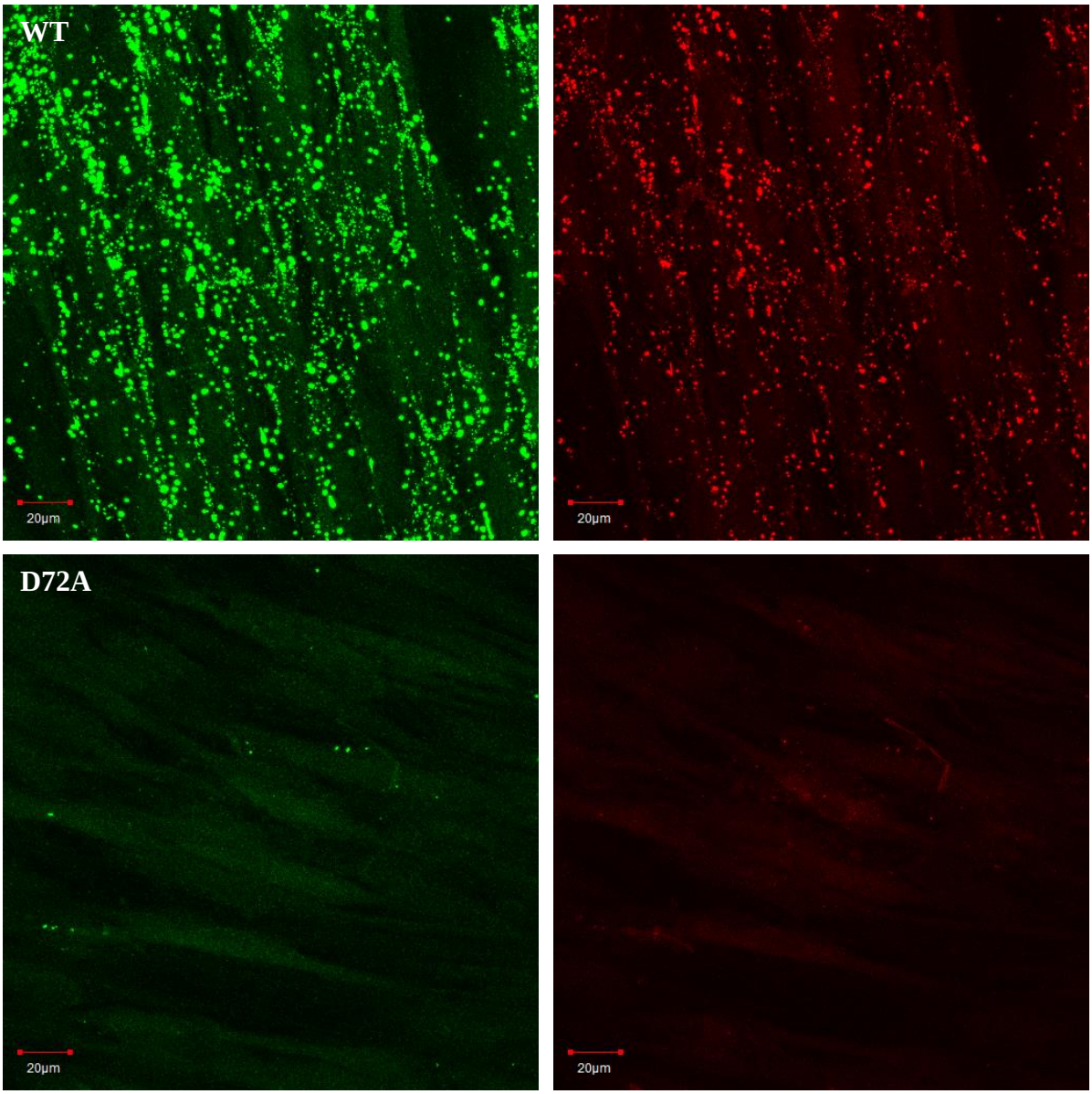

Day 4

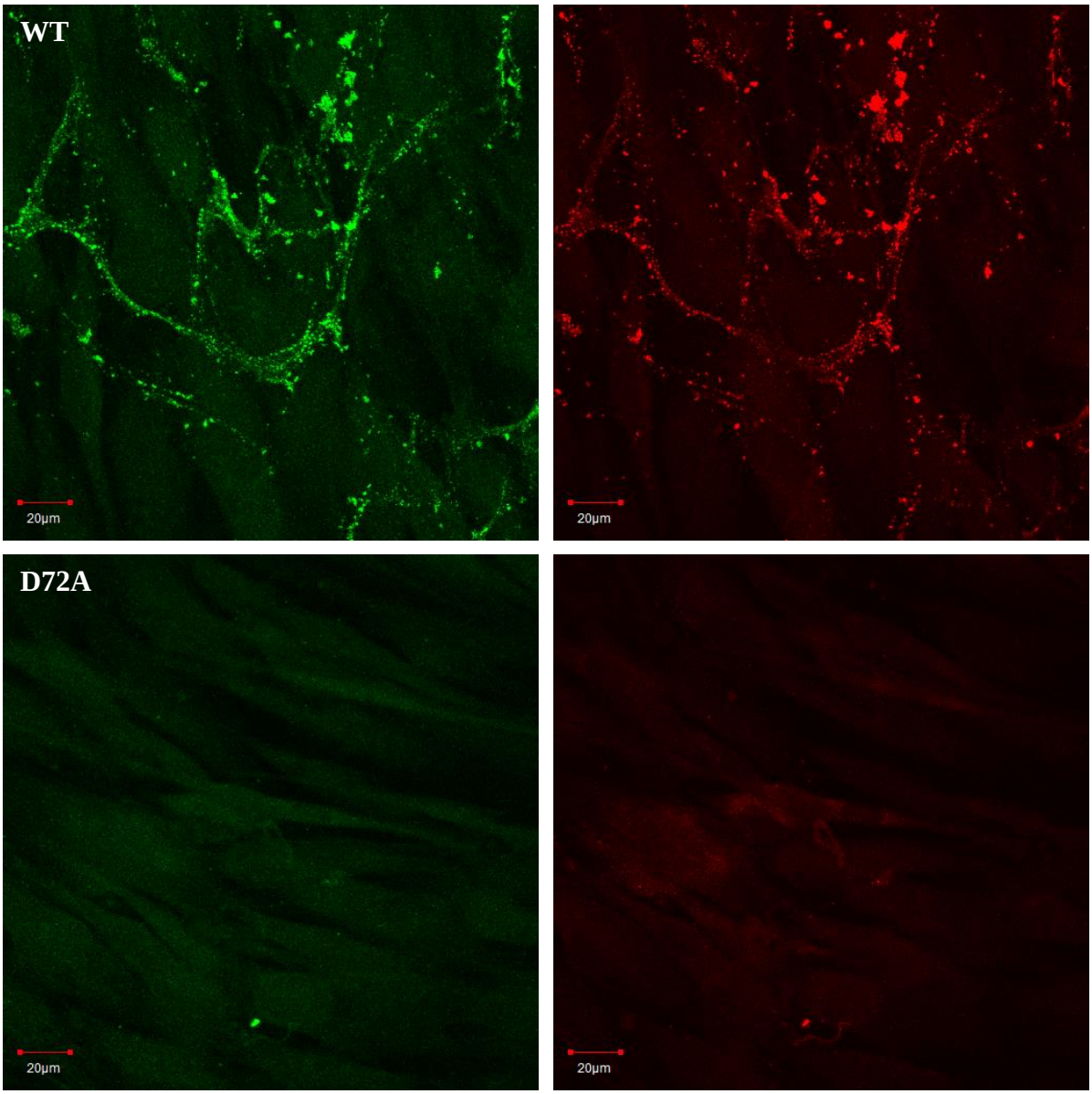

Day 7

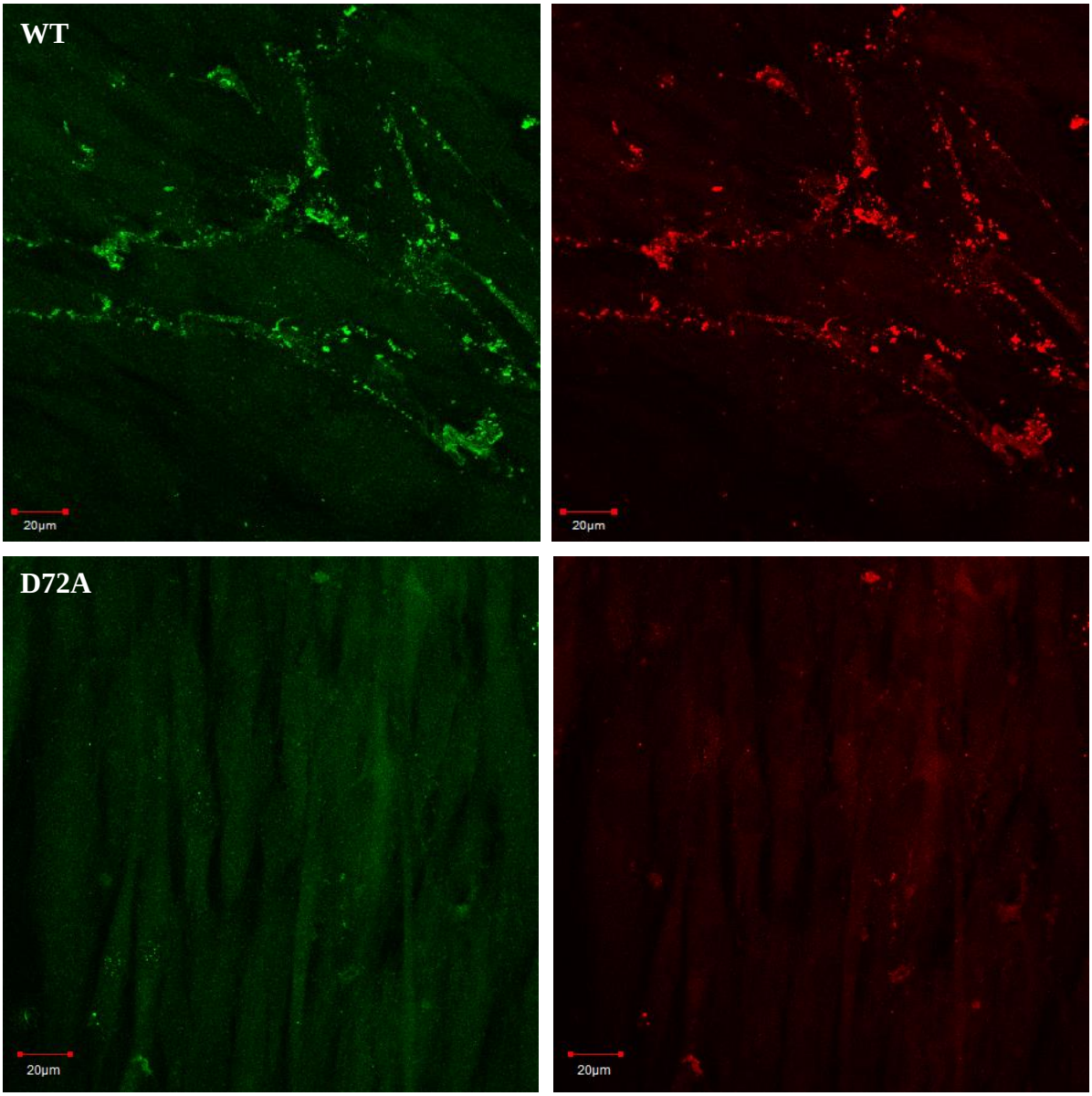

Day 10

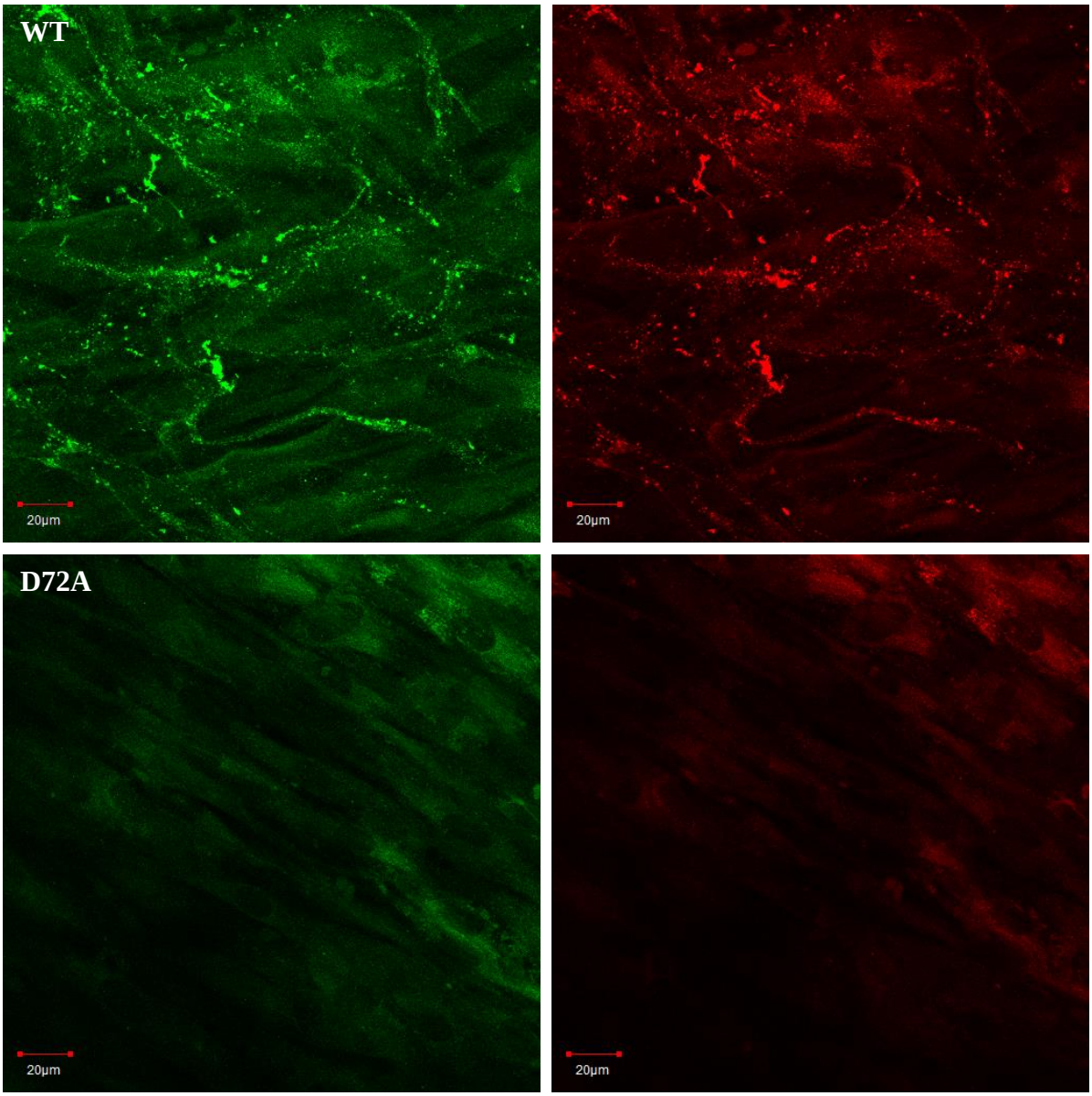

Controls

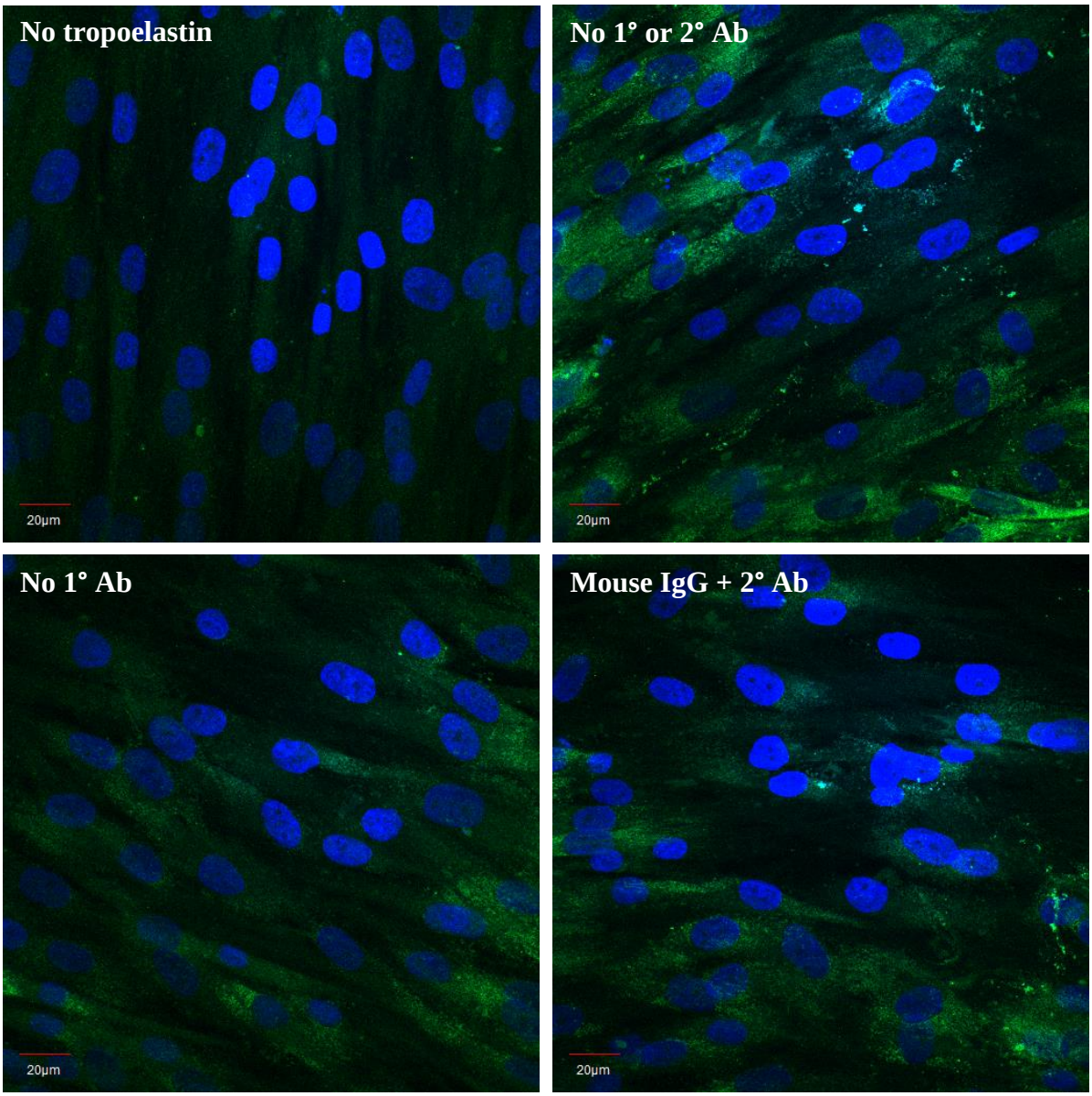

Figure 6.16. Confocal microscope images of elastic fibres formed from 20 µg/mL exogenous WT and D72A tropoelastin by GM3348 human dermal fibroblasts. Cells were fixed and stained 1, 4, 7 and 10 days after tropoelastin addition. The immunofluorescence and autofluorescence signals from each field of view are shown. Staining controls include cells with no added tropoelastin, and samples with added tropoelastin but no primary or secondary antibody, no primary antibody, and a non-specific primary mouse antibody with the anti-mouse secondary antibody. Staining

controls show merged fluorescence and autofluorescence signals as well as DAPI-stained cell nuclei.

6.2.6.2 By ARPE-19 cells

The elastogenic capability of WT and D72A tropoelastin was also assessed with ARPE-19 human retinal pigmented epithelial cells, a cell line that naturally expresses major extracellular matrix components but not tropoelastin (Figure 6.17). One day after the addition of WT and D72A tropoelastin to the culture medium, WT spherules were organised linearly while D72A spherules were more scattered throughout the extracellular space. Four days after tropoelastin addition, an expansive WT elastic fibre network had assembled. Several D72A elastic fibres were also visible, but they were significantly fewer in number and exhibited significantly decreased immunofluorescence and autofluorescence than WT fibres. The same pattern was maintained until seven and ten days after tropoelastin addition. D72A elastic fibres consistently stained 45-48% less intensely, displayed 41-47% reduced autofluorescence, and exhibited 57-71% decreased abundance compared to WT fibres (Figure 6.18). Cell numbers were comparable between WT and D72A samples at each time point. Control samples without exogenous tropoelastin showed no elastic fibre formation. Staining controls containing WT tropoelastin but with missing or non-specific antibodies showed faintly visible elastic fibres mainly due to elastin autofluorescence.

Day 1

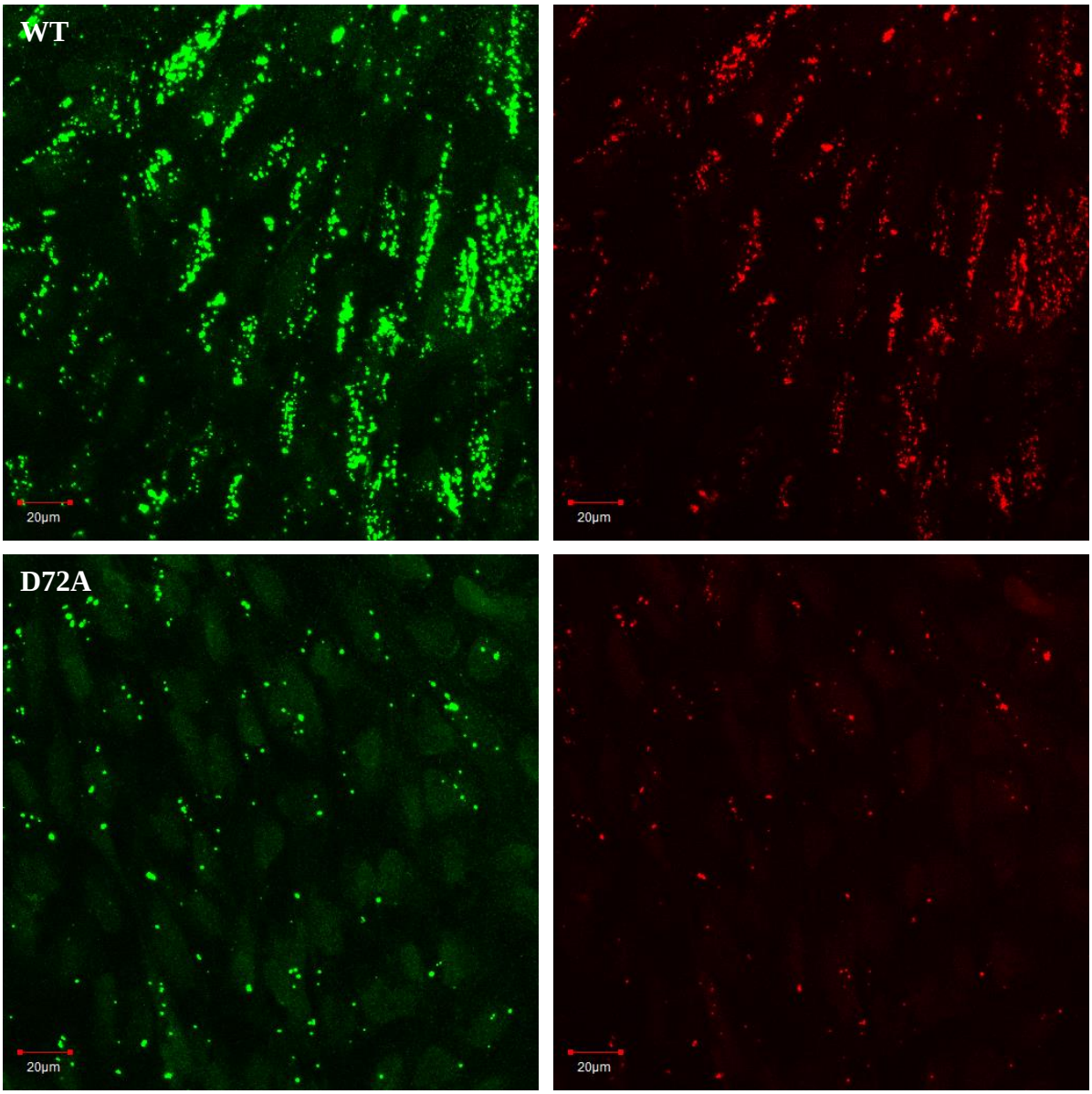

Day 4

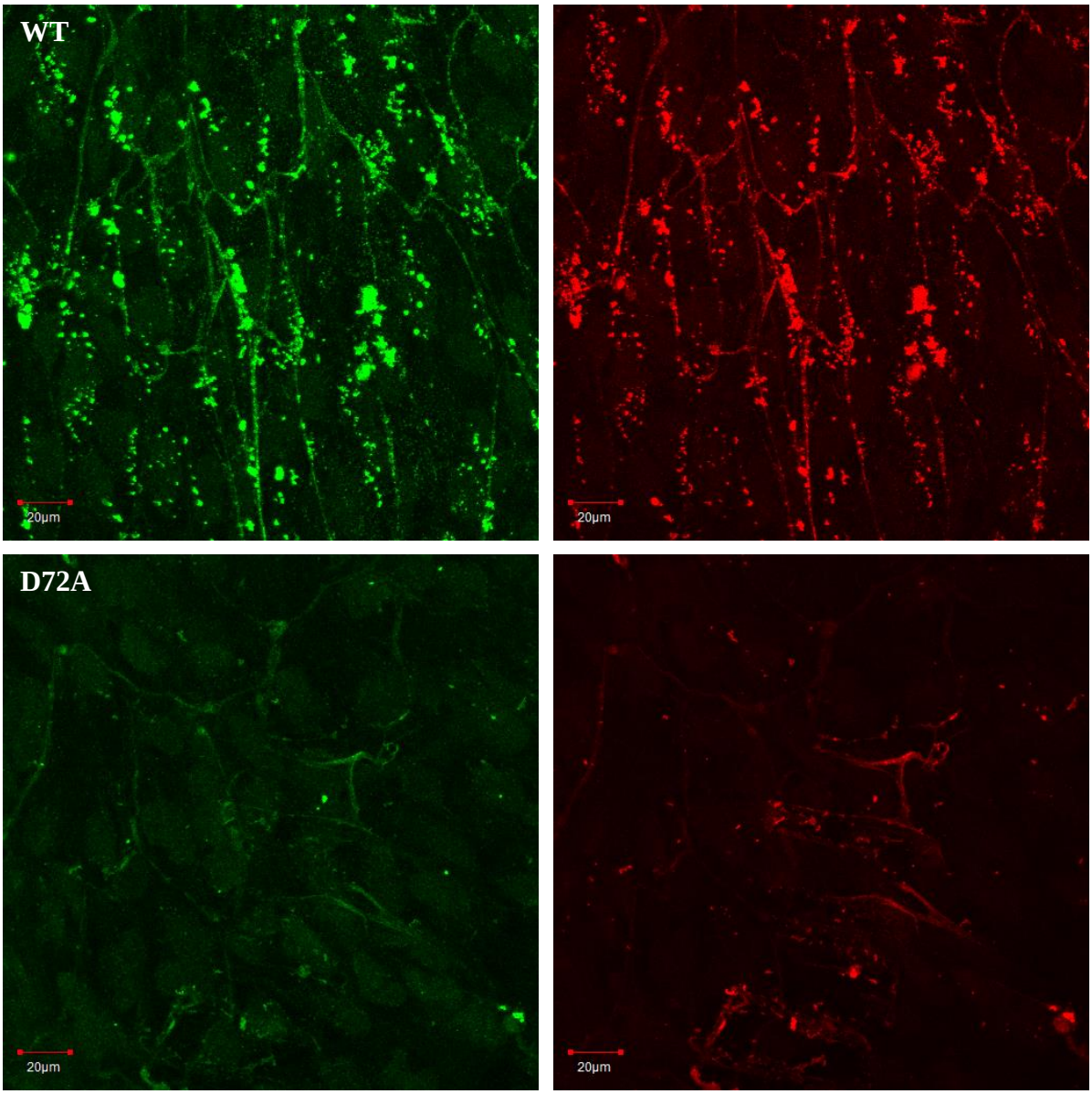

Day 7

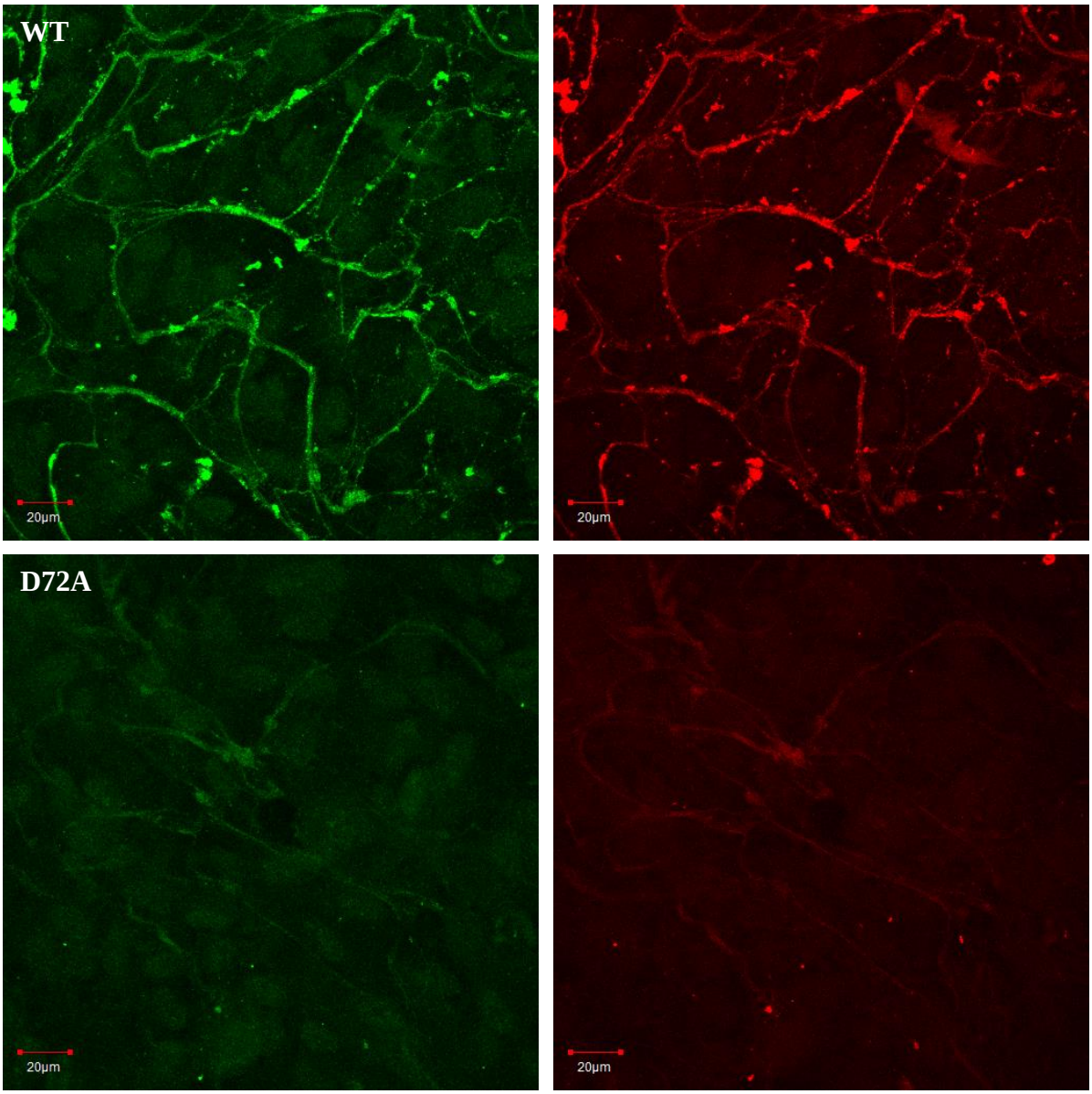

Day 10

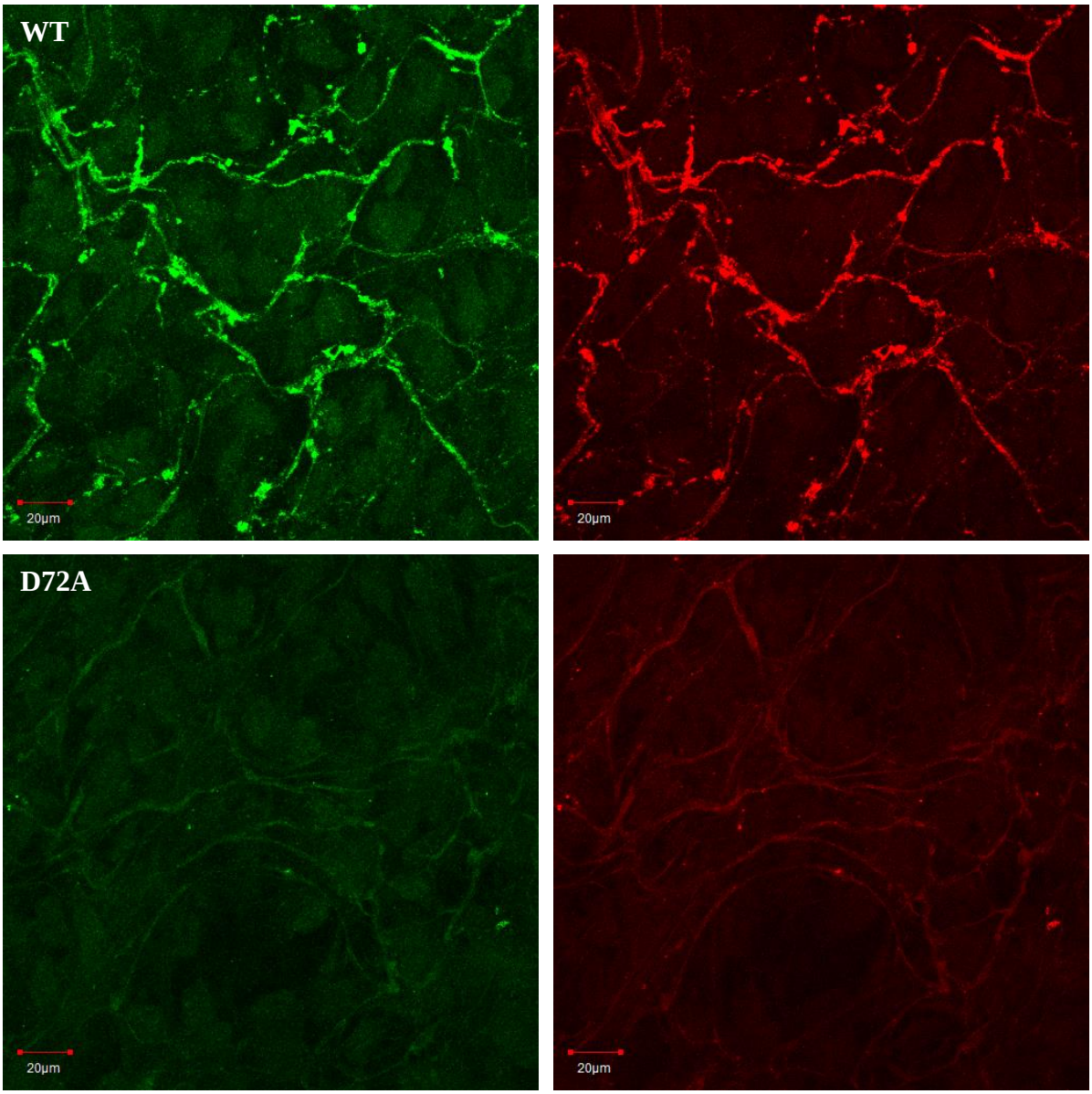

Controls

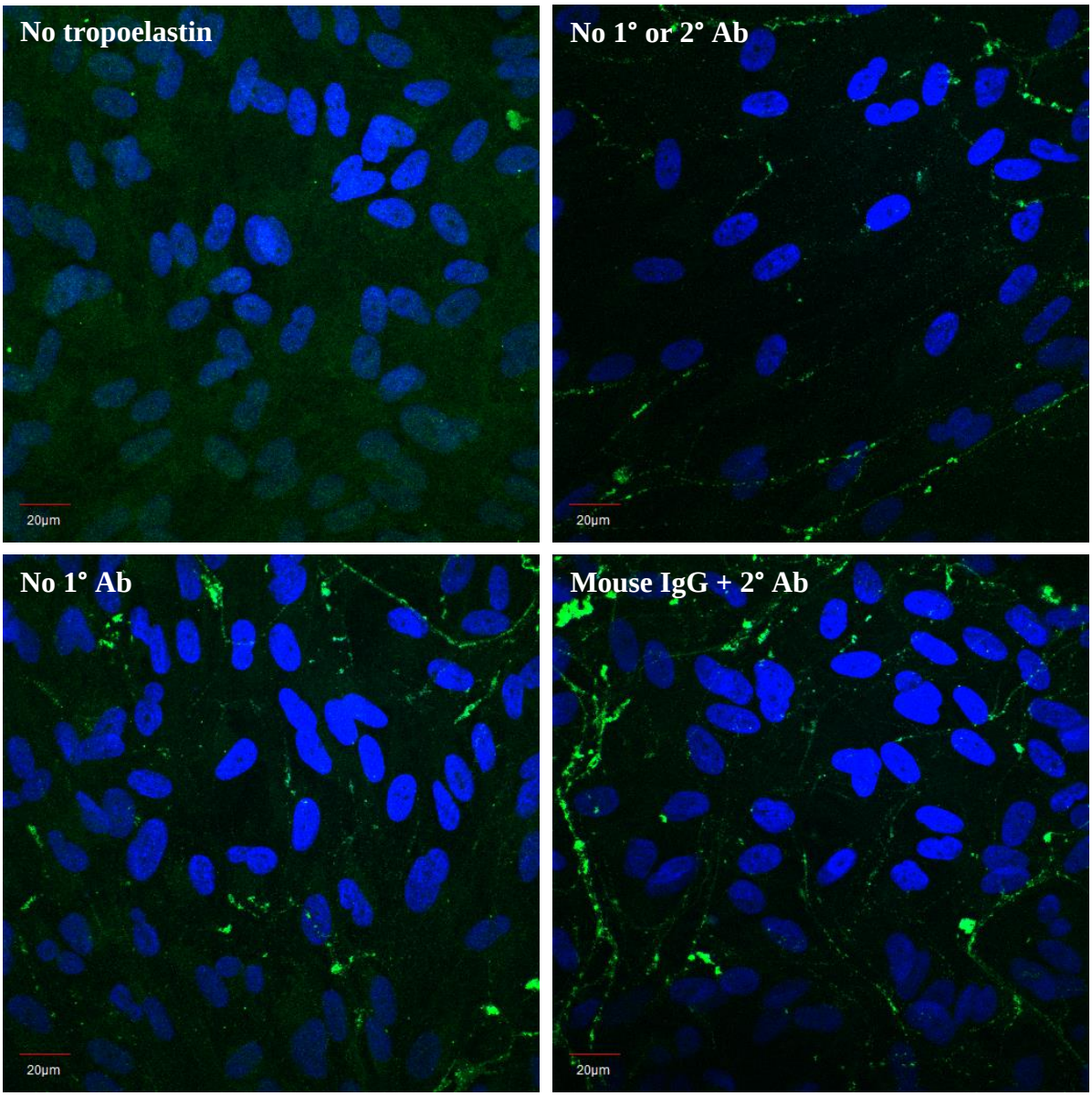

Figure 6.17. Confocal microscope images of elastic fibres formed from 20 µg/mL exogenous WT and D72A tropoelastin by ARPE-19 cells. Cells were fixed and stained 1, 4, 7 and 10 days after tropoelastin addition. The immunofluorescence and autofluorescence signals from each field of view are shown. Staining controls include cells with no added tropoelastin, and samples with added tropoelastin but no primary or secondary antibody, no primary antibody, and a non-specific primary mouse antibody with the anti-mouse secondary antibody. Staining controls show merged fluorescence and autofluorescence signals as well as DAPI-stained cell nuclei.

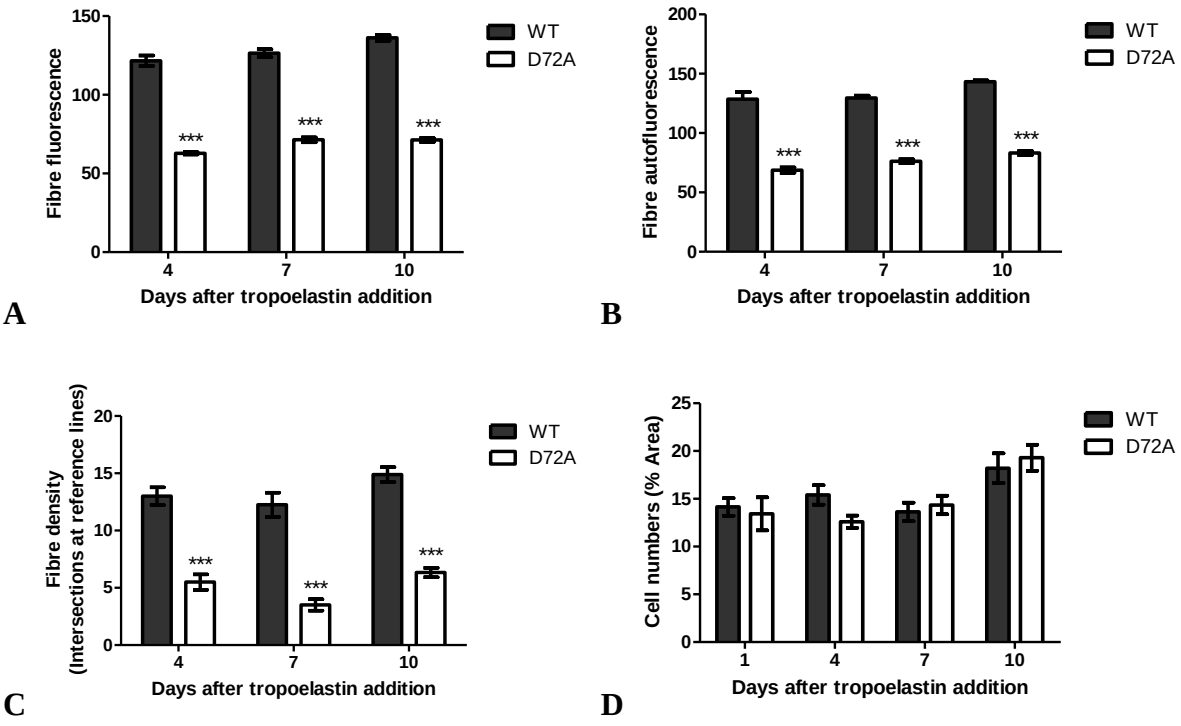

Figure 6.18. Analysis of WT and D72A elastic fibre properties formed with ARPE-19 cells. The (A) immunofluorescence, (B) autofluorescence and (C) abundance of the elastic fibres are indicated. (D) Cell numbers between WT and D72A samples are comparable, as represented by the similar area occupied by cell nuclei.

6.2.7 Structural studies

6.2.7.1 Antibody detection of tropoelastin

Antibodies targeted against different regions within the tropoelastin molecule were used to examine potential conformational changes between WT and D72A species (Figure 6.19). Immunodetection of surface-coated tropoelastin increased as expected with rising tropoelastin concentrations until antibody-specific saturation levels of 5-10 μg/mL tropoelastin. Significantly decreased epitope levels were detected in D72A compared to WT when using a specific antibody against domain 6 which encompasses the mutation site. However, no differences were observed between WT and D72A with antibodies targeted against domains 24 and 36.

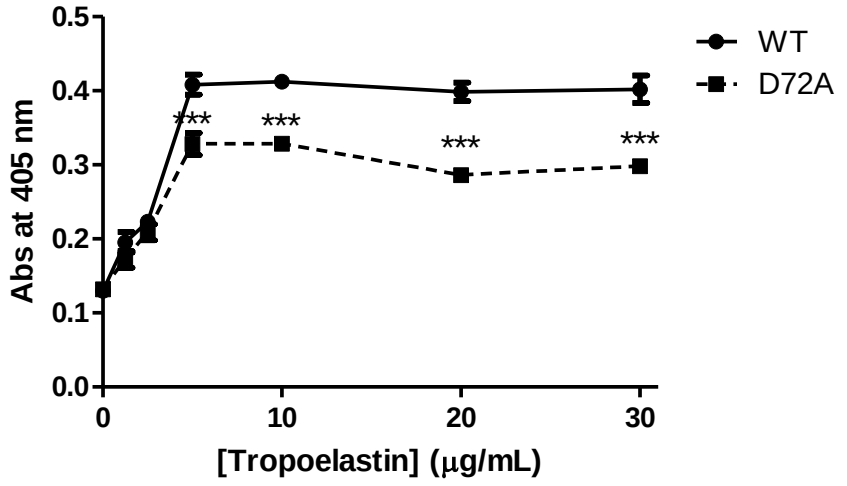

A

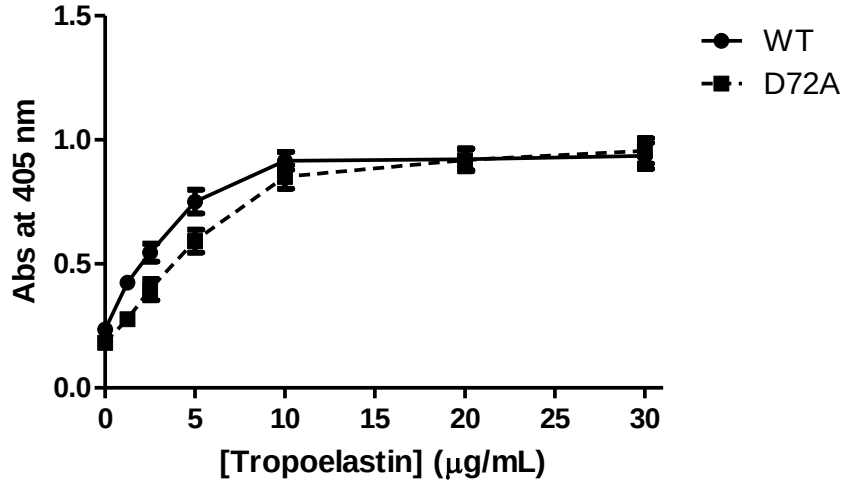

B

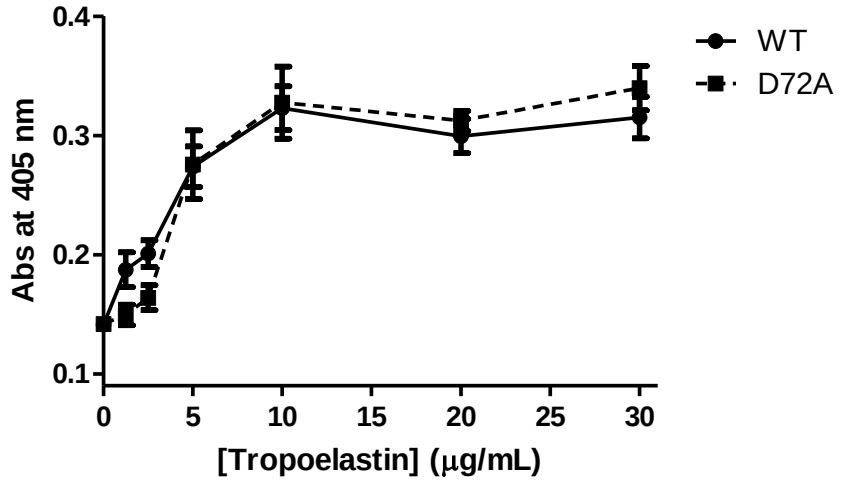

C

Figure 6.19. Detection of surface-bound WT and D72A tropoelastin by ELISA, using antibodies targeted against (A) domain 6, (B) domain 24 and (C) domain 36.

6.2.7.2 Secondary structure analysis

The secondary structures of WT and D72A tropoelastin were analysed using far-UV CD. The spectra of both species displayed similar features characteristic of tropoelastin, including a large negative peak at ~200 nm and a negative shoulder at ~220 nm (Figure 6.20A), although there were slight differences in the CD spectra around these wavelengths corresponding to a slight increase in the alpha-helical content of D72A (Figure 6.20B). The secondary structure composition of WT and D72A tropoelastin were predicted to be statistically similar, consisting of 5.4 and 5.0% alpha helix; 24.6 and 24.4% beta sheet; 13.2 and 13.0% turn region; 10.2 and 10.6% polyproline II helix; and 46.5 and 47% unresolved structure, respectively (Figure 6.20C).

6.2.7.3 Solution structure

The shapes of the tropoelastin constructs in an aqueous environment were determined via small-angle x-ray scattering. Both WT and D72A solution structures possessed similar features including the N-terminal coil region, hinge region, bridge region, and C-terminal foot region (Figure 6.21). Alignment of the WT and D72A structures indicated congruent lengths of their bridge regions, and consequently, a similar distance of their C-termini from the central axis. However, conformational changes were observed along the N-terminal coil. The central section of the D72A coil region displayed a more prominent bend or twist, resulting in an altered curvature compared to that of WT tropoelastin.

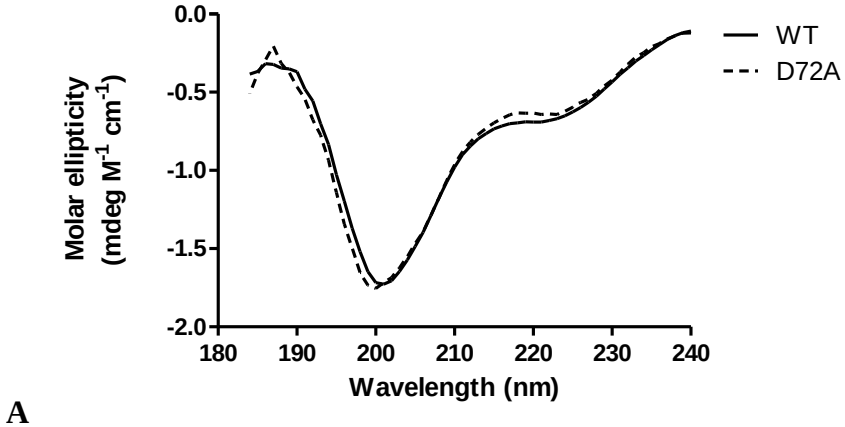

A

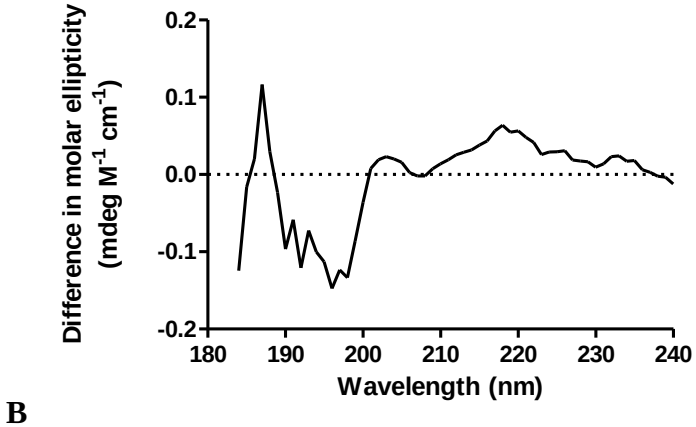

B

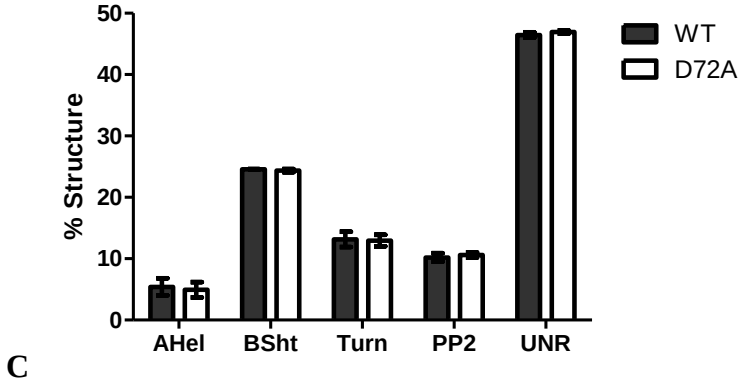

C

Figure 6.20. Secondary structure analysis of WT and D72A tropoelastin. (A) Far-UV CD spectra from 184-240 nm. (B) Difference obtained by subtracting the WT spectrum from the D72A spectrum. (C) Secondary structure composition of both species estimated by the CONTINLL and CDSSTR algorithms. The percentage of alpha-helix (AHel), beta-sheet (BSht), turn, polyproline II helix (PP2) and unresolved structures are indicated.

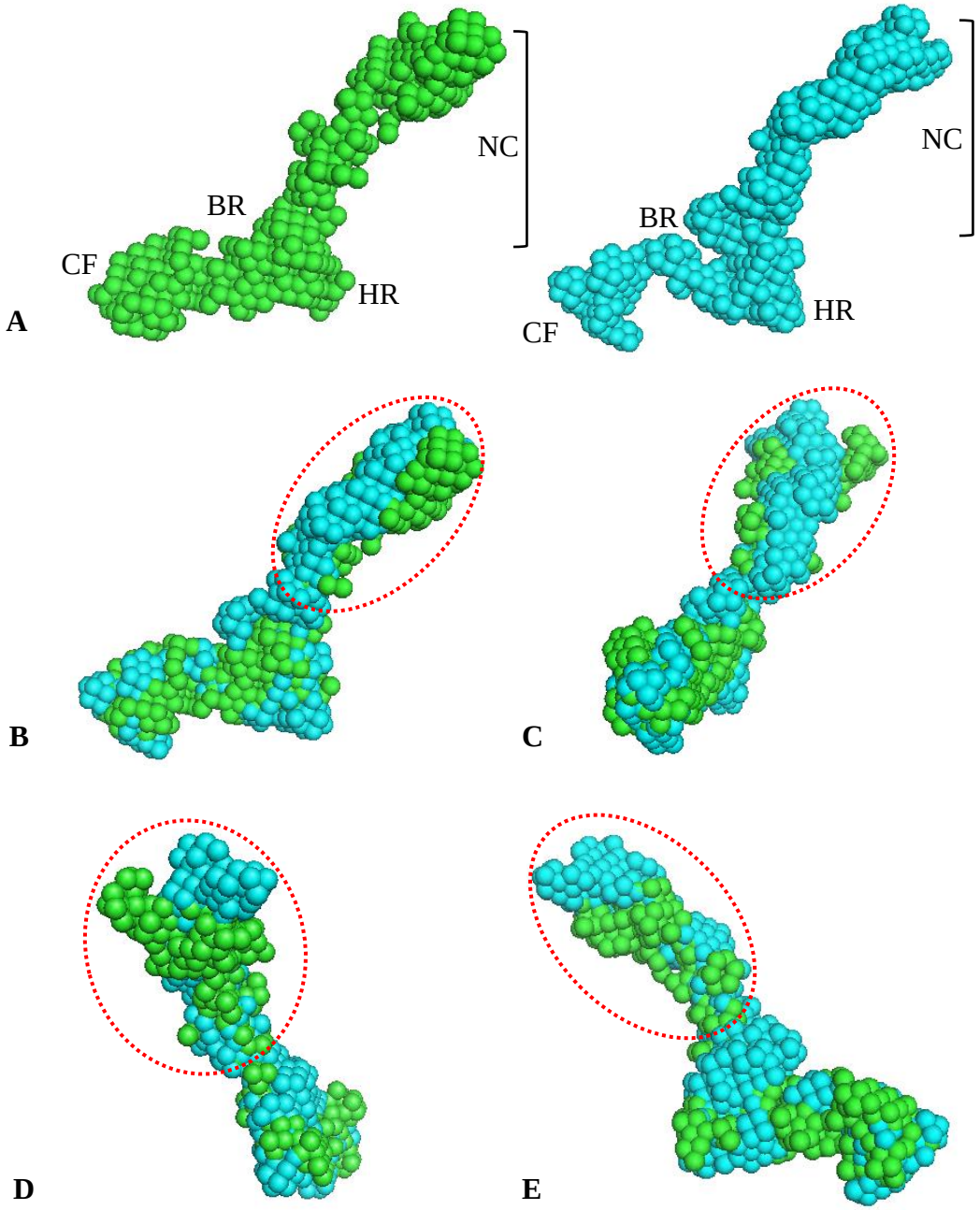

Figure 6.21. (A) Solution structures of WT (green) and D72A (blue) tropoelastin obtained by small-angle x-ray scattering. The N-terminal coil region (NC), hinge region (HR), bridge region (BR), and C-terminal foot region (CF) are indicated. (B-E) Aligned WT and D72A structures rotated around the y-axis. Arrows indicate the structural changes occurring in the N-terminal region.

6.3 Discussion

6.3.1 Conservation of D72A tropoelastin in mammalian tropoelastin

The rarely-occurring negatively-charged residues in mammalian tropoelastin have previously been described as localised around the bridge and N-terminal regions of the monomer protein. In human and several mammalian tropoelastins, only one negatively-charged residue lies within the N-terminal region. This D72 residue in the hydrophilic domain 6 of human tropoelastin is also conserved in the chimpanzee, baboon and pig sequences. Interestingly, in the absence of a D72 site, the bovine and feline tropoelastin species both possess a glutamate residue, which is similarly negatively-charged at physiological pH, at separate positions within domain 6. This suggests that the presence of an N-terminal negatively-charged residue in these mammalian tropoelastin sequences has arisen from at least three independent evolutionary events. Furthermore, such an aspartate or glutamate has been maintained despite significant genetic remodelling of exon 6 among mammalian tropoelastin genes [183]. This includes expanded regions of insertion in the cat sequence, and an alanine insertion in the cat, cow, pig, mouse and rat sequences, all of which are absent in the primate lineage [183]. Such a degree of sequence divergence is atypical in hydrophilic domains, which tolerate fewer substitutions to preserve the spatial arrangement of cross-linking sites. These observations suggest a possible functional significance for the N-terminal domain 6 that involves a negatively-charged residue such as D72, and is likely separate to the conventional cross-linking role of hydrophilic domains in tropoelastin.

6.3.2 Production and confirmation of D72A tropoelastin

Bacterial plasmid containing the WT tropoelastin gene was modified by site-directed mutagenesis to obtain the D72A tropoelastin sequence within the same pET3d vector. Upon transformation of electrocompetent *E. coli* with the mutated vector construct, plasmid DNA was extracted from the transformed bacterial culture and sequenced. Results confirm the presence of a codon change that would give rise to a D72A mutation in the expressed tropoelastin protein.

Production of D72A tropoelastin via a small-scale fermentation system [153] was confirmed by comparative MALDI-TOF mass spectrometry of the purified construct against WT tropoelastin. The Lys-C enzyme, which specifically cleaves at the carboxyl side of lysine residues, was selected to digest the protein constructs to generate large peptides for analysis, due to a maximum of 35 possible cleavage sites in tropoelastin [143]. Within the 5000-6800 m/z window, the WT and D72A spectra were overlapping, with the exception of a mass shift in the peak assigned to the peptide fragment containing residue 72. The shift corresponded to the 43.9 Da mass difference between aspartate and alanine, confirming the presence of a D72A mutation in the purified construct.

SDS-PAGE analysis of the D72A tropoelastin further confirmed an expected size of ~60 kDa and minimal protein degradation, indicating suitable quality for comparison studies with WT tropoelastin.

6.3.3 Coacervation studies

Since coacervation represents the first crucial step of elastogenesis, the ability of tropoelastin molecules to coacervate greatly impacts upon their assembly into elastic fibres. The initial alignment and organisation of tropoelastin monomers during this process are believed to be non-reliant on extracellular components such as microfibrillar proteins due to the excess concentrations of secreted tropoelastin [282]. For this reason, coacervation can be suitably modelled *in vitro* with tropoelastin-only assays in salt and pH conditions approximating the extracellular environment.

Similar to WT tropoelastin and various other tropoelastin isoforms [70, 108, 153, 275], the D72A construct exhibited temperature-dependent aggregation occurring over a narrow temperature range of less than 5°C. This rapid shift from the monomer to polymer state is consistent with the initial assembly process being driven mainly by hydrophobic associations [4] However, the temperature at which D72A achieved maximum coacervation (40°C) was higher compared to WT (35°C). This result paralleled the findings from dynamic light scattering of the tropoelastin solutions at different temperatures. Below 30°C, both constructs were in the monomer form, which corresponded to the absence of sample turbidity observed during light spectrophotometry. At 30°C, a portion of the WT population had aggregated, while the same extent was achieved by D72A only at 35°C, consistent with the partial turbidity of each sample at these temperatures. At 35 and 40°C respectively, all WT and D72A constructs had formed aggregates, reflecting the maximum turbidity seen for both samples at their transition temperatures.

The coacervation temperature of tropoelastin species is conventionally linked to the endothermic energy required to disrupt hydrogen bonds in the structured water shielding hydrophobic domains from self-interaction [289]. The stability of the clathrate water is known to be dictated by protein hydrophobicity, as supported by studies showing a strong

inverse correlation between coacervation temperature and the number of hydrophobic domains [62, 97, 185, 186, 364]. However, WT and D72A possess an equal number of hydrophobic regions, and the substitution of the charged aspartate with a more hydrophobic alanine [97] in D72A should negligibly increase overall hydrophobicity and decrease coacervation temperature. Instead, the increased coacervation temperature of D72A reflects a higher energy requirement for the disruption of bound water, indicating altered protein hydration that is likely unrelated to changes in protein hydropathy. Such changes in protein hydration may conceivably arise from structural differences between WT and D72A.

Kinetic differences were also observed in the initial assembly of WT and D72A tropoelastin. At temperatures up to 50°C, D72A consistently required a longer coacervation time than WT, although the difference was more pronounced within the physiological temperature range. The coacervation time of both constructs decreased with increasing temperatures, similar to previous findings on tropoelastin isoforms [275], until reaching parity at 55-60°C. The rate of tropoelastin coacervation has likewise been associated with protein hydropathy, as greater cooperativity between a larger number of hydrophobic segments would increase the efficiency of self-assembly [70]. However, the slower coacervation of D72A cannot be attributed to a loss of hydrophobic regions, which again suggests possible conformational changes in the mutant construct that alter the exposure or proximity of interacting hydrophobic domains.

Apart from the differences in the coacervation temperature and time of WT and D72A tropoelastin, the full-sized WT coacervates were more than four times larger than those of D72A. This was observed even at high temperatures which allow WT and D72A coacervation to proceed fully and at a similar rate. Tropoelastin assemblies cannot expand indefinitely and reach a maximum of 2-6 μm [11], which suggests an inherent size limitation due to the arrangement of monomers within the coacervated species. The smaller end size of

D72A assemblies therefore implies a different self-organisation of mutant constructs that precludes expansion to the same extent as WT. This may also potentially result from structural changes in the individual D72A monomers that affect intermolecular packing within the coacervated species.

It is interesting that a single amino acid mutation in the hydrophilic domain 6 of tropoelastin impairs its ability to coacervate normally, since the process is thought to be dominated by the large hydrophobic domains in the central region of tropoelastin, such as domains 18, 26, 28 and 30 [70, 108]. Furthermore, multiple site mutations in the more proximal domain 20 did not affect the coacervation profile of full-length tropoelastin variants [35], concordant with the relatively high allowance for sequence polymorphisms in the hydrophobic regions of tropoelastin [21]. The impact of the D72A mutation on tropoelastin coacervation implicates the involvement of the N-terminal segment in this initial assembly process. This is supported by the ability of elastin peptides containing domains 2-7 to coacervate into structures reminiscent of those formed by the full-length monomer [357].

6.3.4 Cross-linking studies

The ability of tropoelastin to be cross-linked strongly corresponds to its propensity to be incorporated into insoluble elastic fibres. Cross-linking of WT and D72A was modelled in extracellular temperature, salt and pH conditions with the amine-reactive homobifunctional chemical cross-linker BS3 [290]. This approach identifies tropoelastin regions aligned by coacervation and approximates *in vivo* enzymatic cross-linking by lysyl oxidase [44, 178]. A six-fold molar excess of BS3 allowed complete cross-linking of WT and D72A, as evidenced by the absence of monomers in the aqueous solution left after hydrogel formation.

The WT and D72A elastin hydrogels showed distinct differences in morphological and functional properties. Three-dimensional reconstruction of the hydrogels by micro-CT illustrated the stark contrast between the open porous network of the WT construct, which was consistent with the fibrous nature of physiological elastin [8, 13, 14, 365], and the compact layered structure of the D72A material. This compositional difference corresponded to a 34% decrease in the calculated porosity of D72A hydrogels compared to WT hydrogels. The porosity of a polymer is known to depend on the separation kinetics of the initially homogeneous mixture into the polymer and aqueous phases [291, 292]. Since the WT and D72A hydrogels were constructed under identical conditions, variations in phase separation are likely due to inherent differences in the rate and extent of the polymerisation, i.e. cross-linking, process between molecules.

The observed structural differences between WT and D72A hydrogels are congruent with their differential swelling properties in water. The D72A material allowed significantly less water uptake compared to the WT, which reflected their reduced porosity and dense structure. The extent of hydrogel swelling is classically reliant upon solvent-polymer interactions. Solvent influx elongates the junctions of the cross-linked material and

decreases the conformational space of flexible hydrophobic segments within the rigid cross-linked domains [76, 188]. This resulting decrease in entropy is compensated for by an increase in entropy attributed to the mixing of solvent and the bulk water within the polymer [189]. In these swelling experiments where the nature of the solvent is kept constant, the primary determinant of hydrogel fluid uptake is the extent and nature of cross-linking within the material.

High resolution analyses of WT and D72A hydrogel surfaces via SEM confirmed the morphological differences initially observed with micro-CT imaging. The top surface of WT hydrogels consisted of a fibrous network with large pore sizes consistent with previously reported values [20]. This composition reflects that expected at the final stage of synthetic elastin assembly, in which linked tropoelastin spheres consolidate to form porous structures [296]. In contrast, the top surface of D72A hydrogels was characterised by a minimally porous, smooth, dense sheet that mirrors the structure formed after tropoelastin coalescence [366], as well as the bottom surfaces of WT and D72A hydrogels. The vastly dissimilar surface features of both types of hydrogels strongly suggest differences between WT and D72A cross-linking and in the resultant cross-linked structures.

Tropoelastin cross-linking, whether by lysyl oxidase or BS3, is known to be enriched in the central region spanning domains 19-25 [143, 282]. The abnormal cross-linking of D72A tropoelastin may result from differential assembly of the initial coacervated species, as misalignments between monomers can potentially affect the formation of native cross-links within the central domains. In addition, domain 6 has also been shown to directly participate in tropoelastin cross-linking. Its K78 residue is thought to bind to the K696 of domain 36 in an intermolecular linkage [143], while its K81 contacts K111 of domain 8 via an intramolecular bond [282]. The involvement of domain 6 in cross-linking is consistent with the surface accessibility of the N-terminal region [362], as supported by the presence of

a protease susceptible K152 site in domain 10 [367]. The participation of domain 6 in cross-linking therefore suggests that the process may be affected even by subtle local conformational shifts arising from the D72A mutation that disturb the juxtaposition of interacting lysine residues. Depending on the scale of the structural changes that occur, cross-link formation by the proximal domains 12-14 [143, 282] may also be altered.

6.3.5 Attachment to human dermal fibroblasts

WT and D72A tropoelastin coated on tissue culture plastic promoted the adhesion of human dermal fibroblasts in a concentration-dependent but saturable manner similar to previous reports [45, 179]. At each tropoelastin concentration, there was no difference in the extent of cell attachment to WT and D72A. However, the comparative binding properties of both tropoelastin constructs cannot be extrapolated to other cell types. Human dermal fibroblasts are known to attach via the $\alpha_v\beta_3$ integrin primarily to the tropoelastin C-terminus [18, 297], specifically the terminal GRKRK residues [179]. While integrins are the major adhesion receptors for most extracellular matrix molecules [45], other cell type-specific receptors also mediate attachment to tropoelastin [18]. These cell-surface glycosaminoglycans such as heparin sulfate and chondroitin sulfate are also thought to interact with tropoelastin at or near its C-terminal domain [45].

The comparable levels of fibroblast adhesion to WT and D72A therefore indicate a similar extent of C-terminal accessibility in the surface-bound tropoelastin constructs. The results further suggest that any structural changes in D72A tropoelastin are most likely localised to the N-terminal segment, as conformational adjustments to the central bridge region can still influence the orientation of the C-terminus [184].

6.3.6 Elastic fibre assembly

Exogenous tropoelastin added to the culture media of elastogenic cells has been shown to be capably assembled into elastic fibres [202, 203]. The addition of WT tropoelastin to human dermal fibroblast cultures induced the linear clustering of tropoelastin spherules after one day, the establishment of defined elastic fibres after four days, and their progressive development into a more extensive network by seven and ten days. In stark contrast, D72A tropoelastin added to the fibroblast cells was unable to form large spherules or elastic fibres. This is less likely to be caused by impaired cellular binding proposed to be essential for the anchorage of the elastic network [179], as D72A displayed comparable fibroblast adhesion to the WT isoform. Rather, its inability to form elastic fibres may be a cumulative effect of impaired self-assembly and deficient interactions with extracellular matrix components. For instance, early contacts between tropoelastin and fibrillin-1, the main component of microfibrils, are thought to be dually important for further alignment of the tropoelastin coacervates prior to cross-linking [368], and for tropoelastin deposition onto microfibrils [128, 130, 369]. The microfibrillar deposition of tropoelastin has classically been attributed to its C-terminal domains [122]; however, the N-terminal domains 4-6 of tropoelastin have also been found to bind the shoulder interbead region [130] of fibrillin-1 with high affinity [135]. This suggests that structural changes in D72A occurring around residue 72 of domain 6 may negatively affect contacts with fibrillin-1, thus impairing tropoelastin deposition on the microfibrillar scaffold and subsequent cross-linking into stable elastic fibres.

The addition of WT and D72A monomers to ARPE-19 cells, which express the major elastogenic components except tropoelastin [140], confirmed the impaired elastogenic ability of the D72A construct, albeit to a lesser degree than that observed in dermal fibroblasts. The WT species efficiently organised into linear assemblies after one day and

into an abundant elastic fibre network after four days. In contrast, the D72A constructs initially remained dispersed in the extracellular space, which may be associated with their reduced propensity for self-association, but subsequently formed elastic fibres with atypical properties. The decreased immunofluorescence of D72A fibres may arise from a fewer number of tropoelastin monomers within the fibre, or from reduced accessibility of antibody-targeted motifs that implies differential tropoelastin packing within the fibre. The decreased autofluorescence of D72A fibres implicates altered elastin cross-linking [257, 258], which may at least partially result from disruptions or modifications to linkages participated in by domain 6 [282]. The impaired coacervation and cross-linking of D72A, coupled with posited deficient interactions with elastogenic proteins, all potentially contribute to the lower abundance of D72A elastic fibres compared to WT.

In addition, the variable elastogenic capability of D72A tropoelastin between fibroblast and ARPE-19 cell types is likely due to the different environments created by tissue-specific expression of cell receptors [260] and extracellular matrix components including fibrillins [261-265], lysyl oxidase enzymes [141] and microfibril-associated glycoproteins [266, 267]. The tissue-specific elastogenic environments may select against D72A constructs to varying degrees, in accordance with specific functional prerequisites for the assembled elastic fibre. This is supported by the visibly different morphology of WT elastic fibres formed in fibroblast and ARPE-19 cell lines.

6.3.7 Structural studies

6.3.7.1 Antibody detection

The altered self-assembly and elastogenic properties of D72A tropoelastin provide strong support for the presence of conformational changes in the monomer. Antibodies targeted against specific tropoelastin regions were used in ELISAs as a preliminary tool for probing the location and extent of these potential structural changes in D72A. Compared to the WT species, D72A displayed equal levels of detection by both the BA4 and the anti-C-terminal peptide antibodies. The BA4 anti-elastin antibody is known to react predominantly with the VGVAPG hexapeptide in domain 24 that serves as the elastin binding protein ligand, and to lesser extent other hydrophobic sequences throughout the molecule that follow the xGxxPG or xGxPGx motifs [298, 299]. On the other hand, the anti-C-terminal peptide antibody has been designed and experimentally validated to specifically target the tropoelastin domain 36, which also contains the main binding site to dermal fibroblasts. Comparable binding of both antibodies to WT and D72A indicates similar exposure of their central and C-terminal regions, thus suggesting preservation of the native conformation of these regions in the D72A mutant.

In contrast, the polyclonal antibody targeted against domain 6 exhibited significantly reduced binding to D72A compared to WT, even at excess tropoelastin coating concentrations. This decreased antibody detection may be caused in part by the mutation-derived abolishment of the recognition site of a number of antibodies within the polyclonal population, and in part by the partial inaccessibility of domain 6 in the D72A construct. This strongly points to the likelihood of a conformational shift in this region of D72A.

6.3.7.2 Secondary structure analysis

The far-UV CD profiles of WT and D72A tropoelastin were compared to determine potential differences in secondary structure composition. The CD spectra of both constructs possessed features characteristic of tropoelastin, such as the negative peak at ~200 nm corresponding to unstructured hydrophobic domains, and the negative shoulder at ~220 nm attributed to alpha-helical content [109, 110, 273]. The secondary structure compositions of WT and D72A were calculated to be similar, with a major percentage allocated to unordered regions consistent with the flexible nature of tropoelastin [54, 320], and decreasing amounts of beta-sheet, turn, polyproline II helix and alpha-helix structures.

By directly comparing the WT and D72A CD spectra, small local differences in secondary structure may not be resolved, particularly in the context of the whole tropoelastin molecule. Subtracting the WT spectrum from that of D72A may help magnify such differences. Using this approach, D72A appears to have a slight reduction in alpha-helical structure, with a concurrent increase in unordered regions. These differences, however, were not statistically significant.

The propensity for alpha-helix formation in peptides has been directly correlated to the number of consecutive alanine residues [75]. As evidence, peptides corresponding to tropoelastin domains 6 and 31, which have 4 alanines each, possessed fewer alpha-helices than the domain 21 peptide which contains 5 alanines [75]. The aspartate-to-alanine mutation in the D72A construct would adjoin the preceding A71 residue to the downstream A73 to A76 tetra-alanines to form a hexa-alanine sequence that would theoretically have a higher predisposition for alpha-helix formation. However, the stability of this nascent helix structure may be affected by the substitution of the N-terminal alpha-helical capping residue from the native aspartate at position 72 to a valine at position 70 in the mutant isoform. While the negatively-charged aspartate is the second most preferred N-capping residue in

alpha-helical peptides, valine is the third least favourable among the 20 amino acids [370]. Given the established role of alpha-helices in positioning lysine residues for cross-linking [58], potential changes to the alpha-helical formation of domain 6 may mechanistically explain the observed impairment in D72A assembly.

6.3.7.3 Solution structure

The WT and D72A solution structures modelled from SAXS data showed a similar overall shape consisting of the rod-like N-terminal coil region, the looped hinge and bridge regions, and the open C-terminal foot region, which are consistent with the reported structural features of human tropoelastin [72]. Alignment of the WT and D72A models localised the main structural difference between the constructs to the N-terminal region. Previous structural characterisation of a truncated tropoelastin isoform spanning domains 2-18 indicated shape congruence with the N-terminal coil, and thus allowed the assignment of domains 2-18 to this region [72]. Domain 6, which contains D72, is expected to lie within this coil region of tropoelastin.

The D72A mutation in tropoelastin is clearly associated with an altered curvature and orientation of the segment spanning the N-terminus to the mid-section of the coil region. This structural deviation may be contributed to by possible destabilisation of alpha-helices in domain 6. These results suggests for the first time a role for the D72 residue in maintaining the native conformation of the tropoelastin N-terminal coil, potentially by stabilising local secondary structure and/or contacting proximal residues via charge interactions. D72 was modelled to contact the positively-charged K78 residue in domain 6 (Figure 6.22). Such an interaction would constrain this region and allow the formation of the reported intra-molecular linkage between K81 of domain 6 and K111 of domain 8 [282] during *in vivo* zero-length cross-linking by lysyl oxidase [371, 372]. The D72A mutation

would potentially preclude the formation of a stabilising D72-K78 salt bridge and lead to the altered N-terminal orientation of the mutant construct.

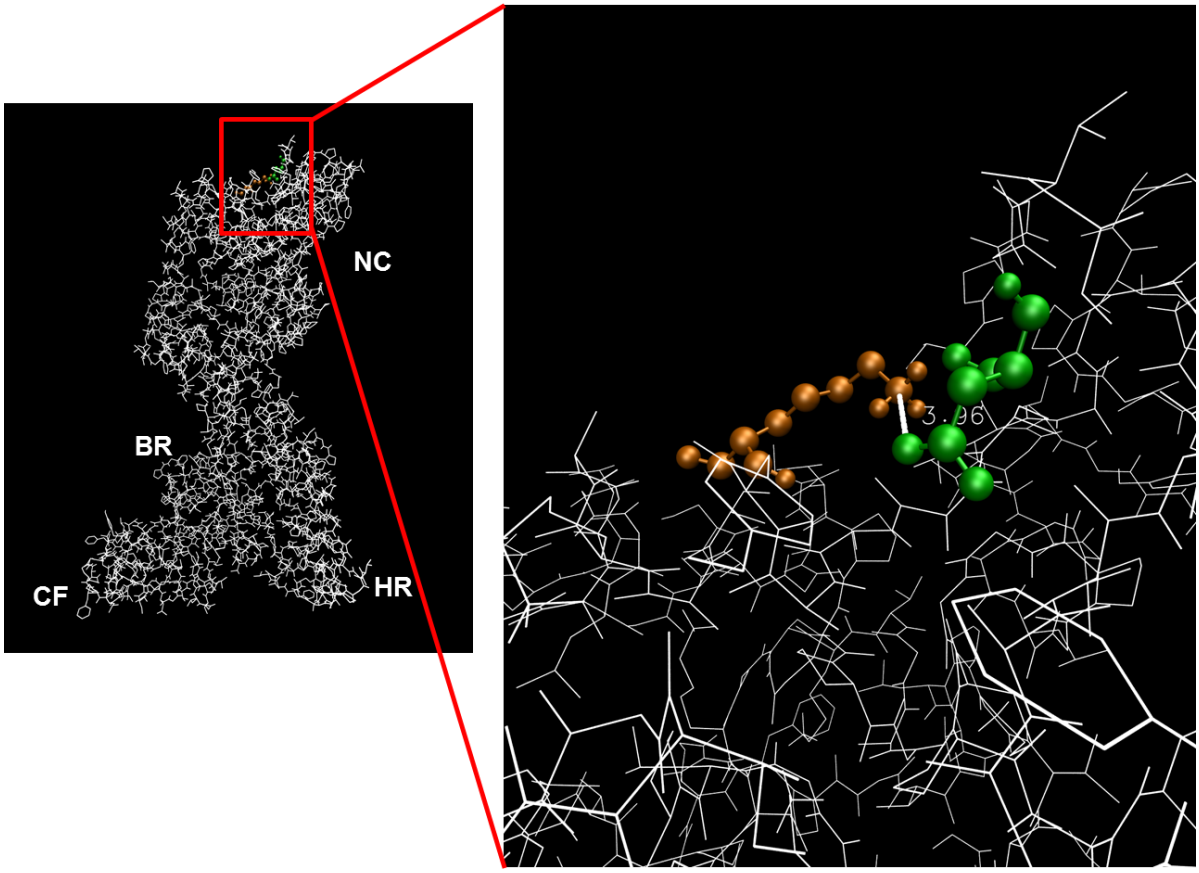

Figure 6.22. Molecular modelling of potential interactions between the D72 and K78 residues of tropoelastin, obtained from Anna Tarakanova. The N-terminal coil, hinge, bridge and C-terminal foot regions are indicated.

An N-terminal structural change at the monomer level may account for the altered assembly of D72A tropoelastin. Protein hydration changes associated with the conformational shift can affect the thermodynamic requirements of coacervation, while modifications to the relative position of domains can decrease the efficiency of association and hinder native molecular packing within the assembled species. The misalignment of cross-linking domains may contribute to deficient or aberrant formation of intramolecular and intermolecular linkages, particularly those involving domain 6 and neighbouring

domains. Atypical cross-linking of the D72A species is consistent with the structural and functional abnormalities of its hydrogel constructs. Evidence of a domain 6-domain 36 cross-link [143] strengthens a head-to-tail model of tropoelastin assembly [72]. The impaired elastogenic ability of D72A tropoelastin directly supports a model in which the assembly and architecture of elastin are affected upon perturbations to the tropoelastin N-terminal segment.

7. General discussion

This thesis explores the structural and functional properties of a number of tropoelastin constructs with sequence mutations at strategic locations within the molecule. The observed effects of these mutations on the elastogenic ability of tropoelastin help shed light on the significance of these classically under-characterised regions in the monomer protein.

7.1 The R515 residue of the tropoelastin bridge region

The tropoelastin bridge region contains a highly-conserved, protease-susceptible R515 site situated at the junctions of domains 25 and 26. However, the functional significance, if any, of the R515 residue and of the tropoelastin bridge region were previously unknown. *In vitro* characterisation of an R515A tropoelastin mutant demonstrated a dramatically impaired self-assembly compared to wild-type tropoelastin, including inefficient coacervation, atypical hydrogel formation, and decreased dermal fibroblast attachment [184]. These properties of the R515A construct were linked to an altered nanostructure which displays greater conformational flexibility around the bridge region and C-terminal regions.

To assess the elastogenic ability of R515A tropoelastin in a cellular environment, the initial approach involved the transfection of ARPE-19 cells and dermal fibroblasts with the synthetic WT or R515A gene. The mammalian cell-specific expression vectors were successfully constructed via linker-mediated cloning after trialling several cloning strategies. The ARPE-19 cells were confirmed to express retinal pigmented epithelium-specific markers CRALBP and RPE65 [227, 229], and essential elastogenic components such as fibrillin-1 and lysyl oxidase but not tropoelastin [140, 201]. Two types of fibroblasts were likewise shown to express the major elastogenic proteins including endogenous tropoelastin, although at transcript levels markedly lower than that expected of the recombinant

tropoelastin after transfection. However, the propagation of stable transfectants in both ARPE-19 cells and fibroblasts was hampered by the loss of the tropoelastin gene over time. In contrast, transiently transfected fibroblasts produced fine fibre structures that were confirmed by FLIM to be elastic fibres. However, the low extent of elastic fibre assembly prevented meaningful analyses of WT and R515A fibre properties.

To circumvent the difficulties with tropoelastin synthesis, purified WT and R515A constructs were directly added to the culture medium of cells following an *in vitro* elastic fibre assembly model [140]. In the ARPE-19 environment, R515A tropoelastin showed a delayed initial self-assembly, and formed fewer fibres with decreased immunofluorescence and autofluorescence compared to WT. However, multiple additions of R515A restored the resulting fibres to a WT morphology, suggesting that the previously observed differences mainly stemmed from monomer loss due to inefficient early-stage assembly. With fibroblasts, R515A exhibited a magnified degree of elastogenic impairment, remaining predominantly as spherical clusters or as sparse fibres even with repeated additions of the construct to the culture medium. These results provide direct evidence of the functional consequences of an altered tropoelastin bridge, and elucidate the critical importance of the R515 site in stabilising this region for elastic fiber assembly.

7.2 The E345 and E414 residues near the tropoelastin hinge region

Negatively-charged residues occur rarely in mammalian tropoelastin sequences, but consistently appear to be clustered in either domain 6 or the central segment spanning domains 19-25. Human tropoelastin contains an E345 in domain 19 and an E414 in domain 21, which are spatially primed for potential interactions with R515 in the bridge region [72]. Three tropoelastin constructs with mutations at either or both glutamate sites were produced to explore the previously undetermined role/s of these negatively-charged residues in tropoelastin function.

Similar to the R515A construct, the E345A, E414A and E345A+E414A mutants all displayed higher temperature and time requirements for self-association than the WT species. At the temperature at which WT tropoelastin achieved full coacervation (35°C), the mutant constructs only partially coacervated to different degrees. They also assembled into full-sized aggregates at a higher temperature and at a slower rate than WT. In addition, the double E345A+E414A mutant showed a more severe impairment than the E345A or E414A species in terms of coacervation.

Chemically cross-linked E345A, E414A and E345A+E414A hydrogels possessed a more compact structure in contrast to the highly porous nature of the WT material. Consequently, the mutant hydrogels swelled 2- to 5-fold less than WT. Their surfaces, partially reminiscent of the bead-like composition of R515A hydrogels, are composed of globules linked by coalesced structures that varied between thin fibres to sheet-like fragments among the mutant constructs. Such structures suggest a variably deficient cross-linking process [271] that appears, however, to have progressed further than that of R515A.

The Glu-to-Ala mutants also exhibited a 21-34% decrease in dermal fibroblast attachment compared to WT, most likely due to a confirmed decrease in the accessibility of their cell-interactive C-terminal regions [179]. The mutant constructs displayed significant

elastogenic impairment when added to cultured fibroblasts. While WT monomers assembled into defined elastic fibres, E414A and E345A+E414A tropoelastin, like R515A, formed fibres with reduced immunofluorescence and abundance, indicating inefficient early-stage assembly and an atypical monomer arrangement within the elastic fibre. The E345A species did not form elastic fibres at all, suggesting an incompatibility of the monomer or assembled species with the elastogenic requirements of the fibroblastic environment.

The WT and mutant constructs indicated no differences in their secondary structure composition. Their solution structures exhibited the known features of normal tropoelastin [72], but with distinct conformational changes in the central to C-terminal regions. E345A possessed a slightly elongated hinge and shortened bridge, leading to a contracted C-terminus. In marked contrast, E414A showed an enlarged hinge and an extended bridge, resulting in a protruded C-terminus. The E345A+E414A shape also possessed a bulkier hinge but without significant changes in the length of the bridge and C-terminal regions. These results contribute to a model in which the central domains 19-25 are positioned symmetrically from the established domain 21/23 hinge [74]. This loop region may be stabilised by interactions between E345 and domains 25/26, and between E414 and domain 23 [73]. The loss of one glutamate may induce aberrant local structures that contract or extend the bridge, which in turn affects the tropoelastin C-terminal orientation as previously reported. The loss of both glutamates may reduce this occurrence, but potential destabilisation of the loop region can alter the positions of coacervation and cross-linking domains that affect elastin assembly. These findings strongly illustrate the significance of negatively-charged sites in the central region of tropoelastin.

7.3 The domain 22 of tropoelastin

The tropoelastin hinge region is formed by the consecutive hydrophilic domains encoded by exons 21 and 23 [73, 74]. The formation of this flexible structure results from the constitutive splicing out of exon 22 in human tropoelastin transcripts [34], which may mechanistically be due to the deviation of the exon 22 acceptor splice and branch point from consensus sequences, and a greater than optimum distance between the branch point and acceptor site. The reasons for the constitutive exclusion of exon 22 in human tropoelastin were previously unknown, particularly since this exon remains expressed in bovine, mouse and rat tropoelastin [33, 317, 318]. The selective pressures against exon 22 in human tropoelastin were explored with an EX22 construct, which contains the hydrophobic domain 22 between domains 21 and 23.

EX22 exhibited normal self-association with a similar coacervation temperature and a slightly higher coacervation rate than WT, indicating that the presence of domain 22 does not significantly affect the intrinsic coacervation ability of tropoelastin. However, EX22 showed aberrant assembly into higher order structures. EX22 hydrogels were densely stacked with very low porosity, and accordingly displayed reduced swelling on hydration. Their atypical composition relative to the WT material is consistent with differential cross-linking.

EX22 was inefficiently utilized by cells for incorporation into the elastic matrix. When added to dermal fibroblasts, EX22 species did not progress beyond spherule assembly at lower concentrations of exogenous tropoelastin. This was only partially compensated for by the addition of excess EX22 monomers. With ARPE-19 cells, EX22 formed elastic fibers that were morphologically different and fewer in number than WT fibres. The thicker EX22 fibres appear characteristic of skin elastic fibres in mammals which express tropoelastin containing domain 22 [326].

The solution structure of EX22 revealed a bulkier hinge/bridge region and a displaced C-terminus, consistent with the decreased antibody exposure of the central and C-terminal regions. The domain 21/23 tropoelastin hinge represents a highly flexible region that can access a broad conformational space [324]. The insertion of domain 22 into the hinge region would most likely induce steric constraints that disrupt the native hinge structure [325]. These structural changes were observed to translate into differences in intermolecular interactions during assembly, and consequentially in the assembled structure. These findings identity for the first time the deleterious impact of domain 22 expression on the structure and assembly of human tropoelastin, supporting strong functional advantages for its constitutive exclusion in human elastin.

7.4 The D72 residue of the tropoelastin N-terminal region

The only other negatively-charged residue in human tropoelastin, other than E345 and E414, lies within the N-terminal domain 6. This D72 site is conserved in a number of mammalian tropoelastin sequences, while others contain a negatively-charged glutamate residue similarly localised in domain 6 [183]. The role of D72 in tropoelastin function has never been explored; in fact, the tropoelastin N-terminal region is largely uncharacterised in terms of its participation in elastin assembly.

A D72A construct was produced to determine the effects of abolishing this D72 site in tropoelastin. The mutant displayed a lower propensity to coacervate, as evidenced by the higher temperature and longer time requirements for self-association. The full-sized D72A coacervates were also markedly smaller than the WT assemblies, suggesting that D72A not only undergoes less efficient early stage assembly but also forms differently-arranged coacervates. Hydrogels constructed from D72A likewise possessed an abnormally compact structure of stacked sheets with significantly reduced porosity and swelling capacity. This strongly implies an altered cross-linking process in D72A tropoelastin, potentially due in part to affected contacts involving the cross-linking domain 6 [143, 282].

Upon addition to a cellular environment, D72A monomers did not assemble into elastic fibres in fibroblast cultures, and formed only sparse, morphologically atypical fibres in ARPE-19 cells. This elastogenic deficiency of D72A is unlikely due to decreased cellular attachment, as evidenced by a comparable cell binding ability to WT. Rather, it is probably attributed to its intrinsically impaired self-assembly and interaction with extracellular matrix components such as fibrillin-1 [135].

Antibody detection of surface-bound D72A indicated equal exposure of the central and C-terminal regions to those of the WT species; however, the D72A N-terminal region is partially inaccessible, suggesting a conformational change in this section of the mutant

construct. The nanostructure of D72A confirmed an altered curvature of the N-terminal coil extending from the N-terminus to the midsection of this region. While no significant secondary structure change was observed in the whole protein, small local changes arising from alpha-helix destabilisation may be present and potentially contribute to the structural deviation of the N-terminal region. These results point to the role of D72 in maintaining the structure of the N-terminal region, which is also critical for normal elastogenic function of tropoelastin.

7.5 Conclusion

This thesis identifies specific residues and regions of human tropoelastin necessary for maintaining its native structure and function. The described results clarify the significance of the R515 residue in the bridge region, the negatively-charged E345, E414 and D72 sites in the central and N-terminal regions, and the constitutive exclusion of domain 22 in the hinge region. The non-conservative substitution of these residues, as well as the addition of domain 22, are associated with conformational changes at specific regions of tropoelastin and a dramatic impairment of protein self-assembly, which ultimately translate to a markedly reduced elastogenic potential. By recognising the independent and cooperative roles of the tropoelastin bridge, hinge and N-terminal regions, this work contributes to an improved understanding of the structure-function relationship in and between human tropoelastin molecules.

8. Appendices

8.1 WT DNA sequence

```
WT          ATGGGTGGCGTTCCGGGTGCTATCCCGGGTGGCGTTCCGGGTGGTGTATTCTACCCAGGC 60
WT          GCGGGTCTGGGTGCACTGGGCGGTGGTGCGCTGGGCCCGGGTGGTAAACCGCTGAAACCG 120
WT          GTTCCAGGCGGTCTGGCAGGTGCTGGTCTGGGTGCAGGTCTGGGCGCGTTCCCGGCGGTT 180
WT          ACCTTCCCGGGTGCTCTGGTTCCGGGTGGCGTTGCAGACGCAGCTGCTGCGTACAAAGCG 240
WT          GCAAAGGCAGGTGCGGGTCTGGGCGGGGTACCAGGTGTTGGCGGTCTGGGTGTATCTGCT 300
WT          GGCGCAGTTGTTCCGCAGCCGGGTGCAGGTGTAAAACCGGGCAAAGTTCCAGGTGTTGGT 360
WT          CTGCCGGGCGTATACCCGGGTGGTGTTCTGCCGGGCGCGCGTTTCCCAGGTGTTGGTGTA 420
WT          CTGCCGGGCGTTCCGACCGGTGCAGGTGTTAAACCGAAGGCACCAGGTGTAGGCGGCGCG 480
WT          TTCGCGGGTATCCCGGGTGTTGGCCCGTTCGGTGGTCCGCAGCCAGGCGTTCCGCTGGGT 540
WT          TACCCGATCAAAGCGCCGAAGCTTCCAGGTGGCTACGGTCTGCCGTACACCACCGGTAAA 600
WT          CTGCCGTACGGCTACGGTCCGGGTGGCGTAGCAGGTGCTGCGGGTAAAGCAGGCTACCCA 660
WT          ACCGGTACTGGTGTTGGTCCGCAGGCTGCTGCGGCAGCTGCGGCGAAGGCAGCAGCAAAA 720
WT          TTCGGCGCGGGTGCAGCGGGTGTTCTGCCGGGCGTAGGTGGTGCTGGCGTTCCGGGTGTT 780
WT          CCAGGTGCGATCCCGGGCATCGGTGGTATCGCAGGCGTAGGTACTCCGGCGGCCGCTGCG 840
WT          GCTGCGGCAGCTGCGGCGAAAGCAGCTAAATACGGTGCGGCAGCAGGCCTGGTTCCGGGT 900
WT          GGTCCAGGCTTCGGTCCGGGTGTTGTAGGCGTTCCGGGTGCTGGTGTTCCGGGCGTAGGT 960
WT          GTTCCAGGTGCGGGCATCCCGGTTGTACCGGGTGCAGGTATCCCGGGCGCTGCGGTTCCA 1020
WT          GGTGTTGTATCCCCGGAAGCGGCAGCTAAGGCTGCTGCGAAAGCTGCGAAATACGGAGCT 1080
WT          CGTCCGGGCGTTGGTGTTGGTGGCATCCCGACCTACGGTGTAGGTGCAGGCGGTTTCCCA 1140
WT          GGTTTCGGCGTTGGTGTTGGTGGCATCCCGGGTGTAGCTGGTGTTCCGTCTGTTGGTGGC 1200
WT          GTACCGGGTGTTGGTGGCGTTCCAGGTGTAGGTATCTCCCCGGAAGCGCAGGCAGCTGCG 1260
WT          GCAGCTAAAGCAGCGAAGTACGGCGTTGGTACTCCGGCGGCAGCAGCTGCTAAAGCAGCG 1320
WT          GCTAAAGCAGCGCAGTTCGGACTAGTTCCGGGCGTAGGTGTTGCGCCAGGTGTTGGCGTA 1380
WT          GCACCGGGTGTTGGTGTTGCTCCGGGCGTAGGTCTGGCACCGGGTGTTGGCGTTGCACCA 1440
WT          GGTGTAGGTGTTGCGCCGGGCGTTGGTGTAGCACCGGGTATCGGTCCGGGTGGCGTTGCG 1500
WT          GCTGCTGCGAAATCTGCTGCGAAGGTTGCTGCGAAAGCGCAGCTGCGTGCAGCAGCTGGT 1560
WT          CTGGGTGCGGGCATCCCAGGTCTGGGTGTAGGTGTTGGTGTTCCGGGCCTGGGTGTAGGT 1620
WT          GCAGGGGTACCGGGCCTGGGTGTTGGTGCAGGCGTTCCGGGTTTCGGTGCTGTTCCGGGC 1680
WT          GCGCTGGCTGCTGCGAAAGCGGCGAAATACGGTGCAGCGGTTCCGGGTGTACTGGGCGGT 1740
WT          CTGGGTGCTCTGGGCGGTGTTGGTATCCCGGGCGGTGTTGTAGGTGCAGGCCCAGCTGCA 1800
WT          GCTGCTGCTGCGGCAAAGGCAGCGGCGAAAGCAGCTCAGTTCGGTCTGGTTGGTGCAGCA 1860
```

```
WT          GGTCTGGGCGGTCTGGGTGTTGGCGGTCTGGGTGTACCGGGCGTTGGTGGTCTGGGTGGC 1920

WT          ATCCCGCCGGCGGCGGCAGCTAAAGCGGCTAAATACGGTGCAGCAGGTCTGGGTGGCGTT 1980

WT          CTGGGTGGTGCTGGTCAGTTCCCACTGGGCGGTGTAGCGGCACGTCCGGGTTTCGGTCTG 2040

WT          TCCCCGATCTTCCCAGGCGGTGCATGCCTGGGTAAAGCTTGCGGCCGTAAACGTAAATAA 2100
```

Figure 8.1. DNA sequence of the WT tropoelastin construct.

8.2 R515A DNA sequence

```
R515A        ATGGGTGGCGTTCCGGGTGCTATCCCGGGTGGCGTTCCGGGTGGTGTATTCTACCCAGGC 60
R515A        GCGGGTCTGGGTGCACTGGGCGGTGGTGCGCTGGGCCCGGGTGGTAAACCGCTGAAACCG 120
R515A        GTTCCAGGCGGTCTGGCAGGTGCTGGTCTGGGTGCAGGTCTGGGCGCGTTCCCGGCGGTT 180
R515A        ACCTTCCCGGGTGCTCTGGTTCCGGGTGGCGTTGCAGACGCAGCTGCTGCGTACAAAGCG 240
R515A        GCAAAGGCAGGTGCGGGTCTGGGCGGGGTACCAGGTGTTGGCGGTCTGGGTGTATCTGCT 300
R515A        GGCGCAGTTGTTCCGCAGCCGGGTGCAGGTGTAAAACCGGGCAAAGTTCCAGGTGTTGGT 360
R515A        CTGCCGGGCGTATACCCGGGTGGTGTTCTGCCGGGCGCGCGTTTCCCAGGTGTTGGTGTA 420
R515A        CTGCCGGGCGTTCCGACCGGTGCAGGTGTTAAACCGAAGGCACCAGGTGTAGGCGGCGCG 480
R515A        TTCGCGGGTATCCCGGGTGTTGGCCCGTTCGGTGGTCCGCAGCCAGGCGTTCCGCTGGGT 540
R515A        TACCCGATCAAAGCGCCGAAGCTTCCAGGTGGCTACGGTCTGCCGTACACCACCGGTAAA 600
R515A        CTGCCGTACGGCTACGGTCCGGGTGGCGTAGCAGGTGCTGCGGGTAAAGCAGGCTACCCA 660
R515A        ACCGGTACTGGTGTTGGTCCGCAGGCTGCTGCGGCAGCTGCGGCGAAGGCAGCAGCAAAA 720
R515A        TTCGGCGCGGGTGCAGCGGGTGTTCTGCCGGGCGTAGGTGGTGCTGGCGTTCCGGGTGTT 780
R515A        CCAGGTGCGATCCCGGGCATCGGTGGTATCGCAGGCGTAGGTACTCCGGCGGCCGCTGCG 840
R515A        GCTGCGGCAGCTGCGGCGAAAGCAGCTAAATACGGTGCGGCAGCAGGCCTGGTTCCGGGT 900
R515A        GGTCCAGGCTTCGGTCCGGGTGTTGTAGGCGTTCCGGGTGCTGGTGTTCCGGGCGTAGGT 960
R515A        GTTCCAGGTGCGGGCATCCCGGTTGTACCGGGTGCAGGTATCCCGGGCGCTGCGGTTCCA 1020
R515A        GGTGTTGTATCCCCGGAAGCGGCAGCTAAGGCTGCTGCGAAAGCTGCGAAATACGGAGCT 1080
R515A        CGTCCGGGCGTTGGTGTTGGTGGCATCCCGACCTACGGTGTAGGTGCAGGCGGTTTCCCA 1140
R515A        GGTTTCGGCGTTGGTGTTGGTGGCATCCCGGGTGTAGCTGGTGTTCCGTCTGTTGGTGGC 1200
R515A        GTACCGGGTGTTGGTGGCGTTCCAGGTGTAGGTATCTCCCCGGAAGCGCAGGCAGCTGCG 1260
R515A        GCAGCTAAAGCAGCGAAGTACGGCGTTGGTACTCCGGCGGCAGCAGCTGCTAAAGCAGCG 1320
R515A        GCTAAAGCAGCGCAGTTCGGACTAGTTCCGGGCGTAGGTGTTGCGCCAGGTGTTGGCGTA 1380
R515A        GCACCGGGTGTTGGTGTTGCTCCGGGCGTAGGTCTGGCACCGGGTGTTGGCGTTGCACCA 1440
R515A        GGTGTAGGTGTTGCGCCGGGCGTTGGTGTAGCACCGGGTATCGGTCCGGGTGGCGTTGCG 1500
R515A        GCTGCTGCGAAATCTGCTGCGAAGGTTGCTGCGAAAGCGCAGCTG<u>**GCA**</u>GCAGCAGCTGGT 1560
R515A        CTGGGTGCGGGCATCCCAGGTCTGGGTGTAGGTGTTGGTGTTCCGGGCCTGGGTGTAGGT 1620
R515A        GCAGGGGTACCGGGCCTGGGTGTTGGTGCAGGCGTTCCGGGTTTCGGTGCTGTTCCGGGC 1680
R515A        GCGCTGGCTGCTGCGAAAGCGGCGAAATACGGTGCAGCGGTTCCGGGTGTACTGGGCGGT 1740
R515A        CTGGGTGCTCTGGGCGGTGTTGGTATCCCGGGCGGTGTTGTAGGTGCAGGCCCAGCTGCA 1800
R515A        GCTGCTGCTGCGGCAAAGGCAGCGGCGAAAGCAGCTCAGTTCGGTCTGGTTGGTGCAGCA 1860
R515A        GGTCTGGGCGGTCTGGGTGTTGGCGGTCTGGGTGTACCGGGCGTTGGTGGTCTGGGTGGC 1920
R515A        ATCCCGCCGGCGGCGGCAGCTAAAGCGGCTAAATACGGTGCAGCAGGTCTGGGTGGCGTT 1980
```

```
R515A        CTGGGTGGTGCTGGTCAGTTCCCACTGGGCGGTGTAGCGGCACGTCCGGGTTTCGGTCTG 2040

R515A        TCCCCGATCTTCCCAGGCGGTGCATGCCTGGGTAAAGCTTGCGGCCGTAAACGTAAATAA 2100
```

Figure 8.2. DNA sequence of the R515A tropoelastin construct. The underlined codon encodes the A515 residue.

8.3 E345A DNA sequence

```
E345A        ATGGGTGGCGTTCCGGGTGCTATCCCGGGTGGCGTTCCGGGTGGTGTATTCTACCCAGGC 60
E345A        GCGGGTCTGGGTGCACTGGGCGGTGGTGCGCTGGGCCCGGGTGGTAAACCGCTGAAACCG 120
E345A        GTTCCAGGCGGTCTGGCAGGTGCTGGTCTGGGTGCAGGTCTGGGCGCGTTCCCGGCGGTT 180
E345A        ACCTTCCCGGGTGCTCTGGTTCCGGGTGGCGTTGCAGACGCAGCTGCTGCGTACAAAGCG 240
E345A        GCAAAGGCAGGTGCGGGTCTGGGCGGGGTACCAGGTGTTGGCGGTCTGGGTGTATCTGCT 300
E345A        GGCGCAGTTGTTCCGCAGCCGGGTGCAGGTGTAAAACCGGGCAAAGTTCCAGGTGTTGGT 360
E345A        CTGCCGGGCGTATACCCGGGTGGTGTTCTGCCGGGCGCGCGTTTCCCAGGTGTTGGTGTA 420
E345A        CTGCCGGGCGTTCCGACCGGTGCAGGTGTTAAACCGAAGGCACCAGGTGTAGGCGGCGCG 480
E345A        TTCGCGGGTATCCCGGGTGTTGGCCCGTTCGGTGGTCCGCAGCCAGGCGTTCCGCTGGGT 540
E345A        TACCCGATCAAAGCGCCGAAGCTTCCAGGTGGCTACGGTCTGCCGTACACCACCGGTAAA 600
E345A        CTGCCGTACGGCTACGGTCCGGGTGGCGTAGCAGGTGCTGCGGGTAAAGCAGGCTACCCA 660
E345A        ACCGGTACTGGTGTTGGTCCGCAGGCTGCTGCGGCAGCTGCGGCGAAGGCAGCAGCAAAA 720
E345A        TTCGGCGCGGGTGCAGCGGGTGTTCTGCCGGGCGTAGGTGGTGCTGGCGTTCCGGGTGTT 780
E345A        CCAGGTGCGATCCCGGGCATCGGTGGTATCGCAGGCGTAGGTACTCCGGCGGCCGCTGCG 840
E345A        GCTGCGGCAGCTGCGGCGAAAGCAGCTAAATACGGTGCGGCAGCAGGCCTGGTTCCGGGT 900
E345A        GGTCCAGGCTTCGGTCCGGGTGTTGTAGGCGTTCCGGGTGCTGGTGTTCCGGGCGTAGGT 960
E345A        GTTCCAGGTGCGGGCATCCCGGTTGTACCGGGTGCAGGTATCCCGGGCGCTGCGGTTCCA 1020
E345A        GGTGTTGTATCCCCG<u>**GCA**</u>GCGGCAGCTAAGGCTGCTGCGAAAGCTGCGAAATACGGAGCT 1080
E345A        CGTCCGGGCGTTGGTGTTGGTGGCATCCCGACCTACGGTGTAGGTGCAGGCGGTTTCCCA 1140
E345A        GGTTTCGGCGTTGGTGTTGGTGGCATCCCGGGTGTAGCTGGTGTTCCGTCTGTTGGTGGC 1200
E345A        GTACCGGGTGTTGGTGGCGTTCCAGGTGTAGGTATCTCCCCGGAAGCGCAGGCAGCTGCG 1260
E345A        GCAGCTAAAGCAGCGAAGTACGGCGTTGGTACTCCGGCGGCAGCAGCTGCTAAAGCAGCG 1320
E345A        GCTAAAGCAGCGCAGTTCGGACTAGTTCCGGGCGTAGGTGTTGCGCCAGGTGTTGGCGTA 1380
E345A        GCACCGGGTGTTGGTGTTGCTCCGGGCGTAGGTCTGGCACCGGGTGTTGGCGTTGCACCA 1440
E345A        GGTGTAGGTGTTGCGCCGGGCGTTGGTGTAGCACCGGGTATCGGTCCGGGTGGCGTTGCG 1500
E345A        GCTGCTGCGAAATCTGCTGCGAAGGTTGCTGCGAAAGCGCAGCTGCGTGCAGCAGCTGGT 1560
E345A        CTGGGTGCGGGCATCCCAGGTCTGGGTGTAGGTGTTGGTGTTCCGGGCCTGGGTGTAGGT 1620
E345A        GCAGGGGTACCGGGCCTGGGTGTTGGTGCAGGCGTTCCGGGTTTCGGTGCTGTTCCGGGC 1680
E345A        GCGCTGGCTGCTGCGAAAGCGGCGAAATACGGTGCAGCGGTTCCGGGTGTACTGGGCGGT 1740
E345A        CTGGGTGCTCTGGGCGGTGTTGGTATCCCGGGCGGTGTTGTAGGTGCAGGCCCAGCTGCA 1800
E345A        GCTGCTGCTGCGGCAAAGGCAGCGGCGAAAGCAGCTCAGTTCGGTCTGGTTGGTGCAGCA 1860
E345A        GGTCTGGGCGGTCTGGGTGTTGGCGGTCTGGGTGTACCGGGCGTTGGTGGTCTGGGTGGC 1920
E345A        ATCCCGCCGGCGGCGGCAGCTAAAGCGGCTAAATACGGTGCAGCAGGTCTGGGTGGCGTT 1980
```

```
E345A        CTGGGTGGTGCTGGTCAGTTCCCACTGGGCGGTGTAGCGGCACGTCCGGGTTTCGGTCTG 2040

E345A        TCCCCGATCTTCCCAGGCGGTGCATGCCTGGGTAAAGCTTGCGGCCGTAAACGTAAATAA 2100
```

Figure 8.3. DNA sequence of the E345A tropoelastin construct. The underlined codon encodes the A345 residue.

8.4 E414A DNA sequence

```
E414A        ATGGGTGGCGTTCCGGGTGCTATCCCGGGTGGCGTTCCGGGTGGTGTATTCTACCCAGGC 60
E414A        GCGGGTCTGGGTGCACTGGGCGGTGGTGCGCTGGGCCCGGGTGGTAAACCGCTGAAACCG 120
E414A        GTTCCAGGCGGTCTGGCAGGTGCTGGTCTGGGTGCAGGTCTGGGCGCGTTCCCGGCGGTT 180
E414A        ACCTTCCCGGGTGCTCTGGTTCCGGGTGGCGTTGCAGACGCAGCTGCTGCGTACAAAGCG 240
E414A        GCAAAGGCAGGTGCGGGTCTGGGCGGGGTACCAGGTGTTGGCGGTCTGGGTGTATCTGCT 300
E414A        GGCGCAGTTGTTCCGCAGCCGGGTGCAGGTGTAAAACCGGGCAAAGTTCCAGGTGTTGGT 360
E414A        CTGCCGGGCGTATACCCGGGTGGTGTTCTGCCGGGCGCGCGTTTCCCAGGTGTTGGTGTA 420
E414A        CTGCCGGGCGTTCCGACCGGTGCAGGTGTTAAACCGAAGGCACCAGGTGTAGGCGGCGCG 480
E414A        TTCGCGGGTATCCCGGGTGTTGGCCCGTTCGGTGGTCCGCAGCCAGGCGTTCCGCTGGGT 540
E414A        TACCCGATCAAAGCGCCGAAGCTTCCAGGTGGCTACGGTCTGCCGTACACCACCGGTAAA 600
E414A        CTGCCGTACGGCTACGGTCCGGGTGGCGTAGCAGGTGCTGCGGGTAAAGCAGGCTACCCA 660
E414A        ACCGGTACTGGTGTTGGTCCGCAGGCTGCTGCGGCAGCTGCGGCGAAGGCAGCAGCAAAA 720
E414A        TTCGGCGCGGGTGCAGCGGGTGTTCTGCCGGGCGTAGGTGGTGCTGGCGTTCCGGGTGTT 780
E414A        CCAGGTGCGATCCCGGGCATCGGTGGTATCGCAGGCGTAGGTACTCCGGCGGCCGCTGCG 840
E414A        GCTGCGGCAGCTGCGGCGAAAGCAGCTAAATACGGTGCGGCAGCAGGCCTGGTTCCGGGT 900
E414A        GGTCCAGGCTTCGGTCCGGGTGTTGTAGGCGTTCCGGGTGCTGGTGTTCCGGGCGTAGGT 960
E414A        GTTCCAGGTGCGGGCATCCCGGTTGTACCGGGTGCAGGTATCCCGGGCGCTGCGGTTCCA 1020
E414A        GGTGTTGTATCCCCGGAAGCGGCAGCTAAGGCTGCTGCGAAAGCTGCGAAATACGGAGCT 1080
E414A        CGTCCGGGCGTTGGTGTTGGTGGCATCCCGACCTACGGTGTAGGTGCAGGCGGTTTCCCA 1140
E414A        GGTTTCGGCGTTGGTGTTGGTGGCATCCCGGGTGTAGCTGGTGTTCCGTCTGTTGGTGGC 1200
E414A        GTACCGGGTGTTGGTGGCGTTCCAGGTGTAGGTATCTCCCCG**GCA**GCGCAGGCAGCTGCG 1260
E414A        GCAGCTAAAGCAGCGAAGTACGGCGTTGGTACTCCGGCGGCAGCAGCTGCTAAAGCAGCG 1320
E414A        GCTAAAGCAGCGCAGTTCGGACTAGTTCCGGGCGTAGGTGTTGCGCCAGGTGTTGGCGTA 1380
E414A        GCACCGGGTGTTGGTGTTGCTCCGGGCGTAGGTCTGGCACCGGGTGTTGGCGTTGCACCA 1440
E414A        GGTGTAGGTGTTGCGCCGGGCGTTGGTGTAGCACCGGGTATCGGTCCGGGTGGCGTTGCG 1500
E414A        GCTGCTGCGAAATCTGCTGCGAAGGTTGCTGCGAAAGCGCAGCTGCGTGCAGCAGCTGGT 1560
E414A        CTGGGTGCGGGCATCCCAGGTCTGGGTGTAGGTGTTGGTGTTCCGGGCCTGGGTGTAGGT 1620
E414A        GCAGGGGTACCGGGCCTGGGTGTTGGTGCAGGCGTTCCGGGTTTCGGTGCTGTTCCGGGC 1680
E414A        GCGCTGGCTGCTGCGAAAGCGGCGAAATACGGTGCAGCGGTTCCGGGTGTACTGGGCGGT 1740
E414A        CTGGGTGCTCTGGGCGGTGTTGGTATCCCGGGCGGTGTTGTAGGTGCAGGCCCAGCTGCA 1800
E414A        GCTGCTGCTGCGGCAAAGGCAGCGGCGAAAGCAGCTCAGTTCGGTCTGGTTGGTGCAGCA 1860
E414A        GGTCTGGGCGGTCTGGGTGTTGGCGGTCTGGGTGTACCGGGCGTTGGTGGTCTGGGTGGC 1920
E414A        ATCCCGCCGGCGGCGGCAGCTAAAGCGGCTAAATACGGTGCAGCAGGTCTGGGTGGCGTT 1980
```

```
E414A        CTGGGTGGTGCTGGTCAGTTCCCACTGGGCGGTGTAGCGGCACGTCCGGGTTTCGGTCTG 2040

E414A        TCCCCGATCTTCCCAGGCGGTGCATGCCTGGGTAAAGCTTGCGGCCGTAAACGTAAATAA 2100
```

Figure 8.4. DNA sequence of the E414A tropoelastin construct. The underlined codon encodes the A414 residue.

8.5 E345A+E414A DNA sequence

```
E345A+E414A    ATGGGTGGCGTTCCGGGTGCTATCCCGGGTGGCGTTCCGGGTGGTGTATTCTACCCAGGC 60
E345A+E414A    GCGGGTCTGGGTGCACTGGGCGGTGGTGCGCTGGGCCCGGGTGGTAAACCGCTGAAACCG 120
E345A+E414A    GTTCCAGGCGGTCTGGCAGGTGCTGGTCTGGGTGCAGGTCTGGGCGCGTTCCCGGCGGTT 180
E345A+E414A    ACCTTCCCGGGTGCTCTGGTTCCGGGTGGCGTTGCAGACGCAGCTGCTGCGTACAAAGCG 240
E345A+E414A    GCAAAGGCAGGTGCGGGTCTGGGCGGGGTACCAGGTGTTGGCGGTCTGGGTGTATCTGCT 300
E345A+E414A    GGCGCAGTTGTTCCGCAGCCGGGTGCAGGTGTAAAACCGGGCAAAGTTCCAGGTGTTGGT 360
E345A+E414A    CTGCCGGGCGTATACCCGGGTGGTGTTCTGCCGGGCGCGCGTTTCCCAGGTGTTGGTGTA 420
E345A+E414A    CTGCCGGGCGTTCCGACCGGTGCAGGTGTTAAACCGAAGGCACCAGGTGTAGGCGGCGCG 480
E345A+E414A    TTCGCGGGTATCCCGGGTGTTGGCCCGTTCGGTGGTCCGCAGCCAGGCGTTCCGCTGGGT 540
E345A+E414A    TACCCGATCAAAGCGCCGAAGCTTCCAGGTGGCTACGGTCTGCCGTACACCACCGGTAAA 600
E345A+E414A    CTGCCGTACGGCTACGGTCCGGGTGGCGTAGCAGGTGCTGCGGGTAAAGCAGGCTACCCA 660
E345A+E414A    ACCGGTACTGGTGTTGGTCCGCAGGCTGCTGCGGCAGCTGCGGCGAAGGCAGCAGCAAAA 720
E345A+E414A    TTCGGCGCGGGTGCAGCGGGTGTTCTGCCGGGCGTAGGTGGTGCTGGCGTTCCGGGTGTT 780
E345A+E414A    CCAGGTGCGATCCCGGGCATCGGTGGTATCGCAGGCGTAGGTACTCCGGCGGCCGCTGCG 840
E345A+E414A    GCTGCGGCAGCTGCGGCGAAAGCAGCTAAATACGGTGCGGCAGCAGGCCTGGTTCCGGGT 900
E345A+E414A    GGTCCAGGCTTCGGTCCGGGTGTTGTAGGCGTTCCGGGTGCTGGTGTTCCGGGCGTAGGT 960
E345A+E414A    GTTCCAGGTGCGGGCATCCCGGTTGTACCGGGTGCAGGTATCCCGGGCGCTGCGGTTCCA 1020
E345A+E414A    GGTGTTGTATCCCCG<u>**GCA**</u>GCGGCAGCTAAGGCTGCTGCGAAAGCTGCGAAATACGGAGCT 1080
E345A+E414A    CGTCCGGGCGTTGGTGTTGGTGGCATCCCGACCTACGGTGTAGGTGCAGGCGGTTTCCCA 1140
E345A+E414A    GGTTTCGGCGTTGGTGTTGGTGGCATCCCGGGTGTAGCTGGTGTTCCGTCTGTTGGTGGC 1200
E345A+E414A    GTACCGGGTGTTGGTGGCGTTCCAGGTGTAGGTATCTCCCCG<u>**GCA**</u>GCGCAGGCAGCTGCG 1260
E345A+E414A    GCAGCTAAAGCAGCGAAGTACGGCGTTGGTACTCCGGCGGCAGCAGCTGCTAAAGCAGCG 1320
E345A+E414A    GCTAAAGCAGCGCAGTTCGGACTAGTTCCGGGCGTAGGTGTTGCGCCAGGTGTTGGCGTA 1380
E345A+E414A    GCACCGGGTGTTGGTGTTGCTCCGGGCGTAGGTCTGGCACCGGGTGTTGGCGTTGCACCA 1440
E345A+E414A    GGTGTAGGTGTTGCGCCGGGCGTTGGTGTAGCACCGGGTATCGGTCCGGGTGGCGTTGCG 1500
E345A+E414A    GCTGCTGCGAAATCTGCTGCGAAGGTTGCTGCGAAAGCGCAGCTGCGTGCAGCAGCTGGT 1560
E345A+E414A    CTGGGTGCGGGCATCCCAGGTCTGGGTGTAGGTGTTGGTGTTCCGGGCCTGGGTGTAGGT 1620
E345A+E414A    GCAGGGGTACCGGGCCTGGGTGTTGGTGCAGGCGTTCCGGGTTTCGGTGCTGTTCCGGGC 1680
E345A+E414A    GCGCTGGCTGCTGCGAAAGCGGCGAAATACGGTGCAGCGGTTCCGGGTGTACTGGGCGGT 1740
E345A+E414A    CTGGGTGCTCTGGGCGGTGTTGGTATCCCGGGCGGTGTTGTAGGTGCAGGCCCAGCTGCA 1800
E345A+E414A    GCTGCTGCTGCGGCAAAGGCAGCGGCGAAAGCAGCTCAGTTCGGTCTGGTTGGTGCAGCA 1860
E345A+E414A    GGTCTGGGCGGTCTGGGTGTTGGCGGTCTGGGTGTACCGGGCGTTGGTGGTCTGGGTGGC 1920
E345A+E414A    ATCCCGCCGGCGGCGGCAGCTAAAGCGGCTAAATACGGTGCAGCAGGTCTGGGTGGCGTT 1980
```

```
E345A+E414A    CTGGGTGGTGCTGGTCAGTTCCCACTGGGCGGTGTAGCGGCACGTCCGGGTTTCGGTCTG 2040

E345A+E414A    TCCCCGATCTTCCCAGGCGGTGCATGCCTGGGTAAAGCTTGCGGCCGTAAACGTAAATAA 2100
```

Figure 8.5. DNA sequence of the E345A+E414A tropoelastin construct. The underlined codons encode the A345 and A414 residues.

8.6 EX22 DNA sequence

EX22	ATGGGTGGCGTTCCGGGTGCTATCCCGGGTGGCGTTCCGGGTGGTGTATTCTACCCAGGC	60
EX22	GCGGGTCTGGGTGCACTGGGCGGTGGTGCGCTGGGCCCGGGTGGTAAACCGCTGAAACCG	120
EX22	GTTCCAGGCGGTCTGGCAGGTGCTGGTCTGGGTGCAGGTCTGGGCGCGTTCCCGGCGGTT	180
EX22	ACCTTCCCGGGTGCTCTGGTTCCGGGTGGCGTTGCAGACGCAGCTGCTGCGTACAAAGCG	240
EX22	GCAAAGGCAGGTGCGGGTCTGGGCGGGGTACCAGGTGTTGGCGGTCTGGGTGTATCTGCT	300
EX22	GGCGCAGTTGTTCCGCAGCCGGGTGCAGGTGTAAAACCGGGCAAAGTTCCAGGTGTTGGT	360
EX22	CTGCCGGGCGTATACCCGGGTGGTGTTCTGCCGGGCGCGCGTTTCCCAGGTGTTGGTGTA	420
EX22	CTGCCGGGCGTTCCGACCGGTGCAGGTGTTAAACCGAAGGCACCAGGTGTAGGCGGCGCG	480
EX22	TTCGCGGGTATCCCGGGTGTTGGCCCGTTCGGTGGTCCGCAGCCAGGCGTTCCGCTGGGT	540
EX22	TACCCGATCAAAGCGCCGAAGCTTCCAGGTGGCTACGGTCTGCCGTACACCACCGGTAAA	600
EX22	CTGCCGTACGGCTACGGTCCGGGTGGCGTAGCAGGTGCTGCGGGTAAAGCAGGCTACCCA	660
EX22	ACCGGTACTGGTGTTGGTCCGCAGGCTGCTGCGGCAGCTGCGGCGAAGGCAGCAGCAAAA	720
EX22	TTCGGCGCGGGTGCAGCGGGTGTTCTGCCGGGCGTAGGTGGTGCTGGCGTTCCGGGTGTT	780
EX22	CCAGGTGCGATCCCGGGCATCGGTGGTATCGCAGGCGTAGGTACTCCGGCGGCCGCTGCG	840
EX22	GCTGCGGCAGCTGCGGCGAAAGCAGCTAAATACGGTGCGGCAGCAGGCCTGGTTCCGGGT	900
EX22	GGTCCAGGCTTCGGTCCGGGTGTTGTAGGCGTTCCGGGTGCTGGTGTTCCGGGCGTAGGT	960
EX22	GTTCCAGGTGCGGGCATCCCGGTTGTACCGGGTGCAGGTATCCCGGGCGCTGCGGTTCCA	1020
EX22	GGTGTTGTATCCCCGGAAGCGGCAGCTAAGGCTGCTGCGAAAGCTGCGAAATACGGAGCT	1080
EX22	CGTCCGGGCGTTGGTGTTGGTGGCATCCCGACCTACGGTGTAGGTGCAGGCGGTTTCCCA	1140
EX22	GGTTTCGGCGTTGGTGTTGGTGGCATCCCGGGTGTAGCTGGTGTTCCGTCTGTTGGTGGC	1200
EX22	GTACCGGGTGTTGGTGGCGTTCCAGGTGTAGGTATCTCCCCGGAAGCGCAGGCAGCTGCG	1260
EX22	GCAGCTAAAGCAGCGAAGTAC**GGTGCGGCGGGTGCGGGTGTTCTGGGTGGCCTGGTTCCG**	1320
EX22	**GGTGCGCCGGGCGCGGTTCCGGGTGTGCCGGGTACCGGCGGTGTTCCG**GGCGTTGGTACT	1380
EX22	CCGGCGGCAGCAGCTGCTAAAGCAGCGGCTAAAGCAGCGCAGTTCGGACTAGTTCCGGGC	1440
EX22	GTAGGTGTTGCGCCAGGTGTTGGCGTAGCACCGGGTGTTGGTGTTGCTCCGGGCGTAGGT	1500
EX22	CTGGCACCGGGTGTTGGCGTTGCACCAGGTGTAGGTGTTGCGCCGGGCGTTGGTGTAGCA	1560
EX22	CCGGGTATCGGTCCGGGTGGCGTTGCGGCTGCTGCGAAATCTGCTGCGAAGGTTGCTGCG	1620
EX22	AAAGCGCAGCTGCGTGCAGCAGCTGGTCTGGGTGCGGGCATCCCAGGTCTGGGTGTAGGT	1680
EX22	GTTGGTGTTCCGGGCCTGGGTGTAGGTGCAGGGGTACCGGGCCTGGGTGTTGGTGCAGGC	1740
EX22	GTTCCGGGTTTCGGTGCTGTTCCGGGCGCGCTGGCTGCTGCGAAAGCGGCGAAATACGGT	1800
EX22	GCAGCGGTTCCGGGTGTACTGGGCGGTCTGGGTGCTCTGGGCGGTGTTGGTATCCCGGGC	1860
EX22	GGTGTTGTAGGTGCAGGCCCAGCTGCAGCTGCTGCTGCGGCAAAGGCAGCGGCGAAAGCA	1920
EX22	GCTCAGTTCGGTCTGGTTGGTGCAGCAGGTCTGGGCGGTCTGGGTGTTGGCGGTCTGGGT	1980

```
EX22            GTACCGGGCGTTGGTGGTCTGGGTGGCATCCCGCCGGCGGCGGCAGCTAAAGCGGCTAAA 2040
EX22            TACGGTGCAGCAGGTCTGGGTGGCGTTCTGGGTGGTGCTGGTCAGTTCCCACTGGGCGGT 2100
EX22            GTAGCGGCACGTCCGGGTTTCGGTCTGTCCCCGATCTTCCCAGGCGGTGCATGCCTGGGT 2160
EX22            AAAGCTTGCGGCCGTAAACGTAAATAA                                   2187
```

Figure 8.6. DNA sequence of the EX22 tropoelastin construct. Exon 22 is underlined.

8.7 D72A DNA sequence

```
D72A            ATGGGTGGCGTTCCGGGTGCTATCCCGGGTGGCGTTCCGGGTGGTGTATTCTACCCAGGC 60
D72A            GCGGGTCTGGGTGCACTGGGCGGTGGTGCGCTGGGCCCGGGTGGTAAACCGCTGAAACCG 120
D72A            GTTCCAGGCGGTCTGGCAGGTGCTGGTCTGGGTGCAGGTCTGGGCGCGTTCCCGGCGGTT 180
D72A            ACCTTCCCGGGTGCTCTGGTTCCGGGTGGCGTTGCAGCAGCAGCTGCTGCGTACAAAGCG 240
D72A            GCAAAGGCAGGTGCGGGTCTGGGCGGGGTACCAGGTGTTGGCGGTCTGGGTGTATCTGCT 300
D72A            GGCGCAGTTGTTCCGCAGCCGGGTGCAGGTGTAAAACCGGGCAAAGTTCCAGGTGTTGGT 360
D72A            CTGCCGGGCGTATACCCGGGTGGTGTTCTGCCGGGCGCGCGTTTCCCAGGTGTTGGTGTA 420
D72A            CTGCCGGGCGTTCCGACCGGTGCAGGTGTTAAACCGAAGGCACCAGGTGTAGGCGGCGCG 480
D72A            TTCGCGGGTATCCCGGGTGTTGGCCCGTTCGGTGGTCCGCAGCCAGGCGTTCCGCTGGGT 540
D72A            TACCCGATCAAAGCGCCGAAGCTTCCAGGTGGCTACGGTCTGCCGTACACCACCGGTAAA 600
D72A            CTGCCGTACGGCTACGGTCCGGGTGGCGTAGCAGGTGCTGCGGGTAAAGCAGGCTACCCA 660
D72A            ACCGGTACTGGTGTTGGTCCGCAGGCTGCTGCGGCAGCTGCGGCGAAGGCAGCAGCAAAA 720
D72A            TTCGGCGCGGGTGCAGCGGGTGTTCTGCCGGGCGTAGGTGGTGCTGGCGTTCCGGGTGTT 780
D72A            CCAGGTGCGATCCCGGGCATCGGTGGTATCGCAGGCGTAGGTACTCCGGCGGCCGCTGCG 840
D72A            GCTGCGGCAGCTGCGGCGAAAGCAGCTAAATACGGTGCGGCAGCAGGCCTGGTTCCGGGT 900
D72A            GGTCCAGGCTTCGGTCCGGGTGTTGTAGGCGTTCCGGGTGCTGGTGTTCCGGGCGTAGGT 960
D72A            GTTCCAGGTGCGGGCATCCCGGTTGTACCGGGTGCAGGTATCCCGGGCGCTGCGGTTCCA 1020
D72A            GGTGTTGTATCCCCGGAAGCGGCAGCTAAGGCTGCTGCGAAAGCTGCGAAATACGGAGCT 1080
D72A            CGTCCGGGCGTTGGTGTTGGTGGCATCCCGACCTACGGTGTAGGTGCAGGCGGTTTCCCA 1140
D72A            GGTTTCGGCGTTGGTGTTGGTGGCATCCCGGGTGTAGCTGGTGTTCCGTCTGTTGGTGGC 1200
D72A            GTACCGGGTGTTGGTGGCGTTCCAGGTGTAGGTATCTCCCCGGAAGCGCAGGCAGCTGCG 1260
D72A            GCAGCTAAAGCAGCGAAGTACGGCGTTGGTACTCCGGCGGCAGCAGCTGCTAAAGCAGCG 1320
D72A            GCTAAAGCAGCGCAGTTCGGACTAGTTCCGGGCGTAGGTGTTGCGCCAGGTGTTGGCGTA 1380
D72A            GCACCGGGTGTTGGTGTTGCTCCGGGCGTAGGTCTGGCACCGGGTGTTGGCGTTGCACCA 1440
D72A            GGTGTAGGTGTTGCGCCGGGCGTTGGTGTAGCACCGGGTATCGGTCCGGGTGGCGTTGCG 1500
D72A            GCTGCTGCGAAATCTGCTGCGAAGGTTGCTGCGAAAGCGCAGCTGCGTGCAGCAGCTGGT 1560
D72A            CTGGGTGCGGGCATCCCAGGTCTGGGTGTAGGTGTTGGTGTTCCGGGCCTGGGTGTAGGT 1620
D72A            GCAGGGGTACCGGGCCTGGGTGTTGGTGCAGGCGTTCCGGGTTTCGGTGCTGTTCCGGGC 1680
D72A            GCGCTGGCTGCTGCGAAAGCGGCGAAATACGGTGCAGCGGTTCCGGGTGTACTGGGCGGT 1740
D72A            CTGGGTGCTCTGGGCGGTGTTGGTATCCCGGGCGGTGTTGTAGGTGCAGGCCCAGCTGCA 1800
D72A            GCTGCTGCTGCGGCAAAGGCAGCGGCGAAAGCAGCTCAGTTCGGTCTGGTTGGTGCAGCA 1860
D72A            GGTCTGGGCGGTCTGGGTGTTGGCGGTCTGGGTGTACCGGGCGTTGGTGGTCTGGGTGGC 1920
D72A            ATCCCGCCGGCGGCGGCAGCTAAAGCGGCTAAATACGGTGCAGCAGGTCTGGGTGGCGTT 1980
```

```
D72A            CTGGGTGGTGCTGGTCAGTTCCCACTGGGCGGTGTAGCGGCACGTCCGGGTTTCGGTCTG 2040

D72A            TCCCCGATCTTCCCAGGCGGTGCATGCCTGGGTAAAGCTTGCGGCCGTAAACGTAAATAA 2100
```

Figure 8.7. DNA sequence of the D72A tropoelastin construct. The underlined codon encodes the A72 residue.

References

[1] Mithieux SM, Weiss AS. Elastin. Advances in Protein Chemistry: Academic Press; 2005. p. 437-61.

[2] Patel A, Fine B, Sandig M, Mequanint K. Elastin biosynthesis: The missing link in tissue-engineered blood vessels. Cardiovascular Research 2006;71:40-9.

[3] Kozel BA, Rongish BJ, Czirol A, Zach J, Little CD, Davis EC, et al. Elastic fiber formation: A dynamic view of extracellular matrix assembly using timer reporters. Journal of Cellular Physiology 2006;207:87-96.

[4] Vrhovski B, Weiss AS. Biochemistry of tropoelastin. European Journal of Biochemistry 1998;258:1-18.

[5] Fukuda Y, Nakazawa N, Yamanaka N. Interactions of elastin and microfibrils in elastogenesis of human pulmonary fibroblasts in culture. Connective Tissue Research 1993;29:301-10.

[6] Kielty CM, Sherratt MJ, Shuttleworth CA. Elastic fibres. Journal of Cell Science 2002;115:2817-28.

[7] Wise SG, Weiss AS. Tropoelastin. International Journal of Biochemistry & Cell Biology 2009;41:494-7.

[8] Ronchetti IP, Baccarani-Contri M, Fornieri C, Mori G, Quaglino D. Structure and composition of the elastin fibre in normal and pathological conditions. Micron 1993;24:75-89.

[9] Ross R, Bornstein P. The elastic fiber I. The separation and partial characterization of its macromolecular components. The Journal of Cell Biology 1969;40:366-81.

[10] Jacob MP, Hornebeck W. Isolation and characterization of insoluble and kappa-elastins. Frontiers in Matrix Biology 1985;10:92-129.

[11] Clarke AW, Arnspang EC, Mithieux SM, Korkmaz E, Braet F, Weiss AS. Tropoelastin massively associates during coacervation to form quantized protein spheres. Biochemistry 2006;45:9989-96.

[12] Hirai M, Ohbayashi T, Horiguchi M, Okawa K, Hagiwara A, Chien KR, et al. Fibulin-5/DANCE has an elastogenic organizer activity that is abrogated by proteolytic cleavage in vivo. The Journal of Cell Biology 2007;176:1061-71.

[13] Ronchetti IP, Baccarani-Contri M. Elastic fiber during development and aging. Microscopy Research and Technique 1997;38:428-35.

[14] Gotte L, Giro MG, Volphin D, Horne RW. The ultrastructural organization of elastin. Journal of Ultrastructure Research 1974;46.

[15] Milewicz DM, Urban Z, Boyd C. Genetic disorders of the elastic fiber system. Matrix Biology 2000;19:471-80.

[16] Li DY, Brooke B, Davis EC, Mecham RP, Sorensen LK, Boak BB, et al. Elastin is an essential determinant of arterial morphogenesis. Nature 1998;393:276-80.

[17] Pezet M, Jacob MP, Escoubet B, Gheduzzi D, Tillet E, Perret P, et al. Elastin haploinsufficiency induces alternative aging processes in the aorta. Rejuvenation Research 2008;11:97-112.

[18] Rodgers UR, Weiss AS. Cellular interactions with elastin. Pathologie Biologie 2005;53:390-8.

[19] Bisaccia F, Castiglione-Morelli MA, De Biasi M, Traniello S, Spisani S, Tamburro AM. Migration of monocytes in the presence of elastolytic fragments of elastin and in synthetic derivates. Structure-activity relationships. International Journal of Peptide Protein Research 1994;44:332-41.

[20] Mithieux SM, Rasko JEJ, Weiss AS. Synthetic elastin hydrogels derived from massive elastic assemblies of self-organized human protein monomers. Biomaterials 2004;25:4921-7.

[21] Bashir MM, Indik Z, Yeh HS, Ornstein-Goldstein N, Rosenbloom J, Abrams WR, et al. Characterization of the complete human elastin gene. The Journal of Biological Chemistry 1989;264:8887-91.

[22] Sage H, Gray WR. Studies on the evolution of elastin. I. Phylogenetic distribution. Comparative Biochemistry and Physiology B: Comparative Biochemistry 1979;64:313-27.

[23] Fazio M, M. M, Passage E, Chu M, Black D, Solomon E, et al. Human elastin gene: new evidence for localisation to the long arm of chromosome 7. American Journal of Human Genetics 1991;48:696-703.

[24] Indik Z, Yeh H, Ornstein-Goldstein N. Alternative splicing of human elastin mRNA indicated by sequence analysis of cloned genomic and complementary DNA. Proceedings of the National Academy of Sciences USA 1987;84:5680-4.

[25] Rosenbloom J, Abrams WR, Indik Z, Yeh HS, Ornstein-Goldstein N, Bashir MM. Structure of the elastin gene. CIBA Foundation Symposium 1995;192:59-80.

[26] Martin SL, Vrhovski B, Weiss AS. Total synthesis and expression in Escherichia coli of a gene encoding human tropoelastin. Gene 1995;154:159-66.

[27] Cicila G, May M, Ornstein-Goldstein N, Indik Z, Morrow S, Yeh HS, et al. Structure of the 3' portion of the bovine elastin gene. Biochemistry 1985;24:3075-80.

[28] Debelle L, Tamburro AM. Elastin: molecular description and function. The International Journal of Biochemistry & Cell Biology 1999;31:261-72.

[29] Holzenberger M, Levi-Minzi SA, Herzog CP, Deak S, Robert L, Boyd C. Quantitation of tropoelastin mRNA and assessment of alternative splicing in human skin fibroblasts by reverse transcriptase-polymerase chain reaction. PCR Methods and Applications 1993;3:107-14.

[30] Sato F, Wachi H, Starcher BC, Murata H, Amano S, Tajima S, et al. The characteristics of elastic fiber assembled with recombinant tropoelastin isoform. Clinical Biochemistry 2006;39:746-53.

[31] Fazio M, Olsen DR, Kauh EA, Baldwin CT, Indik Z, Ornstein-Goldstein N, et al. Cloning of full-length elastin cDNAs from a human skin fibroblast recombinant cDNA library: Further elucidation of alternative splicing utlizing exon-specific oligonucleotides. Journal of Investigative Dermatology 1988;91:458-64.

[32] Hirano E, Knutsen RH, Sugitani H, Ciliberto CH, Mecham RP. Functional rescue of elastin insufficiency in mice by the human elastin gene - Implications for mouse models of human disease. CircRes 2007;101:523-31.

[33] Sugitani H, Hirano E, Knutsen RH, Shifren A, Wagenseil JE, Ciliberto C, et al. Alternative splicing and tissue-specific elastin misassembly act as biological modifiers of human elastin gene frame shift mutations associated with dominant cutis laxa. Journal of Biological Chemistry 2012.

[34] Urban Z, Agapova O, Hucthagowder V, Yang P, Starcher BC, Hernandez MR. Population differences in elastin maturation in optic nerve head tissue and astrocytes. Investigative Ophthalmology & Visual Science 2007;48:3209-15.

[35] Megarbane H, Florence J, Sass JO, Schwonbeck S, Foglio M, de Cid R, et al. An autosomal-recessive form of cutis laxa is due to homozygous elastin mutations, and the phenotype may be modified by a heterozygous fibulin 5 polymorphism. Journal of Investigative Dermatology 2009;129:1650-5.

[36] Heinz A, Jung MC, Jahreis G, Rusciani A, Duca L, Debelle L, et al. The action of neutrophil serine proteases on elastin and its precursor. Biochimie 2012;94:192-202.

[37] Lipta MJ, Bolney MD, Mecham RP, Rosenbloom J, Cooper L, Kaiser LR. The detection of a unique isoform of elastin in human hypertensive pulmonary arteries. Surgical Forum 1991;42:287-9.

[38] Barrineau LL, Rich CB, Przybyla A, Foster JA. Differential expression of aortic and lung elastin genes during chick embryogenesis. Developmental Biology 1981;87:46-51.

[39] Parks WC, Roby JD, Wu LC, Grosso LE. Cellular expression of tropoelastin mRNA splice variants. Matrix 1992;12:156-62.

[40] Rich CB, Foster JA. Characterization of rat heart tropoelastin. Archives of Biochemistry and Biophysics 1989;268.

[41] Song HY, Parkinson J. Modelling the self-assembly of elastomeric proteins provides insights into the evolution of their domain architectures. Plos Computational Biology 2012;8.

[42] Lee J, Macosko CW, Urry DW. Elastomeric polypentapeptides cross-linked into matrixes and fibers. Biomacromolecules 2001;2:170-9.

[43] Kielty CM. Elastic fibres in health and disease. Expert reviews in molecular medicine 2006;8:1-23.

[44] Dyksterhuis LB, Baldock C, Lammie D, Wess TJ, Weiss AS. Domains 17-27 of tropoelastin contain key regions of contact for coacervation and contain an unusual turn-containing crosslinking domain. Matrix Biology 2007;26:125-35.

[45] Broekelmann TJ, Kozel BA, Ishibashi H, Werneck CC, Keeley Fred W, Zhang L, et al. Tropoelastin interacts with cell-surface glycosaminoglycans via its COOH-terminal domain. The Journal of Biological Chemistry 2005;280:40939-47.

[46] Mecham RP. Trypsin-like neutral protease associated with soluble elastin. Biochemistry 1977;16:3825-31.

[47] He D, Chung M, Chan E, Alleyne T, Ha KCH, Miao M, et al. Comparative genomics of elastin: Sequence analysis of a highly repetitive protein. Matrix Biology 2007;26:524-40.

[48] Wachi H, Seyama Y, Yamashita S, Suganami H, Uemura Y, Okamoto K, et al. Stimulation of cell proliferation and autoregulation of elastin expression by elastin peptide VPGVG in cultured chick vascular smooth muscle cells. FEBS Letters 1995;368:215-9.

[49] Chung MIS, Ming M, Stahl RJ, Chan E, Parkinson J, Keeley FW. Sequences and domain structures of mammalian, avian, amphibian and teleost tropoelastins: Clues to the evolutionary history of elastins. Matrix Biology 2006;25:492-504.

[50] Brown PL, Mecham L, Tisdale C, Mecham RP. The cysteine residues in the carboxy terminal domain of tropoelastin form an intrachain disulfide bond that stabilizes a loop structure and positively charged pocket. Biochemical and Biophysical Research Communications 1992;186:549-55.

[51] Floquet N, Pepe A, Dauchez M, Bochicchio B, Tamburro AM, Alix AJP. Structure and modeling studies of the carboxy-terminus region of human tropoelastin. Matrix Biology 2005;24:271-82.

[52] Mammi M, Gotte L, Pezzin G. Evidence for order in the structure of alpha-elastin. Nature 1968;220:371-3.

[53] Lyerla JR, Torchia DA. Molecular mobility and structure of elasitn deducted from the solvent and temperature dependence of ^{13}C magnetic resonance relaxation data. Biochemistry 1975;14:5175-83.

[54] Muiznieks LD, Weiss AS. Flexibility in the solution structure of human tropoelastin. Biochemistry 2007;46:8196-205.

[55] He D, Miao M, Sitarz EE, Muiznieks LD, Reichheld S, Stahl RJ, et al. Polymorphisms in the human tropoelastin gene modify *in vitro* self-assembly and mechanical properties of elastin-like polypeptides. PLoS ONE 2012;7:e46130.

[56] Rauscher S, Baud S, Miao M, Keeley Fred W, Pomès R. Proline and glycine control protein self-organization into elastomeric or amyloid fibrils. Structure 2006;14:1667-76.

[57] Villani V, Tamburro AM. Conformational chaos of an elastin-related peptide in aqueous solution. Annals of the New York Academy of Sciences 1999;879:284-7.

[58] Bochicchio B, Pepe A. Role of polyproline II conformation in human tropoelastin structure. Chirality 2011;23:694-702.

[59] Martino M, Coviello A, Tamburro AM. Synthesis and structural characterization of poly(LGGVG), an elastin-like polypeptide. International Journal of Biological Macromolecules 2000;27:59-64.

[60] Tamburro AM, Guantieri V, Gordini DD. Synthesis and structural studies of a pentapeptide sequence of elastin. Poly (Val-Gly-Gly-Leu-Gly). Journal of Biomolecular Structure and Dynamics 1992;10:441-54.

[61] Muiznieks LD, Keeley F. Proline periodicity modulates the self-assembly properties of elastin-like polypeptides. Journal of Biological Chemistry 2010;285:39779-89.

[62] Miao M, Bellingham CM, Stahl RJ, Sitarz EE, Lane CJ, Keeley FW. Sequence and structure determinants for the self-aggregation of recombinant polypeptides modeled after human elastin. Journal of Biological Chemistry 2003;278:48553-62.

[63] Tamburro AM, Bochicchio B, Pepe A. The dissection of human tropoelastin: from the molecular structure to the self-assembly to the elasticity mechanism. Pathologie Biologie 2005;53:383-9.

[64] Pepe A, Guerra D, Bochicchio B, Quaglino D, Gheduzzi D, Pasquali Ronchetti I, et al. Dissection of human tropoelastin: Supramolecular organization of polypeptide sequences coded by particular exons. Matrix Biology 2005;24:96-109.

[65] Maeda I, Fukumoto Y, Nose T, Shimohigashi Y, Nezu T, Terada Y, et al. Structural requirements essential for elastin coacervation: favorable spatial arrangements of valine ridges on the three-dimensional structure of elastin-derived polypeptide (VPGVG)n. J Pept Sci 2011;17:735-43.

[66] Muiznieks LD, Weiss AS, Keeley FW. Structural disorder and dynamics of elastin. Biochemistry and Cell Biology 2010;88:239-50.

[67] Muiznieks LD, Jensen SA, Weiss AS. Structural changes and facilitated association of tropoelastin. Archives of Biochemistry and Biophysics 2003;410:317-23.

[68] Rucker RB, Goettlich-Riemann W, Tom K. Properties of chick tropoelastin. Biochimica et Biophysica Acta 1973;317:193-211.

[69] Tamburro AM, Bochicchio B, Pepe A. Dissection of human tropoelastin: Exon-by-exon chemical synthesis and related conformational studies. Biochemistry 2003;42:13347-62.

[70] Jensen SA, Vrhovski B, Weiss AS. Domain 26 of tropoelastin plays a dominant role in association by coacervation. J Biol Chem 2000;275:28449-54.

[71] Gosline JM, Yew FF, Weisfogh T. Reversible structural changes in a hydrophobic protein, elastin, as indicated by fluorescence probe analysis. Biopolymers 1975;14:1811-26.

[72] Baldock C, Oberhauser AF, Ma L, Lammie D, Siegler V, Mithieux SM, et al. Shape of tropoelastin, the highly extensible protein that controls human tissue elasticity. Proceedings of the National Academy of Sciences 2011;108:4322-7.

[73] Djajamuliadi J, Kagawa TF, Ohgo K, Kumashiro KK. Insights into a putative hinge region in elastin using molecular dynamics simulations. Matrix Biology 2009;28:92-100.

[74] Miao M, Cirulis JT, Lee S, Keeley FW. Structural determinants of cross-linking and hydrophobic domains for self-assembly of elastin-like polypeptides. Biochemistry 2005;44:14367-75.

[75] Tamburro AM, Pepe A, Bochicchio B. Localizing alpha-helices in human tropoelastin: Assembly of the elastin "puzzle". Biochemistry 2006;45:9518-30.

[76] Hoeve CA, Flory PJ. The elastic properties of elastin. Biopolymers 1974;13:677-86.

[77] Rauscher S, Pomes R. Molecular simulations of protein disorder. Biochemistry and Cell Biology 2010;88:269-90.

[78] Rauscher S, Pomes R. Structural disorder and protein elasticity. Advances in Experimental Medicine and Biology 2012;725:159-83.

[79] Werth VP, Williams KJ, Fisher EA, Bashir M, Rosenbloom J, Shi XM. UVB irradiation alters cellular responses to cytokines: Role in extracellular matrix gene expression. Journal of Investigative Dermatology 1997;108:290-4.

[80] Mecham RP. Elastin synthesis and fiber assembly. Annals of the New York Academy of Sciences 1991;624:137-46.

[81] Davidson J, Giro MG, Sutcliffe M, Zoia O, Quaglino D, Liu JM, et al. Regulation of elastin synthesis. In: Tamburro AM, Davidson J, editors. Elastin: chemical and biological aspects. Galatina, Italy: Congedo Editore; 1990.

[82] Zhang J, Wu L, Qu JM, Bai CX, Merrilees MJ, Black PN. Pro-inflammatory phenotype of COPD fibroblasts not compatible with repair in COPD lung. Journal of Cellular and Molecular Medicine 2012;16:1522-32.

[83] Akhtart K, Broekelnnann TJ, Song HW, Turk J, Brett TJ, Mecham RP, et al. Oxidative modifications of the C-terminal domain of tropoelastin prevent cell binding. Journal of Biological Chemistry 2011;286:13574-82.

[84] Grosso LE, Mecham RP. In vitro processing of tropoelastin: Investigation of a possible transport function associated with the carboxy-terminal domain. Biochemical and Biophysical Research Communications 1988;151:822-6.

[85] Saunders NA, Grant ME. Elastin biosynthesis in chick-embryo arteries. Studies on the intracellular site of synthesis of tropoelastin. Biochemical Journal 1984;221:393-400.

[86] Hinek A, Rabinovitch M. 67-kD elastin binding protein is a protective companion of extracellular insoluble elastin and intracellular tropoelastin. J Cell Biol 1994;126:563-74.

[87] Davis EC, Mecham RP. Selective degradation of accumulated secretory proteins in the endoplasmic reticulum - A possible clearance pathway for abnormal tropoelastin. Journal of Biological Chemistry 1996;271:3787-94.

[88] Hucthagowder V, Morava E, Kornak U, Lefeber DJ, Fischer B, Dimopoulou A, et al. Loss-of-function mutations in ATP6V0A2 impair vesicular trafficking, tropoelastin secretion and cell survival. Hum Mol Genet 2009;18:2149-65.

[89] Thyberg J, Hinek A, Nilsson J, Friberg U. Electron microscopic and cytochemical studies of rat aorta - intracellular vesicles containing elastin-like and collagen-like material. HistochemJ 1979;11:1-17.

[90] Hinek A, Mecham RP, Keeley F, Rabinovitch M. Impaired elastin fiber assembly related to reduced 67-kD elastin-binding protein in fetal lamb ductus-arteriosus and in cultued aortic smooth muscle cells treated with chrondroitin sulfate. J Clin Invest 1991;88:2083-94.

[91] Tu YD, Weiss AS. Glycosaminoglycan-mediated coacervation of tropoelastin abolishes the critical concentration, accelerates coacervate formation, and facilitates spherule fusion: Implications for tropoelastin microassembly. Biomacromolecules 2008;9:1739-44.

[92] Perrimon N, Bernfield M. Specificities of heparan sulphate proteoglycans in developmental processes. Nature 2000;404:725-8.

[93] Wu WJ, Vrhovski B, Weiss AS. Glycosaminoglycans mediate the coacervation of human tropoelastin through dominant charge interactions involving lysine side chains. The Journal of Biological Chemistry 1999;274:21719-24.

[94] Kozel BA, Ciliberto CH, Mecham RP. Deposition of tropoelastin into the extracellular matrix requires a competent elastic fiber scaffold but not live cells. Matrix Biology 2004;23:23-34.

[95] Jamieson AM, Simic-Glavaski B, Tansey K, Walton AG. Studies of elastin coacervation by quasielastic light scattering. Faraday Discussions of the Chemical Society 1976;61:194-204.

[96] Urry DW. Entropic elastic processes in protein mechanisms. I. Elastic structure due to an inverse temperature transition and elasticity due to internal chain dynamics. Journal of Protein Chemistry 1988;7:1-34.

[97] Urry DW. The change in Gibbs free energy for hydrophobic association - Derivation and evaluation by means of inverse temperature transitions. Chem Phys Lett 2004;399:177-83.

[98] Li B, Alonso DOV, Daggett V. The molecular basis for the inverse temperature transition of elastin. Journal of Molecular Biology 2001;305:581-92.

[99] Luan CH, Parker TM, Prasad KU, Urry DW. Differential Scanning Calorimetry Studies of Nacl Effect on the Inverse Temperature Transition of Some Elastin-Based Polytetrapeptides, Polypentapeptides, and Polynonapeptides. Biopolymers 1991;31:465-75.

[100] Keeley Fred W, Bellingham CM, Woodhouse K. Elastin as a self-organizing biomaterial: use of recombinantly expressed human elastin polypeptides as a model for investigations of structure and self-assembly of elastin. Philosophical Transactions of the Royal Society London B 2002;357:185-9.

[101] Cox BA, Starcher B, Urry DW. Coacervation of tropoelastin results in fiber formation. The Journal of Biological Chemistry 1973;249:997-8.

[102] Sato F, Wachi H, Ishida M, Nonaka R, Onoue S, Urban Z, et al. Distinct steps of cross-linking, self-association, and maturation of tropoelastin are necessary for elastic fiber formation. Journal of Molecular Biology 2007;369:841-51.

[103] Wachi H, Sato F, Nakazawa N, Nonaka R, Szabo Z, Urban Z, et al. Domains 16 and 17 of tropoelastin in elastic fibre formation. Biochemical Journal 2007;402:63-70.

[104] Boyd CD, Christiano AM, Pierce RA, Stolle CA, Deak SB. Mammalian Tropoelastin - Multiple Domains of the Protein Define an Evolutionarily Divergent Amino-Acid-Sequence. Matrix 1991;11:235-41.

[105] Brown-Augsburger P, Tisdale C, Broekelmann TJ, Sloan C, Mecham RP. Identification of an elastin cross-linking domain that joins three peptide chains. Possible role in nucleated assembly. Journal of Biological Chemistry 1995;270:17778-83.

[106] Kaibara K, Akinari Y, Okamoto K, Uemura Y, Yamamoto S, Kodama H, et al. Characteristic interaction of Ca2+ ions with elastin coacervate: Ion transport study across coacervate layers of agr-elastin and elastin model polypeptide, (Val-Pro-Gly-Val-Gly)n. Biopolymers 1996;39:189-98.

[107] Kaibara K, Watanabe T, Miyakawa K. Characterizations of critical processes in liquid-liquid phase separation of the elastomeric protein-water system: Microscopic observations and light scattering measurements. Biopolymers 2000;53:369-79.

[108] Toonkool P, Jensen SA, Maxwell AL, Weiss AS. Hydrophobic domains of human tropoelastin interact in a context-dependent manner. The Journal of Biological Chemistry 2001;276:44575-80.

[109] Starcher BC, Saccoman.G, Urry DW. Coacervation and ion-binding studies on aortic elastin. Biochimica et Biophysica Acta 1973;310:481-6.

[110] Urry DW, Starcher B, Partridg.Sm. Coacervation of solubilized elastin effects a notable conformational change. Nature 1969;222:795-&.

[111] Cox BA, Starcher BC, Urry DW. Coacervation of tropoelastin results in fiber formation. Journal of Biological Chemistry 1974;249:997-8.

[112] Li B, Daggett V. The molecular basis of the temperature- and pH-induced conformational transitions in elastin-based peptides. Biopolymers 2003;68:121-9.

[113] Reguera J, Lagaron JM, Alonso M, Reboto V, Calvo B, Rodriguez-Cabello JC. Thermal behavior and kinetic analysis of the chain unfolding and refolding and of the concomitant nonpolar solvation and desolvation of two elastin-like polymers. Macromolecules 2003;36:8470-6.

[114] Toonkool P, Regan DG, Kuchel PW, Morris MB, Weiss AS. Thermodynamic and hydrodynamic properties of human tropoelastin - Analytical ultracentrifuge and pulsed field-gradient spin-echo NMR studies. Journal of Biological Chemistry 2001;276:28042-50.

[115] Cirulis JT, Keeley FW. Kinetics and morphology of self-assembly of an elastin-like polypeptide based on the alternating domain arrangement of human tropoelastin. Biochemistry 2010;49:5726-33.

[116] Long MM, Rapaka RS, Volpin D, Pasqualironchetti I, Urry DW. Spectroscopic and electron micrographic studies on the repeat tetrapeptide of tropoelastin - (Val-Pro-Gly-Gly)n. Archives of Biochemistry and Biophysics 1980;201:445-52.

[117] Foster JA, Bruenger E, Rubin L, Imberman M, Kagan HM, Mecham RP, et al. Circular dichroism studies of an elastin cross-linked peptide. Biopolymers 1976;15:833-41.

[118] Urry DW. Molecular perspectives of vascular wall structure and disease - elastic component. Perspect Biol Med 1978;21:265-95.

[119] Narayanan AS, Page RC, Kuzan F, Cooper CG. Elastin cross-linking in vitro. Studies on factors influencing the formation of desmosines by lysyl oxidase action on tropoelastin. Biochemical Journal 1978;173:857-62.

[120] Long MM, King VJ, Prasad KU, Urry DW. Chemotaxis of fibroblasts toward nonapeptide of elastin. Biochimica et Biophysica Acta 1988;968:300-11.

[121] Sato F, Wachi H, Starcher B, Seyama Y. Biochemical analysis of elastic fiber formation with a frameshift-mutated tropoelastin (fmTE) at the C-terminus of tropoelastin. Journal of Health Science 2006;52:259-67.

[122] Kozel BA, Wachi H, Davis EC, Mecham RP. Domains in tropoelastin that mediate elastin deposition in vitro and in vivo. The Journal of Biological Chemistry 2003;278:18491-8.

[123] Kielty CM, Baldock C, Lee D, Rock MJ, Ashworth JL, Shuttleworth CA. Fibrillin: from microfibrillar assembly to biomechanical function. Philosophical Transactions of the Royal Society London B 2002;357:207-17.

[124] Clarke AW, Weiss AS. Microfibril-associated glycoprotein-1 binding to tropoelastin. European Journal of Biochemistry 2004;271:3085-90.

[125] Nakamura T, Lozano PR, Ikeda Y, Iwanaga Y, Hinek A, Minamisawa S, et al. Fibulin-5/DANCE is essential for elastogenesis in vivo. Nature 2002;415:171-5.

[126] Nonaka R, Onoue S, Wachi H, Sato F, Urban Z, Starcher B, et al. DANCE/fibulin-5 promotes elastic fiber formation in a tropoelastin isoform-dependent manner. Clinical Biochemistry 2009;42:713-21.

[127] Jensen SA, Reinhardt DP, Gibson MA, Weiss AS. Protein interaction studies of MAGP-1 with tropoelastin and fibrillin-1. The Journal of Biological Chemistry 2001;276:39661-6.

[128] Trask TM, Trask BC, Ritty TM, Abrams WR, Rosenbloom J, Mecham L. Interaction of tropoelastin with the amino-terminal domains of fibrillin-1 and fibrillin-2 suggests a role for fibrillines in elastic fibre assembly. The Journal of Biological Chemistry 2000;275:24400-6.

[129] Hurle JM, Corson G, Daniels K, Reiter RS, Sakai LY, Solursh M. Elastin exhibits a distinctive temporal and spatial pattern of distribution in the developing chick limb in association with the establishment of the cartilaginous skeleton. Journal of Cell Science 1994;107:2623-34.

[130] Rock MJ, Cain SA, Freeman LJ, Morgan A, Mellody K, Marson A, et al. Molecular basis of elastic fiber formation: critical interactions and a tropoelastin-fibrillin-1 cross-link. The Journal of Biological Chemistry 2004;279:23748-58.

[131] Cirulis JT, Bellingham CM, Davis EC, Hubmacher D, Reinhardt DP, Mecham RP, et al. Fibrillins, Fibulins, and Matrix-Associated Glycoprotein Modulate the Kinetics and Morphology of in Vitro Self-Assembly of a Recombinant Elastin-like Polypeptide. Biochemistry 2008;47:12601-13.

[132] Hu QR, Loeys BL, Coucke PJ, De Paepe A, Mecham RP, Choi J, et al. Fibulin-5 mutations: mechanisms of impaired elastic fiber formation in recessive cutis laxa. Hum Mol Genet 2006;15:3379-86.

[133] Yamauchi Y, Tsuruga E, Nakashima K, Sawa Y, Ishikawa H. Fibulin-5 and -5, but not fibulin-2, are associated with tropoelastin deposition in elastin-producing cell culture. Acta Histochemica et Cytochemica 2010;43:131-8.

[134] Fahrenbach WH, Sandberg LB, Cleary EG. Ultrastructural studies on early elastogenesis. The Anatomical Record 1966;155:563-75.

[135] Clarke AW, Wise SG, Cain SA, Kielty CM, Weiss AS. Coacervation is promoted by molecular interactions between the PF2 segment of fibrillin-1 and the domain 4 region of tropoelastin. Biochemistry 2005;44:10271-81.

[136] Liu X, Zhao Y, Gao J, Pawlyk B, Starcher B, Spencer JA, et al. Elastin fiber homeostasis requires lysyl oxidase-like 1 protein. Nature Genetics 2004;36:178-82.

[137] Kagan HM, Sullivan KA. Lysyl oxidase: preparation and role in elastin biosynthesis. Methods in Enzymology 1982;82:637-50.

[138] Lelievre E, Hinek A, Lupu F, Buquet C, Soncin F, Mattot V. VE-statin/egfl7 regulates vascular elastogenesis by interacting with lysyl oxidases. The EMBO Journal 2008;27:1658-70.

[139] Bedell-Hogan D, Trackman P, Abrams W, Rosenbloom J, Kagan HM. Oxidation, cross-linking, and insolubilization of recombinant tropoelastin by purified lysyl oxidase. The Journal of Biological Chemistry 1993;268:10345-50.

[140] Wachi H, Sato F, Murata H, Nakazawa N, Starcher B, Seyama Y. Development of a new in vitro model of elastic fiber assembly in human pigmented epithelial cells. Clinical Biochemistry 2005;38:643-53.

[141] Behmoaras J, Slove S, Seve S, Vranckx R, Sommer P, Jacob MP. Differential expression of lysyl oxidases LOXL1 and LOX during growth and aging suggests specific roles in elastin and collagen fiber remodeling in rat aorta. Rejuvenation Research 2008;11:883-9.

[142] Choi J, Bergdahl A, Zheng Q, Starcher B, Yanagisawa H, Davis EC. Analysis of dermal elastic fibers in the absence of fibulin-5 reveals potential roles for fibulin-5 in elastic fiber assembly. Matrix Biology 2009;28:211-20.

[143] Wise SG, Mithieux SM, Raftery MJ, Weiss AS. Specificity in the coacervation of tropoelastin: solvent exposed lysines. Journal of Structural Biology 2005;149:273-81.

[144] Bressan GM, Pasqualironchetti I, Fornieri C, Mattioli F, Castellani I, Volpin D. Relevance of aggregation properties of tropoelastin to the assembly and structure of elastic fibers. Journal of Ultrastructure and Molecular Structure Research 1986;94:209-16.

[145] Wender DB, Treiber LR, Bensusan HB, Walton AG. Synthesis and characterization of poly(LysAla3). Biopolymers 1974;13:1929-41.

[146] Mecham RP, Foster JA. A structural model for desmosine cross-linked peptides. Biochemical Journal 1978;173:617-25.

[147] Bellingham CM, Lillie MA, Gosline JM, Wright GM, Starcher BC, Bailey AJ, et al. Recombinant human elastin polypeptides self-assemble into biomaterials with elastin-like properties. Biopolymers 2003;70:445-55.

[148] Daamen WF, Hafmans T, Veerkamp JH, van Kuppevelt TH. Comparison of five procedures for the purification of insoluble elastin. Biomaterials 2001;22:1997-2005.

[149] Romero N, Tinker D, Hyde D, Rucker RB. Role of plasma and serum proteases in the degradation of elastin. Archives of Biochemistry and Biophysics 1986;244:161-8.

[150] Yanagisawa H, Davis EC. Unraveling the mechanism of elastic fiber assembly: The roles of short fibulins. The International Journal of Biochemistry & Cell Biology 2010;42:1084-93.

[151] Morris CA. Genetic aspects of supravalvular aortic stenosis. Curr Opin Cardiol 1998;13:214-9.

[152] Urbán Z, Riazi S, Seidl TL, Katahira J, Smoot LB, Chitayat D, et al. Connection between elastin haploinsufficiency and increased cell proliferation in patients with supravalvular aortic stenosis and Williams-Beuren Syndrome. The American Journal of Human Genetics 2002;71:30-44.

[153] Wu WJ, Weiss AS. Deficient coacervation of two forms of human tropoelastin associated with supravalvular aortic stenosis. European Journal of Biochemistry 1999;266:308-14.

[154] Boeckel T, Dierks A, Vergopoulos A, BÃ¤hring S, Knoblauch H, MÃ¼ller-Myhsok B, et al. A new mutation in the elastin gene causing supravalvular aortic stenosis. The American Journal of Cardiology 1999;83:1141-3.

[155] Li DY, Toland AE, Boak BB, Atkinson DL, Ensing GJ, Morris CA, et al. Elastin point mutations cause an obstructive vascular disease, supravalvular aortic stenosis. Hum Mol Genet 1997;6:1021-8.

[156] Tassabehji M, Metcalfe K, Donnai D, Hurst J, Reardon W, Burch M, et al. Elastin: genomic structure and point mutations in patients with supravalvular aortic stenosis. Hum Mol Genet 1997;6:1029-36.

[157] Urbán Z, Simone P, Henri P, Marie-Therese Z, Mark L, Kurt S, et al. Elastin gene deletions in Williams syndrome patients result in altered deposition of elastic fibers in skin and a subclinical dermal phenotype. Pediatric Dermatology 2000;17:12-20.

[158] Urban Z, Michels VV, Thibodeau SN, Davis EC, Bonnefont JP, Munnich A, et al. Isolated supravalvular aortic stenosis: functional haploinsufficiency of the elastin gene as a result of nonsense-mediated decay. Hum Genet 2000;106:577-88.

[159] Merla G, Brunetti-Pierri N, Piccolo P, Micale L, Loviglio MN. Supravalvular aortic stenosis elastin arteriopathy. Circulation-Cardiovascular Genetics 2012;5:692-6.

[160] Li DY, Faury G, Taylor DG, Davis EC, Boyle WA, Mecham RP, et al. Novel arterial pathology in mice and humans hemizygous for elastin. J Clin Invest 1998;102:1783-7.

[161] Urban Z, Zhang J, Davis EC, Maeda GK, Kumar A, Stalker H, et al. Supravalvular aortic stenosis: genetic and molecular dissection of a complex mutation in the elastin gene. Hum Genet 2001;109:512-20.

[162] Callewaert B, Renard M, Hucthagowder V, Albrecht B, Hausser I, Blair E, et al. New insights into the pathogenesis of autosomal dominant cutis laxa with report of five ELN mutations. Hum Mutat 2011;32:445-55.

[163] Damkier A, Brandrup F, Starklint H. Cutis laxa: autosomal dominant inheritance in five generations. Clinical Genetics 1991;39:321-9.

[164] Sarkar R, Kaur C, Kanwar AJ, Basu S. Cutis laxa in seven members of a north-Indian family. Pediatric Dermatology 2002;19:229-31.

[165] Graul-Neumann LM, Hausser I, Essayie M, Rauch A, Kraus C. Highly variable cutis laxa resulting from a dominant splicing mutation of the elastin gene. American Journal of Medical Genetics Part A 2008;146A:977-83.

[166] Rodriguez-Revenga L, Iranzo P, Badenas C, Puig S, Carrio A, Mila M. A novel elastin gene mutation resulting in an autosomal dominant form of cutis laxa. Archives of Dermatology 2004;140:1135-9.

[167] Szabo Z, Crepeau MW, Mitchell AL, Stephan MJ, Puntel RA, Yin Loke K, et al. Aortic aneurysmal disease and cutis laxa caused by defects in the elastin gene. J Med Genet 2006;43:255-8.

[168] Tassabehji M, Metcalfe K, Hurst J, Ashcroft GS, Kielty CM, Wilmot C, et al. An elastin gene mutation producing abnormal tropoelastin and abnormal elastic fibres in a patient with autosomal dominant cutis laxa. Hum Mol Genet 1998;7:1021-8.

[169] Urban Z, Gao J, Pope M, Davis EC. Autosomal dominant cutis laxa with severe lung disease: synthesis and matrix deposition of mutant tropoelastin. Journal of Investigative Dermatology 2005;124:1193-9.

[170] Zhang MC, He L, Giro M, Yong SL, Tiller GE, Davidson JM. Cutis laxa arising from frameshift mutations in exon 30 of the elastin gene (ELN). Journal of Biological Chemistry 1999;274:981-6.

[171] Markova D, Zou YQ, Ringpfeil F, Sasaki T, Kostka G, Timpl R, et al. Genetic heterogeneity of cutis laxa: A heterozygous tandem duplication within the fibulin-5 (FBLN5) gene. American Journal oF Human Genetics 2003;72:998-1004.

[172] Kelleher CM, Silverman EK, Broekelmann TJ, Litonjua AA, Hernandez M, Sylvia JS, et al. A functional mutation in the terminal exon of elastin in severe, early-onset chronic obstructive pulmonary disease. American Journal of Respiratory Cell and Molecular Biology 2005;33:355-62.

[173] Sreerama N, Woody RW. Estimation of protein secondary structure from circular dichroism spectra: Comparison of CONTIN, SELCON, and CDSSTR methods with an expanded reference set. Analytical Biochemistry 2000;287:252-60.

[174] Konarev PV, Volkov VV, Sokolova AV, Koch MHJ, Svergun D. PRIMUS - a Windows-PC based system for small-angle scattering data analysis. Journal of Applied Crystallography 2003;36:1277-82.

[175] Svergun DI, Petoukhov MV, Koch MHJ. Determination of domain structure of proteins from X-ray solution scattering. Biophys J 2001;80:2946-53.

[176] Volkov VV, Svergun DI. Uniqueness of ab-initio shape determination in small-angle scattering. Journal of Applied Crystallography 2003;36:860-4.

[177] Holst J, Watson S, Lord MS, Eamegdool SS, Bax DV, Nivison-Smith LB, et al. Substrate elasticity provides mechanical signals for the expansion of hemopoietic stem and progenitor cells. Nature Biotechnology 2010;28:1123-8.

[178] Dyksterhuis LB, Weiss AS. Homology models for domains 21-23 of human tropoelastin shed light on lysine crosslinking. Biochemical and Biophysical Research Communications 2010;396:870-3.

[179] Bax DV, Rodgers UR, Bilek MM, Weiss AS. Cell adhesion to tropoelastin is mediated via the C-terminal GRKRK motif and integrin alphaVbeta3 Journal of Biological Chemistry 2009;284:28616-23.

[180] Broekelmann TJ, Ciliberto CH, Shifren A, Mecham RP. Modification and functional inactivation of the tropoelastin carboxy-terminal domain in cross-linked elastin. Matrix Biology 2008;27:631-9.

[181] Foster JA, Rich CB, Miller MF. Pulmonary fibroblasts: an in vitro model of emphysema. Regulation of elastin gene expression. Journal of Biological Chemistry 1990;265:15544-9.

[182] Mcgowan SE, Liu R, Harvey CS, Jaeckel E. Serine proteinase inhibitors influence the stability of tropoelastin mRNA in neonatal rat lung fibroblast cultures. American Journal of Physiology - Lung Cellular and Molecular Physiology 1996;270:L376-L85.

[183] Piontkivska H, Zhang Y, Green E, Elnitski L. Multi-species sequence comparison reveals dynamic evolution of the elastin gene that has involved purifying selection and lineage-specific insertions/deletions. BMC Genomics 2004;5:31.

[184] Yeo GC, Baldock C, Tuukkanen A, Roessle M, Dyksterhuis LB, Wise SG, et al. Tropoelastin bridge region positions the cell-interactive C terminus and contributes to elastic fiber assembly. Proceedings of the National Academy of Sciences 2012;109:2878-83.

[185] Urry DW, Peng SQ, Xu J, McPherson DT. Characterization of waters of hydrophobic hydration by microwave dielectric relaxation. J Am Chem Soc 1997;119:1161-2.

[186] Urry DW, Luan CH, Parker TM, Gowda DC, Prasad KU, Reid MC, et al. Temperature of polypeptide inverse temperature transition depends on mean residue hydrophobicity. J Am Chem Soc 1991;113:4346-8.

[187] Yeo GC, Keeley FW, Weiss AS. Coacervation of tropoelastin. Advances in Colloid and Interface Science 2011;167:94-103.

[188] Flory PJ, Rehner JJ. Statistical mechanics of cross-Linked polymer networks II. Swelling. The Journal of Chemical Physics 1943;11:521-6.

[189] Nickerson MT, Farnworth R, Wagar E, Hodge SM, Rousseau D, Paulson AT. Some physical and microstructural properties of genipin-crosslinked gelatin-maltodextrin hydrogels. International Journal of Biological Macromolecules 2006;38:40-4.

[190] Lee J, Macosko CW, Urry DW. Swelling behavior of gamma-irradiation cross-linked elastomeric polypentapeptide-based hydrogels. Macromolecules 2001;34:4114-23.

[191] Vieth S, Bellingham CM, Keeley FW, Hodge SM, Rousseau D. Microstructural and tensile properties of elastin-based polypeptides crosslinked with Genipin and pyrroloquinoline quinone. Biopolymers 2007;85:199-206.

[192] Ross R. Smooth muscle cell. 2. Growth of smooth muscle in culture and formation of elastic fibers. J Cell Biol 1971;50:172-&.

[193] Mecham RP, Madaras J, McDonald JA, Ryan U. Elastin production by cultured calf pulmonary artery endothelial cells. Journal of Cellular Physiology 1983;116:282-8.

[194] Giro MG, Oikarinen AI, Oikarinen H, Sephel G, Uitto J, Davidson J. Demonstration of elastin gene expression in human skin fibroblast cultures and reduced tropoelastin production by cells from a patient with atrophoderma. J Clin Invest 1985;75:672-8.

[195] Field JM, Rodger GW, Hunter JC, Serafinifracassini A, Spina M. Isolation of elastin from bovine auricular cartilage. Archives of Biochemistry and Biophysics 1978;191:705-13.

[196] Quintarelli G, Starcher BC, Vocaturo A, Digianfilippo F, Gotte L, Mecham RP. Fibrogenesis and biosynthesis of elastin in cartilage. Connective Tissue Research 1979;7:1-19.

[197] Mecham RP. Modulation of elastin synthesis - in vitro models. Methods in Enzymology 1987;144:232-46.

[198] Olson MD. Development of Bruch's membrane in the chick: an electron microscopic study. Investigative Ophthalmology & Visual Science 1979;18:329-38.

[199] Campochiaro PA, Jerdon JA, Glaser BM. The extracellular matrix of human retinal pigment epithelial cells in vivo and its synthesis in vitro. Investigative Ophthalmology & Visual Science 1986;27:1615-21.

[200] Sekiyama E, Saint-Geniez M, Yoneda K, Hisatomi T, Nakao S, Walshe TE, et al. Heat treatment of retinal pigment epithelium induces production of elastic lamina components and antiangiogenic activity. Faseb J 2012;26:567-75.

[201] Robb BW, Wachi H, Schaub T, Mecham RP, Davis EC. Characterization of an in vitro model of elastic fiber assembly. Molecular Biology of the Cell 1999;10:3595-605.

[202] Faris B, Jackson LE, Schreiber BM, Martin BM, Jones HV, Franzblau C. A controlled precursor add-back model of elastogenesis in smooth muscle cell cultures. Matrix 1991;11:367-72.

[203] Stone PJ, Morris SM, Griffin S, Mithieux S, Weiss AS. Building elastin - incorporation of recombinant human tropoelastin into extracellular matrices using nonelastogenic Rat-1 fibroblasts as a source for lysyl oxidase. American Journal of Respiratory Cell and Molecular Biology 2001;24:733-9.

[204] Thomas P, Pande P, Clubb F, Adame J, Jo JA. Biochemical imaging of human atherosclerotic plaques with fluorescence lifetime angioscopy. Photochemistry and Photobiology 2010;86:727-31.

[205] Sharp PM, Li WH. The codon adaptation index - a measure of directional synonymous codon usage bias, and its potential applications. Nucleic Acids Research 1987;15:1281-95.

[206] Zhang L, Kasif S, Cantor CR, Broude NE. GC/AT-content spikes as genomic punctuation marks. Proc Natl Acad Sci U S A 2004;101:16855-60.

[207] Pozzoli U, Menozzi G, Fumagalli M, Cereda M, Comi G, Cagliani R, et al. Both selective and neutral processes drive GC content evolution in the human genome. BMC Evolutionary Biology 2008;8:99.

[208] Sambrook J, Russell DW. Cloning PCR products by addition of restriction sites to the termini of amplified DNA. Cold Spring Harbor Protocols 2006;2006:pdb.prot3835.

[209] Kaufman DL, Evans GA. Restriction endonuclease cleavage at the termini of PCR products. Biotechniques 1990;9:304-6.

[210] Polsky F, Edgell MH, Seidman JG, Leder P. High-capacity gel preparative electrophoresis for purification of fragments of genomic DNA. Analytical Biochemistry 1978;87:397-410.

[211] Ulrich A, Shine J, Chirgwin J, Pictet R, Tischer E, Rutter WJ, et al. Rat insulin genes: construction of plasmids containing the coding sequences. Science 1977;196:1313-9.

[212] Erickson J, Rushford CL, Dorney DJ, Wilson GN, Schmickel RD. Structure and variation of human ribosomal DNA: molecular analysis of cloned fragments. Gene 1981;16:1-9.

[213] Clark JM. Novel non-templated nucleotide addition reactions catalyzed by procaryotic and eucaryotic DNA polymerases. Nucleic Acids Research 1988;16:9677-86.

[214] Mole SE, Iggo RD, Lane DP. Using the polymerase chain reaction to modify expression plasmids for epitope mapping. Nucleic Acids Research 1989;17:3319.

[215] Klenow H, Henningsen I. Selective elimination of the exonuclease activity of the deoxyribonucleic acid polymerase from *Escherichia coli* B by limited proteolysis. Proceedings of the National Academy of Sciences 1970;65:168-75.

[216] Aslanidis C, de Jong PJ. Ligation-independent cloning of PCR products (LIC-PCR). Nucleic Acids Research 1990;18:6069-74.

[217] Paithankar KR, Prasad KS. Precipitation of DNA by polyethylene glycol and ethanol. Nucleic Acids Research 1991:1346.

[218] Lund AH, Duch M, Skou Pedersen F. Increased cloning efficiency by temperature-cycle ligation. Nucleic Acids Research 1996;24:800-1.

[219] Koster H, Blieffert J. New type of linker useful for cloning experiments. Journal of Biochemical and Biophysical Methods 1986;13:251-7.

[220] Helfman DM, Fiddes JC, Hanahan D. Directional cDNA cloning in plasmid vectors by sequential addition of oligonucleotide linkers. Methods in Enzymology 1987;152:349-59.

[221] Kurtz DT, Nicodemus CF. Cloning of alpha-2U globulin cDNA using a high-efficiency technique for the cloning of trace messenger-RNAs. Gene 1981;13:145-52.

[222] Nikfarjam L, Farzaneh P. Prevention and detection of mycoplasma contamination in cell culture. Cell J 2012;13:203-12.

[223] Hay RJ, Macy ML, Chen TR. Mycoplasma infection of cultured cells. Nature 1989;339:487-8.

[224] Hopert A, Uphoff CC, Wirth M, Hauser Hr, Drexler HG. Specifity and sensitivity of polymerase chain reaction (PCR) in comparison with other methods for the detection of mycoplasma contamination in cell lines. Journal of Immunological Methods 1993;164:91-100.

[225] Dunn KC, AotakiKeen AE, Putkey FR, Hjelmeland LM. ARPE-19, a human retinal pigment epithelial cell line with differentiated properties. Exp Eye Res 1996;62:155-69.

[226] Kennedy BnN, Goldflam S, Chang MA, Campochiaro P, Davis AA, Zack DJ, et al. Transcriptional regulation of cellular retinaldehyde-binding protein in the retinal pigment epithelium: a role for the photoreceptor consensus element. Journal of Biological Chemistry 1998;273:5591-8.

[227] John C, Nawrot M, Kennedy BN, Garwin GG, Hurley JB, Huang J, et al. Visual cycle impairment in cellular retinaldehyde binding protein (CRALBP) knockout mice results in delayed dark adaptation. Neuron 2001;29:739-48.

[228] Hamel CP, Tsilou E, Harris E, Pfeffer BA, Hooks JJ, Detrick B, et al. A developmentally regulated microsomal protein specific for the pigment epithelium of the vertebrate retina. Journal of Neuroscience Research 1993;34:414-25.

[229] Hamel CP, Tsilou E, Pfeffer BA, Hooks JJ, Detrick B, Redmond TM. Moleuclar cloning and expression of RPE65, a novel retinal pigment epithelium-specific microsomal protein that is post-transcriptionally regulated in vitro. Journal of Biological Chemistry 1993;268:15751-7.

[230] Boulanger A, Redmond TM. Expression and promoter activation of the Rpe65 gene in retinal pigment epithelium cell lines. Curr Eye Res 2002;24:368-75.

[231] Sakai LY, Keene DR, Engvall E. Fibrillin, a new 350-kD glycoprotein, is a component of extracellular microfibrils. J Cell Biol 1986;103:2499-509.

[232] Piha-Gossack A, Sossin W, Reinhardt DP. The evolution of extracellular fibrillins and their functional domains. PLoS ONE 2012;7:e33560.

[233] Mariko B, Pezet M, Escoubet B, Bouillot S, Andrieu JP, Starcher B, et al. Fibrillin-1 genetic deficiency leads to pathological ageing of arteries in mice. J Pathol 2011;224:33-44.

[234] Siegel RC, Pinnell SR, Martin GR. Cross-linking of collagen and elastin - properties of lysyl oxidase. Biochemistry 1970;9:4486-&.

[235] Hawley-Nelson P, Ciccarone V. Transfection of cultured eukaryotic cells using cationic lipid reagents. Current Protocols in Neuroscience: John Wiley & Sons, Inc.; 2001.

[236] Vigneron JP, Oudrhiri N, Fauquet M, Vergely L, Bradley JC, Basseville M, et al. Guanidinium-cholesterol cationic lipids: efficient vectors for the transfection of eukaryotic cells. Proceedings of the National Academy of Sciences 1996;93:9682-6.

[237] Felgner PL, Gadek TR, Holm M, Roman R, Chan HW, Wenz M, et al. Lipofection: a highly efficient, lipid-mediated DNA-transfection procedure. Proceedings of the National Academy of Sciences 1987;84:7413-7.

[238] Shih PJ, Evans K, Schifferli K, Ciccarone V, Lichaa F, Masoud M, et al. High efficiency transfection with minimal optimization using the Lipofectamine PLUS reagent. Focus 1997;19:52-6.

[239] Paludan K, Duch M, Jorgensen P, Kjeldgaard NO, Pedersen FS. Graduated resistance to G418 leads to differential selection of cultured mammalian cells expressing the neo gene. Gene 1989;85:421-6.

[240] del Pozo-Rodriguez A, Delgado D, Solinis MA, Gascon AR, Pedraz JL. Solid lipid nanoparticles for retinal gene therapy: Transfection and intracellular trafficking in RPE cells. Int J Pharm 2008;360:177-83.

[241] Hsu CYM, Uludag H. Cellular uptake pathways of lipid-modified cationic polymers in gene delivery to primary cells. Biomaterials 2012;33:7834-48.

[242] Wolff JA, Ludtke JJ, Acsadi G, Williams P, Jani A. Long-term persistence of plasmid DNA and foreign gone expression in mouse muscle. Hum Mol Genet 1992;1:363-9.

[243] Li WH, Ishida T, Tachibana R, Almofti MR, Wang XY, Kiwada H. Cell type-specific gene expression, mediated by TFL-3, a cationic liposomal vector, is controlled by a post-transcription process of delivered plasma DNA. Int J Pharm 2004;276:67-74.

[244] von Gersdorff K, Sanders NN, Vandenbroucke R, De Smedt SC, Wagner E, Ogris M. The internalization route resulting in successful gene expression depends on both cell line and polyplex type. Molecular Therapy 2006;14:745-53.

[245] Wachi H, Nonaka R, Sato F, Shibata-Sato K, Ishida M, Iketani S, et al. Characterization of the molecular interaction between tropoelastin and DANCE/Fibulin-5. J Biochem 2008;143:633-9.

[246] Kagan HM, Trackman P. Properties and function of lysyl oxidase. American Journal of Respiratory Cell and Molecular Biology 1991;5:206-10.

[247] Faury G. Function-structure relationship of elastic arteries in evolution: from microfibrils to elastin and elastic fibres. Pathologie Biologie 2001;49:310-25.

[248] Ronchetti IP, Alessandrini A, Contri MB, Fornieri C, Mori G, Quaglino D, et al. Study of elastic fiber organization by scanning force microscopy. Matrix Biology 1998;17:75-83.

[249] Ronchetti IP, Fornieri C, BaccaraniContri M, Quaglino D. Ultrastructure of elastin. In: Chadwick DJ, Goode JA, editors. Molecular Biology and Pathology of Elastic Tissues. Chichester: John Wiley & Sons Ltd; 1995. p. 31-50.

[250] Ronchetti IP, Fornieri C, Baccaranicontri M, Volpin D. Ultrastructure of elastin revealed by freeze-fracture electron microscopy. Micron 1979;10:89-99.

[251] Suhling K, French PM, Phillips D. Time-resolved fluorescence microscopy. Photochemical and Photobiological Sciences 2005;4:13-22.

[252] Arakawa K, Isoda K, Ito T, Nakajima K, Shibuya T, Ohsuzu F. Fluorescence analysis of biochemical constituents identifies atherosclerotic plaque with a thin fibrous cap. Arteriosclerosis, Thrombosis, and Vascular Biology 2002;22:1002-7.

[253] Patalay R, Talbot C, Alexandrov Y, Munro I, Breunig HG, Konig K, et al. Non-invasive imaging of skin cancer with fluorescence lifetime imaging using two photon tomography. In: Ramanujam N, Popp J, editors. Clinical and Biomedical Spectroscopy and Imaging Ii. Bellingham: Spie-Int Soc Optical Engineering; 2011.

[254] Lakowicz JR, Gryczynski I, Malak H, Schrader M, Engelhardt P, Kano H, et al. Time-resolved fluorescence spectroscopy and imaging of DNA labeled with DAPI and Hoechst 33342 using three-photon excitation. Biophys J 1997;72:567-78.

[255] Maarek JMI, Marcu L, Snyder WJ, Grundfest WS. Time-resolved fluorescence spectra of arterial fluorescent compounds: Reconstruction with the laguerre expansion technique. Photochemistry and Photobiology 2000;71:178-87.

[256] Marcu L, Grundfest WS, Maarek JMI. Photobleaching of arterial fluorescent compounds: Characterization of elastin, collagen and cholesterol time-resolved spectra during prolonged ultraviolet irradiation. Photochemistry and Photobiology 1999;69:713-21.

[257] Deyl Z, Macek K, Adam M, Vancíková O. Studies on the chemical nature of elastin fluorescence. Biochimica et Biophysica Acta (BBA) - Protein Structure 1980;625:248-54.

[258] Wang HW, Simianu V, Locker MJ, Sturek M, Cheng JX. Imaging arterial cells, atherosclerosis, and restenosis by multimodal nonlinear optical microscopy. Proceedings of SPIE 2008;6860:68600W.

[259] Swatland HJ. Fiber-optic reflectance and autofluorescence of bovine elastin and differences between intramuscular and extramuscular tendon. J Anim Sci 1987;64:1038-43.

[260] Hertle MD, Adams JC, Watt FM. Integrin expression during human epidermal development in vivo and in vitro. Development 1991;112:193-206.

[261] Zhang H, Hu W, Ramirez F. Developmental expression of fibrillin genes suggests heterogeneity of extracellular microfibrils. J Cell Biol 1995;129:1165-76.

[262] Mariencheck MC, Davis EC, Zhang H, Ramirez F, Rosenbloom J, Gibson MA, et al. Fibrillin-1 and fibrillin-2 show temporal and tissue-specific regulation of expression in developing elastic tissues. Connective Tissue Research 1995;31:87-97.

[263] Koo HP, Macarak EJ, Chang SL, Rosenbloom J, Howard PS. Temporal expression of elastic fiber components in bladder development. Connective Tissue Research 1998;37:1-11.

[264] Charbonneau NL, Dzamba BJ, Ono RN, Keene DR, Corson GM, Reinhardt DP, et al. Fibrillins can co-assemble in fibrils, but fibrillin fibril composition displays cell-specific differences. Journal of Biological Chemistry 2003;278:2740-9.

[265] Sabatier L, Miosge N, Hubmacher D, Lin GQ, Davis EC, Reinhardt DP. Fibrillin-3 expression in human development. Matrix Biology 2011;30:43-52.

[266] Gibson MA, Finnis ML, Kumaratilake JS, Cleary EG. Microfibril-associated glycoprotein-2 (MAGP-2) is specifically associated with fibrillin-containing microfibrils but exhibits more restricted patterns of tissue localization and developmental expression than its structural relative MAGP-1. J Histochem Cytochem 1998;46:871-85.

[267] Weber E, Rossi A, Solito R, Agliano M, Sacchi G, Gerli R. The pattern of fibrillin deposition correlates with microfibril-associated glycoprotein 1 (MAGP-1) expression in cultured blood and lymphatic endothelial cells. Lymphology 2004;37:116-26.

[268] Burchett ME, Ling IF, Estus S. FBN1 isoform expression varies in a tissue and development-specific fashion. Biochemical and Biophysical Research Communications 2011;411:323-8.

[269] Horiguchi M, Inoue T, Ohbayashi T, Hirai M, Noda K, Marmorstein LY, et al. Fibulin-4 conducts proper elastogenesis via interaction with cross-linking enzyme lysyl oxidase. Proc Natl Acad Sci U S A 2009;106:19029-34.

[270] Indik Z, Yeh H, Ornsteingoldstein N, Kucich U, Abrams W, Rosenbloom JC, et al. Structure of the elastin gene and alternative splicing of elastin messenger-RNA - implications for human disease. Am J Med Genet 1989;34:81-90.

[271] Tu Y, Weiss AS. Transient tropoelastin nanoparticles are early-stage intermediates in the coacervation of human tropoelastin whose aggregation is facilitated by heparan sulfate and heparin decasaccharides. Matrix Biology 2010;29:152-9.

[272] Gheduzzi D, Guerra D, Bochicchio B, Pepe A, Tamburro AM, Quaglino D, et al. Heparan sulphate interacts with tropoelastin, with some tropoelastin peptides and is present in human dermis elastic fibers. Matrix Biology 2005;24:15-25.

[273] Tamburro AM, Guantieri V, Daga-Gordini D, Abatangelo G. Conformational transitions of alpha-elastin. Biochimica et Biophysica Acta 1977;492:370-6.

[274] Mammi M, Gotte L, Pezzin G. Comparision of soluble and native elastin conformations by far-ultraviolet circular dichroism. Nature 1970;225:380-1.

[275] Vrhovski B, Jensen SA, Weiss AS. Coacervation characteristics of recombinant human tropoelastin. European Journal of Biochemistry 1997;250:92-8.

[276] BrownAugsburger P, Broekelmann T, Rosenbloom J, Mecham RP. Functional domains on elastin and microfibril-associated glycoprotein involved in elastic fibre assembly. Biochemical Journal 1996;318:149-55.

[277] Baccarani Contri M, Vincenzi D, Cicchetti F, Mori G, Pasquali Ronchetti I. lmmuno-cytochemical localization of proteoglycans within normal elastin fibers. European Journal of Cell Biology 1990;53:305-12.

[278] Fornieri C, Baccaranicontri M, Quaglino D, Pasqualironchetti I. Lysyl oxidase activity and elastin glycosaminoglycan interactions in growing chick and rat aortas. J Cell Biol 1987;105:1463-9.

[279] McGowan SE, Liu RG, Harvey CS. Effects of heparin and other glycosaminoglycans on elastin production by cultured neonatal rat lung fibroblasts. Archives of Biochemistry and Biophysics 1993;302:322-31.

[280] Wrenn DS, Parks WC, Whitehouse LA, Crouch EC, Kucich UK, Rosenbloom J, et al. Identification of multiple tropoelastins secreted by bovine cells. The Journal of Biological Chemistry 1987;262:2244-9.

[281] Franzblau C, Pratt CA, Faris B, Colannino NM, Offner GD, Mogayzel PJ, et al. Role of tropoelastin fragmentation in elastogenesis in rat smooth muscle cells. The Journal of Biological Chemistry 1989;264:15115-9.

[282] Mithieux SM, Wise SG, Raftery MJ, Starcher B, Weiss AS. A model two-component system for studying the architecture of elastin assembly in vitro. Journal of Structural Biology 2005;149:282-9.

[283] Drake AF, Siligardi G, Gibbons WA. Reassessment of the electronic circular dichroism criteria for random coil conformations of poly(L-lysine) and the implications for protein folding and denaturation studies. Biophysical Chemistry 1988;31:143-6.

[284] Forood B, Feliciano EJ, Nambiar KP. Stabilization of alpha-helical structures in short peptides via end capping. Proceedings of the National Academy of Sciences 1993;90:838-42.

[285] Presta LG, Rose GD. Helix signals in proteins. Science 1988;240:1632-41.

[286] Thompson JD, Higgins DG, Gibson TJ. ClustalW - improving the sensitivity of progressive multiple sequence alignment through sequence weighting, position-specific gap penalties and matrix choice. Nucleic Acids Research 1994;22:4673-80.

[287] Gilad Y, Wiebe V, Przeworski M, Lancet D, Paabo S. Loss of olfactory receptor genes coincides with the acquisition of full trichromatic vision in primates. PLoS Biol 2004;2:e5.

[288] Ferguson-Smith MA, Trifonov V. Mammalian karyotype evolution. Nature Reviews Genetics 2007;8:950-62.

[289] Urry DW, Trapane TL, Prasad KU. Phase-structure transitions of the elastin polypentapeptide-water system within the framework of composition-temperature studies. Biopolymers 1985;24:2345-56.

[290] Cuatrecasas P, Parikh I. Adsorbents for Affinity Chromatography - Use of N-Hydroxysuccinimide Esters of Agarose. Biochemistry 1972;11:2291-&.

[291] Annabi N, Mithieux SM, Weiss AS, Dehghani F. The fabrication of elastin-based hydrogels using high pressure CO2. Biomaterials 2009;30:1-7.

[292] Mano JF, Silva GA, Azevedo HS, Malafaya PB, Sousa RA, Silva SS, et al. Natural origin biodegradable systems in tissue engineering and regenerative medicine: present status and some moving trends. J R Soc Interface 2007;4:999-1030.

[293] Mark JE. Dependence of swelling of elastin on elongation, and its importance in fluorescence probe analysis. Biopolymers 1976;15:1853-6.

[294] Gosline JM. Temperature-dependent swelling of elastin. Biopolymers 1978;17:697-707.

[295] Trabbic-Carlson K, Setton LA, Chilkoti A. Swelling and mechanical behaviors of chemically cross-linked hydrogels of elastin-like polypeptides. Biomacromolecules 2003;4:572-80.

[296] Tu YD, Wise SG, Weiss AS. Stages in tropoelastin coalescence during synthetic elastin hydrogel formation. Micron 2010;41:268-72.

[297] Rodgers UR, Weiss AS. Integrin alpha(v)beta(3) binds a unique non-RGD site near the C-terminus of human tropoelastin. Biochimie 2004;86:173-8.

[298] Wrenn DS, Griffin GL, Senior RM, Mecham RP. Characterization of biologically-active domains on elastin - identification of a monoclonal antibody to a cell recognition site. Biochemistry 1986;25:5172-6.

[299] Grosso LE, Scott M. Peptide sequences selected by BA4, a tropoelastin-specific monoclonal antibody, are ligands for the 67-kilodalton bovine elastin receptor. Biochemistry 1993;32:13369-74.

[300] Debelle L, Alix AJP. Optical spectroscopic determination of bovine tropoelastin molecular model. Journal of Molecular Structure 1995;348:321-4.

[301] Debelle L, Alix AJP, Jacob MP, Huvenne J, Berjot M, Sombret B, et al. Bovine elastin and κ-elastin secondary structure determination by optical spectroscopies. Journal of Biological Chemistry 1995;270:26099-103.

[302] Urry DW. Characterization of soluble peptides of elastin by physical techniques. Methods in Enzymology 1982;82:673-716.

[303] Frushour BG, Koenig JL. Raman scattering of collagen, gelatin, and elastin. Biopolymers 1975;14:379-91.

[304] Prescott B, Renugopalakrishnan V, Thomas GJ. Raman spectrum and structure of elastin in relation to type-II β-turns. Biopolymers 1987;26:934-6.

[305] Urry DW. What is elastin; what is not. Ultrastructural Pathology 1983;4:227-51.

[306] Ruigrok YM, Seitz U, Wolterink S, Rinkel GJE, Wijmenga C, Urban Z. Association of polymorphisms and haplotypes in the elastin gene in Dutch patients with sporadic aneurysmal subarachnoid hemorrhage. Stroke 2004;35:2064-8.

[307] Yamashiro K, Mori K, Nakata I, Tsuchihashi T, Horie-Inoue K, Nakanishi H, et al. Association of elastin gene polymorphism to age-related macular degeneration and polypoidal choroidal vasculopathy. Investigative Ophthalmology & Visual Science 2011;52:8780-4.

[308] Deng LH, Huang R, Chen ZY, Wu L, Xu DL. A Study on Polymorphisms of Elastin Gene in Chinese Han Patients With Isolated Systolic Hypertension. Am J Hypertens 2009;22:656-62.

[309] Micale L, Turturo MG, Fusco C, Augello B, Jurado LAP, Izzi C, et al. Identification and characterization of seven novel mutations of elastin gene in a cohort of patients affected by supravalvular aortic stenosis. Eur J Hum Genet 2010;18:317-23.

[310] Jakob A, Arnold R, Grohmann J, Unger S, Zabel B, Stiller B. New mutation in elastin gene as cause for critical supra valvular aorta stenosis (SVAS). Klinische Padiatr 2009;221:111-.

[311] Jakob A, Unger S, Arnold R, Grohmann J, Kraus C, Schlensak C, et al. A family with a new elastin gene mutation: broad clinical spectrum, including sudden cardiac death. Cardiol Young 2011;21:62-5.

[312] Szabo Z, Levi-Minzi SA, Christiano AM, Struminger C, Stoneking M, Batzer MA, et al. Sequential loss of two neighboring exons of the tropoelastin gene during primate evolution. J Mol Evol 1999;49:664-71.

[313] Martin RD. Primate origins - plugging the gaps. Nature 1993;363:223-34.

[314] Fazio M, Olsen DR, Kuivaniemi H, Chu M, Davidson J, Rosenbloom J, et al. Isolation and characterization of human elastin cDNAs, and age-associated variation in elastin gene expression in cultured skin fibroblasts. Laboratory Investigation 1988;58:270-7.

[315] Lander ES, Linton LM, Birren B, Nusbaum C, Zody MC, Baldwin J, et al. Initial sequencing and analysis of the human genome. Nature 2001;409:860-921.

[316] Chen Z, Shin MH, Moon YJ, Lee SR, Kim YK, Seo JE, et al. Modulation of elastin exon 26A mRNA and protein expression in human skin in vivo. Exp Dermatol 2009;18:378-86.

[317] Raju K, Anwar RA. A comparative analysis of the amino acid and cDNA sequences of bovine elastin a and chick elastin. Biochemistry and Cell Biology 1987;65:842-5.

[318] Heim RA, Pierce RA, Deak SB, Riley DJ, Boyd CD, Stolle CA. Alternative splicing of rat tropoelastin mRNA is tissue-specific and developmentally regulated. Matrix 1991;11:359-66.

[319] Pierce RA, Deak SB, Stolle CA, Boyd CD. Heterogeneity of rat tropoelastin messenger-RNA revealed by cDNA cloning. Biochemistry 1990;29:9677-83.

[320] Dyksterhuis LB, Carter EA, Mithieux SM, Weiss AS. Tropoelastin as a thermodynamically unfolded premolten globule protein: The effect of trimethylamine N-oxide on structure and coacervation. Archives of Biochemistry and Biophysics 2009;487:79-84.

[321] Debelle L, Wei SM, Jacob MP, Hornebeck W, Alix AJP. Predictions of the secondary structure and antigenicity of human and bovine tropoelastins. Eur Biophys J Biophys Lett 1992;21:321-9.

[322] Kumashiro KK, Ohgo K, Niemczura WP, Onizuka AK, Asakura T. Structural insights into the elastin mimetic (LGGVG)6 using solid-state 13C NMR experiments and statistical analysis of the PDB. Biopolymers 2008;89:668-79.

[323] Perry A, Stypa MP, Tenn BK, Kumashiro KK. Solid-state 13C NMR reveals effects of temperature and hydration on elastin. Biophys J 2002;82:1086-95.

[324] Pometun MS, Chekmenev EY, Wittebort RJ. Quantitative observation of backbone disorder in native elastin. Journal of Biological Chemistry 2004;279:7982-7.

[325] Kumashiro KK, Ho JP, Niemczura WP, Keeley FW. Cooperativity between the hydrophobic and cross-linking domains of elastin. Journal of Biological Chemistry 2006;281:23757-65.

[326] Starcher B, Aycock RL, Hill CH. Multiple roles for elastic fibers in the skin. J Histochem Cytochem 2005;53:431-43.

[327] Starcher B, Conrad M. A role for neutrophil elastase in the progression of solar elastosis. Connective Tissue Research 1995;31:133-40.

[328] Sephel GC, Davidson JM. Elastin production in human skin fibroblast cultures and its decline with age. J Investig Dermatol 1986;86:279-85.

[329] Starcher B, Pierce R, Hinek A. UVB irradiation stimulates deposition of new elastic fibers by modified epithelial cells surrounding the hair follicles and sebaceous glands in mice. Journal of Investigative Dermatology 1999;112:450-5.

[330] Desmet FO, Hamroun D, Lalande M, Collod-BÃ©roud G, Claustres M, BÃ©roud C. Human Splicing Finder: an online bioinformatics tool to predict splicing signals. Nucleic Acids Research 2009;37:e67.

[331] Shapiro MB, Senapathy P. RNA splice junctions of different classes of eukaryotes: sequence statistics and functional implications in gene expression. Nucleic Acids Research 1987;15:7155-74.

[332] Green MR. Biochemical mechanisms of constitutive and regulated pre-messenger-RNA splicing. Annual Review of Cell Biology 1991;7:559-99.

[333] Hallegger M, Sobala A, Smith CWJ. Four exons of the serotonin receptor 4 gene are associated with multiple distant branch points. RNA 2010;16:839-51.

[334] Taggart AJ, DeSimone AM, Shih JS, Filloux ME, Fairbrother WG. Large-scale mapping of branchpoints in human pre-mRNA transcripts in vivo. Nature Structural & Molecular Biology 2012;19:719-+.

[335] Tavares R, Renaud G, Oliveira PSL, Ferreira CG, Dias-Neto E, Passetti F. Identical sequence patterns in the ends of exons and introns of human protein-coding genes. Comput Biol Chem 2012;36:55-61.

[336] Stenson PD, Ball EV, Mort M, Phillips AD, Shiel JA, Thomas NST, et al. Human Gene Mutation Database (HGMD®): 2003 update. Hum Mutat 2003;21:577-81.

[337] Graham IR, Hamshere M, Eperon IC. Alternative splicing of a human alpha-tropomyosin muscle-specific exon - identification of derermining sequences. Mol Cell Biol 1992;12:3872-82.

[338] Pierce RA, Alatawi A, Deak SB, Boyd CD. Elements of the rat tropoelastin gene associated with alternative splicing. Genomics 1992;12:651-8.

[339] Kane JF, Violand BN, Curran DF, Staten NR, Duffin KL, Bogosian G. Novel in-frame 2 codon translational hop during synthesis of bovine placental lactogen in a recombinant strain of *Escherichia coli* Nucleic Acids Research 1992;20:6707-12.

[340] Pozharski EV, McWilliams L, MacDonald RC. Relationship between turbidity of lipid vesicle suspensions and particle size. Analytical Biochemistry 2001;291:158-62.

[341] Urry DW. Elastic biomolecular machines. SciAm 1995;272:64-9.

[342] Bellingham CM, Woodhouse KA, Robson P, Rothstein SJ, Keeley FW. Self-aggregation characteristics of recombinantly expressed human elastin polypeptides. Biochim Biophys Acta-Protein Struct Molec Enzym 2001;1550:6-19.

[343] Till O, Schmidt M, Linss W, Baumann E. Detection of bis(sulfosuccinimidyl) suberate binding in electrophoresis: Determination of membrane sidedness of proteins. ELECTROPHORESIS 2007;28:740-5.

[344] Annabi N, Mithieux SM, Weiss AS, Dehghani F. Cross-linked open-pore elastic hydrogels based on tropoelastin, elastin and high pressure CO2. Biomaterials 2010;31:1655-65.

[345] Tu YD, Mithieux SM, Annabi N, Boughton EA, Weiss AS. Synthetic elastin hydrogels that are coblended with heparin display substantial swelling, increased porosity,

and improved cell penetration. Journal of Biomedical Materials Research Part A 2010;95A:1215-22.

[346] Ruponen M, Rönkkö S, Honkakoski P, Pelkonen J, Tammi M, Urtti A. Extracellular glycosaminoglycans modify cellular trafficking of lipoplexes and polyplexes. Journal of Biological Chemistry 2001;276:33875-80.

[347] Naumann C, Mithieux SM, Szekely D, Tu Y, Weiss AS, Kuchel PW. "Setting paint" analogy for the hydrophobic self-association of tropoelastin into elastin-like hydrogel. Biopolymers 2009;91:321-30.

[348] Silver FH, Siperko LM. Mechanosensing and mechanochemical transduction: how is mechanical energy sensed and converted into chemical energy in an extracellular matrix? Critical reviews in biomedical engineering 2003;31:255-331.

[349] Parks WC, Pierce R, Lee KA, Mecham RP. Elastin. Advances in Molecular and Cell Biology 1993;6:133-81.

[350] Indik Z, Abrams WR, Kucich U, Gibson CW, Mecham RP, Rosenbloom J. Production of recombinant human tropoelastin: Characterization and demonstration of immunologic and chemotactic activity. Archives of Biochemistry and Biophysics 1990;280:80-6.

[351] Senior RM, Griffin GL, Mecham RP. Chemotactic responses of fibroblasts to tropoelastin and elastin-derived peptides. J Clin Invest 1982;70:614-8.

[352] Grosso LE, Parks WC, Wu L, Mecham RP. Fibroblast adhesion to recombinant tropoelastin expressed as a Protein A-fusion protein. Biochemical Journal 1991;273:517-22.

[353] Jung S, Rutka JT, Hinek A. Tropoelastin and elastin degradation products promote proliferation of human astrocytoma cell lines. Journal of Neuropathology and Experimental Neurology 1998;57:439-48.

[354] Faury G, Gamier S, Weiss AS, Wallach J, FÃ¼lÃ¶p Jr T, Jacob MP, et al. Action of tropoelastin and synthetic elastin sequences on vascular tone and on free Ca 2+ level in human vascular endothelial cells. CircRes 1998;82:328-36.

[355] Hinek A, Rabinovitch M. The ductus arteriosus migratory smooth muscle cell phenotype processes tropoelastin to a 52-kDa product associated with impaired assembly of elastic laminae. The Journal of Biological Chemistry 1993;268:1405-13.

[356] Hsiao H, Stone PJ, Toselli P, Rosenbloom J, Franzblau C, Schreiber BM. The role of the carboxy terminus of tropoelastin in its assembly into the elastic fiber. Connective Tissue Research 1999;40:83-95.

[357] Ostuni A, Bochicchio B, Armentano MF, Bisaccia F, Tamburro AM. Molecular and supramolecular structural studies on human tropoelastin sequences. Biophys J 2007;93:3640-51.

[358] Bochicchio B, Pepe A, Tamburro AM. Investigating by CD the molecular mechanism of elasticity of elastomeric proteins. Chirality 2008;20:985-94.

[359] Olsen DR, Fazio M, Shamban AT, Rosenbloom J, Uitto J. Cutis laxa: reduced elastin gene expression in skin fibroblast cultures as determined by hybridizations with a homologous cDNA and an exon 1-specific oligonucleotide. Journal of Biological Chemistry 1988;263:6465-7.

[360] Sephel GC, Byers PH, Holbrook KA, Davidson JM. Heterogeneity of elastin expression in cutis laxa fibroblast strains. J Investig Dermatol 1989;93:147-53.

[361] Mecham RP, Broekelmann TJ, Fliszar CJ, Shapiro SD, Welgus HG, Senior RM. Elastin degradation by matrix metalloproteinases - Cleavage site specificity and mechanisms of elastolysis. Journal of Biological Chemistry 1997;272:18071-6.

[362] Heinz A, Jung MC, Duca L, Sippl W, Taddese S, Ihling C, et al. Degradation of tropoelastin by matrix metalloproteinases - cleavage site specificities and release of matrikines. Febs J 2010;277:1939-56.

[363] Taddese S, Weiss AS, Neubert RHH, Schmelzer CEH. Mapping of macrophage elastase cleavage sites in insoluble human skin elastin. Matrix Biology 2008;27:420-8.

[364] Luan CH, Urry DW. Solvent deuteration enhancement of hydrophobicity: DSC study of the inverse temperature transition of elastin-based polypeptides. The Journal of Physical Chemistry 1991;95:7896-900.

[365] Gotte L, Mammi M, Pezzin G. Scanning electron microscope observations on elastin. Connective Tissue Research 1972;1:61-7.

[366] Mithieux SM, Tu YD, Korkmaz E, Braet F, Weiss AS. In situ polymerization of tropoelastin in the absence of chemical cross-linking. Biomaterials 2009;30:431-5.

[367] Waterhouse A, Bax DV, Wise SG, Yin YB, Dunn LL, Yeo GC, et al. Stability of a therapeutic layer of immobilized recombinant human tropoelastin on a plasma-activated coated surface. Pharmaceutical Research 2010;28:1415-21.

[368] Ross R, Fialkow PJ, Altman LK. The morphogenesis of elastic fibers. Advances in Experimental Medicine and Biology 1977;79:7-17.

[369] Sherratt MJ, Holmes DF, Shuttleworth CA, Kielty CM. Scanning transmission electron microscopy mass analysis of fibrillin-containing microfibrils from foetal elastic tissues. International Journal of Biochemistry & Cell Biology 1997;29:1063-70.

[370] Doig AJ, Baldwin RL. N- and C-capping preferences for all 20 amino acids in alpha-helical peptides. Protein Sci 1995;4:1325-36.

[371] Gosline JM, Lillie MA, Carrington E, Guerrette P, Ortlepp C, Savage K. Elastic proteins: biological roles and mechanical properties. Philosophical Transactions of the Royal Society London B 2002;357:121-32.

[372] Urry DW, Hugel T, Seitz M, Gaub HE, Sheiba L, Dea J, et al. Elastin: a representative ideal protein elastomer. Philosophical Transactions of the Royal Society London B 2002;357:169-84.